ABSTRACT

DUNAWAY, LARS ERIK. Advancing Voltammetric Strategies at Carbon-Fiber Ultramicroelectrodes for Improved Monitoring of Chemical Communication in Live Tissue. (Under the direction of Dr. Leslie A. Sombers).

Over the past 25 years or so, the field of neuroscience has been propelled forward by the advent of fast-scan cyclic voltammetry (FSCV). Paired with carbon-fiber ultramicroelectrodes, FSCV offers precise spatiotemporal resolution and high chemical selectivity for molecular measurements in live tissue, lending valuable insight into fundamental aspects of chemical communication. FSCV can be tailored to meet certain experimental requirements, both by modifying the waveform to detect specific analytes, and by changing the sensor geometry to exploit mass transport to and from the electrode surface. The work presented herein describes development of custom waveforms to aid in the study of neuropeptides, as well as the development of innovative carbon-fiber sensors for advancing investigations of the dynamics of vesicular fusion at cells. These advancements in electrochemical monitoring were implemented to investigate fundamental questions regarding neurochemical function.

Voltammetric measurements are heavily influenced by oxygen-group functionalization inherent to the carbon sensing surface. Raman spectroscopy was utilized to study the changing carbon surface in response to application of positive potentials in buffered solution. It was found that preconditioning the electrode with positive potentials results in increased sensitivity to many analytes of interest by modifying the carbon surface. For monitoring exocytosis at single cells in culture, ultramicroelectrodes are fabricated in a disc geometry and positioned directly above a single cell. Herein, the electrode design was modified by a plasma-etching method to recess the carbon sensor inside the insulation, forming a cavity. The cavity

electrodes were characterized using FSCV, and the sensor was used to monitor individual vesicular release events at single cells in culture. These electrodes detected more molecules per exocytotic release event than disc electrodes. The results demonstrate that a number of molecules released may go undetected with the conventional approach, and that the cavity design offers improved performance over disc electrodes. In additional studies, vesicular cargo was interrogated inside chromaffin cells, prior to exocytotic release. A carbon fiber nanoelectrode was designed in order to gain access to the cytoplasm. We monitored discrete, phasic catecholamine events with this approach as vesicles lysed onto the electrode surface, in the first intracellular FSCV study to date. Importantly, epinephrine and norepinephrine signals were distinguishable.

Measurements of endogenous opioid peptides remain challenging due to their low abundance and rapid degradation in the extracellular space. In fact, very little is known regarding where and when opioid neuropeptides are released in brain tissue, how far the peptides diffuse in the extracellular space, or the physiological conditions required to evoke release. To combat this, a customized waveform was designed to allow for the direct detection of methionine-enkephalin (M-ENK), an endogenous opioid peptide, in real-time. The development and characterization of the novel waveform and the detection of endogenous M-ENK dynamics in live tissue are reported herein. Next, the modulatory effects of M-ENK in live adrenal tissue were evaluated while monitoring catecholamine release. Another custom waveform was designed to allow for the detection of catecholamines being released in response to M-ENK, a molecule that tends to foul the electrode surface, preventing reliable measurements. A mechanism was discovered by which M-ENK elicited catecholamine secretion by these cells. This phenomenon was further investigated using electrophysiology.

The data demonstrate a novel mechanism for activation of mu opioid receptors via a synergistic mechanism with occupied muscarinic acetylcholine receptors, to depolarize chromaffin cells and elicit catecholamine efflux.

Overall, the work presented herein demonstrates substantial improvements to ultramicroelectrode technology and electrochemical monitoring with FSCV, and also uses these advances to make exciting new discoveries about cellular chemical communication. Thus, it serves to advance two separate fields, analytical electrochemistry and neuroscience.

Advancing Voltammetric Strategies at Carbon-Fiber Ultramicroelectrodes for Improved Monitoring of Chemical Communication in Live Tissue.

by
Lars Erik Dunaway

A dissertation submitted to the Graduate Faculty of
North Carolina State University
in partial fulfillment of the
requirements for the degree of
Doctor of Philosophy

Chemistry

Raleigh, North Carolina

2017

APPROVED BY:

_____	_____
Leslie A. Sombers Committee Chair	David A. Shultz
_____	_____
Gufeng Wang	John E. Meitzen

DEDICATION

This work is dedicated to my wife, Anna Dunaway, and to the family we will build together. I hope that everything I do, including the work presented herein, may serve you and our family, as well as God, before myself.

The work is also dedicated to my parents, who always encouraged my curiosity in the natural world around me, and reinforced continually, that I could do anything I wanted to with my life.

Lastly, this dissertation is dedicated to my late grandparents- Mayhu, Frances, Stig, and Hanne, and Aunt Sarah, whom I had too short a time with in this world, and my late best friend, Michael Schwab, who was so looking forward to celebrating the day that I would finish my degree.

BIOGRAPHY

Lars Erik Dunaway was born in Chesterfield County, VA, on August 17th, 1989, to parents Dave and Isa Dunaway. He lived there and studied in Chesterfield County Public Schools until leaving for college at the age of 18. Along the way, Lars participated in sports including soccer, tennis, swimming, cross country, and track and field, as well as studying piano, and classical and bluegrass violin. Many of his hobbies and extracurricular activities were picked up from observing his older brother, Chris Dunaway, and wanting to be like him. In middle school, he picked up a life-long interest in cars and all things mechanical. From before he could walk on his own, he was interested in sciences and mathematics, creating obscure patterns with silverware on the kitchen floor, and taking apart toys to see if he could put them back together.

Lars left for college in 2008, attending The College of William & Mary to attain a B.S. in Chemistry. There, he joined the Alpha Tau Omega fraternity, forming friendships that would influence him profoundly and shape the man he turned out to be. He also participated in undergraduate research in Dr. Robert D. Pike's chemistry research laboratory all four years. This research experience opened his eyes to the intellectual satisfaction and joy in doing research, encouraging him to attend graduate school for a Ph.D in chemistry.

After graduating in 2012, Lars went to North Carolina State University to pursue his Ph.D in chemistry. He joined Dr. Leslie Sombers' analytical chemistry research laboratory, falling under her mentorship and guidance for the remainder of his graduate career. Within his first couple of months in Raleigh, he met his future wife, Anna Lamm, at a church function.

They hit it off and got married a little over three years later on April 23rd, 2016. It was the best decision he ever made.

When not in the lab, Lars is active in his church, working with the high school youth and mentoring them. He also continues his love for working on mechanical things including cars, motorcycles, and his 1963 John Deere farm tractor. Additionally, he races motorcycles, having won two regional amateur championships with WERA Road Racing in 2016.

ACKNOWLEDGMENTS

I would like to express my deepest gratitude to all of my friends and family, who have supported me and my path throughout the years. Thank you to my amazing, beautiful wife, Anna Dunaway, for believing in me, encouraging me in my academic pursuits, and keeping me focused when necessary. Thank you to my parents for raising me with an appreciation for learning, and encouraging my curiosity in the world. Thank you also for constantly reminding me that I can do anything that I want to do in life. Thank you to my older brother, Chris Dunaway, for serving as a role model throughout my entire life. I have always looked up to you and wanted to do things the way that you did them.

In addition to the support that I have received from my family, I owe an enormous debt of gratitude to my advisor and mentor, Dr. Leslie Sombers. Thank you for encouraging and supporting me in my research, and for pouring so much energy not only into my science, but also into teaching me how to communicate my research effectively, in both written and verbal form. I would also like to thank the others in the Sombers Lab with whom I have had the privilege of working, particularly Dr. James Roberts and Dr. Andreas Schmidt, for taking me under their wings from the beginning and teaching me the ropes. Thank you to Dr. Gregory McCarty for the continual help in my research, helping both with technical problems, as well as overall guidance in my projects. I also deeply appreciate the many contributions from Christie Lee, in the form of our many conversations about research, as well as help reviewing my manuscripts. A special thank you to my chemistry committee members as well for your guidance in this process, Dr. David Shultz and Dr. Gufeng Wang. Finally, thank you to Dr. John Meitzen for serving both as a committee member, and as a second mentor in the latter

part of my graduate career. Thank you for welcoming me into your lab and giving me access to your resources, for teaching me about electrophysiology, and for your valuable support in the months leading up to my defense.

This work would not have been possible without funding from the North Carolina State University Department of Chemistry, and from the National Science Foundation.

TABLE OF CONTENTS

LIST OF TABLES

LIST OF FIGURES

CHAPTER 1

Introduction to Neurotransmission and Electrochemical Methods for Studying Neurochemical Dynamics

1.1 Introduction to Neuronal Communication

Neurons are specialized, electrically excitable cells that transmit information through chemical messengers and electrical signals. The many types are distributed throughout the central and the peripheral nervous systems, and can be coupled through ~20 nm wide junctions called chemical synapses (Figure 1). Chemical communication happens when the presynaptic neuron releases neurotransmitters into the synapse, which can then bind to specialized receptors on the postsynaptic neuron, thus propagating information between two neurons.

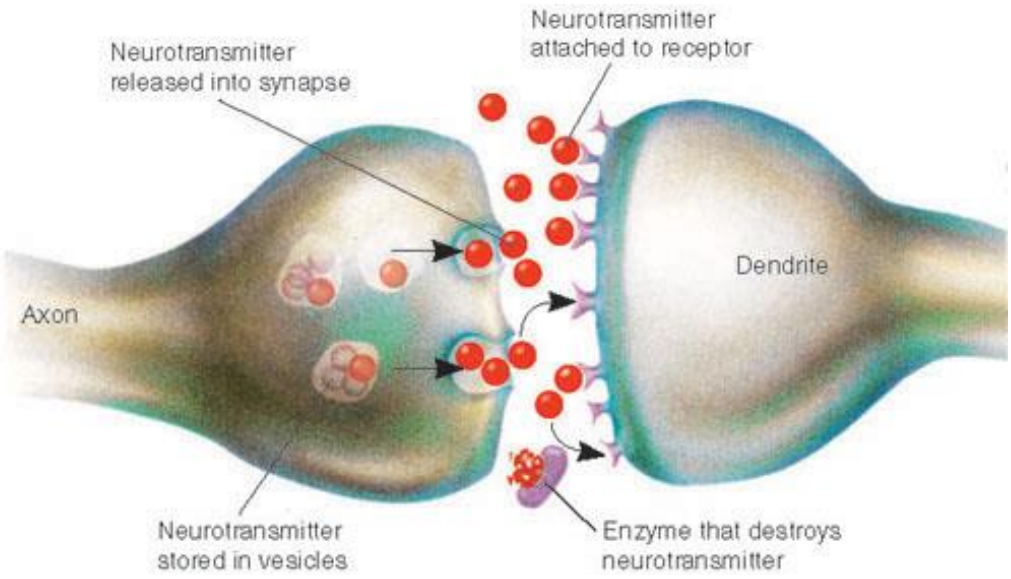

Figure 1.1. Chemical synapse between two neurons[1]

The events that lead to release of neurotransmitters from a neuron begin with the firing and propagation of an action potential. The potential across the cell membrane rests at a negative voltage, often around -70 mV, due to concentration gradients of certain ions across the cell membrane. There is a positive Na^+ gradient outside the cell, and a positive K^+ gradient inside the cell. There are voltage-gated ion channels for each of these ions, which open at certain voltages and allow the ions to flow down their concentration gradients. When the neuron becomes depolarized, generally by the influx of cations, voltage-gated Na^+ channels open up, causing further depolarization as Na^+ flows into the cell. This is the rising phase of an action potential. The Na^+ channels close rapidly after opening, and when the cell is depolarized, it causes voltage-gated K^+ channels to open. This allows for the efflux of K^+ from the cell, which repolarizes the membrane. This is described as the falling phase of the action potential. Once the membrane is repolarized, the voltage-gated K^+ channels close again. Potassium channels are slower to close, resulting in a brief refractory period during which the membrane potential is hyperpolarized, due to overshooting the resting potential. This action potential propagates down the axon of a neuron, ending at the terminal.[1]

When the action potential reaches a particular part of the axon, often but not always the terminal, it triggers vesicular release of neurotransmitters, or exocytosis. The neurotransmitters are stored in large dense core vesicles (LDCVs) and small synaptic vesicles (SSV) inside the cell, a population of which is docked to the inside of the membrane. SSVs are thought to store only small molecule neurotransmitters, while LDCVs can store small and large molecules, including peptides, in their chromogranin core. When the cell depolarizes, it opens voltage-gated Ca^{2+} channels, which allows Ca^{2+} to flow into the cell. The Ca^{2+} binds to synaptotagmin,

a pre-synaptic membrane-bound protein, which triggers the fusion of vesicles docked to the membrane. While there is a wide body of literature showing that different isoforms of synaptotagmin result in either full or partial release of the contents of LDCVs,[2-3] other researchers propose that under normal conditions, LDCVs never release their contents fully.[4-5] Rather, they propose that the vesicle releases the portion of its contents in the halo around the chromogranin core, and then pinches back into the cell membrane, still containing the chemical contents that are electrostatically associated with the core.

There is a wide variety of endogenous neurotransmitters, ranging from simple amines to large peptides.[6] Once neurotransmitters are released, they can bind to specific receptors on the cell membrane and act as agonists or antagonists, as well as performing other functions. Receptors are proteins embedded in the cell membrane that elicit some physiological response when bound by a ligand. An agonist binds to the receptor and provokes a particular physiological response, whereas an antagonist binds to the receptor and blocks or attenuates the response. Most receptors have an endogenous agonist. However many other endogenous and synthetic ligands can also act as agonists, which is the basis for pharmacological manipulation.

Another common fate of neurotransmitters, following release into the extracellular space, is reuptake. This is a process whereby specialized proteins, called transporters, transport the neurotransmitters back inside the cell from which they were released, fine tuning extracellular lifetime and diffusion distances. Reuptake is generally restricted to small molecules, and not larger peptides.[7] Neuropeptides are generally degraded enzymatically in the extracellular space. In many cases these processes are not well described.

1.2 Neurotransmission in the Adrenal Gland

Neurotransmission occurs in the periphery as well, including in the adrenal gland. The adrenal glands are located above the kidneys and have two regions, the medulla and the cortex that surrounds it. Chromaffin cells in the adrenal medulla are similar to neurons in their function and machinery, and are thus a commonly used model for studying exocytosis, both in cell culture preparations as well as tissue slice preparations.[8-12] They secrete hormones, and serve as the body's principal source of norepinephrine and epinephrine in the fight-or-flight response.[3] The adrenal glands are innervated by the splanchnic nerve, which secretes acetylcholine onto chromaffin cells in order to excite the cells. Acetylcholine binds to both nicotinic acetylcholine receptors (nAChR) and muscarinic (mAChR) acetylcholine receptors on chromaffin cells. This depolarizes the cells, causing them to secrete norepinephrine and epinephrine into the bloodstream in response to a threat. Opioid peptides are also secreted, both by the splanchnic nerve and by chromaffin cells, although their precise role in adrenal signaling is not well understood.[13-15] In chromaffin cells, these peptides are stored in LDCVs and released simultaneously with catecholamines.

1.3 Common Techniques for Monitoring Cell Communication in Neuroscience

There are many established approaches to chemical measurements that offer valuable information to the field of neuroscience. These include immunoassay, high-performance liquid chromatography, capillary electrophoresis, and mass spectrometry.[16-22] Significant effort has been put into refining and advancing these techniques. As such, they can offer excellent

sensitivity and selectivity in resolving analytes. However, these techniques require extraction from the tissue or coupling with a method for sampling from the tissue before analysis. Microdialysis, a very common technique for sampling brain tissue, uses a probe to remove extracellular fluid for further separation and detection *ex vivo*. Microdialysis probes used to sample from the brain are typically between 200 and 400 μm in diameter and millimeters in length. These allow for analyte molecules to flow down a concentration gradient across an outer semi-permeable membrane. Artificial cerebral spinal fluid is circulated through the probe to carry the molecules of interest from the probe to the instrument for analysis. Temporal resolution is limited both by sampling time and the separation, resulting in individual measurements that take several minutes to perform. Furthermore, the large size of the probe (with respect to the neurons) can span several brain regions and causes significant damage to the tissue when implanted.[23] Another drawback to sampling by microdialysis is the relatively poor collection efficiency (less than 40% for common neurotransmitters).[24] This is made worse for extraction of peptides, which can adsorb to the walls of the tubing, and are also rapidly digested by peptidases present in the extracellular space before analysis.[25]

Immunoassay suffers its own set of limitations. It is a static technique, measuring the presence of particular molecules by binding labeled antibodies to the molecule of interest. As such, it provides a chemical measurement at a single point in time, post-mortem. Quantification can be difficult and selectivity is limited as well. Detection of peptides is generally done indirectly. Rather than measuring the molecule of interest directly, immunoassays generally target the prepropeptides which are later cleaved into the target molecules. The prepropeptides are not an active form of the target molecule, and can even have opposing actions to the

molecules of interest. Thus, immunoassay is effective at determining where a particular molecule may be likely to be, however it offers little insight into where it truly is in live tissue, and when it is released.

Electrophysiology is another invaluable technique commonly used in the field of neuroscience. Rather than identifying and quantifying the chemicals being released by cells, electrophysiology monitors the electrical activity of cells as they respond to chemical messengers. There are multiple experimental approaches to electrophysiology; one can measure the voltage of the cell membrane or the current moving across the cell membrane. Additionally, it can be performed on a population of cells, a single cell in patch-clamp mode, or even single ion-channels. This discussion is limited to whole-cell patch electrophysiology, since it is most relevant to the work presented herein. Briefly, a micropipette is placed against the cell membrane and negative pressure is applied to "patch" the pipette onto the cell (Figure 2). This opens up a small portion of the cell membrane, which seals against the edge of the micropipette with a very high resistance, allowing the pipette electrical access to the inside of the cell. The micropipette contains an electrode, and is filled with an internal cell solution and connected to an amplifier so that electrical activity can be measured between the inside of the cell and the outside, where a reference electrode is placed. The highly resistive seal between the cell and the pipette allows current between the working electrode and the reference electrode to flow through the cell and across the membrane, with minimal current leaking across the seal. The two common modes for patch-clamp electrophysiology are current-clamp, and voltage-clamp. In the voltage-clamp mode, potential is held constant by the amplifier, and passage of current across the cell membrane is measured. In current-clamp, the current is

controlled, and cell membrane voltage recorded. Patch-clamp electrophysiology is beneficial for looking at the direct effects of drugs and other stimuli on individual neurons, and has been used extensively throughout the field of neuroscience.[26-27] It has even been coupled to electrochemistry, since both can provide different types of valuable information, with very high temporal resolution.[28]

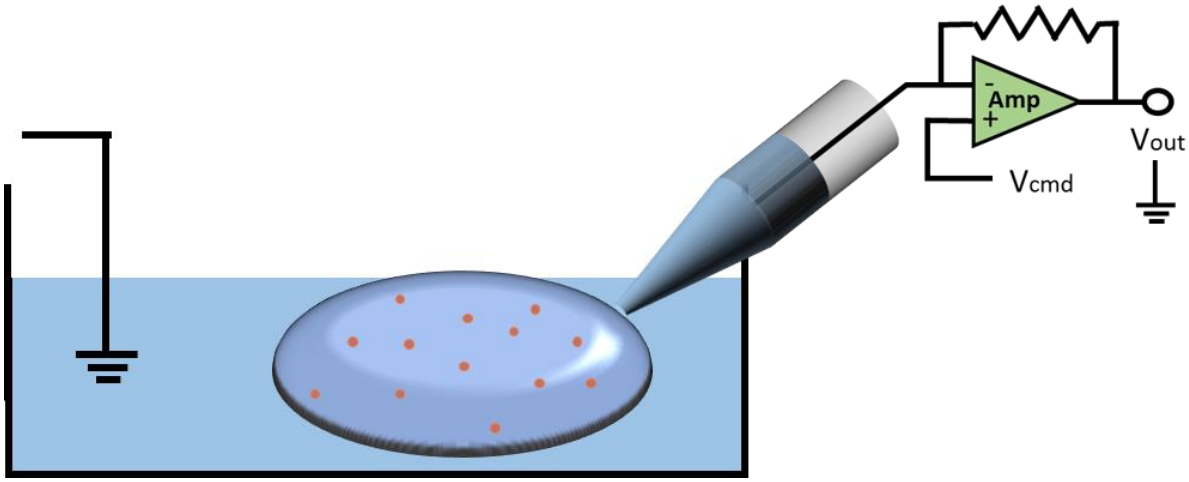

Figure 1.2. Typical whole cell patch-clamp electrophysiology setup. A pipette containing an electrode is sealed to the cell membrane, with the inside of the pipette continuous with the cytosol of the cell to allow for passage of fluid and current between the two.

1.4 Electrochemical Techniques in Neuroscience

Rather than monitoring cell activity, electrochemical approaches allow for the direct detection of chemical messengers being released from the cells. These approaches are capable of measuring chemical concentrations on the sub-second time scale, and offer precise measurements of chemical dynamics. They also offer a high degree of spatial resolution when coupled to micrometer-scale electrodes, or ultramicroelectrodes. Electrochemistry involves the

transfer of electrons from one phase to another, such as from aqueous solution to the electrode substrate, and can be used to monitor electroactive species *in situ*. Typical experiments in neuroscience involve only two electrodes: a working electrode and a reference. A counter electrode is not necessary because of the lower ohmic drop inherent to ultramicroelectrodes. The potential at the working electrode is controlled, and at a particular potential, an electroactive species will either be oxidized or reduced, resulting in a flow of electrons. This electron flow is described as current, measured in amperes, and can be used to quantitate electroactive species at the surface of the electrode. The two most common electrochemical techniques used in neuroscience are amperometry and voltammetry.[29]

Amperometry entails holding the working electrode at a set potential with respect to the reference electrode, typically Ag/AgCl. For detection of catecholamines the electrode is generally held at 650 to 800 mV. At these potentials dopamine is oxidized to dopamine-*o*-quinone through a two-electron process (Figure 3). The data is displayed with oxidation current on the y-axis, and time on the x-axis (Figure 4). Temporal resolution is limited only by adsorption of dopamine to the electrode and by the data sampling rate. Thus, single vesicular release events are detectable and distinguishable by amperometry, with events lasting a few milliseconds (Figure 4). Utilizing high-end potentiostats, the noise of the recording is less than a picoamp, so high sensitivity is also attained. The area under each current spike is integrated to give charge, which can be related to the amount of analyte oxidized using Faraday's Law:

$$Q = nNF$$

where Q is charge, N is moles of analyte, n is number of electrons transferred per molecule, and F is Faraday's constant.

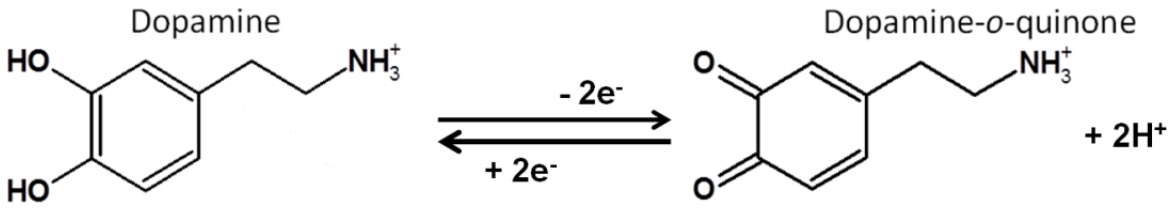

Figure 1.3. Reversible oxidation of dopamine to dopamine-*o*-quinone

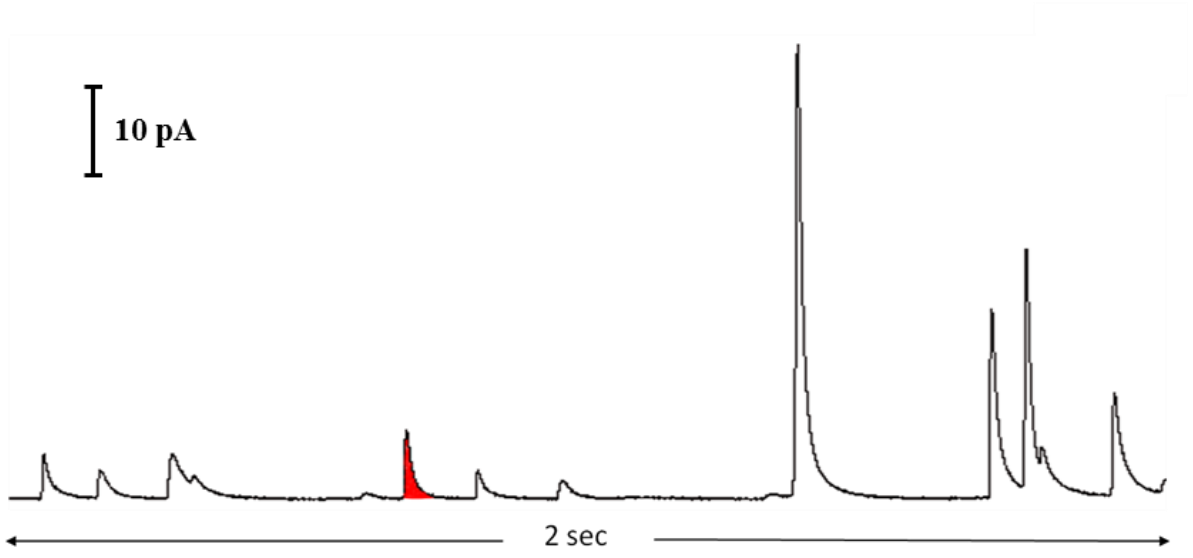

Figure 1.4. Sample amperometric trace. Each spike corresponds to release of a single vesicle via exocytosis. Red shading indicates the area under a curve integrated to give charge, which corresponds to moles of analyte detected.

One drawback to this approach is the limited selectivity, since any species that oxidizes at or below the holding potential is detected and adds to the current on the trace. Thus, amperometry is well-suited to experiments requiring high temporal resolution and sensitivity, such as those at single cells, but limited when used in a complex environment where there are interfering analytes or unknown species (such as in the brain).

Background-subtracted fast scan cyclic voltammetry (FSCV) is another electrochemical technique, with improved selectivity over amperometry. Compared to amperometry, where the potential at the working electrode is held constant, FSCV entails scanning across a set potential window repeatedly in a cyclic fashion, in a pattern called a waveform. The traditional dopamine waveform involves holding the electrode at -0.4 V, scanning up to +1.3 V and immediately back down to -0.4 V at 400 V/s, and repeating at a frequency of 10 Hz. Thus dopamine is oxidized to dopamine-*o*-quinone on the forward scan, and a fraction of the product is subsequently reduced back to dopamine on the return scan, while the rest diffuses away after oxidation. Each cycle yields a plot called a voltammogram, with the potential of the electrode on the x-axis and the resultant current on the y-axis. Selectivity results from the differences in oxidation/reduction potentials and electron transfer kinetics of varying analytes, thus providing a means for identification of analytes, with different classes of analytes giving rise to different shaped voltammograms. Background subtraction is required because the majority of the current collected is a result of charging the electrode, however this current is relatively stable over time and can be subtracted out of the voltammogram, giving rise to the background-subtracted voltammogram that serves as the chemical fingerprint (Figure 5).

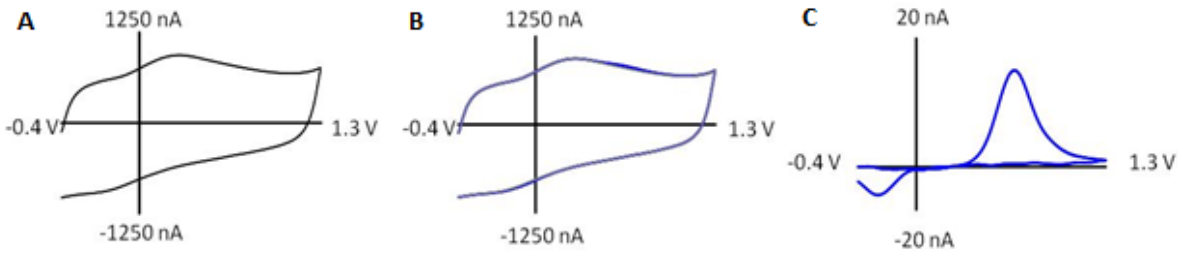

Figure 1.5. Cyclic voltammograms. (A) Stable background current. (B) Background current plus faradaic current resultant from oxidation of dopamine and reduction of dopamine-*o*-quinone. (C) Background-subtracted voltammogram showing faradaic current only

In order to display multiple voltammograms collected successively, a three dimensional color plot is utilized. Time is plotted on the x-axis, with successive voltammograms stacked next to each other. To show the voltammograms on the color plot, they are "unfolded" at the switching potential, so that current is plotted with respect to data point rather than potential (Figure 6A). The data point, or potential, is shown on the y-axis of the color plot, and the resultant current shown in false color (Figure 6B); green and blue indicate oxidation and reduction currents, respectively. This facilitates the observation of successive voltammograms collected over a given time period. The background current is generally stable for at least 90 seconds.

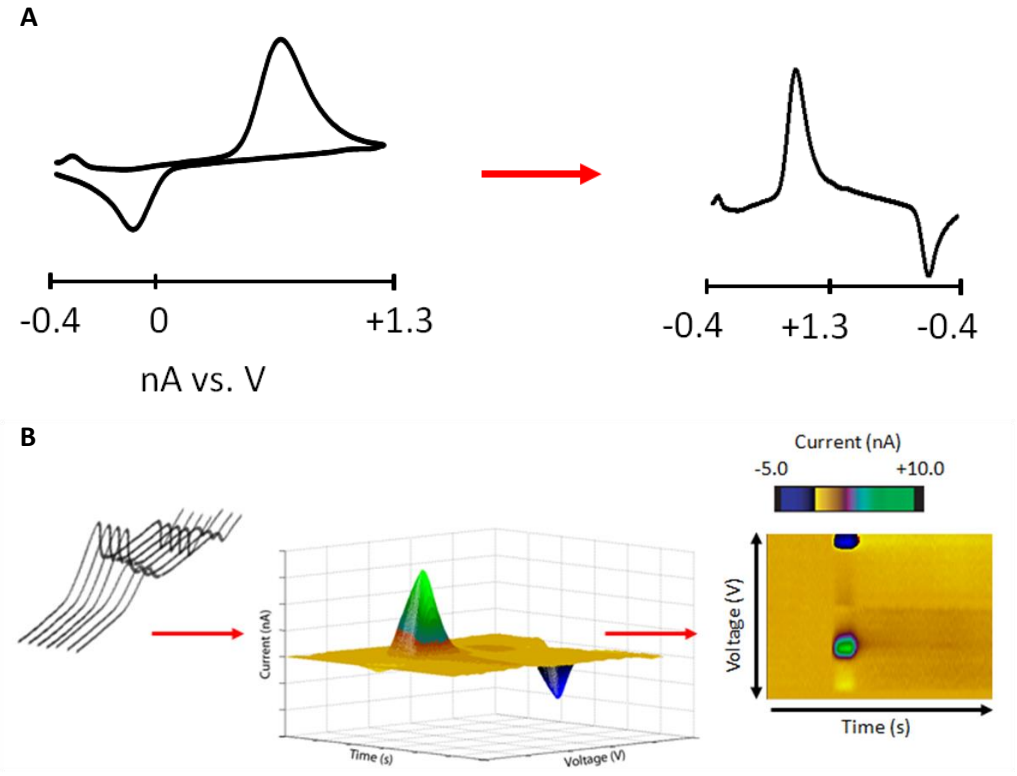

Figure 1.6. Color plot. (A) Unfolding a voltammogram. (B) Stacking unfolded voltammograms to generate the color plot

While most conventional electrochemical experiments on the benchtop are generally performed at platinum electrodes, electrochemical experiments in tissue are most often carried out at carbon electrodes (Figure 7) due to their small size and high tensile strength.[30] Carbon also resists biofouling better than platinum and other metals, where large biomolecules adhere to the surface, decreasing the usable surface area of the electrode and shifting background currents. Overall, the carbon fiber is an electrode material with beneficial properties: high tensile strength, ease of manufacture, wide aqueous potential window, chemical inertness, renewable surface[31] and rapid (sub-second) electron transfer.[32-34] Typical electrode geometries include the "cylinder", where the carbon fiber protrudes from the insulation 50-300 μm (Figure

7A), and the “disk”, where the carbon fiber is polished to an angle flush with the insulation (Figure 7B).

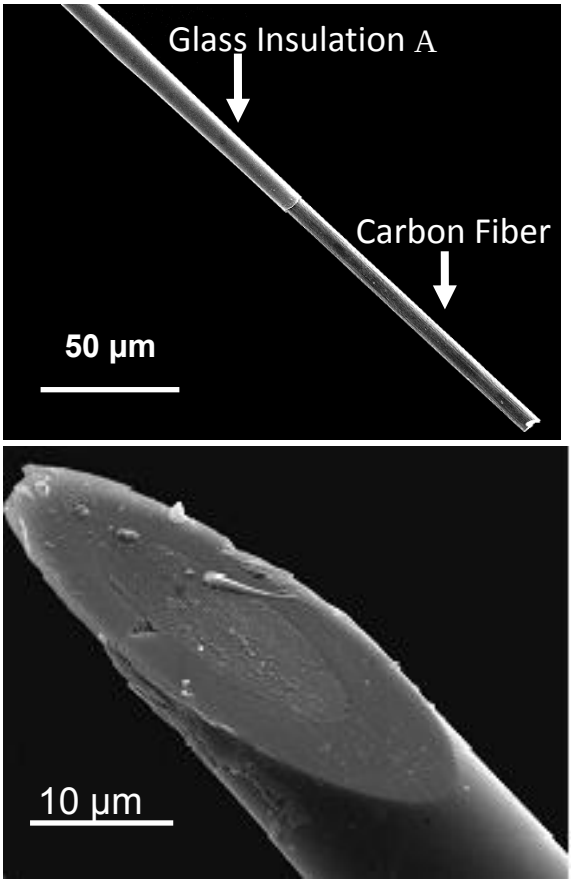

Figure 1.7. Representative scanning electron micrographs of carbon fiber microelectrodes insulated by pulled glass capillaries. A) Cylinder geometry. B) Disk geometry.

For experiments aimed at developing or optimizing new electrochemical detection techniques for neurochemical studies, neurotransmitter release can be simulated *in vitro* using a flow injection apparatus, or flow cell. Flow cells consist of an electrochemical cell with a

constant flow of buffered electrolyte over an electrode, allowing for short bolus injections of an analyte into the flowing buffer. Injections are generally carried out using a six port HPLC valve, which allows for precise control of the concentration and volume of the analyte being injected. The bolus injection serves to mimic rapid neurotransmitter release *in vivo* in a reproducible fashion, while keeping other variables constant. This is useful for characterizing a voltammetric response to a given analyte, and for calibrating electrodes.

1.5 Electrochemistry in Live Tissue

There are a variety of applications where electrochemical methods are coupled to ultramicroelectrodes in order to monitor rapid changes in chemical concentrations in live tissue. While the scope of these experiments ranges from single cell experiments to experiments in the brain of freely-moving animals engaged in behavioral challenges, the work presented herein will focus on the single cell, brain slice and adrenal slice preparations (male Sprague-Dawley rat).

Amperometry is typically used to study exocytosis events at single cells due to its ability to distinguish single-vesicle fusion events. Disk electrodes are placed directly over the cell using micromanipulators, with the sensing surface of the carbon fiber in physical contact with the cell membrane (Figure 8). Thus, vesicle contents are released directly onto the carbon fiber for rapid and sensitive detection. Vesicular release is typically stimulated by introducing a small amount of buffer with elevated potassium content onto the cell, which depolarizes the

membrane, opening up calcium channels and eliciting exocytosis. The electrode is held at a potential sufficient to oxidize vesicular content. Thus, single cell experiments are valuable for studying dynamics of exocytosis, and the physiochemical factors that can modulate this process.

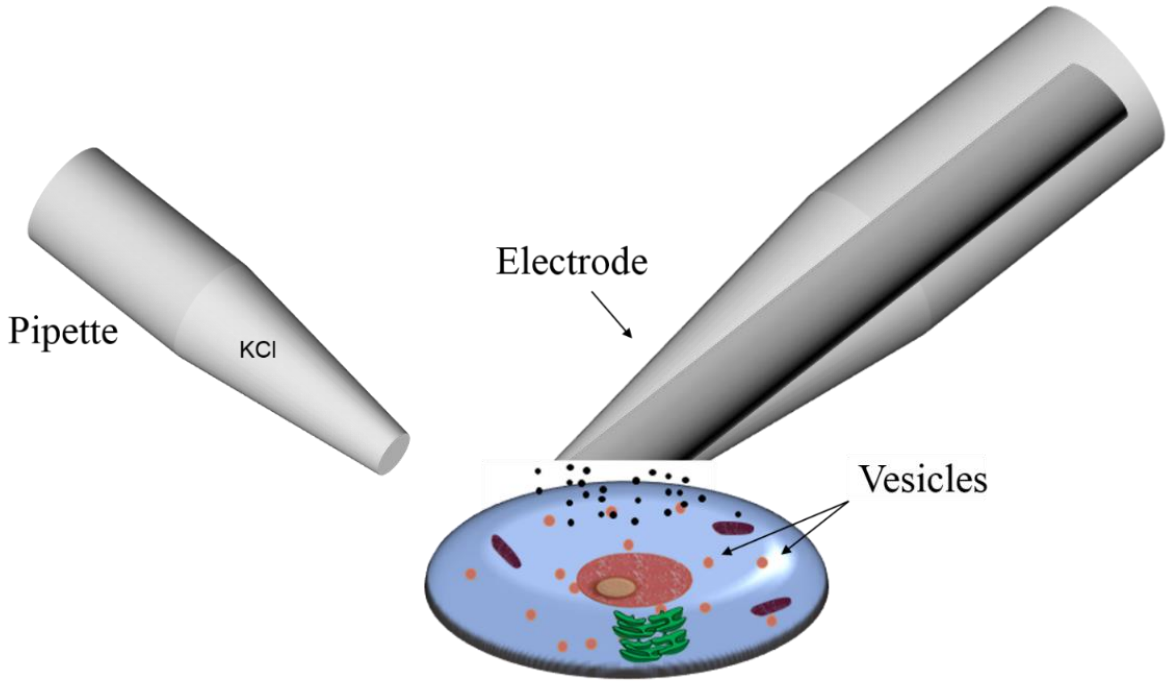

Figure 1.8. Typical setup for single cell electrochemical experiment. Electrode is positioned above a live cell, with the pipette placed nearby to eject secretagogue onto the cell.

Ex vivo experiments with tissue slices are another biological preparation that allows one to study specific aspects of neurotransmission. Organs of interest, typically the brain or the adrenal gland, are removed from an animal and kept alive in oxygenated, temperature-controlled buffer. The tissue is sliced to a thickness of 200-400 μm and perfused with buffer

under a microscope. A micromanipulator is used to position a cylinder electrode inside the tissue in the region of interest. Exocytosis can be triggered in a variety of ways. Electrical stimulation is common, whereby two tungsten microelectrodes are placed next to one another in the region of interest, and an electrical current pulse is passed between them to depolarize the cell and elicit exocytosis. Potassium stimulation is also used to depolarize the cells. Slice experiments permit one to study discrete neural circuits without the effect of afferent projections to the region, and also allow pharmacological manipulation of the system. Voltammetry is well-suited to make electrochemical measurements in complex tissue because of its inherent chemical selectivity.

1.6 Dissertation Overview

This work describes my investigations of opioids and catecholamines in the nervous system, and the interactions between the two. The Sombers Lab has a strong interest in motivated behaviors, which are dependent on these two classes of neurotransmitters, however their precise interactions are largely unknown. Dopamine is a key molecule in physiological function related to reward and learning, while opioids play a fundamental role in nociception and motivation, yet many questions remain. I have taken a technique commonly used to study dopamine and advanced it to allow for the detection for another class of molecules, opioid peptides, and used these advanced to extend a hypothesis about how these two classes of molecules work together. The remaining five chapters in this dissertation will describe the efforts undertaken in this work to improve electrochemical sensors for providing foundational

knowledge of the nervous system and its function. Novel findings made with these improved sensors will be presented.

Chapters 2 and 3 are my own independent work, and detail large research projects that I performed in the Sombers Lab.

Chapter 2 describes the fabrication and characterization of a cavity ultramicroelectrode, made by plasma-etching a disc electrode to recess the carbon sensing surface inside the glass insulation. The cavity electrode outperforms the traditional disc electrode in terms of sensitivity when used with FSCV, and is also compared to the disc electrode when coupled to amperometry to study exocytosis events at single chromaffin cells. The cavity electrode detects more molecules per exocytotic event compared to the disc, leading to the conclusion that discs are likely not detecting all of the molecules.

Chapter 3 demonstrates that M-ENK in the adrenal gland can elicit catecholamine secretion directly, by binding to the mu-opioid receptor on the chromaffin cell membrane. This response is observed with FSCV, and further investigated with electrophysiology. This chapter describes an excitatory action by the MOR when the muscarinic acetylcholine receptor is also occupied, which is most likely masked in prior works by the long time-scale of the measurements.

Chapters 4-6 describe large projects spearheaded by other researchers in the Sombers Lab, where I used my skills and tools to answer specific questions within each work. For each project, the entire work is presented in its own chapter in order to provide a framework for my own contributions within these projects.

Chapter 4 details a multiple scan rate waveform, developed specifically for the detection of M-ENK. The waveform and its response to M-ENK, along with common interferents, are characterized, and the waveform is utilized in adrenal tissue for the first real-time voltammetric detection of M-ENK in live tissue. I contributed to this work by utilizing this new waveform at a microelectrode in an adrenal slice preparation to perform the first detection of M-ENK in live tissue with FSCV.

Chapter 5 examines the functionality of the sensing surface on carbon-fiber electrodes. The carbon surface is constantly changing with the application of a waveform, and this dynamic surface is interrogated spectroelectrochemically by performing Raman spectroscopy while applying a waveform in a buffered solution. In this work, I performed slow scan cyclic voltammetry in order to characterize the electrode surface, as well as contributing heavily to overall manuscript preparation.

Chapter 6 outlines the fabrication of a nano-scale conical electrode, capable of monitoring molecules inside of a single cell. The nanoelectrode is inserted into cultured chromaffin cells, and FSCV used to detect norepinephrine and epinephrine. This is the first time that FSCV has been used to monitor neurotransmitters solely inside of a cell, prior to release. I contributed by helping to establish primary bovine chromaffin cell culture, as well as interfacing instrumentation for the collection of voltammetric data on the single cell experimental rig that I built for a previous work. I also assisted with data collection and analysis.

Additionally, an appendix is provided to supply supplemental information. This is intended to describe thoroughly many of the methods employed herein, and assist other researchers in reproducing this work.

1.7 References

1. Bear, M. F.; Connors, B. W.; Paradiso, M. A., *Neuroscience : exploring the brain*. Fourth edition. ed.; Wolters Kluwer: Philadelphia, 2016; p xlii, 975 pages.

2. Rao, T. C.; Passmore, D. R.; Peleman, A. R.; Das, M.; Chapman, E. R.; Anantharam, A., Distinct fusion properties of synaptotagmin-1 and synaptotagmin-7 bearing dense core granules. *Molecular Biology of the Cell* **2014,** *25* (16), 2416-2427.

3. Cardenas, A. M.; Marengo, F. D., How the stimulus defines the dynamics of vesicle pool recruitment, fusion mode, and vesicle recycling in neuroendocrine cells. *J. Neurochem.* **2016,** *137* (6), 867-879.

4. Li, X.; Majdi, S.; Dunevall, J.; Fathali, H.; Ewing, A. G., Quantitative measurement of transmitters in individual vesicles in the cytoplasm of single cells with nanotip electrodes. *Angew. Chem. Int. Ed. Engl.* **2015,** *54* (41), 11978-82.

5. Hu, R.; Ren, B.; Lin, C. J.; Oleinick, A.; Svir, I.; Tian, Z. Q.; Amatore, C., How "Full" is "Full Fusion" during Exocytosis from Dense Core Vesicles? Effect of SDS on "Quantal" Release and Final Fusion Pore Size. *J. Electrochem. Soc.* **2016,** *163* (9), H853-H865.

6. Bear, Mark F., Connors, Barry W., Paradiso, Michael A. Neuroscience: Exploring the Brain, 3rd ed.; Lippincott Williams & Wilkins: Baltimore, 2007.

7. Stein, W. D.; Lieb, W. R., *Transport and diffusion across cell membranes*. Academic Press: Orlando, 1986; p xvii, 685 p.

8. Bader, M. F.; Holz, R. W.; Kumakura, K.; Vitale, N., Exocytosis: The chromaffin cell as a model system. *Chromaffin Cell: Trnsmitter Biosynthesis, Storage, Release, Actions, and Informatics* **2002,** *971*, 178-183.

9. Strittmatter, W. J., Molecular Mechanisms of Exocytosis - the Adrenal Chromaffin Cell as a Model System. *Cellular and Molecular Neurobiology* **1988,** *8* (1), 19-25.

10. Suchard, S. J.; Rubin, R. W.; Pressman, B. C., Cultured Adrenal Chromaffin Cells as a Model System for the Study of Secretory Events. *J. Cell Biol.* **1980,** *87* (2), A303-A303.

11. Travis, E. R.; Wightman, R. M., Spatio-temporal resolution of exocytosis from individual cells. *Annu. Rev. Biophys. Biomol. Struct.* **1998,** *27*, 77-103.

12. Borges, R.; Camacho, M.; Gillis, K. D., Measuring secretion in chromaffin cells using electrophysiological and electrochemical methods. *Acta Physiol (Oxf)* **2008,** *192* (2), 173-84.

13. Wilson, S. P.; Chang, K. J.; Viveros, O. H., Synthesis of enkephalins by adrenal medullary chromaffin cells: reserpine increases incorporation of radiolabeled amino acids. *Proc Natl Acad Sci U S A* **1980,** *77* (7), 4364-8.

14. Livett, B. G.; Dean, D. M.; Whelan, L. G.; Udenfriend, S.; Rossier, J., Co-release of enkephalin and catecholamines from cultured adrenal chromaffin cells. *Nature* **1981,** *289* (5795), 317-9.

15. Whim, M. D., Near simultaneous release of classical and peptide cotransmitters from chromaffin cells. *J. Neurosci.* **2006,** *26* (24), 6637-42.

16. Hughes, J.; Smith, T. W.; Kosterlitz, H. W.; Fothergill, L. A.; Morgan, B. A.; Morris, H. R., Identification of two related pentapeptides from the brain with potent opiate agonist activity. *Nature* **1975,** *258* (5536), 577-80.

17. Schultzberg, M.; Dreyfus, C. F.; Gershon, M. D.; Hokfelt, T.; Elde, R. P.; Nilsson, G.; Said, S.; Goldstein, M., VIP-, enkephalin-, substance P- and somatostatin-like immunoreactivity in neurons intrinsic to the intestine: immunohistochemical evidence from organotypic tissue cultures. *Brain Res* **1978,** *155* (2), 239-48.

18. Schultzberg, M.; Hokfelt, T.; Lundberg, J. M.; Terenius, L.; Elfvin, L. G.; Elde, R., Enkephalin-like immunoreactivity in nerve terminals in sympathetic ganglia and adrenal medulla and in adrenal medullary gland cells. *Acta Physiol Scand* **1978,** *103* (4), 475-7.

19. Wallingford, R. A.; Ewing, A. G., Capillary zone electrophoresis with electrochemical detection. *Anal Chem* **1987,** *59* (14), 1762-6.

20. Hook, V. Y.; Yasothornsrikul, S.; Hwang, S. R., Novel chromaffin granule serpins, endopin 1 and endopin 2: endogenous protease inhibitors with distinct target protease specificities. *Ann N Y Acad Sci* **2002,** *971*, 426-44.

21. Hook, V. Y.; Toneff, T.; Aaron, W.; Yasothornsrikul, S.; Bundey, R.; Reisine, T., Beta-amyloid peptide in regulated secretory vesicles of chromaffin cells: evidence for multiple cysteine proteolytic activities in distinct pathways for beta-secretase activity in chromaffin vesicles. *J. Neurochem.* **2002,** *81* (2), 237-56.

22. Wegrzyn, J.; Lee, J.; Neveu, J. M.; Lane, W. S.; Hook, V., Proteomics of neuroendocrine secretory vesicles reveal distinct functional systems for biosynthesis and exocytosis of peptide hormones and neurotransmitters. *J Proteome Res* **2007,** *6* (5), 1652-65.

23. Nesbitt, K. M.; Jaquins-Gerstl, A.; Skoda, E. M.; Wipf, P.; Michael, A. C., Pharmacological mitigation of tissue damage during brain microdialysis. *Anal Chem* **2013,** *85* (17), 8173-9.

24. Shippenberg, T. S.; Thompson, A. C., Overview of microdialysis. *Curr Protoc Neurosci* **2001,** *Chapter 7*, Unit7 1.

25. Zhou, Y.; Wong, J. M.; Mabrouk, O. S.; Kennedy, R. T., Reducing adsorption to improve recovery and in vivo detection of neuropeptides by microdialysis with LC-MS. *Anal. Chem.* **2015,** *87* (19), 9802-9.

26. Scanziani, M.; Hausser, M., Electrophysiology in the age of light. *Nature* **2009,** *461* (7266), 930-9.

27. Dorris, D. M.; Cao, J.; Willett, J. A.; Hauser, C. A.; Meitzen, J., Intrinsic excitability varies by sex in prepubertal striatal medium spiny neurons. *J Neurophysiol* **2015,** *113* (3), 720-9.

28. Takmakov, P.; McKinney, C. J.; Carelli, R. M.; Wightman, R. M., Instrumentation for fast-scan cyclic voltammetry combined with electrophysiology for behavioral experiments in freely moving animals. *Rev. Sci. Instrum.* **2011,** *82* (7).

29. Michael, A. C.; Borland, L. M. Electrochemical methods for neuroscience; CRC Press/Taylor & Francis: Boca Raton, 2007.

30. Jaquins-Gerstl, A.; Michael, A. C. J. Neurosci. Methods 2009, 183, 127.

31. Takmakov, P.; Zachek, M. K.; Keithley, R. B.; Walsh, P. L.; Donley, C.; McCarty, G. S.; Wightman, R. M., Carbon microelectrodes with a renewable surface. *Anal Chem* **2010,** *82* (5), 2020-8.

32. Cahill, P. S.; Walker, Q. D.; Finnegan, J. M.; Mickelson, G. E.; Travis, E. R.; Wightman, R. M., Microelectrodes for the measurement of catecholamines in biological systems. *Analytical Chemistry* **1996,** *68* (18), 3180-3186.

33. Wightman, R. M., Probing cellular chemistry in biological systems with microelectrodes. *Science* **2006,** *311* (5767), 1570-1574.

34. McCreery, R. L., Advanced carbon electrode materials for molecular electrochemistry. *Chemical Reviews* **2008,** *108* (7), 2646-2687.

CHAPTER 2

Recessed Carbon-Fiber Microelectrodes Reveal Exciting New Insights into Measurements of Exocytosis from Single Cells

This work was completed in collaboration with: Dunaway, L.E., Schmidt, A.C, Calhoun, S. E., Roberts, J.G., Shogren, T.J., Zach, M.P., and Sombers, L.A., and is in preparation for submission to *Analytical Chemistry*.

2.1 Introduction

The development of carbon-fiber microelectrodes in the late 1970's[1] had a tremendous impact on the field of neuroscience, as it enabled the detection of rapid chemical events in very small places. Carbon-fiber microelectrodes have been used for the quantitative investigation of individual exocytosis events from single chromaffin cells in culture since 1990.[2-3] Owing to the excellent temporal resolution and sensitivity inherent to amperometric measurements at carbon microelectrodes, single-vesicle exocytosis can be resolved when the electrode is positioned immediately adjacent to the cell in an 'artificial synapse' configuration, and held at a potential sufficient to oxidize catecholamines, typically + 0.65 V to + 0.8 V. Thus, extensive research has been done on multiple aspects of exocytosis at single cells, including investigations examining neurotransmitter content,[4-5] the spatial heterogeneity of exocytosis along the cell membrane,[6-7] the dynamics of the fusion pore,[8-11] mass transport at the electrode surface,[12] and catecholamine storage.[10] Recently, Ewing *et. al* have developed a new method deemed 'intracellular vesicle electrochemical cytometry', in which amperometry is performed with a conical nanotip microelectrode inserted into the cell cytoplasm.[13] This work uses

amperometry to quantitatively compare vesicle content in the cytoplasm to that released onto an extracellular electrode in the exocytosis process. Interestingly, the data show that more catecholamine is detected when intracellular vesicles fuse with the microelectrode inserted into the cytoplasm than when vesicles fuse with the plasma membrane, releasing contents into the extracellular space via exocytosis.

Background-subtracted fast-scan cyclic voltammetry (FSCV) has been coupled with carbon-fiber microelectrodes to monitor neurotransmitter release in intact tissue since the 1980s.[14-15] This approach provides the appropriate selectivity for the detection of neurotransmitter dynamics in the complex chemical environment of the brain, while still retaining outstanding sensitivity and temporal resolution. Since its inception, FSCV has emerged as one of the leading techniques used for the detection of dopamine dynamics in the brain, because it enables electrochemical measurements to be correlated with specific aspects of an animal subject's behavior.[16-17] While initially implemented for the detection of dopamine, is has been further developed to allow for detection of various other monoamines,[18] oxygen,[19] hydrogen peroxide,[20] adenosine,[21] and even opioid peptide dynamics,[22] in real time.

Carbon-fiber microelectrodes are typically constructed with either cylindrical[23-26] or disk geometries (see Figure 1.7).[14, 27-30] Consideration of geometry is critical in experimental design, as disk electrodes sample from a smaller area and provide better spatial resolution, while cylinder-shaped electrodes are much larger and feature an increased surface area as compared to the planar surface of a disk electrode. Experiments at single cells require an electrode that samples from an area on the order of the cell size, typically less than 20 μm in diameter.[31] Thus, the disk geometry is preferred for these experiments. Low-noise instruments

are used to collect exocytotic events that generate pA of current. However, many events occur near the limit of detection, and single cell studies could benefit from a more sensitive electrode, particularly when it is necessary to quantify the entirety of the neurotransmitter released in an individual vesicular fusion event.

A recessed carbon-fiber disk geometry (cavity) would be advantageous for a variety of applications, as a cavity helps to confine the analyte proximal to the sensing surface (Figure 2.3D). [32-34] A recessed sensing surface is also shielded from convection, allowing detection of electroactive molecules with less contribution from this contribution to mass transport.[32, 35] In theory, this should allow for more efficient and sensitive detection of individual exocytosis events. Further, cavity electrodes could be coupled with fast-scan cyclic voltammetry to amplify the signal in the detection of chemically reversible reactions, such as the oxidation of dopamine and subsequent reduction of its product, dopamine-*ortho*-quinone. The glass shroud inherent to the cavity electrode could help to retaining the analyte near the sensing surface, allowing for detection of the same molecule multiple times (redox cycling), thus amplifying the signal (Figure 1.1 E,F).[36-38]

Recessed cavity microelectrodes have been constructed by others through combinations of complex fabrication techniques, often involving oxidative etching, various types of lithography, layer-by-layer deposition, and/or ion etching.[36, 39-41] While cavity electrodes offer numerous advantages over traditional disk electrodes, a simpler fabrication method is necessary in order for them to become widely employed in various research laboratories. In this work, single carbon-fiber microelectrodes are etched using a simple and straightforward plasma-etching strategy developed in-house, generating a plasma by applying

a high potential across an air gap. This method reliably produces electrodes with a controllable cavity depth, which are characterized and compared to traditional disk electrodes herein using FSCV. Scanning electron microscopy, Raman spectroscopy, and traditional slow-scan voltammetry are utilized to study structural changes that occur during the etching process. The cavity electrodes are tested in an acute brain slice to evaluate their performance in complex tissue, and also compared to disk electrodes at single cells, detecting more molecules per release event than the widely used disk electrode. Overall, the data suggest that current approaches to measuring exocytotic release at disk electrodes result in an underestimation of quantal size. There is still much to be learned about the dynamics and fundamental nature of exocytosis, and having a tool to more fully describe neurotransmitter release events will offer an improved understanding of quantal release.

2.2 Experimental Section

2.2.1 Chemicals

All chemicals were purchased from Sigma-Aldrich (St. Louis, MO) and used as received, unless otherwise specified. FSCV experiments were carried out in phosphate-buffered saline (0.1 M PBS) at physiological pH 7.4. Brain slice experiments were carried out in aCSF saturated with 95% O_2 and 5% CO_2, at physiological pH 7.4. aCSF consisted of 124 mM NaCl, 26 mM $NaHCO_3$, 3.7 mM KCl, 1.3 mM NaH_2PO_4, 2.4 mM $CaCl_2$, 1.3 mM $MgCl_2$, and 10 mM glucose. All aqueous solutions were made from doubly deionized water >18 MΩ·cm (Millipore, Billerica, MA).

2.2.2 Microelectrode Fabrication

The microdisk electrodes were fabricated from Thornel P-55 (Cytec, Tempe, AZ.) carbon fibers as previously described (fiber diameter = ~10 µm).[42] Briefly, the disk electrodes were prepared by sealing standard carbon-fiber cylinder electrodes with epoxy (301 Epoxy; Epoxy Technology, Inc., Billerica, MA), curing overnight at 105˚C, and polishing the electrode tip to the glass insulation at a 35˚ angle using a diamond dust-embedded micropipette beveling wheel (BV-10; Sutter Instrument Co., Novato, CA). For fabrication of cavity microelectrodes, microdisk electrodes were fabricated from Thornel T-650 (Cytec) carbon fibers as a starting point (fiber diameter = ~7 µm). Wet etching was performed in a flow injection apparatus, applying a waveform with a holding potential of +2.5 V and a negative ramp to +1.5 V, then returning to +2.5 V at 10 Hz. Plasma etching was performed in a custom-made apparatus (Figure 1.1). The carbon-fiber electrode (positive lead) and a conical stainless steel electrode (negative lead) were sealed in a glass chamber with a tip separation of ~1 cm. A picoammeter (Keithley Instruments, Inc., Cleveland, OH) was used to monitor the passage of current. The applied DC potential was sourced from a linear power supply (Lambda Electronics, Inc., Melville, NY) and regulated using a high voltage power supply (Bertan High Voltage Corp, Hicksville, NY). Custom written LabVIEW® software was used to control the applied potential. The carbon fiber was etched 6 µm past the middle of the beveled section of the electrode, 11 µm from the end of the beveled tip. Electrodes were preconditioned by applying a static +1.0 V holding potential for at least 30 minutes prior to the start of experiments.

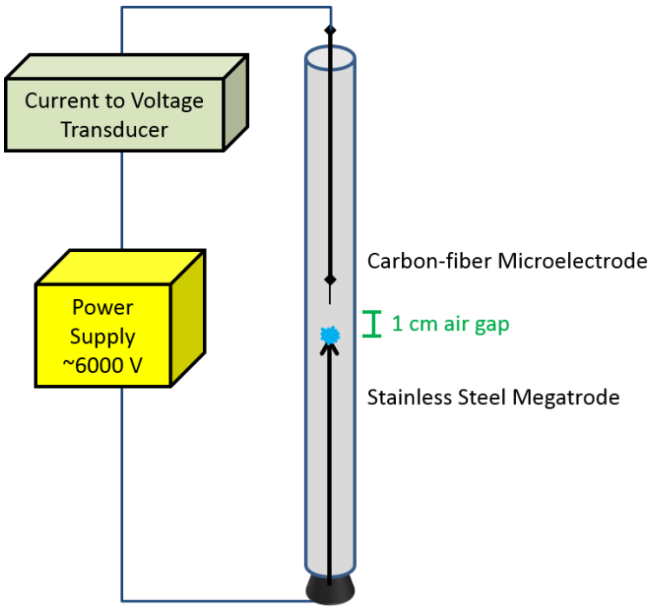

Figure 2.1. Plasma etching apparatus. The carbon-fiber electrodes were mounted inside a glass chamber with a ~1 cm tip separation. The DC potential was ramped in 25V increments using a high-voltage power supply, until the desired electrical current was reached. The etch-rate at this potential was constant, and held for a given amount of time to control how far the carbon-fiber recessed.

2.2.3 Data Acquisition

All *in vitro* FSCV data were collected in a custom-built flow injection apparatus housed within a Faraday cage. A syringe pump (New Era Pump Systems, Inc., Wantagh, NY) supplied a continuous buffer flow of 1 mL/min across both the working and reference electrode. The working electrode was lowered into the electrochemical cell *via* a micromanipulator (World Precision Instruments, Inc., Sarasota, FL). Bolus injections of analyte were accomplished using a six-port HPLC valve and air actuator controlled by a digital valve interface (Valco Instruments Co., Inc., Houston, TX).

2.2.4 Fast-Scan Cyclic Voltammetry

A triangular waveform was used for analyte detection. The applied potential ranged from -0.4 to +1.3 V vs. Ag/AgCl reference, scanned at a rate of 400 V/s, and applied at a frequency of 10 Hz. The waveform was output using a custom-built instrument for potential application to the electrochemical cell and current transduction (University of North Carolina at Chapel Hill, Department of Chemistry, Electronics Facility). HDCV software (University of North Carolina at Chapel Hill, Department of Chemistry)[43] was used for waveform output with a DAC/ADC card (NI 6363). Signal processing (background subtraction and signal averaging) was software-controlled.

2.2.5 Raman Spectroscopy

Raman analysis was done using a custom spectrometer previously described.[44] To mimic the electrochemical environment, spectra were collected while the carbon-fiber electrodes were immersed in PBS solution. A 60x objective was used with collection times of 60 seconds. Prior to plasma etching, spectra were taken of carbon-fiber electrodes after polishing and electrochemical conditioning. The electrodes were subsequently etched and reconditioned and spectra were recollected at the same set of electrodes.

2.2.6 Brain Slice Preparation

Male Sprague-Dawley rats (250-300 g, Charles River Laboratories, Raleigh, NC) were decapitated after being deeply anesthetized with urethane (1.5 g/kg, i.p.). The brain was rapidly removed, mounted, and placed in cold aCSF. 400 μm thick coronal slices were cut with a

vibratome (World Precision Instruments, Sarasota, FL). The slices were allowed to rest in aCSF for at least one hour, and were subsequently placed in a recording chamber (Warner Instruments, Hamden, CT) and superfused with buffered aCSF maintained at 34 °C for at least another hour. The working electrode and bipolar stimulating electrode placements were made with the aid of a microscope (Nikon Instruments, Inc., Melville, NY), and the microelectrodes were positioned about 50 μm below the surface of the slice. Electrical stimulation of nerve terminals consisted of five 500 μA biphasic pulses at 60 Hz using a pulse width of 4 msec. Animal care and use was in complete accordance with institutional guidelines and IACUC.

2.2.7 Primary Bovine Chromaffin Cell Culture

Six bovine adrenal glands were obtained to establish primary culture, and immediately trimmed of excess fat and submerged in ice-cold W3 buffer (145 mM NaCl, 5.4 mM KCl, 1 mM NaH_2PO_4, 11.2 mM glucose, and 15 mM HEPES). Glands were perfused with cold W3 through the adrenal vein until the fluid coming out was clear and free of blood. The glands were trimmed of fat and perfused with warm W3, then incubated at 37 ˚C for 10 minutes and washed with W3, repeated three times. Next, glands were perfused with a digestion mixture containing 1.4 mg/mL DNAase and 0.035 mg/mL collagenase in W3 and incubated for 15 minutes, again three times. After the first wash, nystatin (5mL/L) was added to W3 solution and this was used for the remainder of the steps involving W3. Glands were then dissected, removing and finely mincing the medullae. Minced medullae were placed in stirred digestion mixture for 30 minutes, filtered, and centrifuged at 1500 RPM to pellet the cells. Pellets were resuspended in W3 and mixed with a Percoll gradient. The Percoll gradient containing

suspended cells was centrifuged at 10,000 RPM to separate red blood cells, chromaffin cells, and cellular debris. The chromaffin cell layer was collected and filtered through a 40 μm sterile nylon filter. The filtrate was added to DMEM (Dulbecco's Modified Eagle Medium) and centrifuged at 800 RPM to pellet the cells. Supernatant was removed and pellets were resuspended in DMEM containing 10% FBS and 1% 100X Pen-strep. Using a hemocytometer, cells were diluted to a density of 3 x 10^5 cells/mL and plated on 35 mm culture dishes, with 2 mL in each dish.

2.2.8 Single Cell Experiments

Cells were prepared for the experiment by replacing the medium with an isotonic buffer containing calcium (150 mM NaCl, 5 mM KCl, 1.2 mM $MgCl_2$, 5 mM glucose, 10 mM HEPES, and 2 mM $CaCl_2$ at pH 7.4). The electrodes were lowered onto individual cells, maneuvering the electrode downward until the cell surface was slightly perturbed by the electrode, and lifting back up until the surface was no longer perturbed by the electrode. Exocytosis was stimulated with a 3 second, 20 psi pulse (Picospritzer II; General Valve Corporation, Fairfield, NJ) of high potassium isotonic stimulating buffer (55 mM NaCl, 100 mM KCl, 1.2 mM $MgCl_2$, 5 mM glucose, 10 mM HEPES, and 2 mM $CaCl_2$) using a micropipette polished to a 10 μm opening. The culture dish containing the cells was maintained at 37 ˚C during the experiment using a culture dish incubator (DH-35iL; Warner Instruments, LLC., Camden, CT).

2.2.9 Amperometry Data Acquisition and Analysis

Electrodes were held at +0.8 V vs. Ag/AgCl (World Precision Instruments, Inc., Sarasota, FL) using a patch-clamp amplifier (Axopatch 200B; Molecular Devices, LLC., Sunnyvale, CA). Amperometric output was filtered at 1 kHz using an internal four-pole low-pass Bessel filter and digitized at 2 kHz using an Axon Digidata 1440A (Molecular Devices). The amplifier was set to Whole Cell (ß = 1) configuration in voltage-clamp mode. Data were collected and stored using Axoscope software (version 10.4.1.9; Molecular Devices). Electrodes were not used if the baseline current in buffered solution was greater than + 20 pA. Peaks with intensity exceeding three times the standard deviation of the noise were identified as exocytotic spikes using Mini Analysis software (version 6.0.3, Synaptosoft). These spikes were evaluated for peak area (femtocoulombs), $t_{1/2}$ (milliseconds), and i_{max} (picoamperes). All peaks identified by the program were visually inspected, and artifacts or other misidentified peaks were excluded from the analysis. Double peaks were separated into their constituent peaks. Peaks manually excluded or reevaluated (double peaks) accounted for approximately 5% of the total number of peaks identified by the program.

2.2.10 Slow-Scan Cyclic Voltammetry

Data were collected in 0.1 M $NaPO_4$, pH 7.0, using a WaveNano potentiostat (Pine Instruments Company, Durham, NC). The applied waveform ran from +200 mV to -800 mV and back, at a sweep rate of 100 mV/s. This scan rate proved to be low enough to maintain steady state in all conditions. The cycle was performed twice on each electrode, with a rest

period between segments of 1 second. Data were analyzed using Aftermath software (version 1.4.7714, Pine Instruments Company) to obtain the steady state current.

2.2.11 Data Analysis and Statistics

All data presented are shown as the mean ± standard error of the mean (SEM). Unpaired *t* tests were used to determine the significance of means between two groups. Statistical and graphical analyses were carried out using GraphPad Prism 5 (GraphPad Software, Inc., La Jolla, CA).

2.3 Results

2.3.1 Etching Carbon-Fiber Microelectrodes

Previous research[25] has demonstrated that the surface of a carbon-fiber microelectrode (CFME) is etched in solution when potentials ≥ +1.3 V *vs.* Ag/AgCl are applied, and the etching rate increases with application of higher potentials. Thus, it stands to reason that a carbon-fiber disk electrode could be etched to form a recessed disk (cavity) geometry by applying a sufficient potential. In the present work, cavity electrodes were initially fabricated from T-650 carbon-fiber disk electrodes by applying a waveform in PBS with a holding potential of +2.5 V, and scanning down to +1.5 V and back up to +2.5 V at 400 V/s, repeating at 10 Hz (Figure 2.2a). Though some degree of success was achieved, this method was inconsistent in creating reproducible electrodes. When etching electrodes in solution, gases evolved from the electrode surface (observed through a microscope, data not shown), leading

to damage in the glass insulation. Furthermore, application of such high potentials in solution results in a high level of background noise inherent to the electrode, as shown in Figure 2.2. A plasma-etching technique was developed that enables reproducible fabrication of cavity microelectrodes. The electrochemical performance of these electrodes is consistent, and superior to that of carbon-fiber microdisk electrodes.

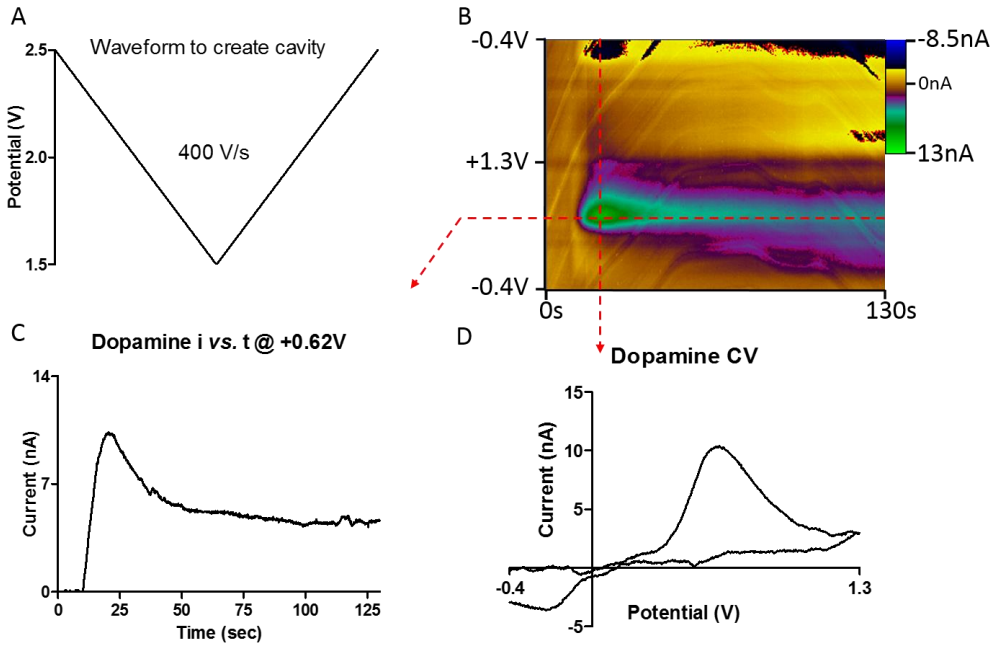

Figure 2.2. Cavity carbon-fiber electrodes can be created using FSCV. (A) A holding potential of +2.5 V was applied to the electrode while it was resting in phosphate buffered saline (PBS). The potential was then scanned down to +1.5 V at 400 V/s and back up to +2.5 V repeated at 10 Hz. After successful recession of the carbon-fiber, which was determined through periodical checks with a microscope, the applied waveform was changed to one used for dopamine detection. (B) The potential was held at -0.4 V, then scanned up to +1.3 V before scanning back to -0.4 V at 400 V/s, repeated at 10 Hz. 4 µM dopamine was then injected and the representative colorplot is shown. (C) The current *vs.* time trace extracted at peak oxidative current shows the limited diffusion of the analyte in the cavity. (D) The cyclic voltammogram is indicative of successful dopamine detection. However, a significant amount of noise is evident in the colorplot and the extracted current traces. Furthermore, only a few of the electrodes prepared in this manner were reliable enough to use.

Figure 2.3 A-C provides a simple step-by-step progression for reliable fabrication of cavity electrodes. Carbon-fiber microelectrodes are placed into the plasma etching chamber, such that a 1 cm gap is established between the carbon-fiber tip and a stainless steel electrode (Figure 1.1). A potential is applied and increased in 25 V increments at a frequency of 4 Hz, while monitoring the passage of current between the electrodes. Once the target current is reached, it is retained for a predetermined length of time (5-30 seconds, depending on experimental needs), resulting in formation of a plasma between the electrodes that etches the carbon fiber, leaving the glass insulation intact and creating a cavity (2.1C).

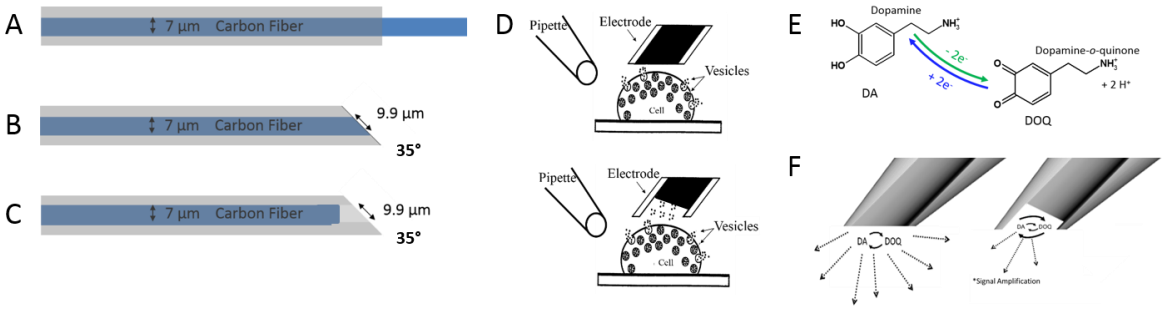

Figure 2.3. Fabrication of cavity electrodes. (A-C) Etching scheme. Cylinder electrodes are fabricated (A), sealed with epoxy, and polished to a 35º angle (B). By applying a high voltage across a 1 cm air gap, these electrodes are etched to ablate the carbon and create a cavity (C). (D) Schematic comparing cavity electrode and disk electrodes placed on a single cell, with the cavity restricting mass transport of molecules from the surface. (E) Electrochemical oxidation of dopamine to dopamine-*o*-quinone and subsequent reduction back to dopamine. (F) Restricted diffusion at the electrode surface allows for detection of the same redox pair multiple times when using FSCV (redox cycling), amplifying the signal.

2.3.2 Controlling Cavity Depth

Scanning electron micrographs are shown of a representative electrode with a 15 μm cavity (Figure 2.4A-D). Using a high voltage beam reveals the position of the carbon underneath the glass insulation, while a low voltage beam images the surface of the glass insulation. The depth of the cavity is dependent on both the target current and the duration of etching. Typically, the target current is reached at a potential of ~+6 kV. While multiple target currents were evaluated, 15 μA yielded the most controllable and reproducible results. Even though the applied potential remains constant once the target is reached, the measured current fluctuates within a few μA of the target (Figure 2.4E). The amount of time the potential is applied proportionally affects the distance the carbon fiber recessed. Integrating the measured current with respect to the etching time yields the total charge (mC) passed through the electrode. Figure 2.4F plots this charge versus the distance etched. The linear relationship (r^2 = 0.83, n = 38 electrodes) allows for precise control of cavity depth. Interestingly, other types of carbon fibers have different etch rates. Pitch-based P-55 carbon-fibers etch at a slower rate than polyacrylonitrile (PAN) based T-650 carbon-fibers (data not shown).

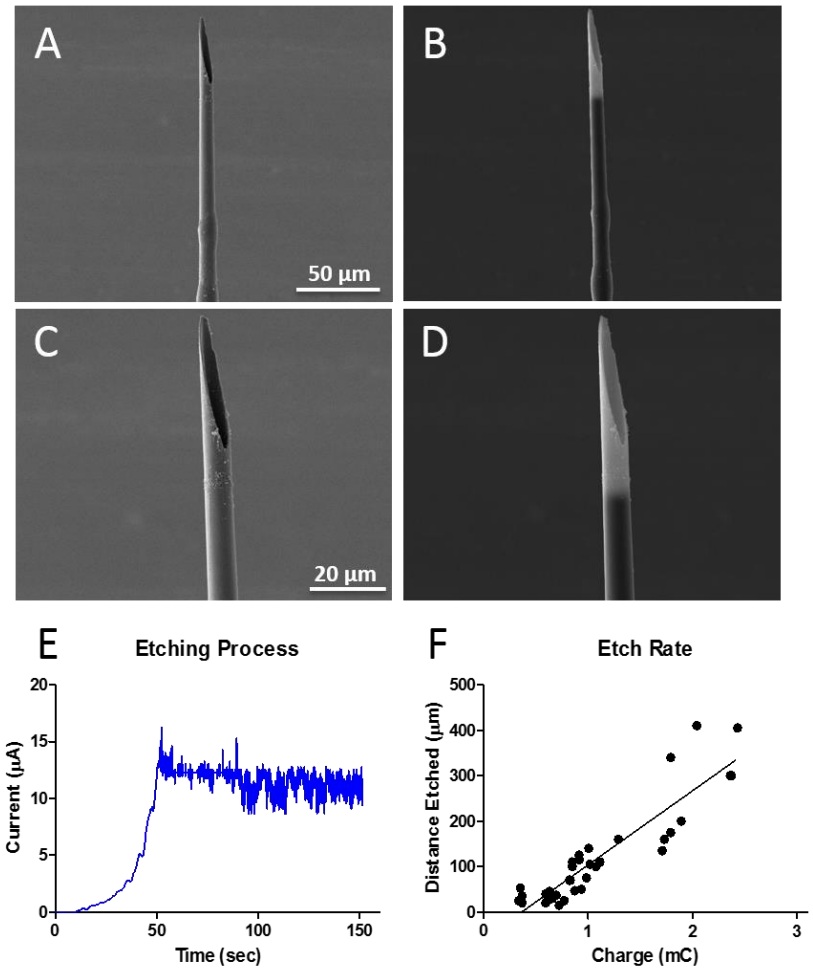

Figure 2.4. Cavity electrodes. **(**A-D) Variable pressure SEM images of a representative electrode etched to a 15 µm cavity depth. Panels A and C are collected with a 5.0 kV beam, and panels B and D with a 20.0 kV beam. (E) Representative current *vs.* time trace collected as the potential is increased and then held once the target current (15 µA) is reached. (F) The amount of charge passed through each electrode correlates linearly with the distance etched (r^2 = 0.83, n = 38)

2.3.3 Electrochemical Characterization

Broadly speaking, traditional carbon-fiber electrodes have been well characterized, especially for the detection of dopamine.[23, 45-46] Thus, the performance of the recessed carbon-

fiber electrodes was compared to carbon-fiber disk electrodes made of the same substrate, using FSCV. Compared to disk electrodes, the cavity electrodes generate greater charging current by approximately 3-fold (Figure 2.5A). However, the disk electrodes have a slightly larger geometric surface area due to their elliptical shape, when compared to the presumed circular shape of the sensing surface in the cavity CFME (Figure 2.3). In theory, charging current (i) is related to surface area by capacitance (C_d) of the electrode, which is proportional to surface area (Equation 2.2),[47] through Equation 2.1[48]:

$$i = \nu C_d(1 - e^{-\frac{t}{R_s C_d}}) \quad (2.1)$$

where R_s is solution resistance, and t is time.

$$C = \epsilon \frac{A}{d} \quad (2.2)$$

where C is capacitance, ϵ is permittivity, A is area of the plates of a capacitor, and d is distance between the plates.

While geometric surface area cannot account for the substantially increased charging current at the cavity electrode, there may be discrete changes at the surface that contribute to an increased capacitance that facilitates more efficient electron transfer at the etched sensing surface. Sensitivities are compared using calibration plots for detection of dopamine, with concentrations ranging from 0.25 μM to 2 μM (Figure 2.5B). The sensitivity inherent to the

cavity electrode (5.23 ± 0.22 nA/μM) is significantly higher than that inherent to the disk electrodes (1.86 ± 0.13 nA/μM, $p < 0.05$, $n = 11$). The ratio of the peak reductive and oxidative currents was also significantly greater ($p < 0.01$) for recessed carbon-fiber electrodes (0.65 ± 0.03, $n = 11$) when compared to disk electrodes (0.39 ± 0.04, $n = 3$), as shown in Figure 2.5C. This is due to decreased mass transport at the sensing surface, as more dopamine-*o*-quinone would efficiently diffuse away at an electrode with disk geometry before being reduced back to dopamine. The effects of this diminished mass transport are also evident in the current *vs*. time trace extracted at the peak oxidation potential (Figure 2.5D). Current returns to baseline 10 to 12 seconds after oxidation using the disk electrodes, but remains above the baseline for a longer period of time (~20 seconds) with the recessed electrodes.

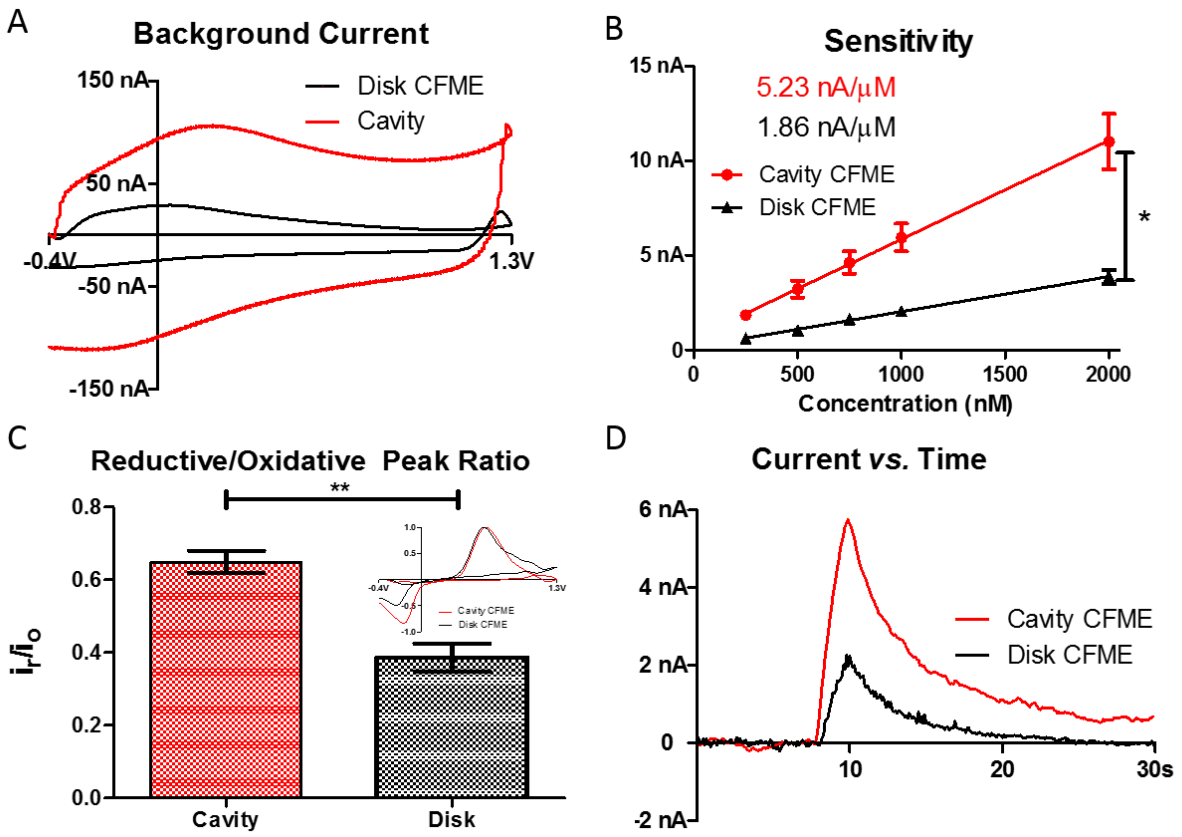

Figure 2.5. Electrochemical characterization of cavity carbon-fiber microelectrodes. (A) The background charging current is larger at cavity electrodes compared to disk electrodes. (B) Calibration plot shows that cavity electrodes are significantly more sensitive than disk electrodes (ANCOVA, $p < 0.05$, $n = 11$). (C) Bar graph showing reductive/oxidative peak ratio. Normalized representative voltammograms overlayed in the inset (Unpaired t-test, $p < 0.01$, $n = 11, 3$). (D) Current *vs*. time trace extracted at peak oxidation potential for 1 µM DA that shows decreased mass transfer within the cavity. Exponential decay time constant, Tau, is significantly higher for cavity electrodes compared to disk electrodes (data not shown, Cavity: 6.24 ± 0.30 s, n=3; Disk: 3.25 ± 0.31 s, n=3; $p < 0.01$)

Multiple methods were used to study the surface characteristics of the etched and non-etched carbon. Field emission SEM provides a way to visually inspect the physical effects of plasma etching on the surface of the fiber. To prevent the glass insulation from obscuring the

carbon in the image, an uninsulated carbon fiber was etched and imaged with SEM. As seen in Figure 2.6A and 2.6B, this method of plasma etching appears to increase the roughness of the fiber surface. This translates to an increase in the true surface area of the carbon in the cavity electrode, which could contribute to the increased sensitivity inherent to these electrodes.

Raman spectroscopy was employed to gain insight into the microstructure of the carbon fiber (Figure 2.6C, D). Spectra were collected at electrodes prior to and after plasma etching. Very broad peaks were observed in the spectra, which are indicative of a highly disordered surface.[49-51] The two peaks observed are related to the sp^2 hybridized graphitic structure and to a breaking of symmetry along the graphitic lattice, and are referred to as the D and G peaks, at approximately 1560 and 1360 cm^{-1}, respectively. More detailed discussions related to the origins of these peaks have been presented elsewhere.[52-55] The D and G peaks were fit using Lorentzian line shapes. In addition, as described by Ribeiro-Soares *et al,*[49] two Gaussian line shapes were fit at 1253 and 1520 cm^{-1} to account for the broadening of the D and G peaks. [49] [49] [49] [46] [45] [45] [49] The I_D/I_G ratio was calculated by adding the widths of the D related bands and dividing by the sum of the widths of the G related bands. An estimate for the crystallite size was made using Equation 2.3[53]:

$$L_a(nm) = (2.4\ x\ 10^{-10})\lambda_{laser}^4 \left(\frac{I_D}{I_G}\right)^{-1}, \qquad (2.3)$$

The data in Figure 2.6 suggest that the average crystallite dimension of the carbon is 8 $\pm$ 3 nm before and after etching. In order to be consistent with the calibration experiments described in Figure 2.5, the fibers were cycled with the triangular waveform in PBS prior to imaging, both before and after etching. The electrodes were carefully positioned so that spectra were collected from the etched portion of the fiber. Interestingly, despite visible changes in the surface structure evident in SEM images, no significant differences were observed by Raman imaging before and after the etching procedure ($p > 0.05$, two-tailed paired t-test, n=3). This highlights that it is likely the cycling following the etching procedure, rather than the etching itself, that affects the microstructure of the carbon. We have studied this in depth in another work (Chapter 6 of this document) and found that cycling creates a significantly more ordered and oxidized surface.

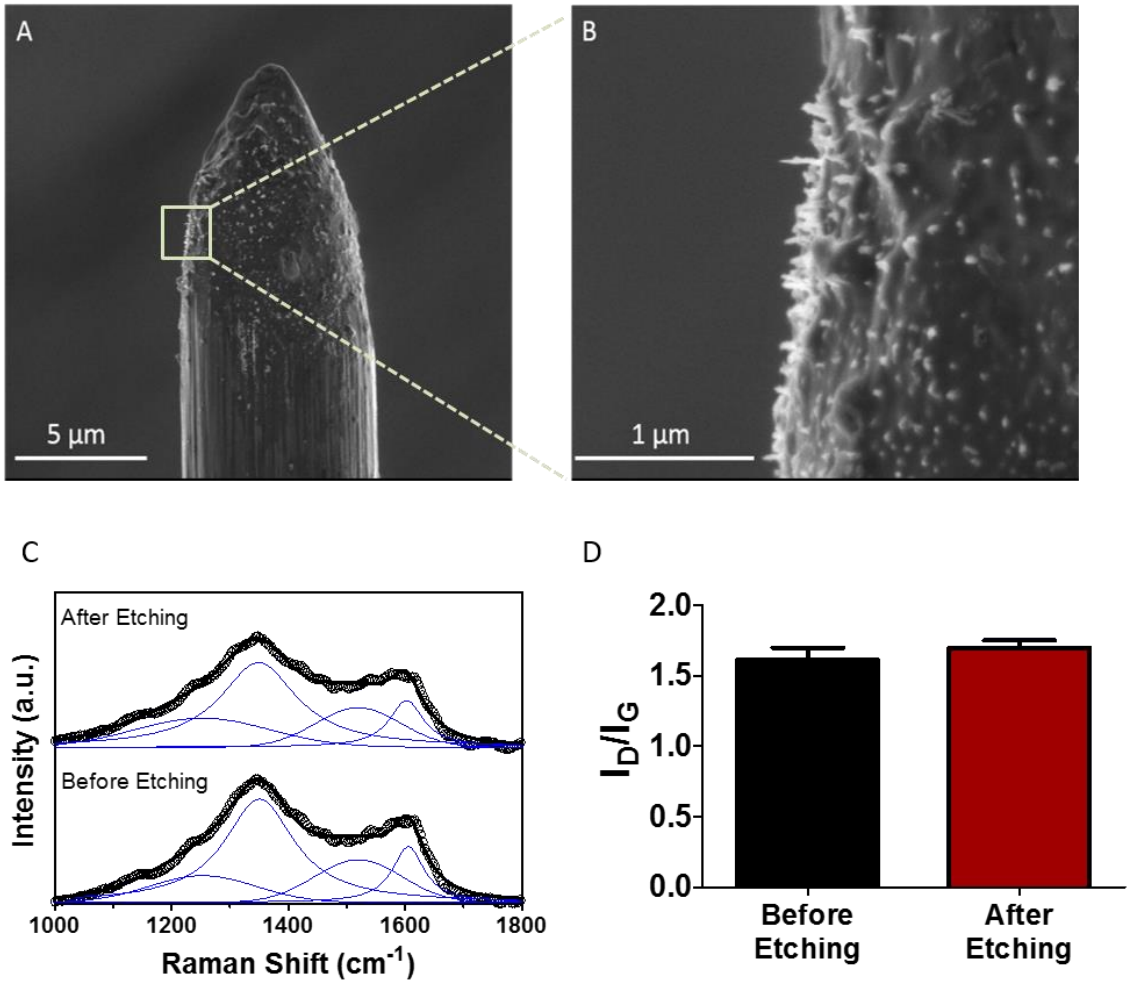

Figure 2.6. Field Emissions SEM and Raman imaging on plasma-etched electrodes. (A) Plasma-etched electrode with tip exposed for imaging. The roughened tip where the etching is taking place visually contrasts with the smooth side of the fiber. (B) 100,000x magnification of the etched tip. (C) Representative spectra (black) and fitted peaks (blue) of a polished and electrochemically conditioned carbon fiber electrode before and after the plasma etching procedure. (D) The ratio of peak amplitudes (I_D/I_G) is unchanged by the etching process ($p>0.05$, two-tailed paired t-test, n=3).

Another possible cause for the increased sensitivity of the cavity electrodes is an increase in surface area at the microscopic level. Peak current in cyclic voltammetry is

described by the Randles-Sevcik equation (Equation 2.4), whereby peak current is proportional to sensing area of the electrode.

$$i_p = 0.4463nFAC\left(\frac{nF\nu D}{RT}\right)^{1/2} \qquad (2.4)$$

where i_p is peak current, n is number of electrons transferred, F is the Faraday constant, A is sensing area of the electrode, C is concentration, ν is scan rate, D is diffusion coefficient, R is the gas constant, and T is temperature.

Assuming a circular geometry, a 7 μm carbon fiber should generate a geometric surface area of 38.5 μm^2, while an electrode created from the same fiber beveled at 35º should have an elliptical surface area of 67.1 μm^2. Slow-scan cyclic voltammetry (100 mV/s) was utilized to estimate the area of the active sensing surface of cavity and standard micro-disk electrodes. Steady-state cyclic voltammograms were collected for 1 mM $Ru(NH_3)_6^{3+}$. Through the steady state current, the geometric area of the electrode was found using the equation for steady state current at a microdisk electrode[48]:

$$i=4nFDCr \qquad (2.5)$$

where i is the measured current, n is the number of electrons transferred, F is the Faraday constant, D is the diffusion coefficient, C is the concentration of the analyte species, and r is the radius of the electrode. The diffusion coefficient for $Ru(NH_3)_6Cl_3$ used in calculations is

5.48×10^{-6} cm^2/s.[56] Once the radius of the electrode was found using Equation 2.5, the surface area was calculated as the area of a circle.

Surface areas for disk electrodes, as well as cavity electrodes with a recessed length of 5, 15 and 20 μm were calculated and are shown in Figure 2.7. The experimentally determined surface area is likely greater than the geometric surface area due to the increased surface roughness. Notably, there is no significant difference in the measured surface area between a disk electrode and cavity electrode, despite the fact that the cavity electrode should have a surface area only 70% of that of a disk. Determining surface area by the steady-state voltammetric limiting current relies on the assumption of a particular geometry, in this case a microdisk. When the actual geometry of the electrode deviates from the geometry assumed by Equation 2.5, this technique is not valid.[57] The disk electrodes examined herein are beveled at a 35º angle, while the cavity electrodes have a glass shroud around the sensing surface, preventing visualization of the true geometry. Thus, increased surface area remains a possible contributor to the heightened sensitivity of the cavity electrodes over disk electrodes. Additionally, it is well-established that plasma-etching of carbon results in a higher oxygen-functionalization on the surface,[58-62] and this is likely a contributor to the heightened sensitivity of these electrodes.[63] This is further supported by Chapter 6 of this work, which shows that a more oxidized surface results in enhanced sensitivity to dopamine.

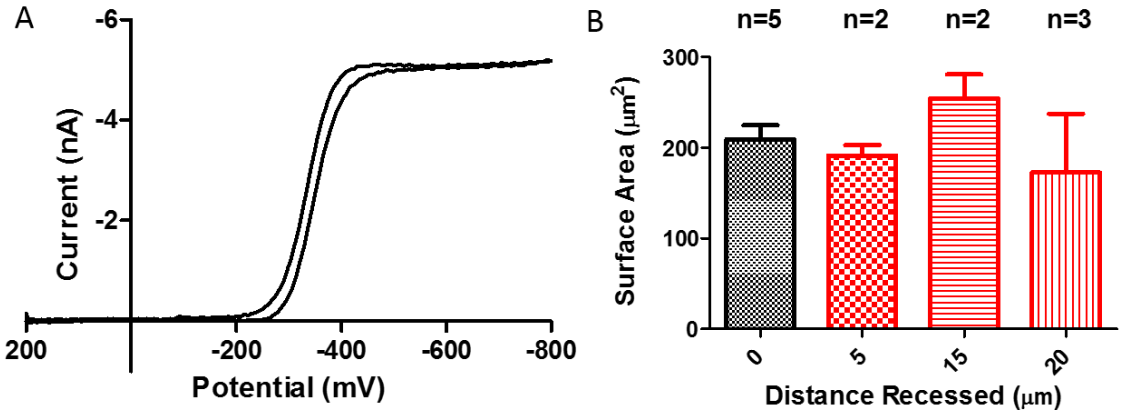

Figure 2.7. Voltammetric estimation of surface area. (A) Representative voltammogram for $Ru(NH_3)_6^{3+}$ collected on an etched cavity electrode. (B) Surface area estimated using limiting current generated in the voltammetric detection of $Ru(NH_3)_6^{3+}$ for unetched disk electrode (black) and cavity electrodes (red) recessed 5, 15, and 20 μm. No significant difference was found (1-way ANOVA, $p > 0.05$, n = 5, 2, 2, and 3, respectively).

2.3.4 Monitoring Neurotransmitter Release in Live Tissue

To assess performance in tissue, a cavity electrode (~10 μm recessed) was placed into an acute rat brain slice encompassing the striatum, a region rich in dopaminergic terminals. A bipolar stimulating electrode was placed in the vicinity of the working electrode and five biphasic electrical pulses (500 μA applied at 60 Hz) were used to evoke dopamine release. A representative colorplot is shown in Figure 2.8A, in which time is plotted on the x-axis, the applied potential on the y-axis, and the change in current from the background is depicted in false color. The time of electrical stimulation is indicated by the red arrow, and the release of approximately 2 μM dopamine was detected with a pre-calibrated electrode. The inset shows a voltammogram extracted at the vertical white line (white trace), overlayed with a normalized voltammogram collected in the same preparation using a cylindrical carbon-fiber electrode

(black trace), typically used for this type of experiment. The reductive/oxidative peak ratio is greated at the cavity electrode, consistent with voltammograms collected *in vitro*. Figure 2.8B shows the normalized current *vs.* time trace extracted at the potential of dopamine oxidation, indicated by the horizontal white line in panel A. Much like the *in vitro* results, the current does not return to baseline after peak oxidation current is reached, demonstrating reduced mass transport of the evoked dopamine molecules in the cavity, relative to the trace collected using an unshielded cylindrical carbon-fiber electrode (also shown in Figure 2.8B). Importantly, these results show that the recessed electrodes can be used for studies in live brain tissue.

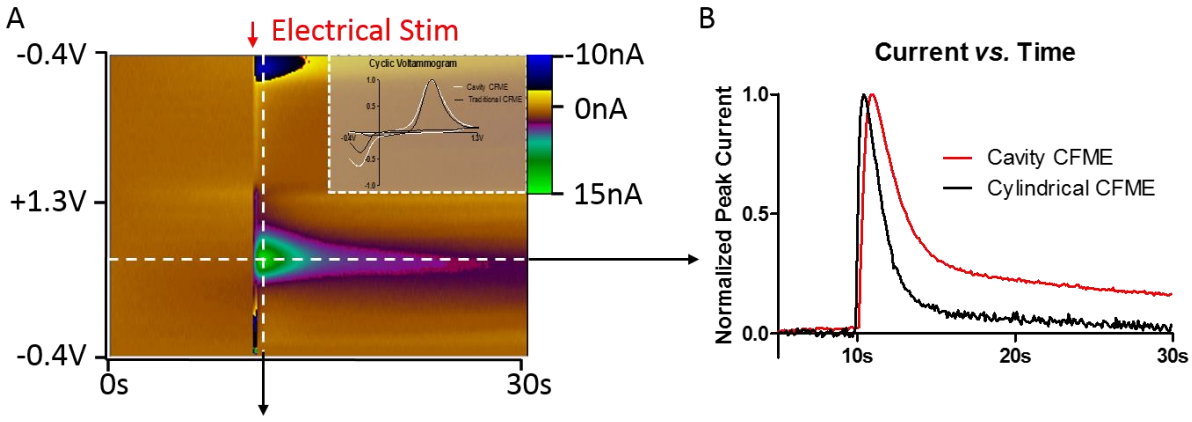

Figure 2.8. Diminished mass transport away from the electrode in live tissue. (A) A representative colorplot showing electrically stimulated (red arrow) dopamine release in striatal region of an acute brain slice, collected using a cavity electrode. Inset: Normalized voltammograms comparing the data extracted at vertical white line to data collected on a cylindrical CFME in the same preparation. (B) Normalized current *vs.* time traces showing the different response times of electrode geometries in this preparation. The response time is reflected in the rising portion of the current *vs.* time trace, showing slowed mass transport to the cavity electrode compared to a cylinder electrode, as well as reduced mass transport away from the electrode surface.

2.3.5 Monitoring Individual Exocytotic Events at Single Cells

Finally, cavity electrodes were utilized for amperometry experiments at single bovine chromaffin cells in culture, detecting individual exocytotic release events. These cells contain dense core vesicles that contain catecholamines, and as such they are a widely used model for studying neurotransmission. Exocytosis was stimulated by pressure-ejecting 100 mM K^+ solution onto the cell, and individual vesicular exocytotic events were monitored by holding the electrode at +0.8 V. Representative traces collected at both the conventional disk electrode and the cavity electrode are shown in Figure 2.9, panels A and C. Spikes on the traces correspond to individual exocytotic release events, as the contents released from each vesicle are oxidized at the electrode surface.

The specific geometry of the cavity electrode could be exerting an effect on the physiology of the cell itself, as the cavity could theoretically trap protons and alter the pH. Alternatively, the glass insulation could exert substantial pressure on the cell itself. To combat this, particular care was taken to ensure that the electrode (both cavity and disk) was lowered just to the point of deforming the cell membrane, and then raised back up slightly such that it was not touching the membrane. Additionally, traces were also collected with both the cavity and the disk electrodes raised 5 μm above the cell membrane, to completely eliminate the possibility of a physiological change in the membrane surface due to the immediate proximity of the electrode (panels B and D). On the left side of each panel, a representative trace is shown for each experimental condition. The shape of amperometric spikes has been analyzed in depth by researchers such as Christian Amatore,[64] with the hypothesis that the rising phase of the spike is largely related to opening and dilation of the fusion pore, while the falling phase

is mainly governed by diffusion of vesicular contents out from the tightly bound core of the vesicles. Thus, the shape of the rising and falling phases of the spikes can convey valuable information related to the biophysical properties of exocytotic release. We compared spike shapes for each condition, to test if the electrode geometry was altering biophysical properties of the membrane and the vesicular release mechanism. The middle of each panel shows averaged spikes for each file from which the representative traces were extracted (dotted black line), overlaid with four individual spikes selected from each trace (indicated by asterisks above the spikes). To directly compare the spike shape, each spike including the averaged spike was normalized to its maximum amplitude, as well as its half-width (width at half of maximum amplitude). These are shown on the right side of each panel, and overlay well with one another. Averaged spikes from each condition are compared in panel E, with raw spikes shown on the left and normalized spikes on the right. The overall shape of the amperometric spikes remains consistent regardless of electrode geometry or vicinity to the cell, indicating similar physiological conditions. These data are consistent with a prior report by Schroeder and Wightman, who modeled the diffusion of molecules to the electrode as it was lifted from the cell, and also observed that the spike shape remained consistent regardless of electrode height above the cell.[65]

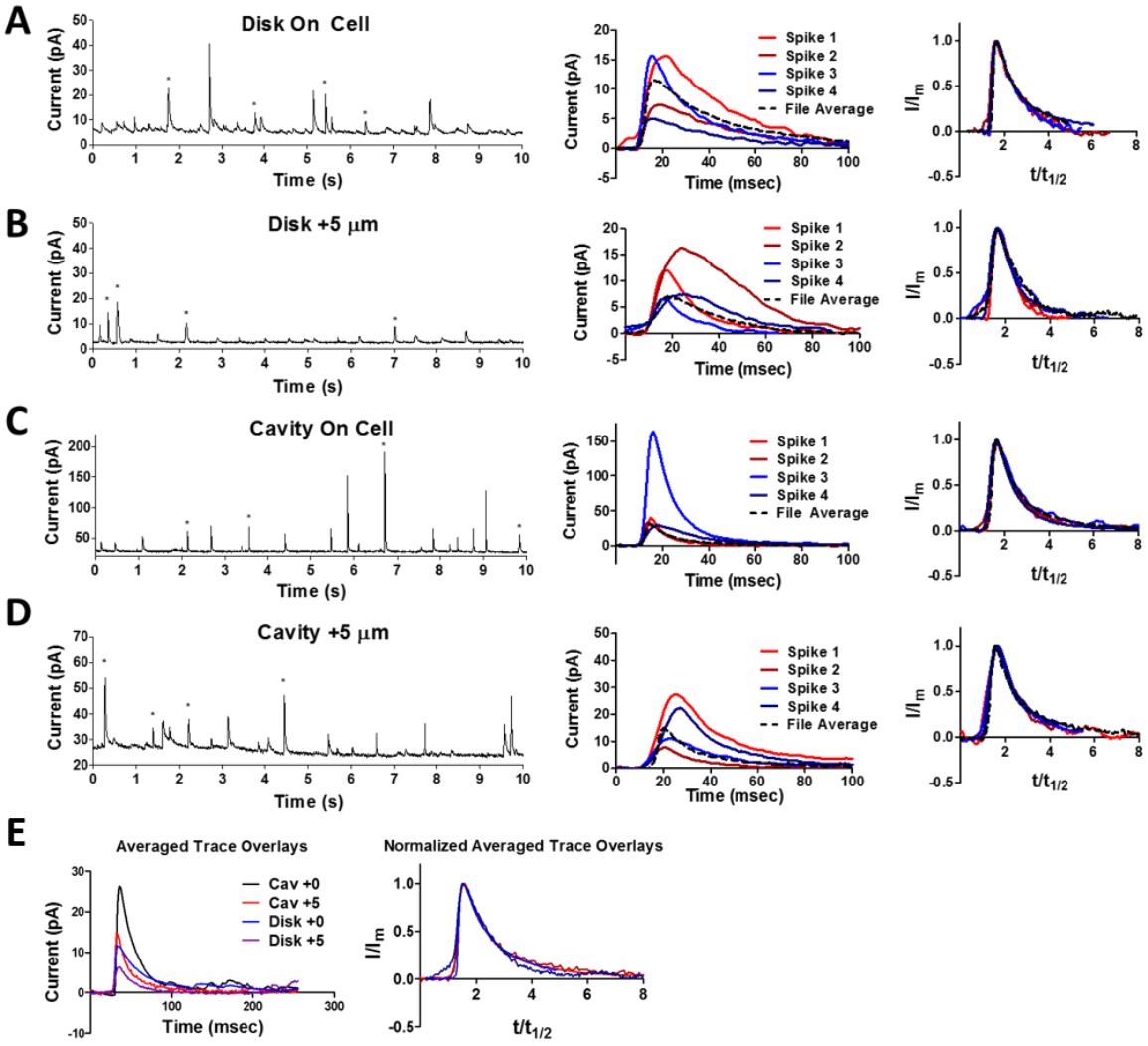

Figure 2.9. Amperometric recordings of individual exocytotic events at single bovine chromaffin cells. Exocytosis is stimulated by pressure ejection of 100 mM K+, and recorded at disk (A, B) electrodes and cavity (C, D) electrodes, with the electrodes located immediately above the cell (A, C) as well as 5 µm above the cell (B, D). Representative traces are shown on the left side of each panel. In the middle is an overlay of four selected spikes from each trace (asterisks), as well as the average of all spikes for each experiment. Right: each of the spikes is normalized by dividing the y-axis by its maximum amplitude, and the x-axis by its half-width (peak width at half maximum height). (E) Averaged spikes for each experimental condition overlaid (left) and normalized then overlaid (right).

After establishing that both the cavity and the disk electrodes are detecting exocytotic release under similar physiological conditions, the exocytotic events were investigated in further detail. The number of molecules detected can be calculated using Faraday's law, Q = nNF, where Q is the charge measured under the peak, n is number of electrons transferred per oxidation event, N is number of molecules, and F is Faraday's constant. Average spike area, spike amplitude, and half-width were calculated for the events recorded at disk and cavity electrodes, and the data are plotted as histograms.

When compared to the disk electrodes, cavity electrodes recorded exocytosis events with a larger area (Figure 2.10A) and higher amplitude (2.10B), and wider half-width (2.10C). Raising the cavity electrode 5 μm above the cell resulted in a 28.3 ± 8.3% decrease in peak area, a 43.6 ± 8.2% decrease in amplitude, and no change in half-width. Raising the disk electrode 5 μm resulted in a 35.2 ± 6.5% decrease in area, a 15.8 ± 7.4% decrease in amplitude, and no significant change in half-width. Our results are in accord with those modeled by Schroeder and Wightman[65] for disk electrodes, as they showed the lifting the electrode 5 μm should result in detection of 36% fewer molecules.

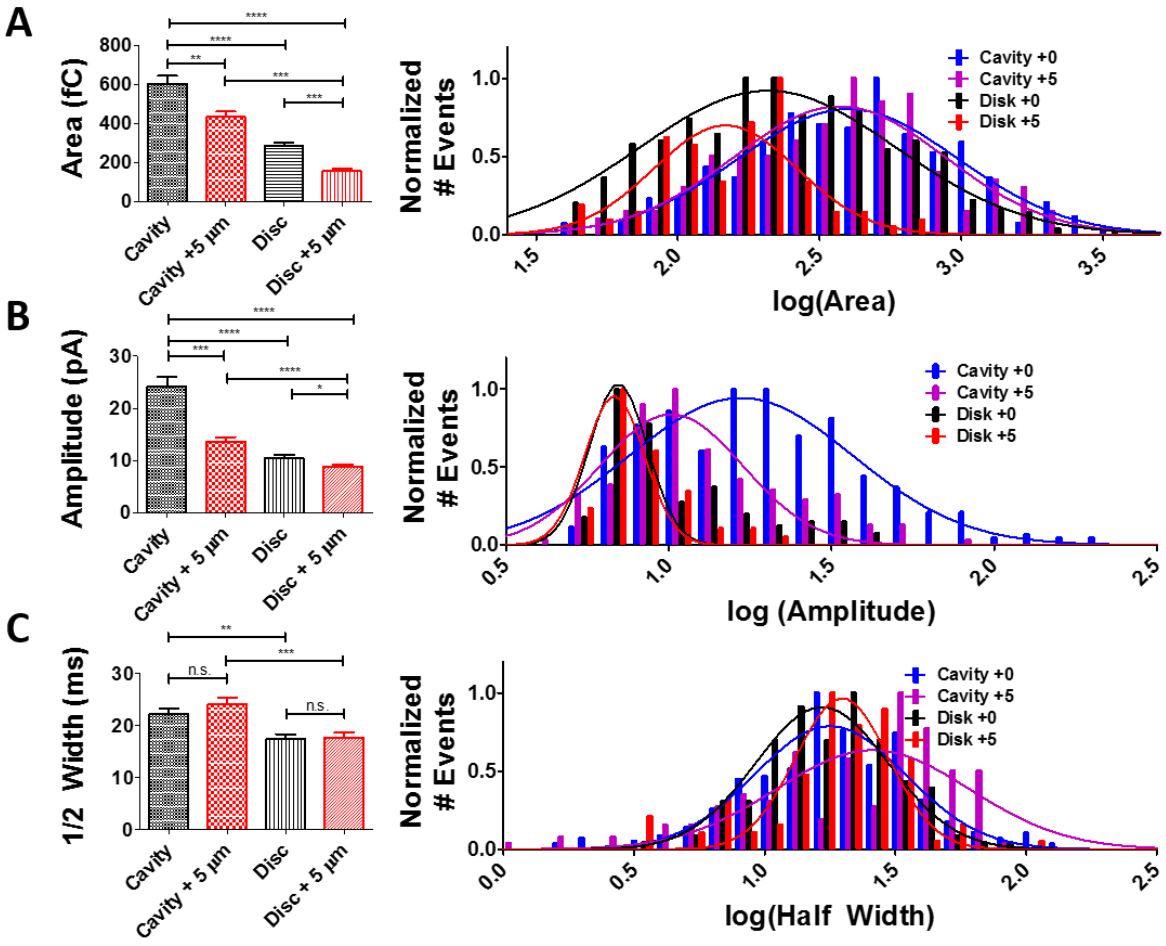

Figure 2.10. Quantitative analysis of individual spikes measured at single cells. (A) Spikes measured at cavity electrodes have 111 ± 15% larger average area (604 ± 41 fC) compared to spikes measured at disk electrodes (287 ± 15 fC). When lifted 5 µm above the cell, there was a 28.3 ± 8.3% decrease in spike area for cavity electrodes (433 ± 29 fC), and a 35.2 ± 6.5% decrease for a disk electrode (186 ± 11 fC). Log transforms of spike area are shown on the right, fit with Gaussian regressions. (B) Peak amplitude (pA) for spikes collected in each experimental condition. Cavity electrodes detect spikes with 133 ± 18% larger amplitude (24.2 ± 1.8 pA) than those measured at disk electrodes (10.43 ± 0.64 pA). When raised 5 µm, cavity electrodes recorded a 43.6 ± 8.2% decrease in amplitude (13.67 ± 0.85 pA), while raising the disk electrodes resulted in a 15.8 ± 7.4% decrease (8.78 ± 0.43 pA). Log transforms of spike amplitude are shown on the right, fit with Gaussian regressions. (C) Cavity electrodes detected spikes with a 28.4± 7.6% wider half-width (22.35 ± 0.90 msec) than disk electrodes (17.40 ± 0.96 msec). Raising the cavity electrode resulted in no change in half-width (24.09 ± 1.35 msec), as neither did raising the disk electrode (17.77 ± 0.92 msec). Log transforms of spike half-width are shown on the right, fit with Gaussian regressions. *$p < 0.05$; ** $p < 0.01$; ***$p < 0.005$; ****$p < 0.001$

Given the surprising nature of our findings, we sought to propose a reason why disk electrodes were not detecting as many molecules per event as cavity electrodes. Presumably, based on the traditional understanding of these types of experiments, all of the molecules that are released and encounter the electrode should be detected. We hypothesized two reasons why this may not be the case, and why the cavity electrodes seemingly detect more of the molecules being released than the disk electrodes. One likely reason for this result is that some molecules released by the cell simply diffuse out from under the disk electrode and go undetected, while the cavity electrode confines them and detects the vesicular contents more completely. Another possible reason is that the norepinephrine transporter (NET) may be binding and transporting some of the molecules immediately after release, prior to detection. The function of the NET, expressed on the chromaffin cell membrane,[66] is to recycle neurotransmitter content released into the extracellular space by transporting it across the membrane back into the cell. As uptake is an incredibly fast process, it is possible that some neurotransmitters are subject to this process, or at least bind to NET on the membrane, prior to detection at the electrode surface. This would serve to decrease the measured quantal size. To test this hypothesis, cells were bathed in a cell buffer containing nomifensine, a potent NET blocker for 90 minutes prior to stimulation. A separate group of cells was incubated with cell buffer sans nomifensine for 90 minutes. Exocytosis was stimulated with 100 mM K+ as with the previous experiments, and recorded at both cavity and disk electrodes. The analysis of spikes recorded in all four experiments is shown in Figure 2.11. Interestingly, in the presence of nomifensine, disk electrodes recorded amperometric spikes with a larger area compared to the control, while cavity electrodes did not record statistically larger events. Analysis of spike amplitude

followed the same trend, with disk electrodes measuring larger amplitudes upon application of nomifensine, where cavity electrodes measured no change in amplitude. Both cavity and disk electrodes recorded wider half-widths upon application of nomifensine. As half-width is dictated both by rise-time and decay time, these two parameters were also analyzed, with rise-time defined as the time taken for the spike to rise from 10% to 90% of maximum amplitude, and decay time defined as time taken to decay from 90% to 10% of maximum amplitude. Spikes measured at cavity electrodes had no change in rise time, and an increase in decay time with nomifensine compared to control. Spikes measured at disk electrodes had longer rise times and decay times with application of nomifensine.

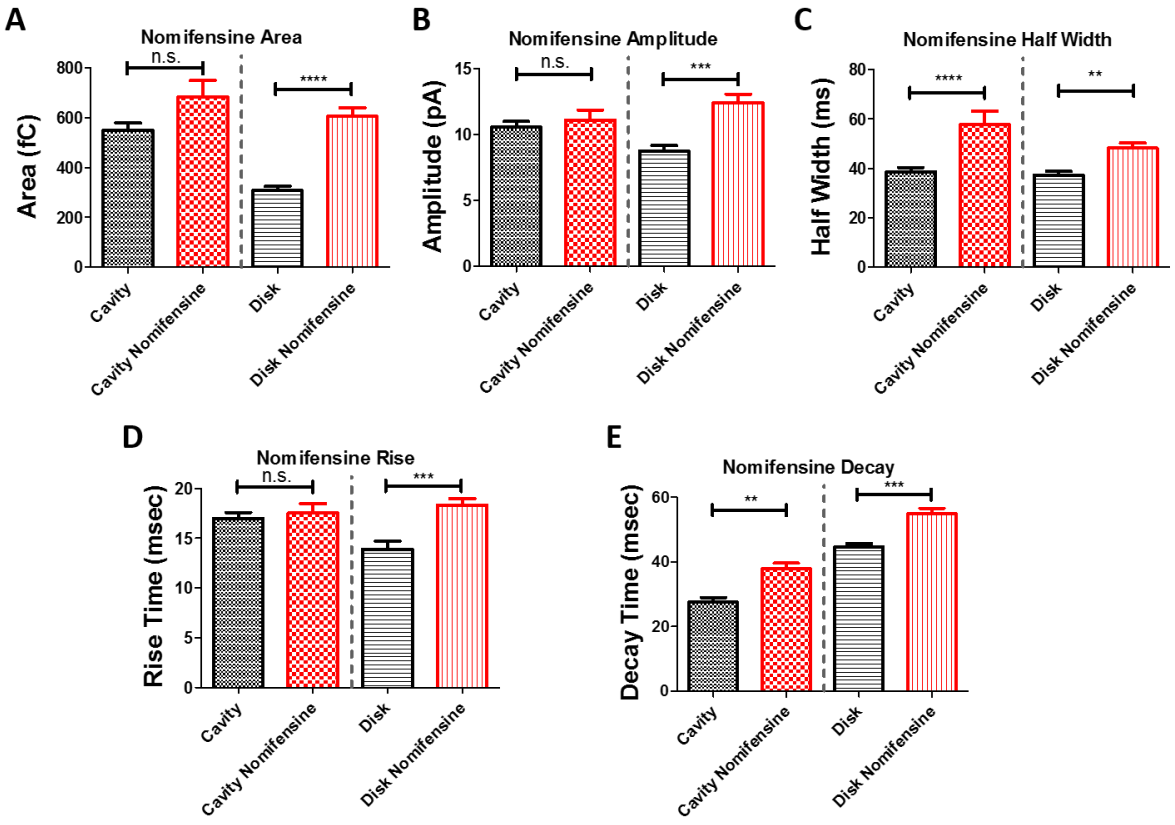

Figure 2.11. The norepinephrine transporter plays a fundamental role in the amperometric detection of vesicular fusion events at microelectrodes. (A) Addition of nomifensine to the cell bath did not change spike area recorded with cavity electrodes (649 ± 59 fC) compared to non-nomifensine control (548 ± 30 fC). By contrast, nomifensine increased spike area at disk electrodes (Non-nomifensine: 307 ± 18 fC; Nomifensine: 604 ± 36 fC) (B) Nomifensine did not affect spike amplitude for spikes measured at cavity electrodes (Non-nomifensine: 10.56 ± 0.46 pA; Nomifensine: 11.12 ± 0.74 pA), but did increase the amplitude of spikes measured at disk electrodes (Non-nomifensine: 8.74 ± 0.44 pA; Nomifensine: 12.45 ± 0.63 pA). (C) Nomifensine increased spike half-width at both cavity (Non-nomifensine: 38.0 ± 1.7 msec; Nomifensine: 54.1 ± 4.9 msec) and disk (Non-nomifensine: 37.3 ± 1.6 msec; Nomifensine: 47.3 ± 1.8) electrodes. (D) Nomifensine did not affect rise time (10% maximum amplitude to 90% maximum amplitude) for events recorded at cavity electrodes (Non-nomifensine: 17.00 ± 0.58 msec; Nomifensine: 17.52 ± 0.98 msec), but did increase rise time for events recorded at disk electrodes (Non-nomifensine: 13.91 ± 0.80 msec; Nomifensine: 18.32 ± 0.66 msec). (E) Nomifensine increased decay times (90% maximum amplitude to 10% maximum amplitude) for events recorded at both cavity (Non-nomifensine: 27.5 ± 1.4 msec; Nomifensine: 37.8 ± 1.7 msec) and disk (Non-nomifensine: 44.6 ± 1.0 msec; Nomifensine: 54.8 ± 1.7) electrodes. *$p < 0.05$; ** $p < 0.01$; ***$p < 0.005$; ****$p < 0.001$

2.4. Discussion

One of the likely reasons that cavity electrodes are more sensitive to dopamine than disk electrodes, when using FSCV, is that they confine the analytes near the electrode surface, resulting in redox cycling. Thus, the same molecule is cycled between dopamine and dopamine-*o*-quinone, and detected multiple times, thus amplifying the signal. When using amperometry, redox cycling does not occur as the potential is held at a constant oxidizing potential. According to Faraday's law, the larger average spike area for the cavity electrodes must be the result of detecting more molecules per individual event. We propose that when monitoring with a disk electrode, some of the molecules released in each event (particularly larger events) can go undetected for one of two reasons: diffusional losses or enhanced reuptake. The cavity electrode has at least two properties which allow it to detect the contents of each fusion event more completely than the disk electrode. One characteristic is the actual geometry of a cavity electrode, which affects both the concentration of released neurotransmitters in the vicinity of the electrode surface, as well as mass transport. This is illustrated in Figure 2.12. The concentration measured at a disk electrode for a single fusion event has been reported to be 40 μM,[67] which creates a large concentration gradient between the artificial synapse (~ 200 nm[68]) and the bath solution. The cavity has a much larger volume into which vesicular content can be released. A cavity electrode recessed 6 μm has a volume of 0.231 pL, which adds to the volume in the artificial synapse to give a total volume of 0.244 pL into which the contents of a vesicle can be released. The 40 μM concentration measured in the space between the cell and a disk electrode would effectively become 4.4 μM for the same number of molecules released into the space between the cavity sensing surface and the cell

membrane. This results in a substantially smaller concentration gradient, which relates to decreased diffusional flux out from under the electrode. Also, the glass insulation serves as a shroud to slow diffusional losses, which should result in more complete oxidation of the molecules being released from the cell.

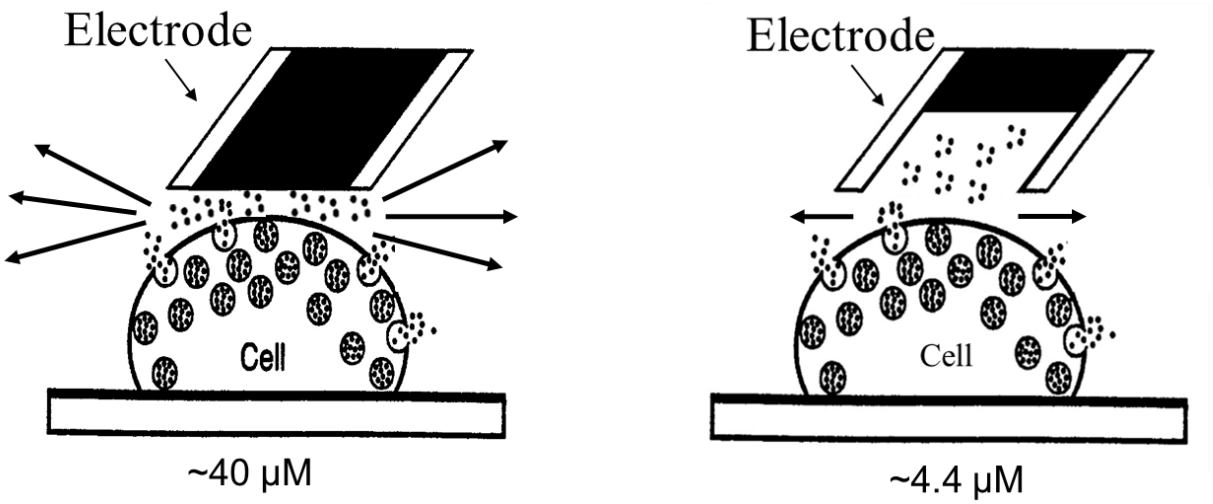

Figure 2.12. Schematic showing amperometric detection of exocytotic events at both a disk (left) and a cavity (right) electrode. There is less volume between a disk electrode and the cell, thus a single exocytotic event can result in concentrations as high as 40 μM. The cavity, on the other hand, has a larger volume for the same number of molecules to be released into, resulting in a 4.4 μM concentration for the same number of molecules. This results in a smaller diffusion gradient.

The other consideration to keep in mind is the potential role that microscopic surface area may play in governing the electrochemical detection of neurotransmitters. As demonstrated by the voltammetric characterization, cavity electrodes are more sensitive to dopamine, which suggests an increased surface area. This results in more efficient oxidation

of molecules when the concentrations are sufficiently high to saturate the surface. To test the adsorption properties of the cavity and disk electrodes, a calibration curve was generated with high concentrations of dopamine outside the linear range (Figure 2.13). The concentration at a disk microelectrode surface during a fusion event can reach 40 μM,[67] which is well outside the linear calibration range ranging from 0.25 μM to 5 μM, suggesting partial surface saturation. This linear range is consistent with the literature,[69] and with the data shown in Figure 3.3. When the surface saturates with molecules, some of the vesicular contents may deflect off of the electrode without being oxidized and detected. Molecules are likely to diffuse out from under the electrode, given the large concentration gradient between the artificial synapse created by the disk electrode (40 μM), and the bath solution. The cavity electrode benefits are twofold here: the proposed increase in microscopic surface area shifts the saturation point to a higher concentration, resulting in more efficient oxidation. Furthermore, the volume added by the cavity effectively lowers the concentration to ~4.5 μM for the same number of molecules released, which heightens the improved ability for the cavity electrode to efficiently oxidize more of the molecules being released.

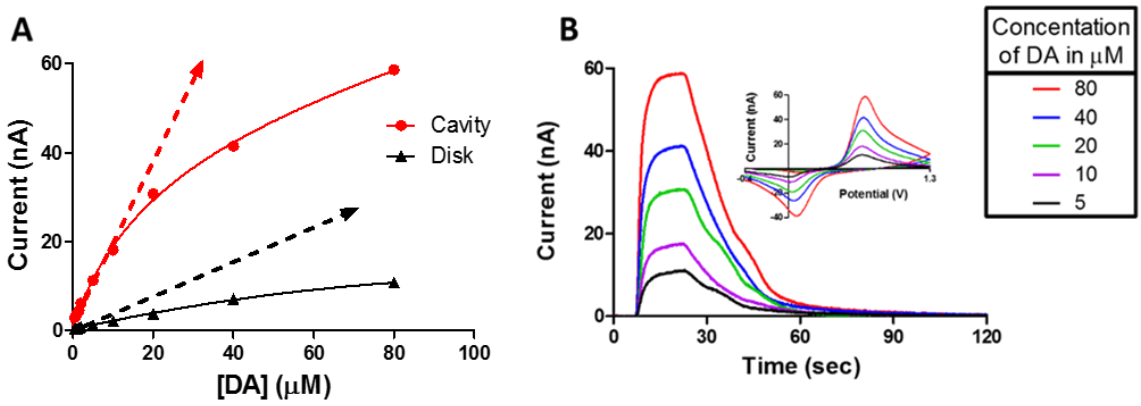

Figure 2.13. Calibration curve for dopamine at a cavity and disk ultramicroelectrode. The electrodes were calibrated to concentrations of dopamine ranging from 0.25 μM to 80 μM. (A) Calibration curves depart from linearity at ~5 μM, indicative of partial surface saturation. (B) Representative current *vs*. time traces and voltammograms (inset) for the higher concentrations measured at the cavity electrode.

Together, these two proposed advantages to the cavity electrodes result in more efficient oxidation of the molecules being released, as well as confined mass transport and a decreased concentration gradient to effectively lengthen the amount of time that molecules are in the vicinity of the electrode for detection.

2.5 Conclusions

Recessed carbon-fiber microelectrodes were successfully and reproducibly fabricated by a plasma-etching procedure developed in-house. This approach allows standard carbon fiber microelectrodes to be made into cavity electrodes that are reliable and adaptable for use with FSCV and amperometry in various live-tissue preparations. The cavity electrodes are more

sensitive to dopamine when used with FSCV, and perform well in the brain slice preparation. Additionally, when used with amperometry at single cells, cavity electrodes detect more molecules per release event than traditional disk electrodes. Raman spectroscopy reveals that the character of the microcrystalline carbon domains at the electrode surface are altered by electrochemical conditioning, but not significantly altered by the plasma-etching process. Scanning electron microscopy demonstrates a roughened surface at the plasma-etched electrodes, which likely increases the sensing surface area. Voltammetric data acquisition gains the added benefit of redox cycling resulting in signal amplification, evident by the increased reductive/oxidative peak ratio for the cavity electrodes over disk electrodes. These electrodes have the potential to reveal new and important insights into cellular exocytosis, since they may detect individual exocytosis events more completely than conventional disk electrodes. In addition, these electrodes offer a more accurate estimation of the quantal size. An accurate estimation of quantal size is of the utmost importance with current research looking into fusion pore dynamics, and whether or not exocytosis results in full release of a vesicle's contents. These cavity electrodes combine the strengths of cylinder electrodes and disk electrodes for use with FSCV in the brain, offering higher sensitivity than disk electrodes, with better spatial resolution than cylinder electrodes. The improved spatial resolution can prove beneficial for study of neurochemical release in discrete brain regions, where the 100 μm cylinder electrodes can span large terminal fields. These findings present a major step forward in creating more sensitive electrodes with a straight-forward plasma-etching strategy, outperforming traditional carbon-fiber microelectrodes in both amperometry and FSCV experiments.

2.6 Acknowledgements

We thank the Chemistry Department (North Carolina State University) for funding this work, and Chuck Mooney (Analytical Instrumentation Facility, North Carolina State University) for assistance with imaging. This material is based upon work supported by the National Science Foundation Graduate Research Fellowship under Grant No. (DGE-1252376).

2.7 References

1. Ponchon, J. L.; Cespuglio, R.; Gonon, F.; Jouvet, M.; Pujol, J. F., Normal pulse polarography with carbon fiber electrodes for in vitro and in vivo determination of catecholamines. *Anal. Chem.* **1979,** *51* (9), 1483-6.

2. Leszczyszyn, D. J.; Jankowski, J. A.; Viveros, O. H.; Diliberto, E. J., Jr.; Near, J. A.; Wightman, R. M., Nicotinic receptor-mediated catecholamine secretion from individual chromaffin cells. Chemical evidence for exocytosis. *J. Biol. Chem.* **1990,** *265* (25), 14736-7.

3. Wightman, R. M.; Jankowski, J. A.; Kennedy, R. T.; Kawagoe, K. T.; Schroeder, T. J.; Leszczyszyn, D. J.; Near, J. A.; Diliberto, E. J., Jr.; Viveros, O. H., Temporally resolved catecholamine spikes correspond to single vesicle release from individual chromaffin cells. *Proc Natl Acad Sci U S A* **1991,** *88* (23), 10754-8.

4. Omiatek, D. M.; Cans, A. S.; Heien, M. L.; Ewing, A. G., Analytical approaches to investigate transmitter content and release from single secretory vesicles. *Anal Bioanal Chem* **2010,** *397* (8), 3269-79.

5. Markov, D.; Mosharov, E. V.; Setlik, W.; Gershon, M. D.; Sulzer, D., Secretory vesicle rebound hyperacidification and increased quantal size resulting from prolonged methamphetamine exposure. *J. Neurochem.* **2008,** *107* (6), 1709-21.

6. Zhang, B.; Adams, K. L.; Luber, S. J.; Eves, D. J.; Heien, M. L.; Ewing, A. G., Spatially and temporally resolved single-cell exocytosis utilizing individually addressable carbon microelectrode arrays. *Anal. Chem.* **2008,** *80* (5), 1394-400.

7. Wang, J.; Ewing, A. G., Simultaneous study of subcellular exocytosis with individually addressable multiple microelectrodes. *Analyst* **2014,** *139* (13), 3290-5.

8. Han, X.; Wang, C. T.; Bai, J.; Chapman, E. R.; Jackson, M. B., Transmembrane segments of syntaxin line the fusion pore of Ca2+-triggered exocytosis. *Science* **2004,** *304* (5668), 289-92.

9. Sombers, L. A.; Hanchar, H. J.; Colliver, T. L.; Wittenberg, N.; Cans, A.; Arbault, S.; Amatore, C.; Ewing, A. G., The effects of vesicular volume on secretion through the fusion pore in exocytotic release from PC12 cells. *J. Neurosci.* **2004,** *24* (2), 303-9.

10. Dong, Y.; Ning, G.; Ewing, A. G.; Heien, M. L., Pituitary adenylate cyclase activating polypeptide modulates catecholamine storage and exocytosis in PC12 cells. *PLoS One* **2014,** *9* (3), e91132.

11. Mellander, L. J.; Trouillon, R.; Svensson, M. I.; Ewing, A. G., Amperometric post spike feet reveal most exocytosis is via extended kiss-and-run fusion. *Sci Rep* **2012,** *2*, 907.

12. Hafez, I.; Kisler, K.; Berberian, K.; Dernick, G.; Valero, V.; Yong, M. G.; Craighead, H. G.; Lindau, M., Electrochemical imaging of fusion pore openings by electrochemical detector arrays. *Proc Natl Acad Sci U S A* **2005,** *102* (39), 13879-84.

13. Li, X.; Majdi, S.; Dunevall, J.; Fathali, H.; Ewing, A. G., Quantitative measurement of transmitters in individual vesicles in the cytoplasm of single cells with nanotip electrodes. *Angew. Chem. Int. Ed. Engl.* **2015,** *54* (41), 11978-82.

14. Dayton, M. A.; Wightman, R. M., Carbon-Fiber Microelectrodes as Invivo Voltammetric Probes of Endogenous Chemical Transmitter Concentration. *Clinical Research* **1980,** *28* (4), A798-A798.

15. Armstrongjames, M.; Millar, J., Carbon-Fiber Micro-Electrodes. *J. Neurosci. Meth.* **1979,** *1* (3), 279-287.

16. Cameron, C. M.; Wightman, R. M.; Carelli, R. M., One month of cocaine abstinence potentiates rapid dopamine signaling in the nucleus accumbens core. *Neuropharmacology* **2016,** *111*, 223-230.

17. Howe, M. W.; Tierney, P. L.; Sandberg, S. G.; Phillips, P. E.; Graybiel, A. M., Prolonged dopamine signalling in striatum signals proximity and value of distant rewards. *Nature* **2013,** *500* (7464), 575-9.

18. Hashemi, P.; Dankoski, E. C.; Lama, R.; Wood, K. M.; Takmakov, P.; Wightman, R. M., Brain dopamine and serotonin differ in regulation and its consequences. *Proc Natl Acad Sci U S A* **2012,** *109* (29), 11510-5.

19. Zimmerman, J. B.; Wightman, R. M., Simultaneous electrochemical measurements of oxygen and dopamine in vivo. *Anal. Chem.* **1991,** *63* (1), 24-8.

20. Sanford, A. L.; Morton, S. W.; Whitehouse, K. L.; Oara, H. M.; Lugo-Morales, L. Z.; Roberts, J. G.; Sombers, L. A., Voltammetric Detection of Hydrogen Peroxide at Carbon Fiber Microelectrodes. *Anal. Chem.* **2010,** *82* (12), 5205-5210.

21. Nguyen, M. D.; Venton, B. J., Fast-scan Cyclic Voltammetry for the Characterization of Rapid Adenosine Release. *Computational and Structural Biotechnology Journal* **2015,** *13*, 47-54.

22. Schmidt, A. C.; Dunaway, L. E.; Roberts, J. G.; McCarty, G. S.; Sombers, L. A., Multiple Scan Rate Voltammetry for Selective Quantification of Real-Time Enkephalin Dynamics. *Anal. Chem.* **2014,** *86* (15), 7806-7812.

23. Roberts, J. G.; Lugo-Morales, L. Z.; Loziuk, P. L.; Sombers, L. A., Real-time chemical measurements of dopamine release in the brain. *Methods Mol Biol* **2013,** *964*, 275-94.

24. Cahill, P. S.; Walker, Q. D.; Finnegan, J. M.; Mickelson, G. E.; Travis, E. R.; Wightman, R. M., Microelectrodes for the measurement of catecholamines in biological systems. *Anal. Chem.* **1996,** *68* (18), 3180-6.

25. Takmakov, P.; Zachek, M. K.; Keithley, R. B.; Walsh, P. L.; Donley, C.; McCarty, G. S.; Wightman, R. M., Carbon microelectrodes with a renewable surface. *Anal. Chem.* **2010,** *82* (5), 2020-8.

26. John, C. E.; Jones, S. R., Fast Scan Cyclic Voltammetry of Dopamine and Serotonin in Mouse Brain Slices. In *Electrochem. Methods Neurosci.*, Michael, A. C.; Borland, L. M., Eds. Boca Raton (FL), 2007.

27. Logman, M. J.; Budygin, E. A.; Gainetdinov, R. R.; Wightman, R. M., Quantitation of in vivo measurements with carbon fiber microelectrodes. *Journal of neuroscience methods* **2000,** *95* (2), 95-102.

28. Roberts, J. G.; Moody, B. P.; McCarty, G. S.; Sombers, L. A., Specific oxygen-containing functional groups on the carbon surface underlie an enhanced sensitivity to dopamine at electrochemically pretreated carbon fiber microelectrodes. *Langmuir* **2010,** *26* (11), 9116-22.

29. Xiao, N.; Venton, B. J., Rapid, sensitive detection of neurotransmitters at microelectrodes modified with self-assembled SWCNT forests. *Anal. Chem.* **2012,** *84* (18), 7816-22.

30. Michael, A. C.; Justice, J. B., Jr., Oxidation of dopamine and 4-methylcatechol at carbon fiber disk electrodes. *Anal. Chem.* **1987,** *59* (3), 405-10.

31. Plattner, H.; Artalejo, A. R.; Neher, E., Ultrastructural organization of bovine chromaffin cell cortex-analysis by cryofixation and morphometry of aspects pertinent to exocytosis. *J. Cell Biol.* **1997,** *139* (7), 1709-17.

32. Bond, A. M.; Luscombe, D.; Oldham, K. B.; Zoski, C. G., A Comparison of the Chronoamperometric Response at Inlaid and Recessed Disk Microelectrodes. *J. Electroanal. Chem.* **1988,** *249* (1-2), 1-14.

33. Godino, N.; Borrise, X.; Munoz, F. X.; del Campo, F. J.; Compton, R. G., Mass Transport to Nanoelectrode Arrays and Limitations of the Diffusion Domain Approach: Theory and Experiment. *Journal of Physical Chemistry C* **2009,** *113* (25), 11119-11125.

34. Fang, D.; Jiang, D.; Lu, H.; Chiel, H. J.; Kelley, T. J.; Burgess, J. D., Observation of Cellular Cholesterol Efflux at Microcavity Electrodes. *J. Am. Chem. Soc.* **2009,** *131* (34), 12038-+.

35. Henry, C. S.; Fritsch, I., Microfabricated recessed microdisk electrodes: characterization in static and convective solutions. *Anal. Chem.* **1999,** *71* (3), 550-6.

36. Ma, C. X.; Contento, N. M.; Gibson, L. R.; Bohn, P. W., Redox Cycling in Nanoscale-Recessed Ring-Disk Electrode Arrays for Enhanced Electrochemical Sensitivity. *Acs Nano* **2013,** *7* (6), 5483-5490.

37. Hu, M. J.; Fritsch, I., Application of Electrochemical Redox Cycling: Toward Differentiation of Dopamine and Norepinephrine. *Anal. Chem.* **2016,** *88* (11), 5574-5578.

38. Hu, M. J.; Fritsch, I., Redox Cycling Behavior of Individual and Binary Mixtures of Catecholamines at Gold Microband Electrode Arrays. *Anal. Chem.* **2015,** *87* (4), 2029-2032.

39. Tokuda, K.; Morita, K.; Shimizu, Y., Cyclic Voltammetry at Microhole Array Electrodes. *Anal. Chem.* **1989,** *61* (15), 1763-1768.

40. He, D. W.; Yan, J. W.; Zhu, F.; Zhou, Y.; Mao, B. W.; Oleinick, A.; Svir, I.; Amatore, C., Enhancing Bipolar Redox Cycling Efficiency of Plane-Recessed Microelectrode Arrays by Adding a Chemically Irreversible Interferent. *Anal. Chem.* **2016**.

41. Morita, K.; Shimizu, Y., Microhole Array for Oxygen-Electrode. *Anal. Chem.* **1989,** *61* (2), 159-162.

42. Kawagoe, K. T.; Zimmerman, J. B.; Wightman, R. M., Principles of Voltammetry and Microelectrode Surface-States. *J. Neurosci. Meth.* **1993,** *48* (3), 225-240.

43. Bucher, E. S.; Brooks, K.; Verber, M. D.; Keithley, R. B.; Owesson-White, C.; Carroll, S.; Takmakov, P.; McKinney, C. J.; Wightman, R. M., Flexible Software Platform for Fast-Scan Cyclic Voltammetry Data Acquisition and Analysis. *Anal. Chem.* **2013,** *85* (21), 10344-10353.

44. Zachek, M.; Takmakov, P.; Moody, B.; Wightman, R.; McCarty, G., Simultaneous Decoupled Detection of Dopamine and Oxygen Using Pyrolyzed Carbon Microarrays and Fast-Scan Cyclic Voltammetry. *Anal. Chem.* **2009,** *81* (15), 6258-6265.

45. Lemos, J. C.; Wanat, M. J.; Smith, J. S.; Reyes, B. A.; Hollon, N. G.; Van Bockstaele, E. J.; Chavkin, C.; Phillips, P. E., Severe stress switches CRF action in the nucleus accumbens from appetitive to aversive. *Nature* **2012,** *490* (7420), 402-6.

46. Roitman, M. F.; Wheeler, R. A.; Wightman, R. M.; Carelli, R. M., Real-time chemical responses in the nucleus accumbens differentiate rewarding and aversive stimuli. *Nature Neuroscience* **2008,** *11* (12), 1376-1377.

47. Boylestad, R. L., *Introductory circuit analysis*. 9th ed.; Prentice Hall: Upper Saddle River, N.J., 2000; p xvi, 1200 p.

48. Bard, A. J.; Faulkner, L. R., *Electrochemical methods : fundamentals and applications*. 2nd ed.; Wiley: New York, 2001; p xxi, 833 p.

49. Ribeiro-Soares, J.; Oliveros, M. E.; Garin, C.; David, M. V.; Martins, L. G. P.; Almeida, C. A.; Martins-Ferreira, E. H.; K. Takai, T. E.; Magalhaes-Paniago, R.; Malachias, A.; Jorio, A.; Archanjo, B. S.; Achete, C. A.; Cancado, L. G., Structural Analysis of Polycrystalline Graphene Systems by Raman Spectroscopy. *Carbon* **2015,** *95*, 646-652.

50. Ferrari, A.; Robertson, J., Interpretation of Raman spectra of disordered and amorphous carbon. *Phys. Rev. B* **2000,** *61* (20), 14095-14107.

51. McCulloch, D. G.; Prawer, S., The Effect of Annealing and Implantation Temperature On the Structure of C Ion-Beam-Irradiated Glassy Carbon. *J. Appl. Phys.* **1995,** *78*, 3040-3047.

52. Ferrari, A. C., Raman spectroscopy of graphene and graphite: Disorder, electron-phonon coupling, doping and nonadiabatic effects. *Solid State Commun.* **2007,** *143*, 47-57.

53. Pimenta, M. A.; Dresselhaus, G.; Dresselhaus, M. S.; Cancado, L. G.; Jorio, A.; Saito, R., Studying disorder in graphite-based systems by Raman spectroscopy. *Phys. Chem. Chem. Phys.* **2007,** *9*, 1276-1291.

54. Wang, Y.; Alsmeyer, D. C.; McCreery, R. L., Raman-Spectroscopy Of Carbon Materials - Structural Basis Of Observed Spectra. *Chem. Mater.* **1990,** *2* (5), 557-563.

55. Mitchell, E. C.; Dunaway, L. E.; McCarty, G. S.; Sombers, L. A., Spectroelectrochemical Characterization of the Dynamic Carbon-Fiber Surface in Response to Electrochemical Conditioning. *Langmuir* **2017**.

56. Baur, J. E.; Wightman, R. M., Diffusion-Coefficients Determined with Microelectrodes. *J. Electroanal. Chem.* **1991,** *305* (1), 73-81.

57. Watkins, J. J.; Chen, J.; White, H. S.; Abruna, H. D.; Maisonhaute, E.; Amatore, C., Zeptomole voltammetric detection and electron-transfer rate measurements using platinum electrodes of nanometer dimensions. *Anal. Chem.* **2003,** *75* (16), 3962-71.

58. Naseh, M. V.; Khodadadi, A. A.; Mortazavi, Y.; Pourfayaz, F.; Alizadeh, O.; Maghrebi, M., Fast and clean functionalization of carbon nanotubes by dielectric barrier discharge plasma in air compared to acid treatment. *Carbon* **2010,** *48* (5), 1369-1379.

59. Coen, M. C.; Keller, B.; Groening, P.; Schlapbach, L., Functionalization of graphite, glassy carbon, and polymer surfaces with highly oxidized sulfur species by plasma treatments. *J. Appl. Phys.* **2002,** *92* (9), 5077-5083.

60. Dongil, A. B.; Bachiller-Baeza, B.; Guerrero-Ruiz, A.; Rodriguez-Ramos, I.; Martinez-Alonso, A.; Tascon, J. M. D., Surface chemical modifications induced on high surface area graphite and carbon nanofibers using different oxidation and functionalization treatments. *J. Colloid Interface Sci.* **2011,** *355* (1), 179-189.

61. Yang, L. F.; Shi, Z.; Yang, W. H., Enhanced capacitive deionization of lead ions using air-plasma treated carbon nanotube electrode. *Surface & Coatings Technology* **2014,** *251*, 122-127.

62. Epifanio, M.; Inguva, S.; Kitching, M.; Mosnier, J. P.; Marsili, E., Effects of atmospheric air plasma treatment of graphite and carbon felt electrodes on the anodic current from Shewanella attached cells. *Bioelectrochemistry* **2015,** *106*, 186-193.

63. Roberts, J. G.; Moody, B. P.; McCarty, G. S.; Sombers, L. A., Specific Oxygen-Containing Functional Groups on the Carbon Surface Underlie an Enhanced Sensitivity to Dopamine at Electrochemically Pretreated Carbon Fiber Microelectrodes. *Langmuir* **2010,** *26* (11), 9116-9122.

64. Amatore, C.; Oleinick, A. I.; Svir, I., Reconstruction of aperture functions during full fusion in vesicular exocytosis of neurotransmitters. *Chemphyschem* **2010,** *11* (1), 159-74.

65. Schroeder, T. J.; Jankowski, J. A.; Kawagoe, K. T.; Wightman, R. M.; Lefrou, C.; Amatore, C., Analysis of diffusional broadening of vesicular packets of catecholamines released from biological cells during exocytosis. *Anal. Chem.* **1992,** *64* (24), 3077-83.

66. Mandela, P.; Ordway, G. A., The norepinephrine transporter and its regulation. *J. Neurochem.* **2006,** *97* (2), 310-333.

67. Wightman, R. M.; Schroeder, T. J.; Finnegan, J. M.; Ciolkowski, E. L.; Pihel, K., Time-Course of Release of Catecholamines from Individual Vesicles during Exocytosis at Adrenal-Medullary Cells. *Biophys. J.* **1995,** *68* (1), 383-390.

68. Sulzer, D.; Pothos, E. N., Regulation of quantal size by presynaptic mechanisms. *Reviews in the Neurosciences* **2000,** *11* (2-3), 159-212.

69. Zachek, M. K.; Hermans, A.; Wightman, R. M.; McCarty, G. S., Electrochemical dopamine detection: Comparing gold and carbon fiber microelectrodes using background subtracted fast scan cyclic voltammetry. *J. Electroanal. Chem.* **2008,** *614* (1-2), 113-120.

CHAPTER 3

Mu-Opioid Receptor Activation Induces Catecholamine Secretion in the Rat Adrenal Gland

This work was completed in collaboration with: Dunaway, L.E., Meitzen, J.E., and Sombers, L.A., and is in preparation for submission to the Journal of Neuroscience. Supplemental information is found in Appendix F.

3.1 Introduction

The adrenal glands are responsible for secretion of catecholamines into the blood stream in response to threats, as part of the fight-or-flight response.[1] The splanchnic nerve innervates the adrenal gland, and modulates the exocytotic release of catecholamines, namely norepinephrine, epinephrine, and dopamine, by way of acetylcholine that can act on ionotropic nicotinic and metabotropic muscarinic acetylcholine receptors.[2-3] Once released, the catecholamines play a key role in regulating the physiological response to stress, including but not limited to cardiac, pulmonary, and metabolic function.[4] Due to the exocytotic nature of neurotransmitter release from these cells, as well as similarities to neurons in terms of key molecular machinery, this system has been widely studied to reveal insights into fundamental aspects of catecholamine release.[5-9] Much of the information learned by using chromaffin cells as a model system for exocytotic function extends beyond the adrenal gland, and applies to exocytotic events that occur throughout the nervous system in general.

Endogenous catecholamines released in the adrenal gland induce systemic sympathetic activation.[10-12] While the mechanisms that underlie the secretion of catecholamines by chromaffin cells have been widely interrogated, the vesicular cargo also includes a variety of peptidergic signaling molecules.[3, 13-14] Neuropeptides are a major class of signaling molecules that are involved in many nervous system functions, such as reward processing,[15-19] nociception,[20] various neuropathologies,[21-24] and the biochemical response to multiple drugs of abuse.[25-30] Subsequently, these molecules influence a wide variety of complex physiological functions ranging from basic endocrine function to motivation.[25, 30-33] Of the known neuropeptides, the enkephalins are one of the most abundant in the adrenal gland.[4] The two principle enkephalins, met-enkephalin (M-ENK) and leu-enkephalin, are both derived from the precursor hormone proenkephalin. They are the smallest of the endogenous opioid peptides, having only five amino acids, and were originally identified in 1975 as potent opioid agonists in the brain.[34] The enkephalins were discovered in the adrenal medulla with immunoassay in 1978.[35-36] The mu- and delta- opioid receptors (MOR and DOR, respectively) are G-protein coupled receptors, generally thought to be inhibitory in nature.[37] However, it is becoming increasingly clear that MOR function is complex and not fully understood.[38] For instance, in a study in 2014,[39] Margolis et. al. examined the functional roles of post-synaptic MORs on dopamine neurons in the ventral tegmental area (VTA) of the rat brain. The conventional understanding of the roles of MORs in this region was posited by Johnson and North in 1992,[40] whereby MORs are present on GABAergic interneurons which project onto and inhibit the dopamine neurons. Inhibition of the GABA neurons by agonism of MOR results in a disinhibition of the dopamine neurons, thus having an indirect excitatory action. However,

Margolis found that even when subject to $GABA_A$ blockade, the MOR agonist DAMGO had a direct excitatory effect on 22 of 110 dopamine neurons tested, while inhibiting 45 of the 110 dopamine neurons tested. In another study, Legorova et. al.[41] found a direct excitatory mechanism for DAMGO in Purkinje neurons. Thus, it is becoming increasingly clear that MORs are not limited to the canonical inhibitory action, but may play other roles as well. In the adrenal gland, M-ENK and other peptides are secreted not only by the chromaffin cells, but also by the splanchnic nerve, which further complicates efforts to determine functional roles of opioid peptides and receptors in the adrenal glands.[14, 42-45] Thus, the precise role that these peptides play in normal endocrine function is not yet clear.

In this work, we sought to examine the modulatory role of M-ENK on dynamic catecholamine release in the adrenal medulla using fast-scan cyclic voltammetry (FSCV), an established electrochemical technique that is often used to monitor rapidly fluctuating catecholamine levels in living brain and adrenal tissue.[46-56] This approach can simultaneously measure rapid fluctuations of multiple chemical species, and also provides excellent spatial resolution when coupled with carbon-fiber microelectrodes. FSCV was used to measure catecholamine release from chromaffin cells in an adrenal slice preparation in response to M-ENK, as well as the selective MOR and DOR agonists, DAMGO and DPDPE. Additionally electrophysiological whole-cell recordings were used to observe changes in chromaffin cell membrane potential. Taken together, the data demonstrate that activation of MORs elicits catecholamine secretion in the adrenal medulla by a mechanism that is dependent on activation of muscarinic acetylcholine receptors.

3.2 Experimental Section

3.2.1 Chemicals

M-ENK was obtained as an acetate salt from LKT Laboratories (St. Paul, MN). All other chemicals were purchased from Sigma-Aldrich (St. Louis, MO) and used as received, unless otherwise specified. All aqueous solutions were made from doubly deionized water >18 MΩ·cm (Millipore, Billerica, MA).

3.2.2 Electrode Fabrication

All electrochemical experiments were carried out with T-650 carbon-fiber microelectrodes (Cytec Industries, West Patterson, NJ), fabricated as described previously.[57] Briefly, a single 7 μm diameter fiber was aspirated into a borosilicate glass capillary (1.0 mm x 0.5 mm, A-M Systems, Carlsburg, WA). Using a micropipette puller (Narishige, Tokyo, Japan) the glass was tapered to form sealed microelectrodes which were then cut to 100 μm under a microscope. To establish an electrical connection with the carbon fiber, the glass capillary was backfilled with ionic solution (4 M potassium acetate, 150 mM KCl) and a stainless steel lead wire was inserted. All measurements were recorded against a Ag/AgCl reference electrode (World Precision Instruments, Inc., Sarasota, FL).

3.2.3 Animal Care and Use

Adult male Sprague-Dawley rats (Charles River Laboratories, Raleigh, NC) weighing 275-300 g were housed on a 12:12 h light cycle with food and water available ad libitum. Animal care and all experimental procedures were in accordance with the North Carolina State

University's institutional animal care and use committee and the Guide for the Care and Use of Laboratory Animals (National Research Council, 2011).

3.2.4 Adrenal Slice Preparation

Animals were deeply anesthetized with urethane (1.5 g/kg, i.p.) and quickly decapitated. The adrenal glands were rapidly removed, trimmed of fat tissue, and embedded in agarose gel containing 3% agarose in BBS. Gel blocks were placed in cold BBS while 400 μm-thick slices were obtained with a vibratome (World Precision Instruments, Sarasota, FL). The slices were allowed to rest in BBS buffer for at least 1 hr. before the start of an experiment. Slices were subsequently placed in a recording chamber (Warner Instruments, Hamden, CT) and superfused with BBS buffer maintained at 29 °C for at least another 1 hr. Carbon-fiber microelectrodes were placed about 100 μm below the surface of the slice, and a micropipette was positioned approximately 1 mm from the recording electrode for the stimulation experiments. Working electrode and stimulating pipette placements were made with the aid of a microscope (Nikon Instruments, Inc., Melville, NY). The micropipette was backfilled with the drug of interest, and chemical stimulation made with short pressure bursts using a Picospritzer II (Parker Hannifin, Hollis, NH).

3.2.5 Brain Slice Preparation

Animals were deeply anesthetized with urethane (1.5 g/kg, i.p.) and quickly decapitated. The brain was rapidly removed, mounted, and placed in cold aCSF. Coronal slices with a thickness of 400 μm containing the striatum were obtained with a vibratome (World

Precision Instruments, Sarasota, FL). The slices were allowed to rest in the buffer for at least 1 hr. before the start of an experiment. Brain slices were subsequently placed in a recording chamber (Warner Instruments, Hamden, CT) and superfused with aCSF buffer maintained at 34 °C for at least another 1 hr. The working electrode and bipolar stimulating electrode placements were made in the nucleus accumbens with the aid of a microscope (Nikon Instruments, Inc., Melville, NY), and the microelectrodes were positioned about 100 μm below the surface of the slice. Electrical stimulation of nerve terminals consisted of five 500 μA pulses at 60 Hz using a pulse width of 4 msec.

3.2.6 Electrochemical Data Acquisition

A sawhorse waveform (Figure 3.1B) was applied at 10 Hz. The potential was held at -0.4 V, then ramped to +1.3 V at 400 V/s. The potential was then held at +1.3 V for 2 msec before scanning back to the holding potential of -0.4 V at 400 V/s. A traditional triangular waveform was also used for comparison. The potential ranged from -0.4 V to +1.3 V and back at 400 V/s (Figure 3.1A). These electrochemical waveforms were output using a custom instrument for potential application and current transduction (University of North Carolina at Chapel Hill, Department of Chemistry, Electronics Facility). High Definition Cyclic Voltammetry software (HDCV, University of North Carolina at Chapel Hill, Department of Chemistry) was used to control waveform output. A 6363 PCIe bus card (National Instruments Corp., Austin, TX) was used for data collection and synchronization of the electrochemical experiment with the flow injection system used for *in vitro* characterization of electrode performance. Signal processing (background subtraction, signal averaging, and digital filtering

(2-pole Sallen-Key Filter, 2 KHz)) was software-controlled. Electrical stimulations were carried out with a DS-4 Biphasic Stimulus Isolator (Digitimer Ltd., Welwyn Garden City, England), controlled by software written in-house through aforementioned PCI bus card.

In vitro characterization of electrode performance was carried out in phosphate buffered saline (0.1 M PBS) or Tris buffer (15 mM Tris, 3.25 mM KCl, 1.20 mM $CaCl_2$, 1.2 mM $MgCl_2$, 2 mM Na_2SO_4, 1.25 mM NaH_2PO_4, 145 mM NaCl), at physiological pH 7.4. Data were collected in a custom-built flow injection apparatus housed within a Faraday cage. A syringe pump (New Era Pump Systems, Inc., Wantagh, NY) supplied a continuous buffer flow of 1.0 mL/min across both the working and reference electrodes. The working electrode was lowered into the electrochemical cell via a micromanipulator (World Precision Instruments, Inc., Sarasota, FL). Two-second bolus injections of analyte were accomplished using a six-port HPLC valve and air actuator controlled by a digital valve interface (Valco Instruments Co., Inc., Houston, TX).

Ex vivo adrenal slice voltammetry experiments used bicarbonate buffered saline (BBS) saturated with 95% O_2 and 5% CO_2, at pH 7.2. BBS consisted of 125 mM NaCl, 26 mM $NaHCO_3$, 2.5 mM KCl, 2.0 mM $CaCl_2$, 1.0 mM $MgCl_2$, 1.3 mM NaH_2PO_4, 10 mM HEPES, and 10 mM glucose. Brain slice voltammetry experiments were carried out in artificial cerebral spinal fluid (aCSF) saturated with 95% O_2 and 5% CO_2, at physiological pH 7.4. aCSF consisted of 124 mM NaCl, 26 mM $NaHCO_3$, 3.7 mM KCl, 2.4 mM $CaCl_2$, 1.3 mM $MgCl_2$, 1.3 mM NaH_2PO_4, and 10 mM glucose.

3.2.7 Electrophysiology Experiments

An Axon MultiClamp 700B amplifier (Molecular Devices, LLC., Sunnyvale, CA) was coupled to an Axon DigiData 1440A digitizer. Data were collected using Axon pCLAMP 10 software. Signals were filtered at 2 kHz and digitized at 10 kHz. Membrane potential was recorded in current-clamp mode. Tissue was visualized using a Zeiss Axioscope, equipped with IR-DIC optics for contrast, a DAGE IR-1000 camera, and 10x and 40x objective lenses with 1.5x optical zoom. Adrenal slices were placed in the recording chamber of the microscope and perfused with ringer flowing buffer saturated with 95% O_2 and 5% CO_2, at pH 7.2, heated to 29°C. Ringer consisted of 150 mM NaCl, 10 mM HEPES, 10 mM Glucose, 2.8 mM $CaCl_2$, 2.8 mM KCl, and 2 mM $MgCl_2$, with osmolarity set to 320 mOsm with sucrose. Whole-cell patch-clamp recordings were made from cells in the medulla showing three-dimensional contour, without a well-defined nuclear envelope indicative of cell death. Recordings were made using glass electrodes (2-4 MΩ) pulled on a Sutter Instrument (Novato, CA) P-97 Micropipette Puller. Electrodes were backfilled with internal pipette solution consisting of 145 mM gluconate, 10 mM HEPES, 8 mM NaCl, 2 mM MgATP, 1 mM $MgCl_2$, 0.1 mM EGTA, 0.3 mM NaGTP, and 10 mM phosphocreatine, osmolarity set to 310 mOsm with sucrose. Air bubbles were removed from the pipette tips either with gentle perturbation, or positive pressure. Cells were patched by applying positive pressure to the pipette and lowering it onto the cell. Negative pressure was then applied until a gigaohm seal was formed, at which point short negative-pressure bursts were applied to break into the membrane. After gaining access to a cell, the membrane potential was allowed to stabilize 3-4 min. Quiescent cells were kept at resting potential with no holding current, while cells firing spontaneous action potentials

were suppressed using negative current (15-30 pA). Three hyperpolarizing current injections were applied in order to calculate input resistance, both before and after each experimental manipulation. When assessing cell response to particular drugs, membrane potential was allowed to rest for 5 minutes before the drug was applied. Drugs were applied via bath application for 8-10 min. before washout. Membrane potential was averaged in 30 sec. increments to assess the response to the drug of interest.

3.2.8 Statistics and Data Analysis

HDCV was used for multivariate calibration using principal component regression (PCR), a combination of principal component analysis and inverse least squares regression. Training sets collected *in vitro* were used to determine chemical contributors to data collected in the biological preparations. All data are shown as the mean ± standard error of the mean. Student's *t*-tests were used to compare means. For data sets containing more than two observations, a one-way ANOVA was used, with Tukey's post-hoc test for multiple comparisons. Repeated measures ANOVA was used for paired observations. When comparing calibration curves, non-linear fits with one-phase decay were generated, and K-values compared using a t-test. Significance was designated at $p < 0.05$. Statistical and graphical analyses were carried out using GraphPad Prism 5 (GraphPad Software, Inc., La Jolla, CA).

3.3 Results

The adrenal glands regulate physiological responses to stressors, in part by secretion of the catecholamines norepinephrine, epinephrine and dopamine. A variety of peptides, including opioid peptides, are thought to be stored in dense core vesicles in adrenal cells.[4, 14, 58] The opioid system is strikingly complex, and the precise interaction between opioid peptides and catecholamines is not well understood. The adrenal medulla contains both mu- and delta-opioid receptors.[10-12] Previous studies have examined the effects of MOR agonists and antagonists on the levels of catecholamine secreted by chromaffin cells in response to splanchnic nerve or nicotinic stimulation. The results have shown that both agonists[12, 59] and antagonists[60-61] can attenuate catecholamine secretion. However, it is important to note that these studies all measured catecholamine levels ex vivo, using an offline detection technique following sampling from the adrenal vein or from the cultured cell bath. Sampling techniques coupled to analytical measurements[62-70] and radioimmunoassay[28, 71-75] have proven invaluable to the study of neuropeptide function; however, utility is limited by poor temporal resolution on the order of tens of minutes. These measurements are sensitive to long-term dynamics in neurotransmitter content, however they lack the ability to monitor sub-second catecholamine release. In this work, we sought to understand the role of met-enkephalin (M-ENK), an endogenous opioid peptide found in the adrenal medulla that acts at both delta and mu opioid receptors,[76] in regulating catecholamine secretion in the adrenal chromaffin cells on the sub-second time scale. In order to do this, background-subtracted fast scan cyclic voltammetry (FSCV) was coupled to carbon-fiber ultramicroelectrodes to measure catecholamine

fluctuations in live tissue, in real time. FSCV has been used extensively for the detection of dopamine in the rodent brain, and is well-characterized for this purpose.[77-78]

3.3.1 Modulatory Role of M-ENK in Response to Nicotine Stimulation

To explore the modulatory role of M-ENK in an adrenal slice preparation, FSCV with was used to monitor nicotine-evoked catecholamine release in real time. Catecholamine release was evoked by pressure ejecting 1 µM nicotine onto the slice at 5 min. intervals for 15 min., and was recorded using a standard triangular waveform ranging from –0.4 V to +1.3 V, applied at a scan rate of 400 V/sec and a frequency of 10 Hz. Addition of 1 µM M-ENK to the running buffer resulted in a 68% increase (Figure 3.1A, pre M-ENK: 1.00 ±0.12; + M-ENK: 1.68 ± 0.26) in the catecholamine levels evoked by nicotine (black vs red). This effect was reversed upon washout of M-ENK (Washout: 0.90 ± 0.04), restoring catecholamine secretion to pre-M-ENK levels (Figure 3.1A, black vs. light gray) ($F(2,24) = 4.78$, $p < 0.05$). Importantly, electrodes were calibrated in both the presence and absence of 250 nM M-ENK. Electrode sensitivity to catecholamine was significantly decreased in the presence of M-ENK ($t(16) = 13.30$, $p < 0.0001$, data not shown), consistent with a previous report.[79] The modulatory role of M-ENK was also investigated in the region of the nucleus accumbens in an acute brain slice. Dopamine release was electrically evoked at 5-min. intervals for 25 min. (Figure 3.1B, pre-M-ENK in black). Addition of 250 nM M-ENK to the aCSF running buffer resulted in a 16% increase (Pre M-ENK: 1.00 ± 0.01; + M-ENK: 1.16 ± 0.03) in dopamine release (Figure 3.1B, red). M-ENK is an agonist of both MOR and DOR, and both receptor subtypes are present in the rat ventral striatum.[80] The increase was reversed (M-ENK + NX: 1.01 ± 0.01)

when 2.5 µM naltrexone (non-specific opioid receptor antagonist) was added to the running buffer (Figure 3.1B, $F(2,14) = 5.23$, $p < 0.05$). Addition of naltrexone to the buffer did not alter sensitivity to dopamine ($t(16) = 0.96$, $p > 0.05$, data not shown)

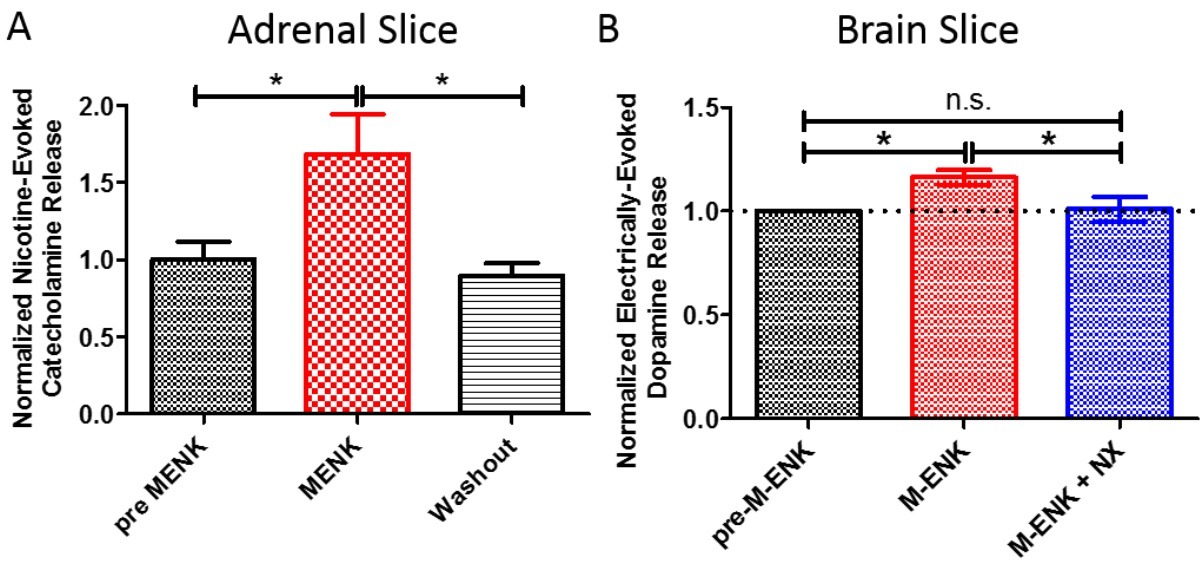

Figure 3.1. M-ENK increases catecholamine secretion in adrenal and brain tissue slices. A) Catecholamine release evoked by 1 µM nicotine in adrenal slice preparation. Addition of 1 µM M-ENK to the running buffer increases the extracellular catecholamine concentrations detected, and this effect was reversed upon washout (ANOVA with Tukey's post hoc, $p = 0.019$, $n = 4$). B) Electrically evoked dopamine release recorded in ventral striatum. Addition of 250 nM M-ENK to the running buffer significantly increased the concentration of dopamine released. This effect was reversed by addition of 2.5 µM naltrexone (ANOVA with Tukey's post-hoc, $p = 0.023$, $n = 5$).

3.3.2 A Sawhorse Waveform Facilitates Detection of Catecholamine Secretion in the Presence of M-ENK

As described above, a carbon-fiber microelectrode is easily fouled when scanning to positive potentials in the presence of M-ENK, likely due to oxidation and subsequent polymerization of the tyrosine residue.[81] Fouling can often be mitigated by briefly holding the potential of the electrode above ~1.0V in order to strip and oxidize the carbon surface.[79, 82-83] Thus, a sawhorse waveform was implemented for the remainder of the electrochemical experiments described herein. This waveform was similar to the triangular waveform commonly employed to detect dopamine – the potential was scanned to +1.3 V at 400 V/sec.; however, the potential was held at +1.3 V for 2 msec before scanning back to the -0.4 V holding potential. Chemical dynamics recorded in an adrenal slice with both waveforms are compared in Figure 3.2. While 1 μM M-ENK is sufficient to elicit catecholamine release (shown in Figure 3.5), a higher concentration (1 mM) was employed here in order to enable the simultaneous detection of M-ENK itself. Fouling is evident in the data collected using the triangular waveform, manifest as a prolonged shift in the background current and no evidence of catecholamines in the voltammograms (Figure 3.2A,C). When using the sawhorse waveform, oxidation of catecholamines is obvious in both the color plot and extracted voltammogram (3.2B,D).

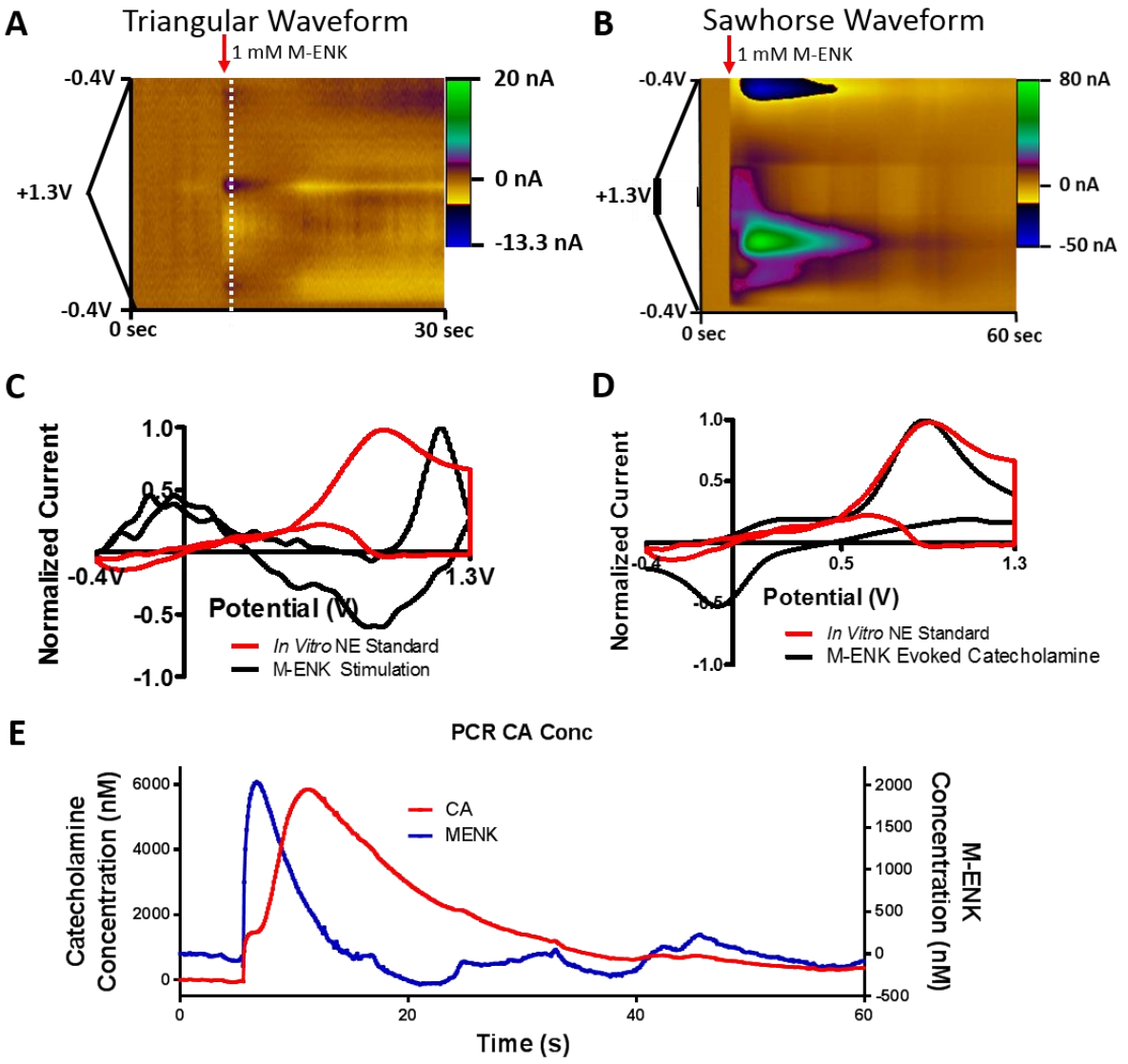

Figure 3.2. A sawhorse waveform allows for detection of catecholamine release in adrenal slice elicited by M-ENK. A) Colorplot collected with a standard triangular waveform, with pressure ejection of 1 mM M-ENK at red arrow. B) Colorplot collected with sawhorse waveform showing catecholamine release elicited upon pressure ejection of 1 mM M-ENK at red arrow. C) Voltammogram extracted from the colorplot shown in 2A, with no evident catecholamine signal (black) overlaid with that for a norepinephrine standard (red) ejected onto the electrode in tissue. D) Voltammogram extracted from colorplot in 2B (black) overlaid with that for a norepinephrine standard (red) ejected onto the electrode in tissue. E) Catecholamine (red) and M-ENK (blue) concentration dynamics extracted from 2B using principal component regression.

Principle component regression (PCR) was employed to distinguish the contribution of the applied M-ENK bolus to the signal, and to discern it from that due to resultant catecholamine release. Training sets were constructed with exogenous applications of norepinephrine and M-ENK onto an electrode implanted in dead adrenal issue. Utilizing the exogenous training sets, PCR successfully accounted for the catecholamine and M-ENK signals in the data. Figure 3.2E shows the dynamic concentration profiles for catecholamine and M-ENK. As expected, M-ENK has a sharp rise corresponding to the pressure ejection, and a quick decay as mass transport carries it away (or possibly enzymatic digestion). The resultant catecholamine secretion follows the M-ENK bolus and has a broader peak. While 1 mM M-ENK was pressure ejected onto the tissue, only 2 μM M-ENK was recorded at the electrode surface following calibration by PCR. This is unsurprising, given the tortuosity of adrenal tissue. These data show that the signals recorded using the sawhorse waveform are indeed resultant from catecholamine secretion in response to stimulation by M-ENK.

While the shape of the signal recorded with the sawhorse waveform resembles that expected for catecholamines, the oxidation peak was shifted to an unusually high potential of +0.84 V. To determine why the oxidation peak was shifted to such a high potential, another experiment was performed where an electrode was lowered into adrenal tissue in 10 μm increments, until the electrode was fully inserted in the tissue. At each increment 10 μM norepinephrine was pressure ejected onto the electrode and the response recorded. The resulting voltammograms are shown in Figure F1A (Appendix F). As the electrode was lowered into the tissue, the magnitude of response decreased and the peak potential shifted to a higher potential. When the electrode was fully inserted into the tissue the peak oxidation

potential for exogenous norepinephrine was +0.84 V. The voltammogram for the bolus ejected onto tissue is overlaid with that for released catecholamine in Figure 3.2D. The shift in peak position matches between both voltammograms, verifying that the collected signal is resultant from oxidation of catecholamine.

Figure F1B shows non-background subtracted voltammograms taken as the electrode was lowered into the tissue without ejecting norepinephrine. As the electrode was lowered into tissue, a feature was observed that increased in magnitude and shifted to higher potential. This feature is the oxidation peak from background level of catecholamines in the adrenal tissues and the shift in peak potential is most likely due to the high impedance of adrenal tissue.[77]

In order to calculate the change in concentration of catecholamines, the new sawhorse waveform's response to epinephrine, norepinephrine and dopamine was characterized and compared that that of the traditional triangular waveform. Due to the high levels of catecholamines in the adrenal medulla, both waveforms were calibrated to concentrations ranging from 0.5 μM to 10 μM. The calibration plots are shown in Figure 3.3, along with representative voltammograms collected with the sawhorse waveform for all three analytes. While the calibration curves depart from linearity at between 2 and 5 μM, the calibration curves are similar for the waveforms in response to dopamine (3.3A) ($t(48) = 0.05$, $p > 0.05$), norepinephrine (3.3B) ($t(48) = 1.01$, $p > 0.05$), and epinephrine (3.3C) ($t(48) = 0.07$, $p > 0.05$). Representative voltammograms for all tested concentrations of these analytes are shown in panels D, E, and F. Since the sawhorse waveform allowed for the detection of catecholamines

in the presence of fouling agents, and had no decrease in sensitivity to catecholamines over the traditional triangular waveform, the sawhorse waveform was employed for the remaining experiments herein.

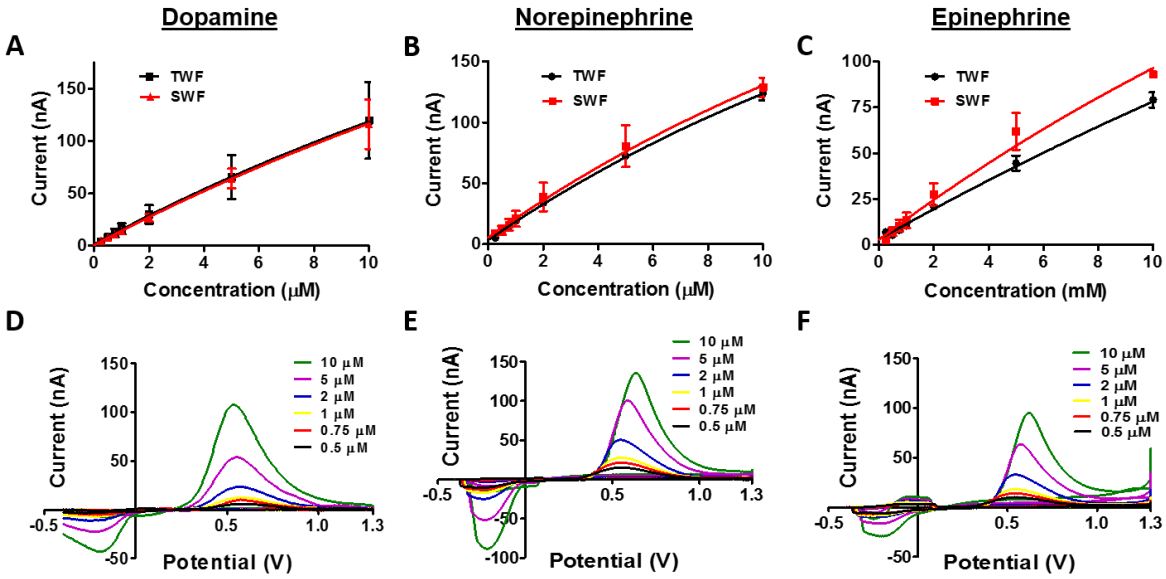

Figure 3.3. Sawhorse waveform calibration. Calibration plots for dopamine (A), norepinephrine (B), and epinephrine (C) reveal no difference in sensitivity to dopamine using the triangular waveform (TWF; black) and the sawhorse waveform (SWF; red). Representative voltammograms are shown for dopamine (D), norepinephrine (E), and epinephrine (F) using the sawhorse waveform. Concentrations span from 0.5 μM to 10 μM, corresponding to the calibration plots.

3.3.3 Pharmacological Validation of Signal

To assess the role of the opioid receptors in facilitating the secretion of catecholamines, a pan-opioid receptor antagonist, naltrexone (NTX) was applied to test whether it would block the response. Catecholamine release was recorded in response to 1 μM M-ENK pressure

ejection in 5-minute intervals for 20 minutes, and then 10 µM NTX was added to the running buffer (Figure 3.4). M-ENK stimulations were continued at 5-minute intervals for 30 minutes. In the presence of NTX, there was a 66% decrease in catecholamine signal evoked by M-ENK (Pre-NTX: 1.00 ± 0.04; + NTX: 0.34 ± 0.06; $t(4) = 9.27$, $p < 0.001$). In a separate set of experiments, stimulation was performed over the same time course (total 50 minutes), with no NTX added to the bath, and the catecholamine release was stable over the course of the experiment (Pre-NTX: 1.00 ± 0.09; - NTX: 0.93 ± 0.12; $t(4) = 0.41$, $p > 0.05$).

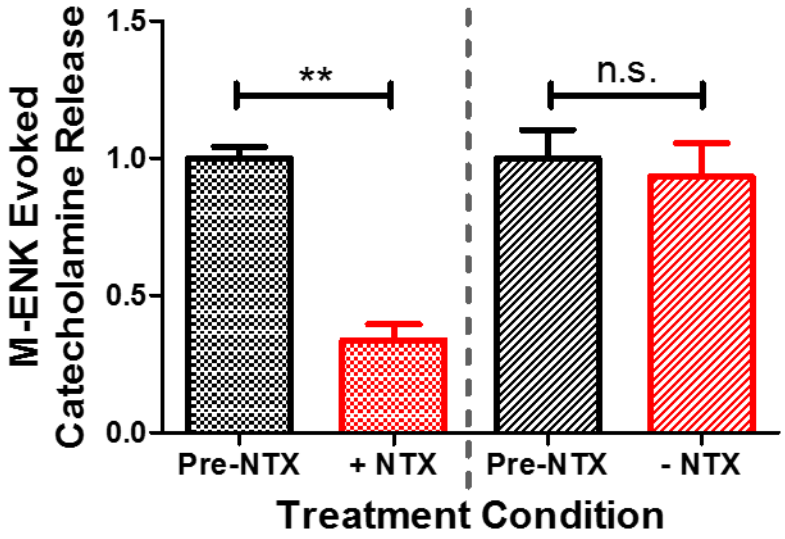

Figure 3.4. Naltrexone attenuates the secretion of catecholamine by M-ENK. Catecholamine release is stimulated by 1 µM M-ENK in 5-minute intervals. After 20 minutes, naltrexone is added to the bath, and recordings made for another 30 minutes at 5-minute intervals. Addition of naltrexone to the bath results in a 66% decrease in the concentration of catecholamine detected in response to M-ENK stimulation. The second set of bars shows experiments where release is stimulated by 1 µM M-ENK in 5 minute intervals for 50 minutes with no naltrexone added to the bath. There is no significant change in evoked catecholamine release between the first 20 minutes and the subsequent 30 minutes. *** $p < 0.001$

M-ENK binds to both mu opioid receptors (MOR) and delta opioid receptors (DOR),[76] and both of these receptors are expressed on chromaffin cells.[10-12] In order to determine at which receptor M-ENK was acting to elicit the catecholamine release, selective agonists for these receptors DAMGO and DPDPE, respectively, were ejected onto the tissue. The data are shown in Figure 3.5. Pressure ejecting the perfusion buffer resulted in no catecholamine release (Figure 3.5A), validating that this was not merely a response to mechanical stimulation[84] and that catecholamine secretion elicited by M-ENK (Figure 3.5B) is indeed a physiological response. The application of M-ENK, Figure 3.5B, and the selective MOR agonist DAMGO, Figure 3.5C, elicited catecholamine secretion. The DOR agonist DPDPE did not (Figure 3.5D). This demonstrates that M-ENK is likely evoking catecholamine secretion by way of agonism of MORs.

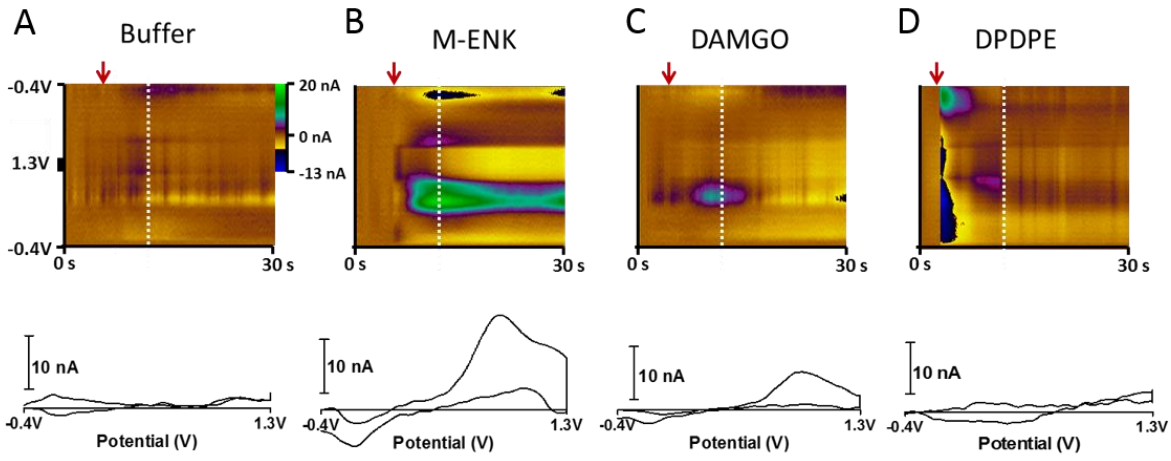

Figure 3.5. Pharmacological verification of M-ENK evoked catecholamine signal. A) Colorplot showing no response to pressure-ejection of BBS buffer onto tissue at the red arrow, with accompanying voltammogram extracted at white dashed line. B) Colorplot showing catecholamine release elicited by pressure ejection of 1 µM M-ENK at red arrow. C) Colorplot showing catecholamine release elicited by pressure ejection of 1 µM DAMGO D) Colorplot showing no response to pressure-ejection of µM DPDPE.

3.4 Observing Membrane Potential in Response to Stimulation

The electrochemical data revealed a unique response whereby M-ENK elicits catecholamine secretion, likely by way of the mu-opioid receptor activation as this effect was seen with MOR agonism (via DAMGO), and attenuated by a non-selective opioid receptor antagonist (NTX). In order to propose a mechanism by which this happens, we performed whole-cell patch electrophysiology to monitor cell membrane potential in response to bath application of the selective MOR agonist, DAMGO. The adrenal slices were prepared in the same manner as those used for FSCV data collection. A single cell in the adrenal slice was targeted and patched in the whole-cell configuration, monitoring membrane potential in response to various drugs. The results are described in Figure 3.6. Initially, cell membrane potential was monitored in response to the nAChR agonist, nicotine. Since the splanchnic nerve secretes acetylcholine onto chromaffin cells in the adrenal gland in order to elicit catecholamine release into the blood stream, this served as a control to ensure that our preparation and methodology was responding as anticipated based on previous studies.[85] As expected, bath application of 1 μM nicotine resulted in depolarization of chromaffin cells (Figure 3.6A), demonstrating that chromaffin cells can be patched and membrane potential can be successfully monitored in response to bath application of drugs (Pre Nicotine: -52.8 ± 10.4 mV; + Nicotine: -54.1 ± 10.9 mV; $t(2) = 7.35$, $p < 0.05$).

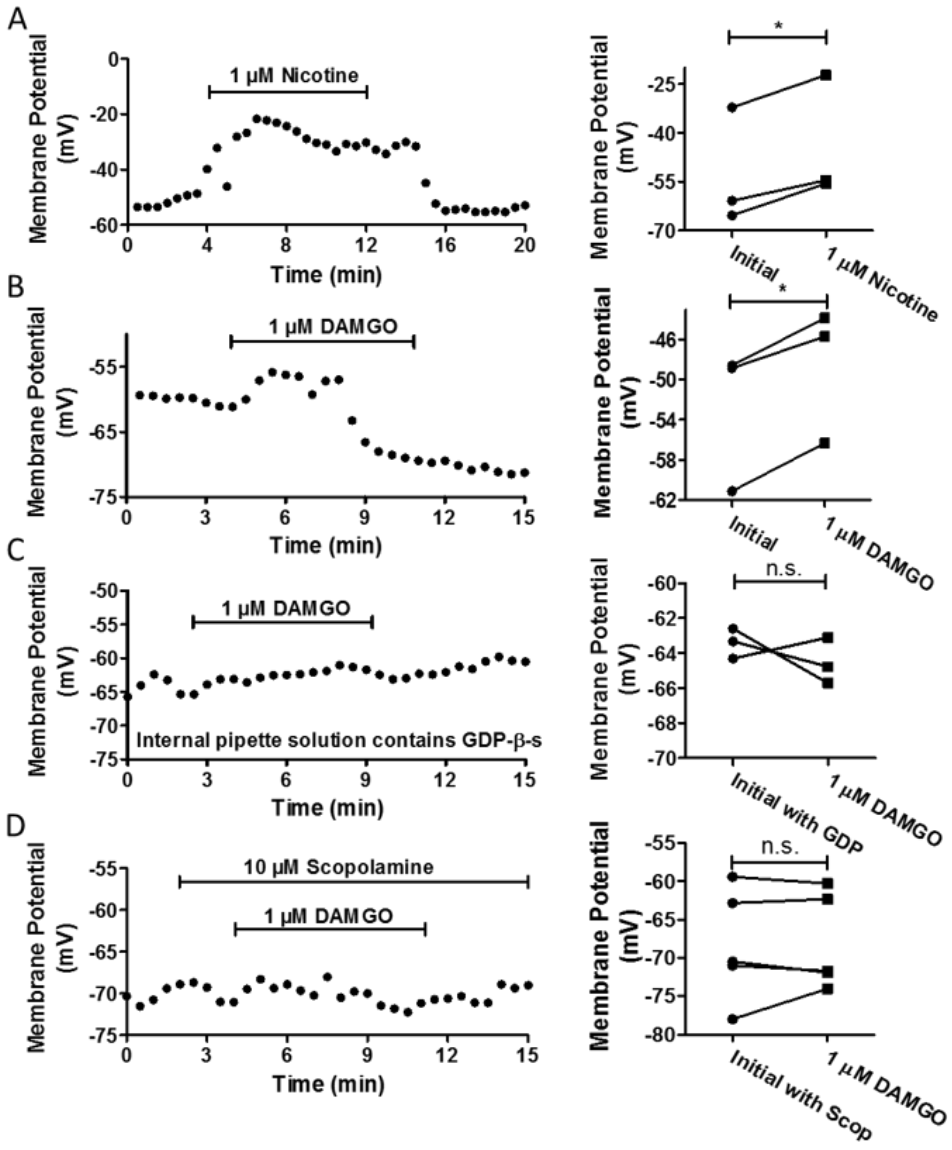

Figure 3.6. DAMGO depolarizes chromaffin cells in a manner dependent on agonism of muscarinic acetylcholine receptors. Membrane potential is monitored in whole-cell patch configuration, with changes observed in response to various drugs. Membrane potential is averaged in 30 second increments and shown with respect to time, with bath-application of drug, designated by horizontal bar over the plot. A) Nicotine in the bath induces a prolonged depolarization from minutes 4 to 14, that washes out thereafter B) DAMGO in the bath induces a depolarization from minutes 5 to 8, which is reversed prior to washout. C) Addition of 0.5 mM GDP-β-s to the internal patch pipette solution abolishes depolarization by DAMGO. D) With 10 µM scopolamine in the perfusion buffer, DAMGO fails to depolarize the cells. * $p < 0.05$

In the next set of experiments, the effect of MOR agonism was investigated while monitoring the membrane potential of patched chromaffin cells. The electrochemical data revealed DAMGO-induced catecholamine secretion, thus our hypothesis was that this manipulation may depolarize the chromaffin cells, despite conventional dogma of opioid receptor activation being inhibitory.[86-87] Indeed, as shown in Figure 3.6B, upon the addition of 1 µM DAMGO to the running buffer, the patched cells depolarized (Pre DAMGO: -52.9 ± 4.1 mV; + DAMGO: -48.6 ± 3.9 mV; $t(2) = 7.96$, $p < 0.05$). This evidence lends strong support of the MOR-mediated catecholamine secretion monitored during the electrochemical experiments with FSCV. Next, we sought to determine whether depolarization by DAMGO was happening locally at the cell of interest, or if it was happening via an indirect mechanism involving neighboring cells or terminals. GDP-β-s was added to the internal solution in the patch pipette, allowing it to diffuse directly into the patched cell. By doing this, we blocked all signaling via G-protein coupled receptors (GPCRs) within the patched cell only. Theoretically, if DAMGO-induced cellular activity changes at splanchnic nerve inputs, this may promote the release of acetylcholine (ACh) and the patched cell could depolarize via the nAChR, which is an ionotropic receptor. However, with GDP-β-s on board, the patched cell failed to depolarize upon the addition of DAMGO to the running buffer (Figure 3.6C) (Pre DAMGO: -63.4 ± 0.5 mV; + DAMGO: -64.5 ± 0.8 mV; $t(2) = 0.89$, $p > 0.05$). Thus, it is evident that chromaffin cell depolarization in the presence of 1 µM DAMGO occurs through a GPCR-mediated mechanism. FSCV experiments have determined that blockade of opioid receptors, which are GPCRs, with naltrexone attenuated this catecholamine secretion. Together with the electrophysiology results, it is likely that this could be due to MOR-activation by DAMGO,

directly on the chromaffin cell of interest, producing a *depolarization*, as this is not the case when GDP-β-s blocks signaling via the MOR.

The last receptor examined in this response was the muscarinic acetylcholine receptor (mAChR), another GPCR located on the chromaffin cell. There are heavy stores of ACh in the splanchnic nerve, thus, it is likely that a basal level of ACh is present in the extracellular space in the slice preparation. It is possible that GDP-β-s results in a blockade of ACh signaling via mAChRs as well. In order to test this hypothesis, the mAChR antagonist scopolamine was added to the running buffer 5 minutes prior to the addition of DAMGO, without GDP-β-s in the internal solution. As shown in Figure 3.6D, in the presence of scopolamine in the buffer, DAMGO failed to depolarize the chromaffin cells (Pre DAMGO: -68.4 ± 4.2 mV; + DAMGO: -68.1 ± 3.6 mV; $t(4) = 0.30$, $p > 0.05$). Thus, it seems that the mAChR may be necessary for depolarization of the cells by DAMGO. Considering naltrexone blocked catecholamine release in the voltammetric experiments, it is clear that both MORs and mAChRs contribute to chromaffin cell depolarization following exposure to DAMGO. Importantly, this is in accord with a report by Samways and Henderson[88] , in which activation of MORs resulted in increased intracellular calcium concentrations, but only when the mAChRs were occupied.

Collectively, the results demonstrate that M-ENK, through MOR agonism, can elicit catecholamine release in the adrenal gland, which is mediated in part by ACh signaling via available mAChRs. Furthermore, this stimulatory influence is evident in the striatal region of the brain as well, as M-ENK augments electrically evoked dopamine release. These results appear contrary to the body of literature which suggests that M-ENK serves to attenuate catecholamine signaling by other mechanisms.[12, 59] However, this traditional understanding has

been arrived at by study with long-term measurement techniques, such as measuring catecholamine content in the cell bath following stimulation. It appears, then, that while there may be a long-term attenuation in catecholamine signaling, there is a short-term potentiation which was previously hidden by the long-term timescale of the chemical measurements.

3.4 Conclusion

The opioid system is strikingly complex, and the precise interaction between opioid peptides and catecholamines in the adrenal gland is not well understood. We have shown that M-ENK serves to modulate catecholamine secretion through acetylcholine signaling in the adrenal medulla, as well as modulating dopamine release in the striatal region of the brain. Addition of M-ENK to the running buffer results in a 68% increase in catecholamine release in the adrenal medulla in response to stimulation by nicotine. Addition of M-ENK to the running buffer in an acute brain slice preparation results in a 16% increase in dopamine release in the striatum, in response to electrical stimulation.

Additionally, catecholamine secretion can be elicited in the adrenal medulla by application of met-enkephalin (M-ENK). This response can be monitored with FSCV by implementing a sawhorse waveform, which remedies the problem of fouling encountered with a conventional triangular waveform. The secretion of catecholamines occurs in response to the MOR agonist DAMGO, while the DOR agonist DPDPE elicits no measurable secretion of catecholamine. The opioid receptor antagonist, naltrexone, attenuates the secretion of

catecholamines by met-enkephalin. Using electrophysiology to monitor cell membrane potential of patched chromaffin cells, we have observed the depolarization of the cells in response to bath application of DAMGO, which is blocked by GDP-β-s, a drug that blocks all GPCR signaling only in the recorded cell. Additionally, application of the muscarinic acetylcholine receptor (mAChR) antagonist, scopolamine, blocks the depolarization of the cell by DAMGO. The combined FSCV and electrophysiology results demonstrate that M-ENK elicits catecholamine secretion by depolarizing chromaffin cells through the mu-opioid receptor, and that this effect is dependent on acetylcholine signaling through the mAChR as well.

The data presented herein provide valuable information into the role that M-ENK plays in eliciting and modulating short-term catecholamine release in the adrenal gland and in the brain. By using FSCV and electrophysiology, we have observed signaling that happens on a rapid time scale which seems opposite to the long term effect of M-ENK administration, which has been studied in depth by sampling techniques. This demonstrates how crucial it is to understand the limitations of each measurement methodology, and to study neurological phenomena with both long-term sampling techniques, and also rapid, real-time measurements such as FSCV.

3.5 Acknowledgements

We thank the Chemistry Department (North Carolina State University) for funding this work, and David Dorris (Biological Sciences, North Carolina State University) for invaluable assistance with electrophysiology experiments. This material is based upon work supported by

the National Science Foundation Graduate Research Fellowship under Grant No. (DGE-1252376).

3.6 Associated Content

Supplemental Figure F1 is found in Appendix F.

3.6 References

1. Barzel, U. S. Textbook of Endocrinology - Williams,Rh. *Journal of the American Geriatrics Society* **1982,** *30* (11), 727-727.

2. Wakade, A. R.; Wakade, T. D. Contribution of Nicotinic and Muscarinic Receptors in the Secretion of Catecholamines Evoked by Endogenous and Exogenous Acetylcholine. *Neuroscience* **1983,** *10* (3), 973-978.

3. Barron, B. A.; Hexum, T. D. Release of catecholamines and [Met5]enkephalin immunoreactive material from perfused bovine adrenal glands. *Eur. J. Pharmacol.* **1984,** *106* (3), 593-9.

4. Podvin, S.; Bundey, R.; Toneff, T.; Ziegler, M.; Hook, V. Profiles of secreted neuropeptides and catecholamines illustrate similarities and differences in response to stimulation by distinct secretagogues. *Mol Cell Neurosci* **2015,** *68*, 177-85.

5. Bader, M. F.; Holz, R. W.; Kumakura, K.; Vitale, N. Exocytosis: The chromaffin cell as a model system. *Chromaffin Cell: Trnsmitter Biosynthesis, Storage, Release, Actions, and Informatics* **2002,** *971*, 178-183.

6. Travis, E. R.; Wightman, R. M. Spatio-temporal resolution of exocytosis from individual cells. *Annu. Rev. Biophys. Biomol. Struct.* **1998,** *27*, 77-103.

7. von Gersdorff, H.; Matthews, G. Electrophysiology of synaptic vesicle cycling. *Annual Review of Physiology* **1999,** *61*, 725-752.

8. Suudhof, T. C. Neurotransmitter release. *Handb. Exp. Pharmacol.* **2008,** (184), 1-21.

9. Borges, R.; Camacho, M.; Gillis, K. D. Measuring secretion in chromaffin cells using electrophysiological and electrochemical methods. *Acta Physiologica* **2008,** *192* (2), 173-184.

10. Kleppisch, T.; Ahnerthilger, G.; Gollasch, M.; Spicher, K.; Hescheler, J.; Schultz, G.; Rosenthal, W. Inhibition of Voltage-Dependent Ca2+ Channels Via Alpha-2-Adrenergic and Opioid Receptors in Cultured Bovine Adrenal Chromaffin Cells. *Pflugers Archiv-European Journal of Physiology* **1992,** *421* (2-3), 131-137.

11. Bunn, S. J.; Marley, P. D.; Livett, B. G. The Distribution of Opioid Binding Subtypes in the Bovine Adrenal-Medulla. *Neuroscience* **1988,** *27* (3), 1081-1094.

12. Kumakura, K.; Karoum, F.; Guidotti, A.; Costa, E. Modulation of Nicotinic Receptors by Opiate Receptor Agonists in Cultured Adrenal Chromaffin Cells. *Nature* **1980,** *283* (5746), 489-492.

13. Stern, A. S.; Lewis, R. V.; Kimura, S.; Rossier, J.; Gerber, L. D.; Brink, L.; Stein, S.; Udenfriend, S. Isolation of the Opioid Heptapeptide Met-Enkephalin [Arg6,Phe7] from Bovine Adrenal-Medullary Granules and Striatum. *Proceedings of the National Academy of Sciences of the United States of America* **1979,** *76* (12), 6680-6683.

14. Livett, B. G.; Dean, D. M.; Whelan, L. G.; Udenfriend, S.; Rossier, J. Co-Release of Enkephalin and Catecholamines from Cultured Adrenal Chromaffin Cells. *Nature* **1981,** *289* (5795), 317-319.

15. Johnson, P. I.; Stellar, J. R.; Paul, A. D. Regional reward differences within the ventral pallidum are revealed by microinjections of a mu opiate receptor agonist. *Neuropharmacology* **1993,** *32* (12), 1305-14.

16. Smith, K. S.; Berridge, K. C. The ventral pallidum and hedonic reward: neurochemical maps of sucrose "liking" and food intake. *Journal of Neuroscience* **2005,** *25* (38), 8637-49.

17. Smith, K. S.; Tindell, A. J.; Aldridge, J. W.; Berridge, K. C. Ventral pallidum roles in reward and motivation. *Behavioural Brain Research* **2009,** *196* (2), 155-67.

18. Kelley, A. E.; Bakshi, V. P.; Haber, S. N.; Steininger, T. L.; Will, M. J.; Zhang, M. Opioid modulation of taste hedonics within the ventral striatum. *Physiology & Behavior* **2002,** *76* (3), 365-77.

19. McBride, W. J.; Murphy, J. M.; Ikemoto, S. Localization of brain reinforcement mechanisms: intracranial self-administration and intracranial place-conditioning studies. *Behavioural Brain Research* **1999,** *101* (2), 129-52.

20. Pasternak, G. W.; Pan, Y. X. Mu opioids and their receptors: evolution of a concept. *Pharmacological Reviews* **2013,** *65* (4), 1257-317.

21. Koprich, J. B.; Fox, S. H.; Johnston, T. H.; Goodman, A.; Le Bourdonnec, B.; Dolle, R. E.; DeHaven, R. N.; DeHaven-Hudkins, D. L.; Little, P. J.; Brotchie, J. M. The selective mu-opioid receptor antagonist ADL5510 reduces levodopa-induced dyskinesia without affecting antiparkinsonian action in MPTP-lesioned macaque model of Parkinson's disease. *Movement disorders : official journal of the Movement Disorder Society* **2011,** *26* (7), 1225-33.

22. Koizumi, H.; Morigaki, R.; Okita, S.; Nagahiro, S.; Kaji, R.; Nakagawa, M.; Goto, S. Response of striosomal opioid signaling to dopamine depletion in 6-hydroxydopamine-lesioned rat model of Parkinson's disease: a potential compensatory role. *Frontiers in cellular neuroscience* **2013,** *7*, 74.

23. Marti, M.; Rodi, D.; Li, Q.; Guerrini, R.; Fasano, S.; Morella, I.; Tozzi, A.; Brambilla, R.; Calabresi, P.; Simonato, M.; Bezard, E.; Morari, M. Nociceptin/orphanin FQ receptor agonists attenuate L-DOPA-induced dyskinesias. *The Journal of neuroscience : the official journal of the Society for Neuroscience* **2012,** *32* (46), 16106-19.

24. Tekes, K.; Tariq, S.; Adeghate, E.; Laufer, R.; Hashemi, F.; Siddiq, A.; Kalasz, H. Nociceptinergic system as potential target in Parkinson's disease. *Mini reviews in medicinal chemistry* **2013,** *13* (10), 1389-97.

25. Gerrits, M. A.; Patkina, N.; Zvartau, E. E.; van Ree, J. M. Opioid blockade attenuates acquisition and expression of cocaine-induced place preference conditioning in rats. *Psychopharmacology* **1995,** *119* (1), 92-8.

26. Mitchell, J. M.; Bergren, L. J.; Chen, K. S.; Rowbotham, M. C.; Fields, H. L. Naltrexone aversion and treatment efficacy are greatest in humans and rats that actively consume high levels of alcohol. *Neurobiology of Disease* **2009,** *33* (1), 72-80.

27. Mitchell, J. M.; O'Neil, J. P.; Janabi, M.; Marks, S. M.; Jagust, W. J.; Fields, H. L. Alcohol consumption induces endogenous opioid release in the human orbitofrontal cortex and nucleus accumbens. *Science Translational Medicine* **2012,** *4* (116), 116ra6.

28. Olive, M. F.; Maidment, N. T. Repeated heroin administration increases extracellular opioid peptide-like immunoreactivity in the globus pallidus/ventral pallidum of freely moving rats. *Psychopharmacology* **1998,** *139* (3), 251-4.

29. Skoubis, P. D.; Maidment, N. T. Blockade of ventral pallidal opioid receptors induces a conditioned place aversion and attenuates acquisition of cocaine place preference in the rat. *Neuroscience* **2003,** *119* (1), 241-9.

30. Tang, X. C.; McFarland, K.; Cagle, S.; Kalivas, P. W. Cocaine-induced reinstatement requires endogenous stimulation of mu-opioid receptors in the ventral pallidum. *Journal of Neuroscience* **2005,** *25* (18), 4512-20.

31. Levine, J. D.; Gordon, N. C.; Fields, H. L. The mechanism of placebo analgesia. *Lancet* **1978,** *2* (8091), 654-7.

32. Trujillo, K. A.; Belluzzi, J. D.; Stein, L. Naloxone blockade of amphetamine place preference conditioning. *Psychopharmacology* **1991,** *104* (2), 265-74.

33. Biala, G.; Langwinski, R. Rewarding properties of some drugs studied by place preference conditioning. *Polish journal of pharmacology* **1996,** *48* (4), 425-30.

34. Hughes, J.; Smith, T. W.; Kosterlitz, H. W.; Fothergill, L. A.; Morgan, B. A.; Morris, H. R. Identification of two related pentapeptides from the brain with potent opiate agonist activity. *Nature* **1975,** *258* (5536), 577-80.

35. Schultzberg, M.; Hokfelt, T.; Lundberg, J. M.; Terenius, L.; Elfvin, L. G.; Elde, R. Enkephalin-like immunoreactivity in nerve terminals in sympathetic ganglia and adrenal medulla and in adrenal medullary gland cells. *Acta Physiol Scand* **1978,** *103* (4), 475-7.

36. Schultzberg, M.; Lundberg, J. M.; Hokfelt, T.; Terenius, L.; Brandt, J.; Elde, R. P.; Goldstein, M. Enkephalin-like immunoreactivity in gland cells and nerve terminals of the adrenal medulla. *Neuroscience* **1978,** *3* (12), 1169-86.

37. Akil, H.; Watson, S. J.; Young, E.; Lewis, M. E.; Khachaturian, H.; Walker, J. M. Endogenous Opioids - Biology and Function. *Annual Review of Neuroscience* **1984,** *7*, 223-255.

38. Murphy, N. P. Dynamic measurement of extracellular opioid activity: status quo, challenges, and significance in rewarded behaviors. *ACS Chem Neurosci* **2015,** *6* (1), 94-107.

39. Margolis, E. B.; Hjelmstad, G. O.; Fujita, W.; Fields, H. L. Direct bidirectional mu-opioid control of midbrain dopamine neurons. *J. Neurosci.* **2014,** *34* (44), 14707-16.

40. Johnson, S. W.; North, R. A. Opioids excite dopamine neurons by hyperpolarization of local interneurons. *J. Neurosci.* **1992,** *12* (2), 483-8.

41. Iegorova, O.; Fisyunov, A.; Krishtal, O. G-protein-independent modulation of P-type calcium channels by mu-opioids in Purkinje neurons of rat. *Neuroscience Letters* **2010,** *480* (2), 106-111.

42. Viveros, O. H.; Diliberto, E. J., Jr.; Hazum, E.; Chang, K. J. Opiate-like materials in the adrenal medulla: evidence for storage and secretion with catecholamines. *Mol Pharmacol* **1979,** *16* (3), 1101-8.

43. O'Connor, D. T.; Klein, R. L.; Thureson-Klein, A. K.; Barbosa, J. A. Chromogranin A: localization and stoichiometry in large dense core catecholamine storage vesicles from sympathetic nerve. *Brain Res* **1991,** *567* (2), 188-96.

44. Neuman, B.; Wiedermann, C. J.; Fischer-Colbrie, R.; Schober, M.; Sperk, G.; Winkler, H. Biochemical and functional properties of large and small dense-core vesicles in sympathetic nerves of rat and ox vas deferens. *Neuroscience* **1984,** *13* (3), 921-31.

45. Klein, R. L.; Wilson, S. P.; Dzielak, D. J.; Yang, W. H.; Viveros, O. H. Opioid peptides and noradrenaline co-exist in large dense-cored vesicles from sympathetic nerve. *Neuroscience* **1982,** *7* (9), 2255-61.

46. van Zessen, R.; Phillips, J. L.; Budygin, E. A.; Stuber, G. D. Activation of VTA GABA neurons disrupts reward consumption. *Neuron* **2012,** *73* (6), 1184-94.

47. Roberts, J. G.; Moody, B. P.; McCarty, G. S.; Sombers, L. A. Specific Oxygen-Containing Functional Groups on the Carbon Surface Underlie an Enhanced Sensitivity to Dopamine at Electrochemically Pretreated Carbon Fiber Microelectrodes. *Langmuir* **2010,** *26*, 9116-9122.

48. Lemos, J. C.; Wanat, M. J.; Smith, J. S.; Reyes, B. A. S.; Hollon, N. G.; Van Bockstaele, E. J.; Chavkin, C.; Phillips, P. E. M. Severe stress switches CRF action in the nucleus accumbens from appetitive to aversive. *Nature* **2012,** *490* (7420), 402-+.

49. John, C. E.; Budygin, E. A.; Mateo, Y.; Jones, S. R. Neurochemical characterization of the release and uptake of dopamine in ventral tegmental area and serotonin in substantia nigra of the mouse. *J. Neurochem.* **2006,** *96* (1), 267-282.

50. Ariansen, J. L.; Heien, M.; Hermans, A.; Phillips, P. E. M.; Hernadi, I.; Bermudez, M. A.; Schultz, W.; Wightman, M. Monitoring extracellular pH, oxygen, and dopamine during reward delivery in the striatum of primates. *Front. Behav. Neurosci.* **2012,** *6*.

51. Sombers, L. A.; Beyene, M.; Carelli, R. M.; Wightman, R. M. Synaptic Overflow of Dopamine in the Nucleus Accumbens Arises from Neuronal Activity in the Ventral Tegmental Area. *J. Neurosci.* **2009,** *29* (6), 1735-1742.

52. Roitman, M. F.; Wheeler, R. A.; Wightman, R. M.; Carelli, R. M. Real-time chemical responses in the nucleus accumbens differentiate rewarding and aversive stimuli. *Nat Neurosci* **2008,** *11* (12), 1376-7.

53. Leszczyszyn, D. J.; Jankowski, J. A.; Viveros, O. H.; Diliberto, E. J.; Near, J. A.; Wightman, R. M. Secretion of Catecholamines from Individual Adrenal-Medullary Chromaffin Cells. *J. Neurochem.* **1991,** *56* (6), 1855-1863.

54. Wightman, R. M.; Jankowski, J. A.; Kennedy, R. T.; Kawagoe, K. T.; Schroeder, T. J.; Leszczyszyn, D. J.; Near, J. A.; Diliberto, E. J.; Viveros, O. H. Temporally Resolved Catecholamine Spikes Correspond to Single Vesicle Release from Individual Chromaffin Cells. *P Natl Acad Sci USA* **1991,** *88* (23), 10754-10758.

55. Walsh, P. L.; Petrovic, J.; Wightman, R. M. Distinguishing splanchnic nerve and chromaffin cell stimulation in mouse adrenal slices with fast-scan cyclic voltammetry. *American Journal of Physiology-Cell Physiology* **2011,** *300* (1), C49-C57.

56. Petrovic, J.; Walsh, P. L.; Thornley, K. T.; Miller, C. E.; Wightman, R. M. Real-time monitoring of chemical transmission in slices of the murine adrenal gland. *Endocrinology* **2010,** *151* (4), 1773-83.

57. Roberts, J. G.; Lugo-Morales, L. Z.; Loziuk, P. L.; Sombers, L. A. Real-time chemical measurements of dopamine release in the brain. *Methods in molecular biology* **2013,** *964*, 275-94.

58. Whim, M. D. Near simultaneous release of classical and peptide cotransmitters from chromaffin cells. *J. Neurosci.* **2006,** *26* (24), 6637-42.

59. Kimura, T.; Katoh, M.; Satoh, S. Inhibition by Opioid Agonists and Enhancement by Antagonists of the Release of Catecholamines from the Dog Adrenal-Gland in Response to Splanchnic Nerve-Stimulation - Evidence for the Functional-Role of Opioid Receptors. *J. Pharmacol. Exp. Ther.* **1988,** *244* (3), 1098-1102.

60. Tome, A. R.; Izaguirre, V.; Rosario, L. M.; Cena, V.; Gonzalez-Garcia, C. Naloxone inhibits nicotine-induced receptor current and catecholamine secretion in bovine chromaffin cells. *Brain Res* **2001,** *903* (1-2), 62-5.

61. Lemaire, S.; Livett, B.; Tseng, R.; Mercier, P.; Lemaire, I. Studies on the inhibitory action of opiate compounds in isolated bovine adrenal chromaffin cells: noninvolvement of stereospecific opiate binding sites. *J. Neurochem.* **1981,** *36* (3), 886-92.

62. Freed, A. L.; Cooper, J. D.; Davies, M. I.; Lunte, S. M. Investigation of the metabolism of substance P in rat striatum by microdialysis sampling and capillary electrophoresis with laser-induced fluorescence detection. *Journal of Neuroscience Methods* **2001,** *109* (1), 23-9.

63. Zhou, Y.; Mabrouk, O. S.; Kennedy, R. T. Rapid preconcentration for liquid chromatography-mass spectrometry assay of trace level neuropeptides. *Journal of the American Society for Mass Spectrometry* **2013,** *24* (11), 1700-9.

64. DiFeliceantonio, A. G.; Mabrouk, O. S.; Kennedy, R. T.; Berridge, K. C. Enkephalin surges in dorsal neostriatum as a signal to eat. *Current Biology* **2012,** *22* (20), 1918-24.

65. Kostel, K. L.; Lunte, S. M. Evaluation of capillary electrophoresis with post-column derivatization and laser-induced fluorescence detection for the determination of substance P and its metabolites. *Journal of Chromatography. B, Biomedical Sciences and Applications* **1997,** *695* (1), 27-38.

66. Haskins, W. E.; Wang, Z.; Watson, C. J.; Rostand, R. R.; Witowski, S. R.; Powell, D. H.; Kennedy, R. T. Capillary LC-MS2 at the attomole level for monitoring and discovering endogenous peptides in microdialysis samples collected in vivo. *Analytical Chemistry* **2001,** *73* (21), 5005-14.

67. Desiderio, D. M.; Zhu, X. Quantitative analysis of methionine enkephalin and beta-endorphin in the pituitary by liquid secondary ion mass spectrometry and tandem mass spectrometry. *Journal of Chromatography A* **1998,** *794* (1-2), 85-96.

68. Sinnaeve, B. A.; Storme, M. L.; Van Bocxlaer, J. F. Capillary liquid chromatography and tandem mass spectrometry for the quantification of enkephalins in cerebrospinal fluid. *Journal of Separation Science* **2005,** *28* (14), 1779-84.

69. Dawson, R., Jr.; Steves, J. P.; Lorden, J. F.; Oparil, S. Reverse-phase separation and electrochemical detection of neuropeptides. *Peptides* **1985,** *6* (6), 1173-8.

70. Shen, H.; Lada, M. W.; Kennedy, R. T. Monitoring of met-enkephalin in vivo with 5-min temporal resolution using microdialysis sampling and capillary liquid chromatography with electrochemical detection. *Journal of Chromatography. B, Biomedical Sciences and Applications* **1997,** *704* (1-2), 43-52.

71. Marinelli, P. W.; Lam, M.; Bai, L.; Quirion, R.; Gianoulakis, C. A microdialysis profile of dynorphin A(1-8) release in the rat nucleus accumbens following alcohol administration. *Alcoholism, Clinical and Experimental Research* **2006,** *30* (6), 982-90.

72. Maidment, N. T.; Brumbaugh, D. R.; Rudolph, V. D.; Erdelyi, E.; Evans, C. J. Microdialysis of extracellular endogenous opioid peptides from rat brain in vivo. *Neuroscience* **1989,** *33* (3), 549-57.

73. Olive, M. F.; Bertolucci, M.; Evans, C. J.; Maidment, N. T. Microdialysis reveals a morphine-induced increase in pallidal opioid peptide release. *Neuroreport* **1995,** *6* (8), 1093-6.

74. Olive, M. F.; Maidment, N. T. Opioid regulation of pallidal enkephalin release: bimodal effects of locally administered mu and delta opioid agonists in freely moving rats. *J. Pharmacol. Exp. Ther.* **1998,** *285* (3), 1310-6.

75. Liu, Z.; Welin, M.; Bragee, B.; Nyberg, F. A high-recovery extraction procedure for quantitative analysis of substance P and opioid peptides in human cerebrospinal fluid. *Peptides* **2000,** *21* (6), 853-60.

76. North, R. A.; Williams, J. T.; Surprenant, A.; Christie, M. J. Mu-Receptor and Delta-Receptor Belong to a Family of Receptors That Are Coupled to Potassium Channels. *Proceedings of the National Academy of Sciences of the United States of America* **1987,** *84* (15), 5487-5491.

77. Meunier, C. J.; Roberts, J. G.; McCarty, G. S.; Sombers, L. A. Background Signal as an in Situ Predictor of Dopamine Oxidation Potential: Improving Interpretation of Fast-Scan Cyclic Voltammetry Data. *ACS Chem. Neurosci.* **2017,** *8* (2), 411-419.

78. Smith, S. K.; Lee, C. A.; Dausch, M. E.; Horman, B. M.; Patisaul, H. B.; McCarty, G. S.; Sombers, L. A. Simultaneous Voltammetric Measurements of Glucose and Dopamine Demonstrate the Coupling of Glucose Availability with Increased Metabolic Demand in the Rat Striatum. *ACS Chem Neurosci* **2017,** *8* (2), 272-280.

79. Schmidt, A. C.; Dunaway, L. E.; Roberts, J. G.; McCarty, G. S.; Sombers, L. A. Multiple Scan Rate Voltammetry for Selective Quantification of Real-Time Enkephalin Dynamics. *Anal. Chem.* **2014,** *86* (15), 7806-7812.

80. Le Merrer, J.; Becker, J. A. J.; Befort, K.; Kieffer, B. L. Reward Processing by the Opioid System in the Brain. *Physiological Reviews* **2009,** *89* (4), 1379-1412.

81. Paras, C. D.; Kennedy, R. T. Amperometry and cyclic voltammetry of tyrosine and tryptophan-containing oligopeptides at carbon fiber microelectrodes applied to single cell analysis. *Electroanalysis* **1997,** *9* (3), 203-208.

82. Takmakov, P.; Zachek, M. K.; Keithley, R. B.; Walsh, P. L.; Donley, C.; McCarty, G. S.; Wightman, R. M. Carbon microelectrodes with a renewable surface. *Anal. Chem.* **2010,** *82* (5), 2020-8.

83. Mitchell, E. C.; Dunaway, L. E.; McCarty, G. S.; Sombers, L. A. Spectroelectrochemical Characterization of the Dynamic Carbon-Fiber Surface in Response to Electrochemical Conditioning. *Langmuir [Just Accepted]* **2017**.

84. Ross, A. E.; Nguyen, M. D.; Privman, E.; Venton, B. J. Mechanical stimulation evokes rapid increases in extracellular adenosine concentration in the prefrontal cortex. *J. Neurochem.* **2014,** *130* (1), 50-60.

85. Di Angelantonio, S.; Matteoni, C.; Fabbretti, E.; Nistri, A. Molecular biology and electrophysiology of neuronal nicotinic receptors of rat chromaffin cells. *Eur J Neurosci* **2003,** *17* (11), 2313-22.

86. Al-Hasani, R.; Bruchas, M. R. Molecular mechanisms of opioid receptor-dependent signaling and behavior. *Anesthesiology* **2011,** *115* (6), 1363-81.

87. Vaughan, C. W.; Ingram, S. L.; Connor, M. A.; Christie, M. J. How opioids inhibit GABA-mediated neurotransmission. *Nature* **1997,** *390* (6660), 611-4.

88. Samways, D. S. K.; Li, W. H.; Conway, S. J.; Holmes, A. B.; Bootman, M. D.; Henderson, G. Co-incident signalling between mu-opioid and M-3 muscarinic receptors at the level of Ca2+ release from intracellular stores: lack of evidence for Ins(1,4,5)P-3 receptor sensitization. *Biochem. J* **2003,** *375*, 713-720.

CHAPTER 4

Multiple Scan Rate Voltammetry for Selective Quantification of Real-Time Enkephalin Dynamics

The following work was reprinted with permission from: Schmidt, A.C., Dunaway, L.E., Roberts, J.G., McCarty, G.S., and Sombers, L.A. *Anal. Chem.*, **2014**, *86 (15)*, pp 7806-7812. Supplemental information is found in Appendix G.

4.1 Introduction

Determining how specific neurochemical fluctuations underlie neurological disorders is a key step in developing appropriate therapies; however, in most cases the neurochemistry is not well understood. This is particularly true in the case of endogenous opioid neuropeptides - a class of signaling molecules that play a key role in modulating a wide variety of complex physiological functions, including reward processing,[1-5] nociception,[6] various neuropathologies,[7-10] and the biochemical response to multiple drugs of abuse.[11-16] However, our understanding of the mechanisms that underlie these functions remain limited, and there is a fundamental gap in our knowledge of when, where, and how these peptides are released. The opioid system is tremendously complex. The mu, delta, and kappa receptors (MOR, DOR, and KOR, respectively) are differentially expressed throughout the brain,[17, 18] and no endogenous opioid peptide family is exclusively associated with a specific receptor type.[19] Gene expression has been used to identify neurons that produce the mRNA of the known precursor molecules for the endogenous opioids: pre-proenkephalin, pre-proopiomelanocortin, and pre-prodynorphin. However, cleavage of neuropeptides, for example of proenkephalin, can yield a

variety of peptides including M-ENK, L-ENK, metorphamide, and peptides E and F.[20] Even more critically, prodynorphin molecules can give rise to either the KOR-acting dynorphin or the MOR/DOR-acting L-ENK; yet KOR and MOR/DOR are generally believed to serve opposing functions in most brain circuits.[19, 21] Therefore, even a thorough anatomical characterization of the opioid system is not sufficient to understand the dynamic contribution of individual opioid peptides to brain function.

Although the potential importance of monitoring specific opioid peptides in living brain tissue is widely appreciated, the experimental tools that are available to date all have known caveats and limitations. Imaging the displacement of radiolabeled agonists is a powerful approach;[13] however, it is expensive, largely static, and usually requires human subjects. Coupling microdialysis to analytical measurements[22-30] or radioimmunoassay[14, 31-35] has proven invaluable to the study of neuropeptide function; however, its utility is limited by poor temporal and spatial resolution. Furthermore, peptide fibers are widely dispersed in brain tissue. If a probe is not contained directly in the field of the release sites, an underestimation in the magnitude of detected chemical changes results.[23] This is a significant drawback when quantifying low abundance molecules, such as opioid neuropeptides.

Fast-scan cyclic voltammetry is an established technique that is often used to monitor fluctuating dopamine levels in living brain tissue,[36-44] and has recently been extended to other molecules such as adenosine,[45, 46] hydrogen peroxide,[47] serotonin,[39, 48-51] local pH changes,[40, 52] and norepinephrine.[53, 54] This electrochemical approach can not only simultaneously measure rapid fluctuations of multiple molecules, but also provides excellent spatial resolution when coupled to carbon-fiber microelectrodes. It boasts chemical selectivity that is not

available with other electrochemical techniques, such as chronoamperometry, by collecting individual data points over a wide range of potentials. However, the electrochemical detection of tyrosine-containing neuropeptides, like the ENKs, is challenging. These molecules are presumably present in the extracellular space for only short periods and tend to foul the electrode surface upon oxidation, making it difficult to obtain reproducible measurements. Furthermore, these peptides generally oxidize at higher potentials than catecholamines and other more abundant electroactive molecules, causing possible interferent problems.[30] To overcome the limitations that have previously inhibited the application of this approach to the detection of peptides, we have designed and characterized a modified sawhorse waveform (MSW) that uses two distinct scan rates in each anodic sweep and a short holding period at the switching potential to eliminate electrode fouling and improve chemical resolution in the detection of tyrosine-containing peptides. The efficacy of this novel approach is demonstrated by simultaneously monitoring the real-time molecular dynamics of catecholamines and M-ENK in living rat adrenal tissue.

4.2 Experimental Section

4.2.1 Chemicals

All chemicals were purchased from Sigma-Aldrich (St. Louis, MO) and used as received, unless otherwise specified. M-ENK, L-ENK, and neurotensin were obtained as acetate salts from LKT Laboratories (St. Paul, MN). Electrochemical experiments were carried out in phosphate buffered saline (0.1 M PBS) or Tris buffer (15 mM Tris, 3.25 mM KCl, 1.20

mM $CaCl_2$, 1.2 mM $MgCl_2$, 2 mM Na_2SO_4, 1.25 mM NaH_2PO_4, 145 mM NaCl), both at physiological pH 7.4. Adrenal slice experiments used bicarbonate buffered saline (BBS) saturated with 95% O_2 and 5% CO_2, at physiological pH 7.4. BBS consisted of 125 mM NaCl, 26 mM $NaHCO_3$, 2.5 mM KCl, 2.0 mM $CaCl_2$, 1.0 mM $MgCl_2$, 1.3 mM NaH_2PO_4, 10 mM HEPES, and 10 mM glucose. All aqueous solutions were made from doubly deionized water >18 MΩ·cm (Millipore, Billerica, MA).

4.2.2 Electrode Fabrication.

All electrochemical experiments were carried out with T-650 carbon-fiber microelectrodes (Cytec Industries, West Patterson, NJ), fabricated as described previously.[55] Briefly, a single 7 μm diameter fiber was aspirated into a single borosilicate glass capillary (1.0 mm x 0.5 mm, A-M Systems, Carlsburg, WA). Using a micropipette puller (Narishige, Tokyo, Japan) the glass was tapered to form sealed microelectrodes which were then cut to 300 μm for experiments involving calibration, reproducibility, and interferent studies. Electrodes cut to 100 μm were used for comparison with conventional waveforms, and 200 μm for the adrenal slice experiment. To establish an electrical connection with the carbon fiber, the glass capillary was backfilled with ionic solution (4 M potassium acetate, 150 mM KCl) and a lead wire was inserted. All measurements were recorded against a Ag/AgCl reference electrode (World Precision Instruments, Inc., Sarasota, FL).

4.2.3 Flow Injection.

All data were collected in a custom-built flow injection apparatus housed within a Faraday cage. A syringe pump (New Era Pump Systems, Inc., Wantagh, NY) supplied a continuous buffer flow of 1 mL/min across both the working and reference electrodes. The working electrode was lowered into the electrochemical cell via a micromanipulator (World Precision Instruments, Inc., Sarasota, FL). Two-second bolus injections of analyte were accomplished using a six-port HPLC valve and air actuator controlled by a digital valve interface (Valco Instruments Co., Inc., Houston, TX).

4.2.4 Electrochemical Waveforms and Data Acquisition.

The novel MSW waveform (Figure 4.1B) was applied at 10 Hz for peptide detection. The potential was held at -0.2 V, then ramped to +0.6 V at 100 V/s, and then raised to +1.2 V at 400 V/s. The potential was then held at +1.2 V for 3 msec before scanning back to the holding potential of -0.2 V at 100 V/s. A more traditional triangular waveform was also used. The potential ranged from -0.2 V to +1.2 V and back at 400 V/s (Figure 4.1A). These waveforms were output using a custom instrument for potential application to the electrochemical cell and current transduction (University of North Carolina at Chapel Hill, Department of Chemistry, Electronics Facility). TH-1 software (ESA, Chelmsford, MA) controlled waveform output. Two PCI bus cards (National Instruments Corp., Austin, TX) were used for collecting data and synchronization of the electrochemical experiment with the flow injection system. Signal processing (background subtraction, signal averaging, and digital

filtering (2-pole Sallen-Key Filter, 2 KHz)) was software-controlled. Electrical stimulations were carried out with a DS-4 Biphasic Stimulus Isolator (Digitimer Ltd., Welwyn Garden City, England), controlled by software written in-house through aforementioned PCI bus cards.

4.2.5 Adrenal Slice Preparation

Animal care and use was in complete accordance with NIH and NC State University institutional guidelines (IACUC). Male Sprague-Dawley rats (250-300 g, Charles River Laboratories, Raleigh, NC) were deeply anesthetized with urethane (1.5 g/kg, ip). The adrenal glands were rapidly removed, trimmed of fat tissue, and embedded in agarose gel containing 3% agarose in BBS. The gel blocks containing the adrenal glands were placed in cold BBS while 400 μm thick slices were obtained with a vibratome (World Precision Instruments, Sarasota, FL). The slices were allowed to rest in the buffer for at least one hour before the start of an experiment. Adrenal slices were subsequently placed in a recording chamber (Warner Instruments, Hamden, CT) and superfused with BBS buffer maintained at 34 °C for at least another 1.5 hours. Carbon-fiber microelectrodes were placed about 100 μm below the surface of the slice, and a twin tungsten electrode was positioned in the tissue approximately 1 mm from the recording electrode for the stimulation experiments. Working electrode and stimulating electrode placements were made with the aid of a microscope (Nikon Instruments, Inc., Melville, NY). Electrical stimulations consisted of trains of 15 biphasic 500 μA pulses, at a frequency of 350 Hz with a pulse-width of 0.5 ms.

4.2.6 Statistics

All data presented are shown as the mean ± standard deviation (stdev). One-tailed Student's *t* tests were used to determine the significance of means. Significance was designated at $p < 0.05$. A Pearson correlation value was calculated for endogenous molecules vs. in vitro standards. Statistical and graphical analysis was carried out using GraphPad Prism 5 (GraphPad Software, Inc., La Jolla, CA).

4.3 Results and Discussion

4.3.1 Met-Enkephalin Cyclic Voltammetry

Cyclic voltammograms (CVs) were initially collected *in vitro* using a standard triangular waveform and a 100 μm long carbon-fiber microelectrode (Figure 4.1A).[47] A scan rate of 400 V/s, ranging from -0.4 V to +1.4 V, was applied at 10 Hz. Figure 4.1C shows a representative background-subtracted CV, as well as the colorplot[56] for a two second bolus injection of 2 μM M-ENK, introduced to electrode surface at the time indicated by the red bar. Current was generated at numerous potentials, and the signal persists long after the end of the injection, indicative of surface fouling (white asterisk, Figure 4.1C). This lowers the sensitivity of the electrode, making reproducible measurements difficult. A modified sawhorse waveform (was developed to retain chemical selectivity and reproducibility, as well as adequate sensitivity and temporal resolution. Specifically, the potential was ramped from -0.2 V to +0.6 V at 100 V/s, then to +1.2 V at 400 V/s and held for 3 msec at this potential. The potential was then ramped back to -0.2 V at 100 V/s (Figure 4.1B). This waveform takes 26.5 msec to apply,

thus allowing measurements to be made at 10 Hz. Since current scales with scan rate, the faster rate was applied only in the potential range of oxidation for our analyte of interest (~1.0 V). By using a slower scan rate in the remainder of the sweep, the faradaic contributions from other analytes were reduced. The potential was held at +1.2 V for 3 msec because research has shown that the adsorption of tyrosine onto the electrode surface weakens above +1.1 V.[57] This waveform produces one resolved peak at about +1.0 V and another less intense peak during the holding time at +1.2 V (Figure 4.1D), suggesting the oxidation of two separate amino acids.

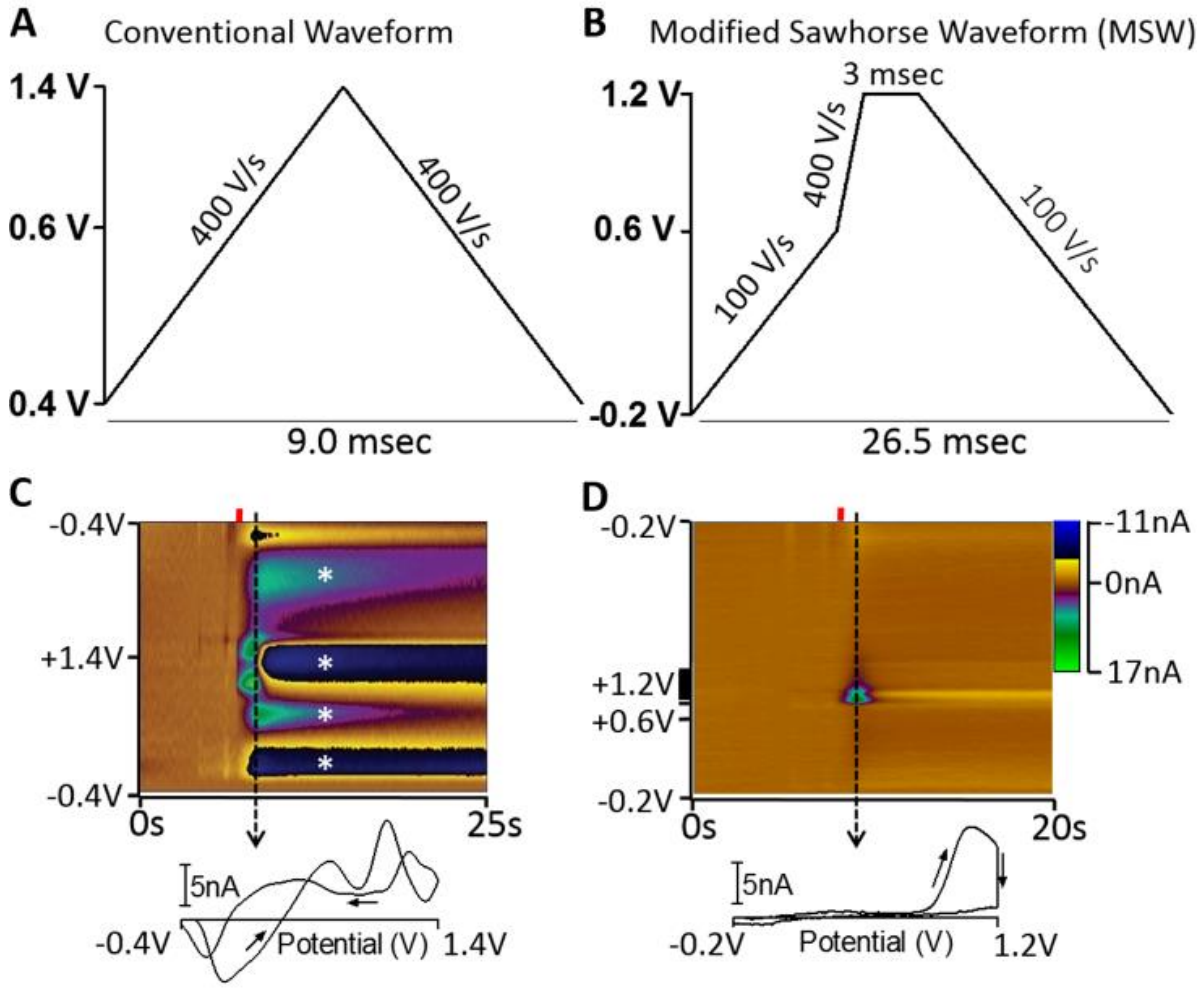

Figure 4.1. (A) Triangular waveform. (B) Modified sawhorse waveform (MSW). (C,D) Representative *in vitro* voltammetric data collected using the waveforms depicted in (A) and (B), respectively, where the ordinate is the potential applied to the carbon-fiber electrode, the abscissa is time in seconds, and the current (nA) is depicted in false color.[56] 2 μM M-ENK was introduced to the microelectrode at the time indicated by the red bar. Displayed voltammograms were extracted at the time indicated by the dashed line.

4.3.2 Electrochemical Moiety.

It was important to isolate which moiety was responsible for the electrochemical response. M-ENK is a five amino-acid chain, as shown in Figure 4.2A (top). The redox activities of tyrosine and methionine have been demonstrated.[58, 59] Conversely, glycine and phenylalanine are not expected to be redox active within the potential window. Voltammograms for tyrosine (left), M-ENK (middle), and methionine (right) are presented as color plots in Figure 4.2A. In Figure 4.2B, the current collected in the hold portion of individual voltammograms for these species is plotted linearly versus waveform point number for the portion of the scan ranging from +0.6 V to +1.2 V and back to +1.0 V, as depicted at the top of the graphic and in Figure G1 (Appendix G). Plotting the data in this manner enables improved visual inspection of both oxidation peaks. Tyrosine is responsible for the first peak in the voltammogram for M-ENK (~1.0V), and methionine contributes to the second peak (during the hold at 1.2V). The slight shift in oxidation potential is likely due to the effect of the additional amino acids on the formal potential of methionine. Tyrosine is the principal contributor to the voltammetry, and was accordingly chosen to be the peak used for quantification purposes. However, tyrosine is a classic example of a molecule that is likely to foul the electrode, thus electrode stability was quantitatively assessed.

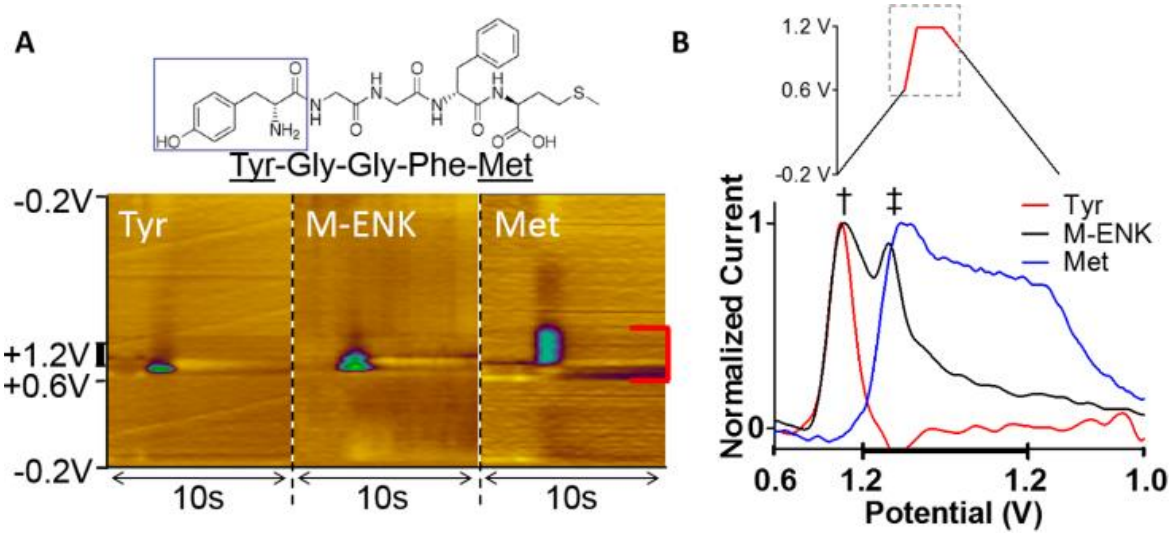

Figure 4.2. M-ENK is a five amino-acid peptide with terminating tyrosine and methionine groups (top). (A) Representative colorplots for 2 μM tyrosine (left), 1 μM M-ENK (middle), and 30 μM methionine (right). (B) To better visualize the current collected during the potential hold period, it is plotted versus waveform point number converted into potential (see Figure G1). The displayed portion is indicated by the dashed box (top). The dagger and double-dagger indicate the first and second oxidation peaks of M-ENK, respectively.

4.3.3 Reproducibility of Met-Enkephalin Electrochemistry

The performance of the novel MSW was compared to a more traditional triangular waveform designed with a holding potential of -0.2 V and a switching potential of +1.2 V, scanned at 400 V/s and applied at 10 Hz. A 2 second bolus of 500 nM M-ENK was introduced to the carbon-fiber electrode for ten consecutive injections (Figure 4.3A). The results demonstrate no loss in measured current when using the MSW (Figure 4.3A), and no distortion in the electrochemical signal after the tenth injection (Figure 4.3A inset). Conversely, the TW showed a significant decrease in signal intensity from baseline ($n = 5$ electrodes, $p < 0.001$) after the sequence of injections (Figure 4.3A), making it impossible to create a linear calibration curve. The electrode fouling increased with higher concentrations of M-ENK when

using the TW waveform, whereas the performance of the MSW was not compromised (Figure G2). These data show that holding the potential at +1.2 V for 3 msec is sufficient to regenerate a clean electrode surface, thus eliminating signal loss due to surface fouling and enabling accurate calibrations for determining sensitivity to M-ENK. Interestingly, increasing the anodic holding potential beyond +1.2 V increased fouling of the electrode, thus constraining the potential to +1.2 V to obtain reproducible results (data not shown).

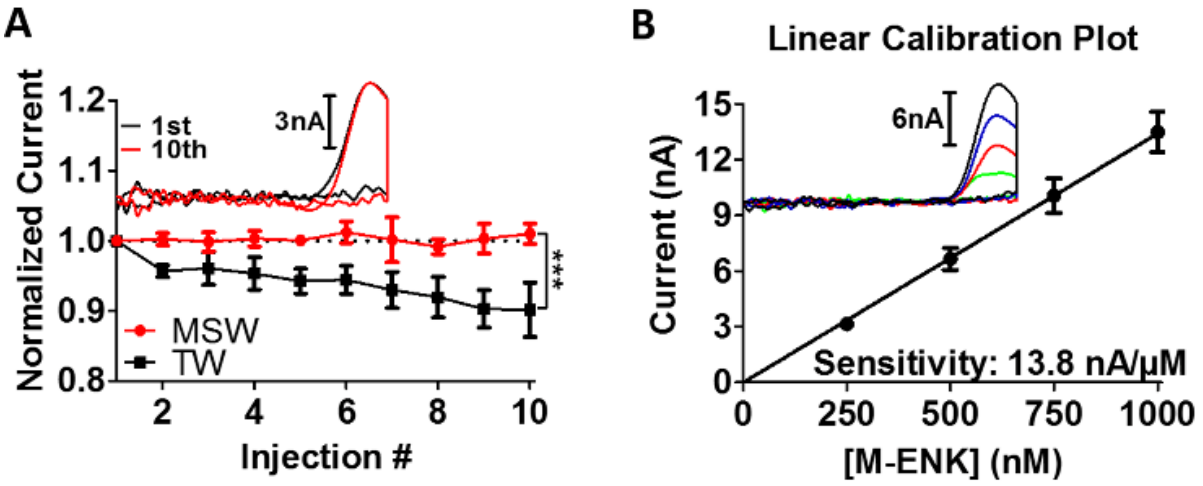

Figure 4.3. Reproducibility. (A) The electrochemical response to 500 nM M-ENK was stable over 10 consecutive injections when using the MSW, but not a more traditional triangular waveform with a potential range from -0.2 V to 1.2 V scanned at 400 V/s (n = 5, $p < 0.001$). The inset shows representative voltammograms corresponding to the first and tenth injection. (B) Calibration curve showing a linear relationship between peak current and M-ENK concentration. Representative voltammograms provided in inset. Data are mean ± stdev, n = 7.

A calibration curve for M-ENK detection using the MSW was created by plotting the linear relationship between peak current (collected at +1.0 V) and analyte concentration (Figure 4.3B). Concentrations ranging from 250 - 1000 nM (n = 7 electrodes, 3 replicates per concentration, $r^2 = 0.99$) were evaluated, affording a sensitivity of 13.8 ± 0.1 nA/µM.

Representative voltammograms are provided in the inset of Figure 4.3B for the various concentrations and show neither a change in peak shape nor a shift in the observed oxidation potential. With this approach, the limit of detection is 27.9 ± 3.5 nM (defined as three times the standard deviation of the noise). The results demonstrate that a reproducible calibration curve can be constructed for M-ENK. However, this single component solution is not representative of the complex recording environment inherent to live tissue.

4.3.4 Selectivity Against Common Interferents

Many electroactive species could potentially interfere with the electrochemical detection of M-ENK in the brain. In the striatum, one of the most likely interferents is dopamine (DA), as it oxidizes more readily than M-ENK and fluctuates at concentrations significantly greater than those expected for M-ENK in tissue.[60] When using a triangular waveform with a typical scan rate of 400 V/s, DA oxidation is evident at approximately +0.6 V (Figure 4.4A, black). The MSW utilizes a relatively slow scan rate (100 V/s) at potentials below 0.6 V, essentially providing two key benefits. Faradaic current scales with scan rate.[61] By slowing the scan rate in the potential region where most interferents oxidize, the current produced for oxidation of those interferents is also significantly reduced, as demonstrated for DA in Figure 4.4A (red). Additionally, for non-Nernstian systems, peak separation increases as scan rate is increased. Thus at a slower scan rate of 100 V/s, the oxidation peak for DA shifts to about +0.4 V (Figure 4.4A, red). Figures 4.4B and 4.4C present voltammograms collected for a mixture containing M-ENK, DA, ascorbic acid (AA), and a pH shift using either a conventional triangular waveform or the novel MSW, respectively. The interferents dominate

the voltammograms collected using the standard triangular waveform, making it difficult to distinguish the analytes. However, when using the MSW with two distinct scan rates in the forward sweep, the current contributed by the possible interferents is diminished, and the signal for M-ENK separates due to the distinct oxidation potentials of these species. (Figure 4.4C). The effects of using different scan rates for the second portion of the anodic scan are further detailed in Figure G3. These results demonstrate the potential of using multiple scan rates in a single sweep to create analyte-specific waveforms that enhance the voltammetric signal due to an analyte of interest by increasing the resolution of the peaks and reducing the contribution to the signal from interferents.

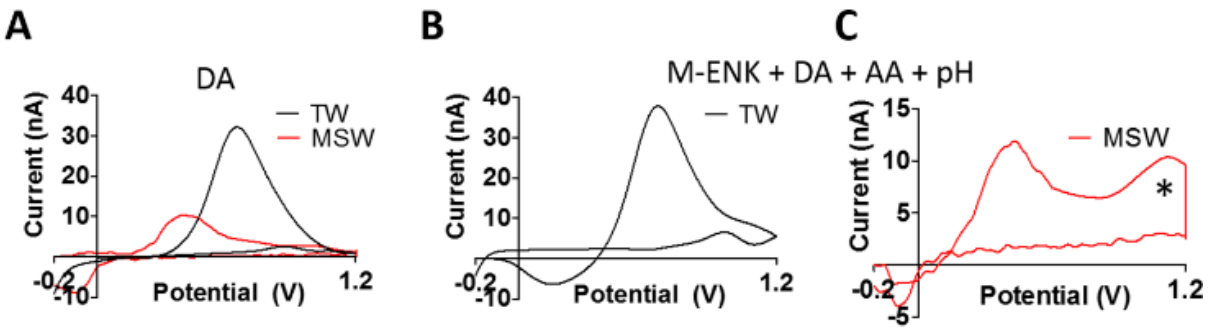

Figure 4.4 (A) Representative voltammetric data for dopamine, and (B,C) a mixture of 0.5 µM M-ENK, 1 µM dopamine, 10 µM ascorbic acid, and a +0.1 pH shift collected using a standard triangular waveform (TW,black) versus the novel MSW (red). Most potential interferents, such as dopamine, oxidize at ~0.6 V. By exploiting scan rate, the MSW reduces the current contributed by potential interferents and shifts their oxidation peaks to a lower potential. This enables the current contributed by M-ENK to be readily distinguished (asterisk) in voltammograms for complex mixtures.

The influence of interfering species was also quantitatively assessed using principal component regression (PCR). PCR is a multivariate statistical analysis technique that first requires principal component analysis to identify the principle components that best describe the variance in the data and then uses linear regression on the selected components to deconvolute these components from the complex data. PCR has been used to distinguish multiple contributors to the voltammetric signal in the past;[62] however, in this case it is not appropriate when using the conventional triangular waveform as the approach requires a linear response to increasing concentrations of the electroactive components and the effects of electrode fouling preclude this. Using the novel MSW, solutions containing varying concentrations of M-ENK in the presence of physiological concentrations of ascorbic acid (AA), dopamine (DA), and pH shifts were interrogated.[63-66] These common biological interferents were selected because they have a known electrochemical response in the potential window used to voltammetrically quantify M-ENK (Figure 4.5A-C). Figure 4.5D shows PCR-predicted concentration versus the actual concentration of M-ENK in mixed solutions that contained each of these analytes. The slope of the regression line for a perfect prediction is unity, and our approach yields a slope of 1.02 (±0.01) (r^2 = 0.99, n = 3 electrodes), indicating that the combination of the novel waveform and PCR was able to appropriately identify and quantify M-ENK in these complex mixtures.

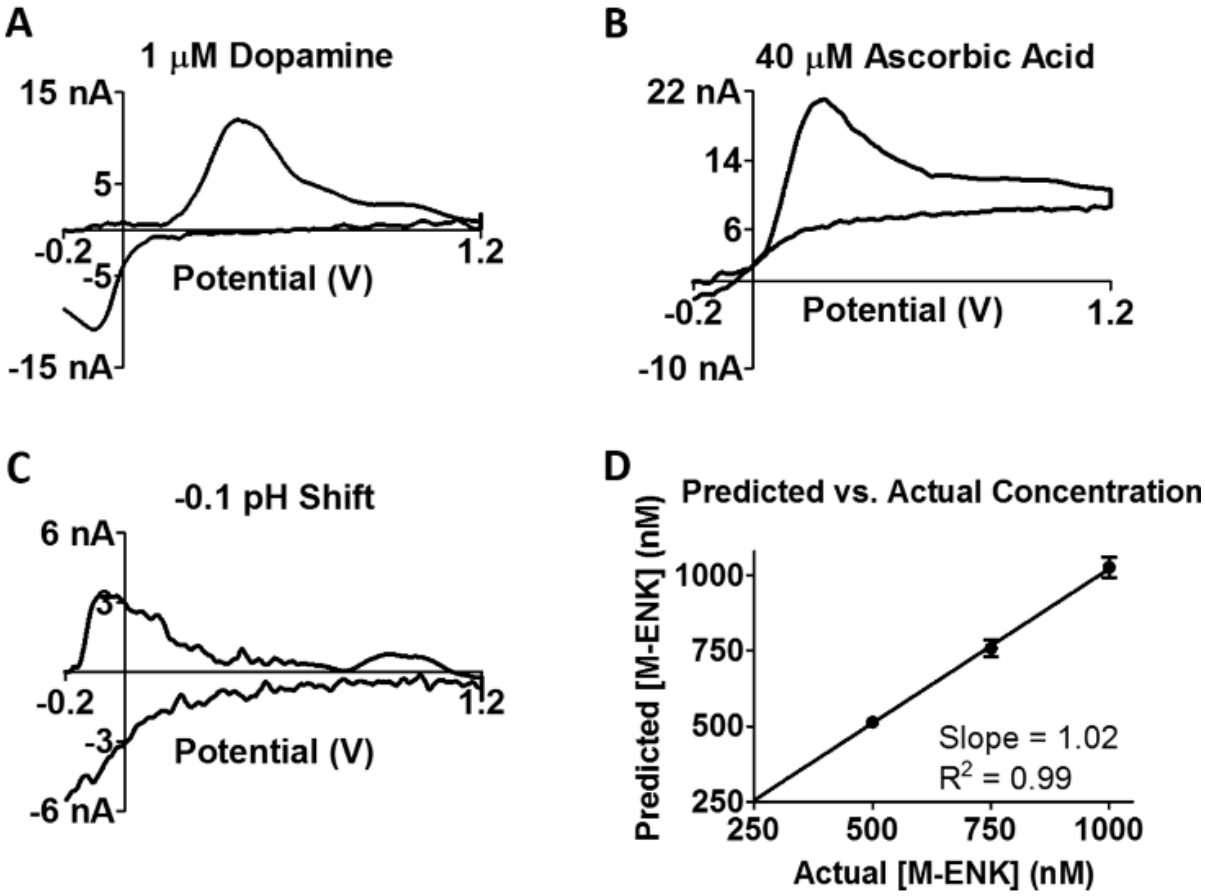

Figure 4.5. Selectivity against common interferents. (A-C) Voltammograms for dopamine, ascorbic acid, and a pH shift collected using the MSW. (D) M-ENK concentrations predicted using PCR compared to known sample concentrations. The diagonal line represents unity for a perfect prediction. The slope of the regression line was 1.02 (±0.01) (r^2 = 0.99, n = 3 electrodes).

4.3.5 Selectivity Against Other Tyrosine-Containing Peptides

There are innumerable peptides present in the brain, and it would be impossible to electrochemically investigate all of them. Having demonstrated that tyrosine was the principal electrochemical moiety, the electrochemical resolution against a few common neuropeptides that contain tyrosine was assessed. Leu-enkephalin (L-ENK) and M-ENK have identical amino acid backbones, but differ only at the C-terminus by either a leucine or a methionine group,

respectively. Neurotensin (NT) is a 13-amino acid neuropeptide containing two tyrosine groups. All three produced an electrochemical response with peak oxidation at ~1.0 V (Figure 4.6A-C). The voltammetric detection of NT produced some electrode fouling, and the color plot is clearly different from those for the enkephalins. Differences between the voltammograms are readily evident when the current is plotted versus point number in the applied waveform (Figure 4.6D). As expected, neither L-ENK nor NT exhibited the second peak inherent to the oxidation of M-ENK (double dagger), as this signal is due to the methionine group. It provides a means of electrochemically distinguishing M-ENK from other peptides including L-ENK, which differs from M-ENK by only a single amino acid. It is important to note that using this approach, any signaling peptides that contained BOTH tyrosine and methionine could not be unequivocally distinguished from M-ENK. However, pharmacology should always be used to verify the electrochemical signal in a biological study, and this approach significantly reduces the number of peptides that could underlie an ambiguous signal.

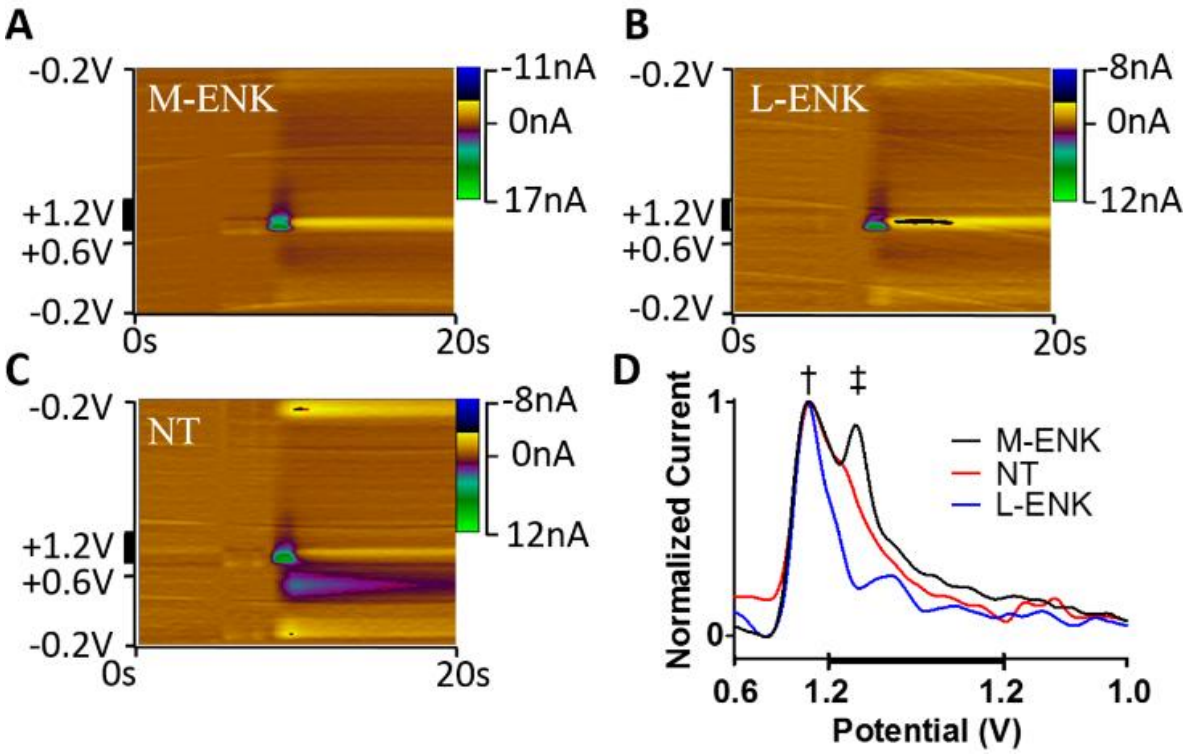

Figure 4.6. Representative voltammetric data collected for 1 μM (A) M-ENK, (B) L-ENK, and (C) NT collected using the MSW. (D) Normalized current plotted versus point number in the applied waveform, focusing on the +0.6 V to +1.2 V to +1.0 V portion of the applied potential. All three analytes share the same first peak (†), but the second peak (‡) inherent to M-ENK allows it to be visually distinguished from the other neuropeptides.

4.3.6 Detecting Met-Enkephalin in Living Adrenal Tissue

Endogenous peptides contribute to the most basic biological systems promoting survival, including managing energy balance and stress responses.[6, 67] To demonstrate the voltammetric detection of endogenous M-ENK in complex living tissue, the novel MSW was used to simultaneously detect electrically evoked catecholamine and M-ENK release in slices of rat adrenal tissue. Proenkephalin-produced peptides are highly concentrated in the adrenal medulla,[67] and adrenal chromaffin cells secrete the ENKs in addition to the catecholamines in

mediating the biological response to stressors.[68] The major catecholamines released are norepinephrine and epinephrine,[69] and the voltammograms for these species are virtually indistinguishable from that for DA. A carbon-fiber microelectrode was inserted at least 100 μm into a section of rat adrenal tissue containing the medulla, and a stimulating electrode was positioned approximately 1 mm away. Representative data collected upon a mild stimulation are shown in Figure 4.7A, with the time of stimulation designated by the red arrow (n = 4). A voltammogram was extracted from these data (white dashed line) and plotted in Figure 4.7B (red) with the voltammogram for a mixture of norepinephrine (NE) and M-ENK standards that were collected *in vitro* (black). The CVs correlate well (r = 0.81), with the first observed peak stemming from catecholamine release (~+0.6 V) and the following 'double-peak' attributed to the release of ~400 nM M-ENK.

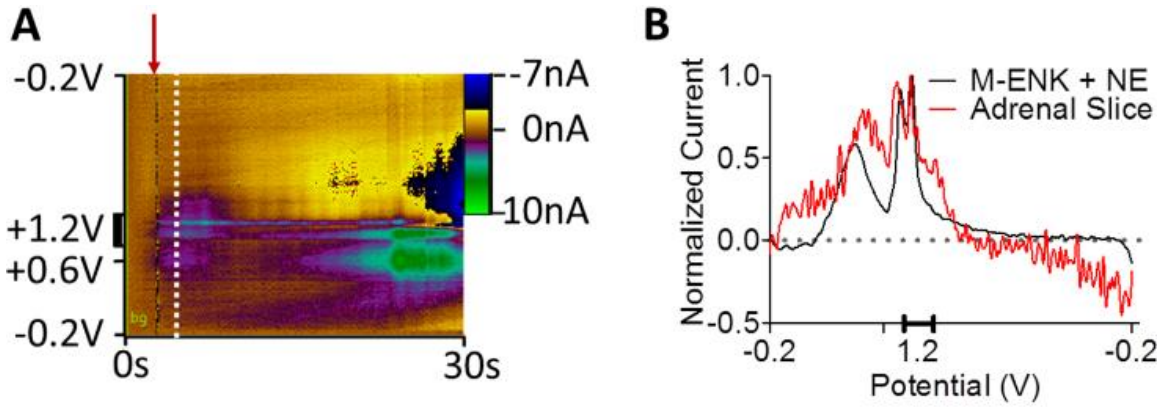

Figure 4.7. M-ENK detection in a rat adrenal slice. (A) The color plot contains 300 background-subtracted cyclic voltammograms recorded over 30 sec, and allows visualization of analytes and interfering species. Electrical stimulation occurred at the time indicated by the red arrow. (B) A background-subtracted cyclic voltammogram (red) extracted from (A) at the time indicated by the dashed white line. The signal corresponds to a voltammogram for a mixed sample of norepinephrine and M-ENK standards collected in the in vitro flow cell (r = 0.81).

4.4 Conclusions

The analyte-specific waveform described herein provides a foundation for directly measuring dynamic fluctuations of tyrosine-containing peptides in living tissue. Simply by using multiple scan rate in the anodic sweep, we have separated the signal for M-ENK from a complex mixture of electrochemically active interferents that are commonly encountered in biological preparations. The data demonstrate that this novel approach has sufficient temporal resolution, sensitivity, reproducibility, and selectivity to monitor real-time molecular dynamics of M-ENK. It is expected that this approach can be adapted for the detection of other tyrosine-containing peptides, and that it can be used to provide functional information on where, when, and how specific neuropeptides are released in tissue.

4.5 Acknowledgments

We thank the Department of Chemistry (North Carolina State University) for funding, as well as Elyssa Margolis and Howard Fields for helpful discussion (University of California – San Francisco).

4.6 Supplemental Information

Supplemental Figures G1-G3 are found in Appendix G. This material is available free of charge via the Internet at http://pubs.acs.org.

4.7 References

1. Johnson, P. I.; Stellar, J. R.; Paul, A. D. Regional reward differences within the ventral pallidum are revealed by microinjections of a mu opiate receptor agonist. *Neuropharmacology* 1993, 32, 1305-14.

2. Smith, K. S.; Berridge, K. C. The ventral pallidum and hedonic reward: neurochemical maps of sucrose "liking" and food intake. *Journal of Neuroscience* 2005, 25, 8637-49.

3. Smith, K. S.; Tindell, A. J.; Aldridge, J. W.; Berridge, K. C. Ventral pallidum roles in reward and motivation. *Behavioural Brain Research* 2009, 196, 155-67.

4. Kelley, A. E.; Bakshi, V. P.; Haber, S. N.; Steininger, T. L.; Will, M. J.; Zhang, M. Opioid modulation of taste hedonics within the ventral striatum. *Physiology & Behavior* 2002, 76, 365-77.

5. McBride, W. J.; Murphy, J. M.; Ikemoto, S. Localization of brain reinforcement mechanisms: intracranial self-administration and intracranial place-conditioning studies. *Behavioural Brain Research* 1999, 101, 129-52.

6. Pasternak, G. W.; Pan, Y. X. Mu opioids and their receptors: evolution of a concept. *Pharmacological Reviews* 2013, 65, 1257-317.

7. Koprich, J. B.; Fox, S. H.; Johnston, T. H.; Goodman, A.; Le Bourdonnec, B.; Dolle, R. E.; DeHaven, R. N.; DeHaven-Hudkins, D. L.; Little, P. J.; Brotchie, J. M. The selective mu-opioid receptor antagonist ADL5510 reduces levodopa-induced dyskinesia without affecting antiparkinsonian action in MPTP-lesioned macaque model of Parkinson's disease. *Movement disorders : official journal of the Movement Disorder Society* 2011, 26, 1225-33.

8. Koizumi, H.; Morigaki, R.; Okita, S.; Nagahiro, S.; Kaji, R.; Nakagawa, M.; Goto, S. Response of striosomal opioid signaling to dopamine depletion in 6-hydroxydopamine-lesioned rat model of Parkinson's disease: a potential compensatory role. *Frontiers in cellular neuroscience* 2013, 7, 74.

9. Marti, M.; Rodi, D.; Li, Q.; Guerrini, R.; Fasano, S.; Morella, I.; Tozzi, A.; Brambilla, R.; Calabresi, P.; Simonato, M.; Bezard, E.; Morari, M. Nociceptin/orphanin FQ receptor agonists attenuate L-DOPA-induced dyskinesias. *The Journal of neuroscience : the official journal of the Society for Neuroscience* 2012, 32, 16106-19.

10. Tekes, K.; Tariq, S.; Adeghate, E.; Laufer, R.; Hashemi, F.; Siddiq, A.; Kalasz, H. Nociceptinergic system as potential target in Parkinson's disease. *Mini reviews in medicinal chemistry* 2013, 13, 1389-97.

11. Gerrits, M. A.; Patkina, N.; Zvartau, E. E.; van Ree, J. M. Opioid blockade attenuates acquisition and expression of cocaine-induced place preference conditioning in rats. *Psychopharmacology* 1995, 119, 92-8.

12. Mitchell, J. M.; Bergren, L. J.; Chen, K. S.; Rowbotham, M. C.; Fields, H. L. Naltrexone aversion and treatment efficacy are greatest in humans and rats that actively consume high levels of alcohol. *Neurobiology of Disease* 2009, 33, 72-80.

13. Mitchell, J. M.; O'Neil, J. P.; Janabi, M.; Marks, S. M.; Jagust, W. J.; Fields, H. L. Alcohol consumption induces endogenous opioid release in the human orbitofrontal cortex and nucleus accumbens. *Science Translational Medicine* 2012, 4, 116ra6.

14. Olive, M. F.; Maidment, N. T. Repeated heroin administration increases extracellular opioid peptide-like immunoreactivity in the globus pallidus/ventral pallidum of freely moving rats. *Psychopharmacology* 1998, 139, 251-4.

15. Skoubis, P. D.; Maidment, N. T. Blockade of ventral pallidal opioid receptors induces a conditioned place aversion and attenuates acquisition of cocaine place preference in the rat. *Neuroscience* 2003, 119, 241-9.

16. Tang, X. C.; McFarland, K.; Cagle, S.; Kalivas, P. W. Cocaine-induced reinstatement requires endogenous stimulation of mu-opioid receptors in the ventral pallidum. *Journal of Neuroscience* 2005, 25, 4512-20.

17. Mansour, A.; Burke, S.; Pavlic, R. J.; Akil, H.; Watson, S. J. Immunohistochemical localization of the cloned kappa 1 receptor in the rat CNS and pituitary. *Neuroscience* 1996, 71, 671-90.

18. Akil, H.; Watson, S. J.; Young, E.; Lewis, M. E.; Khachaturian, H.; Walker, J. M. Endogenous opioids: biology and function. *Annual review of neuroscience* 1984, 7, 223-55.

19. Mansour, A.; Hoversten, M. T.; Taylor, L. P.; Watson, S. J.; Akil, H. The cloned mu, delta and kappa receptors and their endogenous ligands: evidence for two opioid peptide recognition cores. *Brain Research* 1995, 700, 89-98.

20. Breslin, M. B.; Lindberg, I.; Benjannet, S.; Mathis, J. P.; Lazure, C.; Seidah, N. G. Differential processing of proenkephalin by prohormone convertases 1(3) and 2 and furin. *Journal of Biological Chemistry* 1993, 268, 27084-93.

21. Lewis, R. V. Enkephalin biosynthesis in the adrenal medulla. *Advances in biochemical psychopharmacology* 1982, 33, 167-74.

22. Freed, A. L.; Cooper, J. D.; Davies, M. I.; Lunte, S. M. Investigation of the metabolism of substance P in rat striatum by microdialysis sampling and capillary electrophoresis with laser-induced fluorescence detection. *Journal of Neuroscience Methods* 2001, 109, 23-9.

23. Zhou, Y.; Mabrouk, O. S.; Kennedy, R. T. Rapid preconcentration for liquid chromatography-mass spectrometry assay of trace level neuropeptides. *Journal of the American Society for Mass Spectrometry* 2013, 24, 1700-9.

24. DiFeliceantonio, A. G.; Mabrouk, O. S.; Kennedy, R. T.; Berridge, K. C. Enkephalin surges in dorsal neostriatum as a signal to eat. *Current Biology* 2012, 22, 1918-24.

25. Kostel, K. L.; Lunte, S. M. Evaluation of capillary electrophoresis with post-column derivatization and laser-induced fluorescence detection for the determination of substance P and its metabolites. *Journal of Chromatography. B, Biomedical Sciences and Applications* 1997, 695, 27-38.

26. Haskins, W. E.; Wang, Z.; Watson, C. J.; Rostand, R. R.; Witowski, S. R.; Powell, D. H.; Kennedy, R. T. Capillary LC-MS2 at the attomole level for monitoring and discovering endogenous peptides in microdialysis samples collected in vivo. *Analytical Chemistry* 2001, 73, 5005-14.

27. Desiderio, D. M.; Zhu, X. Quantitative analysis of methionine enkephalin and beta-endorphin in the pituitary by liquid secondary ion mass spectrometry and tandem mass spectrometry. *Journal of Chromatography A* 1998, 794, 85-96.

28. Sinnaeve, B. A.; Storme, M. L.; Van Bocxlaer, J. F. Capillary liquid chromatography and tandem mass spectrometry for the quantification of enkephalins in cerebrospinal fluid. *Journal of Separation Science* 2005, 28, 1779-84.

29. Dawson, R., Jr.; Steves, J. P.; Lorden, J. F.; Oparil, S. Reverse-phase separation and electrochemical detection of neuropeptides. *Peptides* 1985, 6, 1173-8.

30. Shen, H.; Lada, M. W.; Kennedy, R. T. Monitoring of met-enkephalin in vivo with 5-min temporal resolution using microdialysis sampling and capillary liquid chromatography with electrochemical detection. *Journal of Chromatography. B, Biomedical Sciences and Applications* 1997, 704, 43-52.

31. Marinelli, P. W.; Lam, M.; Bai, L.; Quirion, R.; Gianoulakis, C. A microdialysis profile of dynorphin A(1-8) release in the rat nucleus accumbens following alcohol administration. *Alcoholism, Clinical and Experimental Research* 2006, 30, 982-90.

32. Maidment, N. T.; Brumbaugh, D. R.; Rudolph, V. D.; Erdelyi, E.; Evans, C. J. Microdialysis of extracellular endogenous opioid peptides from rat brain in vivo. *Neuroscience* 1989, 33, 549-57.

33. Olive, M. F.; Bertolucci, M.; Evans, C. J.; Maidment, N. T. Microdialysis reveals a morphine-induced increase in pallidal opioid peptide release. *Neuroreport* 1995, 6, 1093-6.

34. Olive, M. F.; Maidment, N. T. Opioid regulation of pallidal enkephalin release: bimodal effects of locally administered mu and delta opioid agonists in freely moving rats. *Journal of Pharmacology and Experimental Therapeutics* 1998, 285, 1310-6.

35. Liu, Z.; Welin, M.; Bragee, B.; Nyberg, F. A high-recovery extraction procedure for quantitative analysis of substance P and opioid peptides in human cerebrospinal fluid. *Peptides* 2000, 21, 853-60.

36. van Zessen, R.; Phillips, J. L.; Budygin, E. A.; Stuber, G. D. Activation of VTA GABA neurons disrupts reward consumption. *Neuron* 2012, 73, 1184-94.

37. Roberts, J. G.; Moody, B. P.; McCarty, G. S.; Sombers, L. A. Specific Oxygen-Containing Functional Groups on the Carbon Surface Underlie an Enhanced Sensitivity to Dopamine at Electrochemically Pretreated Carbon Fiber Microelectrodes. *Langmuir* 2010, 26, 9116-9122.

38. Lemos, J. C.; Wanat, M. J.; Smith, J. S.; Reyes, B. A. S.; Hollon, N. G.; Van Bockstaele, E. J.; Chavkin, C.; Phillips, P. E. M. Severe stress switches CRF action in the nucleus accumbens from appetitive to aversive. *Nature* 2012, 490, 402-+.

39. John, C. E.; Budygin, E. A.; Mateo, Y.; Jones, S. R. Neurochemical characterization of the release and uptake of dopamine in ventral tegmental area and serotonin in substantia nigra of the mouse. *J. Neurochem.* 2006, 96, 267-282.

40. Ariansen, J. L.; Heien, M.; Hermans, A.; Phillips, P. E. M.; Hernadi, I.; Bermudez, M. A.; Schultz, W.; Wightman, M. Monitoring extracellular pH, oxygen, and dopamine during reward delivery in the striatum of primates. *Front. Behav. Neurosci.* 2012, 6.

41. Sombers, L. A.; Beyene, M.; Carelli, R. M.; Wightman, R. M. Synaptic Overflow of Dopamine in the Nucleus Accumbens Arises from Neuronal Activity in the Ventral Tegmental Area. *Journal of Neuroscience* 2009, 29, 1735-1742.

42. Roitman, M. F.; Wheeler, R. A.; Wightman, R. M.; Carelli, R. M. Real-time chemical responses in the nucleus accumbens differentiate rewarding and aversive stimuli. *Nat Neurosci* 2008, 11, 1376-7.

43. Leszczyszyn, D. J.; Jankowski, J. A.; Viveros, O. H.; Diliberto, E. J.; Near, J. A.; Wightman, R. M. Secretion of Catecholamines from Individual Adrenal-Medullary Chromaffin Cells. *J. Neurochem.* 1991, 56, 1855-1863.

44. Wightman, R. M.; Jankowski, J. A.; Kennedy, R. T.; Kawagoe, K. T.; Schroeder, T. J.; Leszczyszyn, D. J.; Near, J. A.; Diliberto, E. J.; Viveros, O. H. Temporally Resolved Catecholamine Spikes Correspond to Single Vesicle Release from Individual Chromaffin Cells. *P Natl Acad Sci USA* 1991, 88, 10754-10758.

45. Swamy, B. E. K.; Venton, B. J. Subsecond detection of physiological adenosine concentrations using fast-scan cyclic voltammetry. *Analytical Chemistry* 2007, 79, 744-750.

46. Ross, A. E.; Venton, B. J. Nafion-CNT coated carbon-fiber microelectrodes for enhanced detection of adenosine. *Analyst* 2012, 137, 3045-51.

47. Sanford, A. L.; Morton, S. W.; Whitehouse, K. L.; Oara, H. M.; Lugo-Morales, L. Z.; Roberts, J. G.; Sombers, L. A. Voltammetric Detection of Hydrogen Peroxide at Carbon Fiber Microelectrodes. *Analytical Chemistry* 2010, 82, 5205-10.

48. Swamy, B. E. K.; Venton, B. J. Carbon nanotube-modified microelectrodes for simultaneous detection of dopamine and serotonin in vivo. *Analyst* 2007, 132, 876-884.

49. Borue, X.; Cooper, S.; Hirsh, J.; Condron, B.; Venton, B. J. Quantitative evaluation of serotonin release and clearance in Drosophila. *Journal of Neuroscience Methods* 2009, 179, 300-308.

50. Jackson, B. P.; Dietz, S. M.; Wightman, R. M. FAST-SCAN CYCLIC VOLTAMMETRY OF 5-HYDROXYTRYPTAMINE. *Analytical Chemistry* 1995, 67, 1115-1120.

51. Hashemi, P.; Dankoski, E. C.; Petrovic, J.; Keithley, R. B.; Wightman, R. M. Voltammetric Detection of 5-Hydroxytryptamine Release in the Rat Brain. *Analytical Chemistry* 2009, 81, 9462-9471.

52. Takmakov, P.; Zachek, M. K.; Keithley, R. B.; Bucher, E. S.; McCarty, G. S.; Wightman, R. M. Characterization of Local pH Changes in Brain Using Fast-Scan Cyclic Voltammetry with Carbon Microelectrodes. *Analytical Chemistry* 2010, 82, 9892-9900.

53. Park, J.; Takmakov, P.; Wightman, R. M. In vivo comparison of norepinephrine and dopamine release in rat brain by simultaneous measurements with fast-scan cyclic voltammetry. *J. Neurochem.* 2011, 119, 932-944.

54. Herr, N. R.; Park, J.; McElligott, Z. A.; Belle, A. M.; Carelli, R. M.; Wightman, R. M. In vivo voltammetry monitoring of electrically evoked extracellular norepinephrine in subregions of the bed nucleus of the stria terminalis. *J. Neurophysiol.* 2012, 107, 1731-1737.

55. Roberts, J. G.; Lugo-Morales, L. Z.; Loziuk, P. L.; Sombers, L. A. Real-time chemical measurements of dopamine release in the brain. *Methods in molecular biology* 2013, 964, 275-94.

56. Michael, D.; Travis, E. R.; Wightman, R. M. Color images for fast-scan CV. *Analytical Chemistry* 1998, 70, 586A-592A.

57. Ogura, K.; Kobayashi, M.; Nakayama, M.; Miho, Y. In-situ FTIR studies on the electrochemical oxidation of histidine and tyrosine. *J. Electroanal. Chem.* 1999, 463, 218-223.

58. Harriman, A. Further comments on the redox potentials of tryptophan and tyrosine. *J. Phys. Chem.* 1987, 91, 6102-6104.

59. Tan, W. T.; Goh, J. K. Electrochemical Oxidation of Methionine Mediated by a Fullerene-C(60) Modified Gold Electrode. *Electroanalysis* 2008, 20, 2447-2453.

60. Wightman, R. M.; Heien, M. L.; Wassum, K. M.; Sombers, L. A.; Aragona, B. J.; Khan, A. S.; Ariansen, J. L.; Cheer, J. F.; Phillips, P. E.; Carelli, R. M. Dopamine release is heterogeneous within microenvironments of the rat nucleus accumbens. *The European journal of neuroscience* 2007, 26, 2046-54.

61. Bard, A. J.; Faulkner, L. R. *Electrochemical methods : fundamentals and applications*. 2nd ed.; Wiley: New York, 2001; p xxi, 833 p.

62. Keithley, R. B.; Heien, M. L.; Wightman, R. M. Multivariate concentration determination using principal component regression with residual analysis. *Trends in analytical chemistry : TRAC* 2009, 28, 1127-1136.

63. Gonon, F.; Buda, M.; Cespuglio, R.; Jouvet, M.; Pujol, J. F. Invivo electrochemical detection of catechols in the neostriatum of anesthetized rats - dopamine or dopac. *Nature* 1980, 286, 902-904.

64. Kulagina, N. V.; Shankar, L.; Michael, A. C. Monitoring glutamate and ascorbate in the extracellular space of grain tissue with electrochemical microsensors. *Analytical Chemistry* 1999, 71, 5093-5100.

65. Venton, B. J.; Michael, D. J.; Wightman, R. M. Correlation of local changes in extracellular oxygen and pH that accompany dopaminergic terminal activity in the rat caudate-putamen. *J. Neurochem.* 2003, 84, 373-381.

66. Cheer, J. F.; Wassum, K. M.; Wightman, R. M. Cannabinoid modulation of electrically evoked pH and oxygen transients in the nucleus accumbens of awake rats. *J. Neurochem.* 2006, 97, 1145-1154.

67. Akil, H.; Watson, S. J.; Young, E.; Lewis, M. E.; Khachaturian, H.; Walker, J. M. Endogenous opioids: biology and function. *Annu. Rev. Neurosci.* 1984, 7, 223-55.

68. Toneff, T.; Funkelstein, L.; Mosier, C.; Abagyan, A.; Ziegler, M.; Hook, V. Beta-amyloid peptides undergo regulated co-secretion with neuropeptide and catecholamine neurotransmitters. *Peptides* 2013, 46, 126-35.

69. Verhofstad, A. A.; Coupland, R. E.; Parker, T. R.; Goldstein, M. Immunohistochemical and biochemical study on the development of the noradrenaline- and adrenaline-storing cells of the adrenal medulla of the rat. *Cell and tissue research* 1985, 242, 233-43.

CHAPTER 5

Spectroelectrochemical Characterization of the Dynamic Carbon-Fiber Surface in Response to Electrochemical Conditioning

The following work was reprinted with permission from: Mitchell, E.C., Dunaway, L.E., McCarty, G.M., and Sombers, L.A. *Langmuir*, **2017**, (In Press), DOI: 10.1021/acs.langmuir.7b01443 Supplemental information is found in Appendix H.

5.1 Introduction

Fast-scan cyclic voltammetry (FSCV) continues to grow in popularity, especially for neuroscience research, because it offers considerable advantages over other electrochemical techniques.[1] The cyclic voltammograms enable analyte identification, in contrast to data collected using competing electrochemical techniques. FSCV also provides excellent sensitivity,[2] and data can be collected with millisecond temporal resolution due to the fast scan rates employed. For these reasons, FSCV is well suited for measuring neurochemical release events that happen on the millisecond time scale in the complex chemical environment of the brain. Despite these benefits, the technique is only valuable if it is coupled to an equally powerful sensing platform.

Carbon-fiber microelectrodes are fabricated from individual carbon fibers that are available in a range of sizes (most commonly 5-30 μm in diameter), insulated in glass or silica, and polished or cut to length.[2] The small size of these sensors provides the spatial resolution needed for measurements in discrete brain regions. They are inexpensive and easily fabricated, offer a wide potential window, and resist biofouling.[3-4] Carbon-fiber microelectrodes have

even been shown to have a renewable surface when a sufficiently positive potential is applied.[5-6] These electrodes are effective at detecting a variety of common neurochemicals including dopamine,[7] serotonin,[8] histamine,[9] norepinephrine,[10] hydrogen peroxide,[11] and even met-enkephalin.[12] The fiber surface has also proven amenable to various coatings such as Nafion,[13-14] a well-characterized cation-exchange polymer, or chitosan with entrapped glucose oxidase to enable detection of non-electroactive glucose.[15-16] These properties have made carbon-fiber microelectrodes the preferred sensor for fast-scan voltammetric studies in live tissue.

Most carbon fibers are derived either from polyacrylonitrile or a mesophase pitch-based source subjected to a series of heating processes that result in graphitization of the carbon.[17] The choice of precursor material and differences in the graphitization process give rise to structural variations that result in intrinsic differences in electrical conductivity, thermal conductivity, strength, and other properties across fiber types.[17-18] Performance can be improved by electrochemically pretreating the carbon surface.[19-21] For instance, repetitive excursions to potentials as high as +3.0 V enhances detection of dopamine (but can lead to instability).[22] Indeed, the literature contains many demonstrations of improved performance in the adsorption-controlled detection of molecules after scanning a carbon electrode to a sufficiently positive potential (~1.3-1.5 V).[5, 20-21, 23-26] This treatment alters the carbon structure and increases the population of oxygen-containing functional groups on the surface. However, the chemical and physical effects of an applied potential on the carbon surface are generally not well understood. To gain insight into how potential-driven modifications to the carbon structure and surface chemistry affect electrode performance, this work characterizes the surface microstructure using Raman spectroscopy during application of static (single potential)

and dynamic (triangular) waveforms. Measured changes in the carbon structure are correlated with both electrochemical performance and physical changes evident in scanning electron micrographs. The results will inform the development of improved waveforms when electrochemically targeting complex molecules, or those that are present in low concentrations.

5.2 Experimental

5.2.1 Chemicals

All chemicals were purchased from Sigma Aldrich Co. (St. Louis, MO) and were used without additional processing. Aqueous solutions were made using doubly deionized water (Barnstead Easy Pure II, Dubuque, IA). Unless otherwise noted, all electrochemical experiments were carried out in Tris buffered electrolyte (15 mM Tris, 3.25 mM KCl, 1.20 mM $CaCl_2$, 1.2 mM $MgCl_2$, 2 mM Na_2SO_4, 1.25 mM NaH_2PO_4, and 145 mM NaCl) with a pH of 7.4.

5.2.2 Electrode Fabrication

Elliptical carbon-fiber microdisk electrodes were constructed using pitch based p-55 fibers, as previously described.[4] Briefly, a single carbon fiber was aspirated into a glass capillary (1.0 mm x 0.5 mm, A-M Systems, Carlsburg, WA) and a micropipette puller was used (Narishige, Tokyo, Japan) to form a tapered seal. The carbon fiber was then cut at the glass seal, dipped in epoxy (Epo-Tek 301, Epoxy Technology, Inc., Billerica, MA), and dried overnight at 105 ^{o}C. Electrodes were subsequently polished at 30^{o} using a Sutter Instruments

(Novato, CA) BV-10 micro-pipette beveler and 104D beveling wheel. An electrolyte solution (4 M potassium acetate, 150 mM KCl) was used to backfill the electrode and a lead was inserted to establish an electrical connection with the fiber.

5.2.3 Flow Injection

Electrochemical data were collected using a flow-injection apparatus housed in a custom Faraday cage to reduce interference from outside noise. The working electrode was positioned in the home-built electrochemical cell using a micromanipulator (World Precision Instruments, Inc., Sarasota, FL). Buffered electrolyte was passed continuously over the working and reference electrode at 1 mL/min using a syringe pump (New Era Pump Systems, Inc., Wantagh, NY). A digital valve interface (Valco Instruments Co., Inc., Houston, TX) was used to control an air actuator connected to a six-port HPLC valve in order to make two-second bolus injections of analyte across the working electrode. Electrode sensitivity was determined from calibrations of dopamine using at least three concentrations.

5.2.4 Electrochemical Data Acquisition

All potentials are reported versus a Ag/AgCl reference electrode. Analyte detection was accomplished using triangular waveforms applied at 400 V/s with an application frequency of 10 Hz, a lower potential limit of -0.4 V, and upper potential limits ranging from +1.0 to +1.4 V. Triangular waveform potentials were applied and current transduction was accomplished using custom instrumentation (University of North Carolina at Chapel Hill, Department of Chemistry, Electronics Facility). Waveforms were output using a DAC/ADC

card (NI 6251 M) with TH-1 software (ESA, Chelmsford, MA). Static potentials were applied using a waveform generator (Agilent 33220A). After static conditioning, voltammetric data collection was done using the first potential sweep, with a holding potential of -0.4 V and a positive potential limit equal to the limit used for conditioning, at a scan rate of 400 V/sec. The flow injection system was coordinated with the electrochemical experiment using a second card (NI 6711). Background subtraction and signal averaging was software controlled. Limiting currents generated in the reduction of hexaaminеruthenium(III) chloride were measured with scan rates of 100 mV/s (WaveNano, Pine Instruments Company, Durham, NC). Analysis was done with Aftermath software (Version 1.4.7714, Pine Instruments Company). Solutions deoxygenated with argon prior to use. Electrodes were conditioned with dynamic waveforms in phosphate-buffered saline (0.1 M PBS, pH 7.4) prior to limiting current analysis.

5.2.5 Surface Analysis

Raman spectra were collected for 30 seconds with a 60x objective using a custom spectrometer that has been described previously.[27] Briefly, carbon surfaces were exposed to a 12.0 mW, 632.8 nm HeNe laser (Thorlabs, Newton, NJ) through a 60x dry objective (Olympus Inc., Center Valley, PA) on an inverted microscope (Nikon Inc., Melville, NY). Detection of the Raman signal was performed with a liquid nitrogen cooled CCD camera (PI Acton, Trenton, NJ), and analyzed through an imaging spectrograph (PI Acton). All spectra were collected while the carbon fiber was immersed in Tris buffer (pH 7.4). Scanning electron micrographs were collected using a scanning electron microscope (Hitachi S-3200N) with a

5kV accelerating voltage. To enhance signal-to-noise, electrodes were sputtered with a 60/40 gold/palladium alloy prior to analysis.

5.2.6 Data Analysis and Statistics

Data are shown as the mean ± standard error of the mean, except when otherwise noted. All analysis of Raman spectra was done using Matlab (The Mathworks, Inc., Natick, MA). Background intensity was subtracted and spectra were lowered to the baseline using a spline fitting procedure. The D peak (~1330 cm^{-1}), G peak (~1580 cm^{-1}), and D' peak (~1620 cm^{-1}) were fit using a Lorentzian, Breit-Wigner-Fano, and Gaussian peak shape respectively.[28-29] Graphical and statistical analyses were performed with Graph Pad Prism 5 (GraphPad Software, Inc., La Jolla, CA). Unpaired *t*-tests and one-way analysis of variance (ANOVA) with Tukey's post-hoc tests were used to determine statistical differences with significance designated as $p<0.05$.

5.3 Results and Discussion

5.3.1 Microstructural Characterization with Raman Spectroscopy

Carbon fibers are composed of graphitic sheets aligned along the length of the fiber. These can be oriented in a number of patterns including onion, radial, and random orientation.[19] Upon application of an electrochemical potential, the edge of the graphitic sheets can be oxidized to a state that includes hydroxyl, carbonyl, and carboxyl functionalities (Figure 5.1), as determined using Raman spectroscopy,[23] X-ray photoelectron spectroscopy,[5, 30-31] and

various microscopies[32] (among other techniques). Thus, the orientation of the graphite can substantially impact electrochemical performance. For instance, it is generally considered that the edge plane of the fiber provides more adsorption sites than the basal plane[33-34] (but also see investigations into enhanced electron transfer at basal planes[35-36]). P-55 carbon fibers are pitch-based fibers with a high modulus strength that is thought to be due an alignment of the graphitic planes parallel to the fiber axis.[37-38] For this reason they are particularly useful for electrochemical studies that benefit from a microdisc electrode geometry, such as investigations of single cells. The naïve p-55 carbon fiber surface (prior to application of any potential) was characterized with Raman spectroscopy to determine how the structural morphology varies at different positions on this fiber (Figure 5.1). An electrochemical cell was positioned above the objective so that the electrode could be immersed in buffered electrolyte during Raman data collection. This *in situ* approach is advantageous in that it allows for collection of spectral data during application of an electrochemical waveform, so as to appropriately describe microstructural changes to the carbon fiber that occur over the course of an electrochemical experiment.

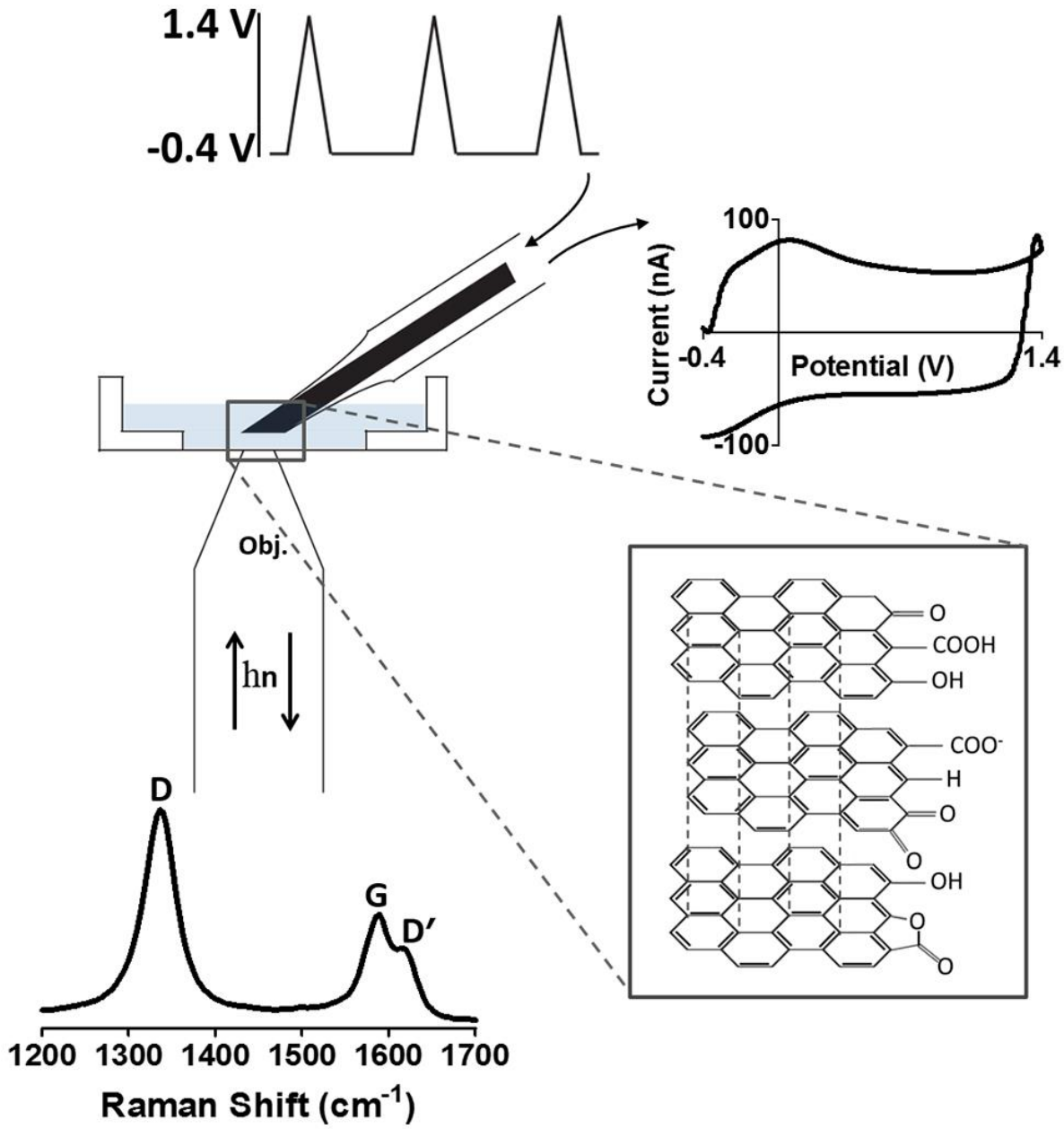

Figure 5.1. *In situ* Raman spectroscopy. Raman spectra were collected at the carbon fiber surface during electrochemical conditioning. A graphical representation of the edge and basal graphitic planes on the oxidized carbon surface is shown in the inset.

A representative Raman spectrum is shown in the bottom of Figure 5.1. Three peaks are clearly identifiable. These comprise the characteristic Raman response for graphitic systems.[19, 39-41] A peak positioned at around 1580 cm^{-1} arises from sp^2 hybridized carbon stretches and is referred to as the 'graphitic' or G peak. The peaks at approximately 1330 cm^{-1} and 1610 cm^{-1}, labeled D and D', respectively, have been related to a breaking of the symmetry in the graphitic lattice. The ratio of the D and G peak amplitudes (I_D/I_G) is commonly used as a measure of graphitic disorder in the system. In a graphitic sample that has long-range crystalline order, the D and D' peaks are low or even undetected. As the highly organized graphitic structure is disrupted, the D and D' peaks grow in intensity, and I_D/I_G increases. This continues until a high level of amorphous carbon is present, at which point I_D/I_G decreases.[42-43] These well-characterized trends make I_D/I_G a common and convenient approach to quantifying relative changes in the carbon structure.

Fibers were analyzed at a spot on the side or at the tip (freshly cut with a scalpel blade). The spectra were normalized to the G peak to highlight differences in I_D/I_G (Figure 5.2). I_D/I_G is significantly greater ($p<0.01$, n=4, two-tailed *t*-test) at the tip of the fiber (1.48 ± 0.11) versus the side (1.22 ± 0.07), which corresponds well with the 'skin-core' morphology that has been described elsewhere (more ordered and larger crystallites in the 'skin' region, and less ordered and smaller crystallites in the 'core').[44] The surface of a freshly polished tip was likewise analyzed. The spectra show a significant increase in I_D/I_G (2.02 ± 0.11) over the values measured at the tip and the side of the freshly cut fiber ($p<0.01$, n=4 tip and side, n=6 polished, one-way ANOVA, Tukey post-hoc test).

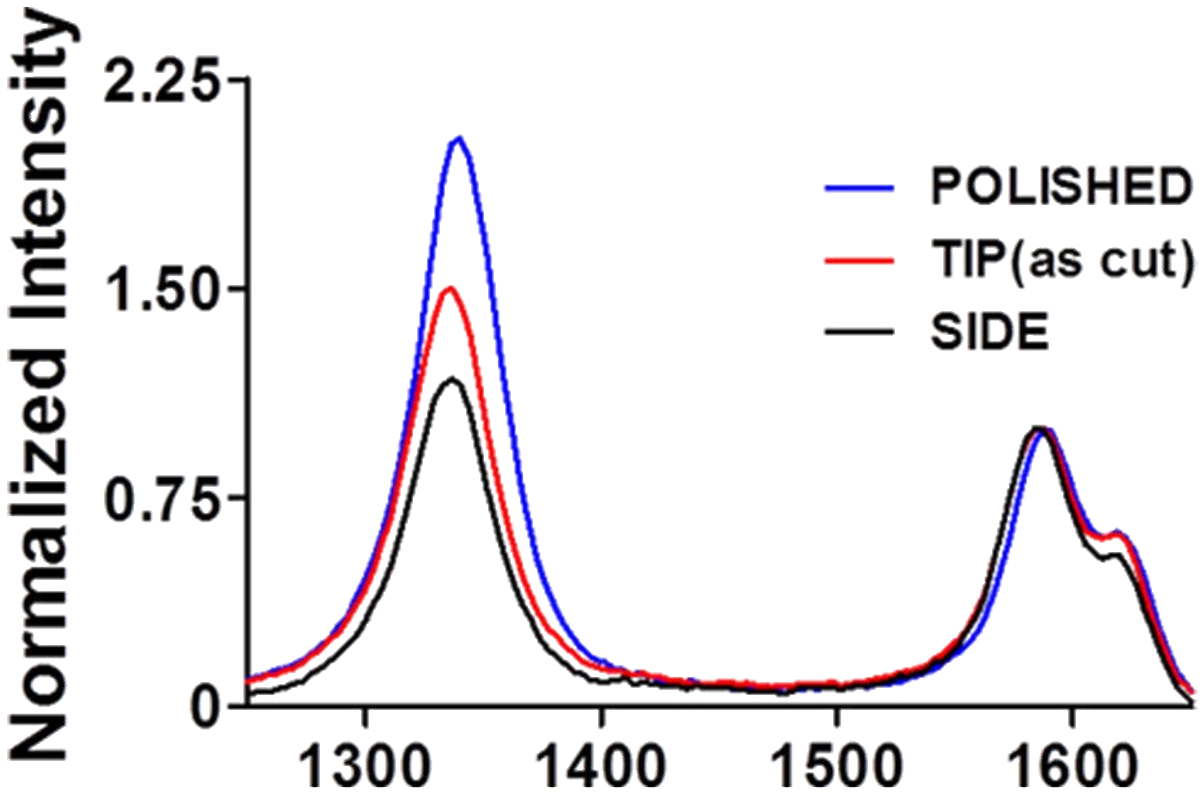

Figure 5.2. Polishing increases disorder on carbon surface. Representative spectra collected at the side, tip (as cut), and polished carbon fiber surfaces.

Previous studies have demonstrated that I_D/I_G is inversely related to the crystallite dimension along the a-axis (L_a), according to the following equation[40]

$$L_a(nm) = (2.4\ x\ 10^{-10})\lambda_{laser}^4 \left(\frac{I_D}{I_G}\right)^{-1}, \qquad (1)$$

where λ_{laser} is the wavelength of the laser in nm. Using this equation, L_a was estimated for the side, tip, and polished surfaces of the carbon fiber (Table 5.1). The L_a dimension at the

polished surface was approximately 7 and 12 nm shorter than L_a measured at the freshly cut tip and side, respectively. While it is possible that the laser itself might cause minor changes to the electrode surface, all three sampling sites would have been equally affected, and a previous study has shown that damage to the carbon surface begins at laser powers ~3 orders of magnitude greater than that used herein.[45] These results indicate two important things: 1) Raman analysis is useful in distinguishing microstructural differences in our sample, and 2) polishing the electrode surface induces crystallite defects (disorder) to the carbon structure, consistent with previous work.[46]

Table 5.1. Microcrystallite dimensions for different states of the P-55 carbon fiber

Surface Type	**L_a (nm)**
Side	31.5 $\pm$ 1.8
Tip (as cut)	26.0 $\pm$ 1.9
Polished	19.1 $\pm$ 1.1

5.3.2 Electrochemical Conditioning Alters the Structure of the Carbon Surface

Dynamic triangular waveforms commonly used in voltammetric experiments (holding potentials of -0.4 V and switching potentials ranging from +1.0 to +1.4 V) were applied for 20 minutes at a frequency of 60 Hz to freshly polished electrodes immersed in Tris buffer. In order to isolate the effect of positive potentials, another set of polished electrodes was subjected to static waveforms (ranging from +1.0 to +1.4 V) for 10 minutes. Representative spectra

collected after conditioning are presented in Figure 5.3A. Each demonstrates the three bands characteristic of graphitic materials (vide supra); however, the intensity of the D and D' bands decreases as the magnitude of the applied potential (dynamic or static) is increased. Figure 5.3B plots the magnitude of I_D/I_G and $I_{D'}/I_G$ versus the highest potential applied to the electrode. In all cases, the ratios decrease as the applied potential is increased. There is a significant difference in I_D/I_G between static and dynamic (triangular) waveforms when potentials of +1.1 to +1.3 V are applied ($p<0.05$, n=4 dynamic, n=4 static). This difference becomes less evident as potentials increase, demonstrating a growing similarity in the surface characteristics of the carbon.

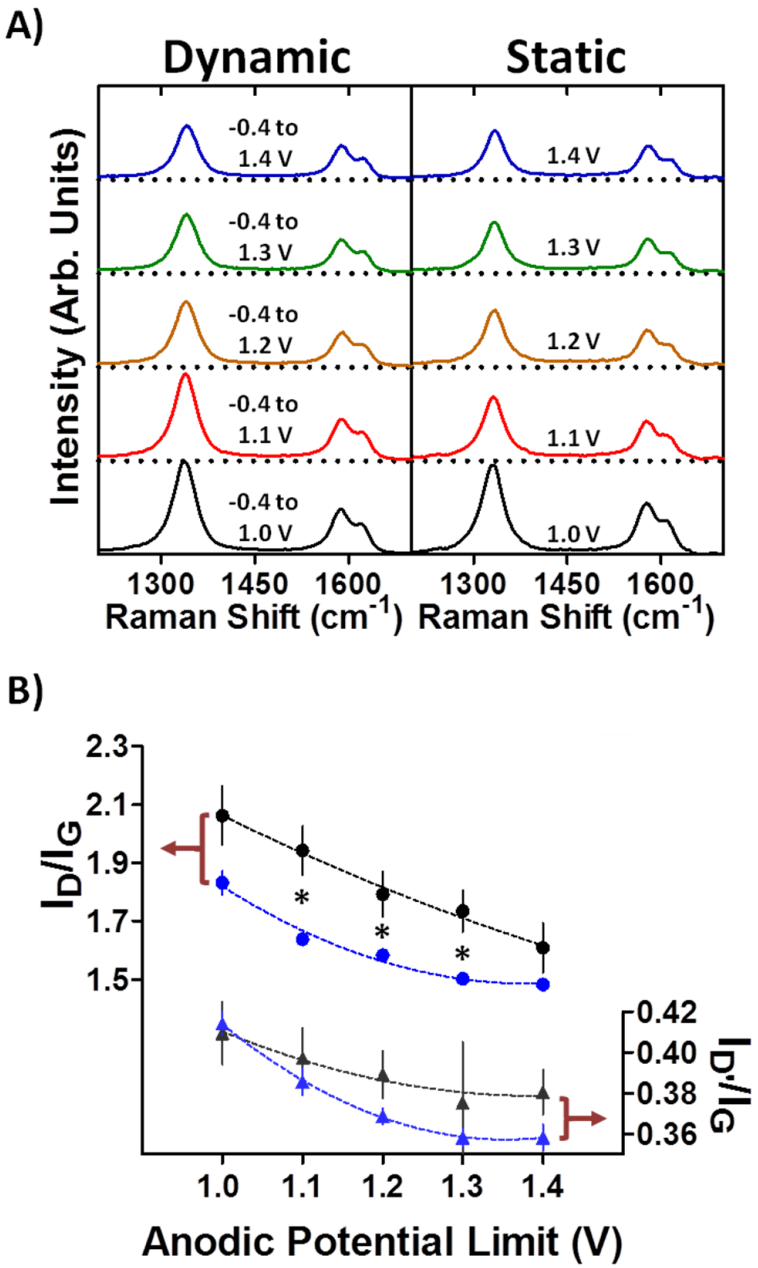

Figure 5.3. Electrochemical conditioning elicits structural changes to the polished carbon surface. A) Representative spectra collected at the carbon fiber surface during application of dynamic (left) and static (right) potentials. Spectra are offset for clarity. B) Plot of I_D/I_G (dots) and $I_{D'}/I_G$ (triangles) vs. dynamic (black) and static (blue) potential limits. The ratios decrease as the applied potential is increased, demonstrating a growing similarity in the surface characteristics of the carbon (*$p<0.05$, two-tailed t-test comparing dynamic and static conditioning, n=4 static, n=4 dynamic).

At first glance, the decreasing trend in I_D/I_G that is observed as the applied potential is increased is surprising, but it is important to note that polishing the carbon surface at the start of the experiment generates a highly disordered state (Figure 5.2). It has been shown that carbon fibers lose mass in what is hypothesized to be a Kolbe-like electrolysis (anodic oxidation of carboxylic acids or carboxylates followed by a decarboxylation step that generates carbon dioxide)[27] when electrodes are conditioned with a dynamic waveform [5, 47], as follows:

$$R - COO^- \rightarrow R - COO^{\cdot} \rightarrow R^{\cdot} + CO_2$$

This idea is supported by the electron micrographs shown in Figure 5.4. Immediately after polishing, the electrode surface does not exhibit distinguishing features indicative of short-range ordering (Figure 5.4A). After application of +1.4 V for 10 minutes, a more ordered carbon microstructure is evident (Figure 5.4B). Taken together, these data suggest that polishing disturbs the graphitic layers, leaving carbon flakes tightly packed in a disordered arrangement. In contrast, electrochemical oxidation results in the formation of more ordered, distinguishing features at the surface.

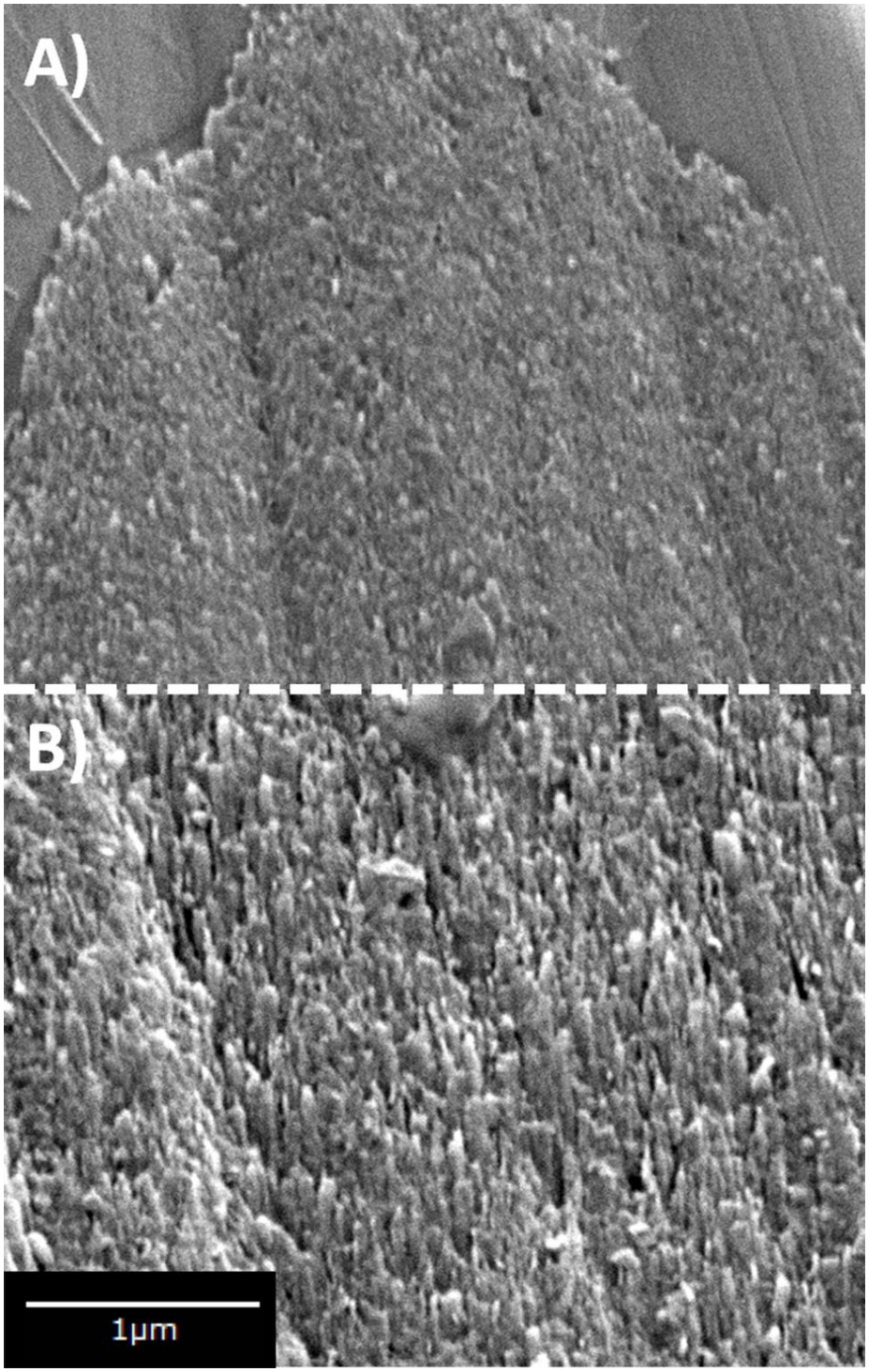

Figure 5.4. Surface changes can be visualized using SEM. Scanning electron micrographs of A) freshly polished carbon fiber surface and B) polished carbon surface after conditioning with a static +1.4 V for 10 minutes.

In an effort to determine the rate at which the preconditioning process alters the surface properties of the carbon, Raman spectra were collected at several time points during the course of electrochemical preconditioning (Figure 5.5). Microstructural changes occurred more gradually with dynamic conditioning (Figure 5.5A) than with static conditioning (Figure 5.5B). Indeed, the rate of decay, as determined from an exponential fit of the data, demonstrates that static conditioning using +1.3 V (*$p<0.05$, two-tailed t-test, n=5 static, n=9 dynamic) and +1.4 V (*$p<0.05$, two-tailed t-test, n=7 static, n=7 dynamic) changes the surface significantly faster than dynamic conditioning with these potential limits (Figure 5.5C). It is worth noting that dynamic conditioning at +1.0 V and static conditioning at -0.4 V lead to no noticeable changes in the carbon microstructure, whereas static conditioning with +1.0 V generates structural changes similar to those observed in response to higher applied potentials. Indeed, a dynamic triangular waveform only affords brief periods of time at potentials sufficient to etch the carbon surface. For instance, a cyclic sweep to 1.3 V at 400 V/sec affords approximately 1.5 msec above 1.0 V, and only 0.5 msec above 1.2 V. The spectral data are plotted as a function of the total time spent above 1.0 V (Figure 5.6A, C) or 1.2 V (Figure 5.6B, D), as the precise potential required to oxidatively etch the carbon surface is unknown. The data collected with the two conditioning methods do not significantly differ in either plot (A-B: $p>0.05$, two-tailed *t*-test, n=11 dynamic, n=7 static; C-D: $p>0.05$, two-tailed *t*-test, n=11 dynamic, n=7 static), suggesting that the time spent at a potential sufficient to break bonds and rearrange the surface is a critical factor in generating an ordered, oxidized carbon surface for electrochemical measurements.

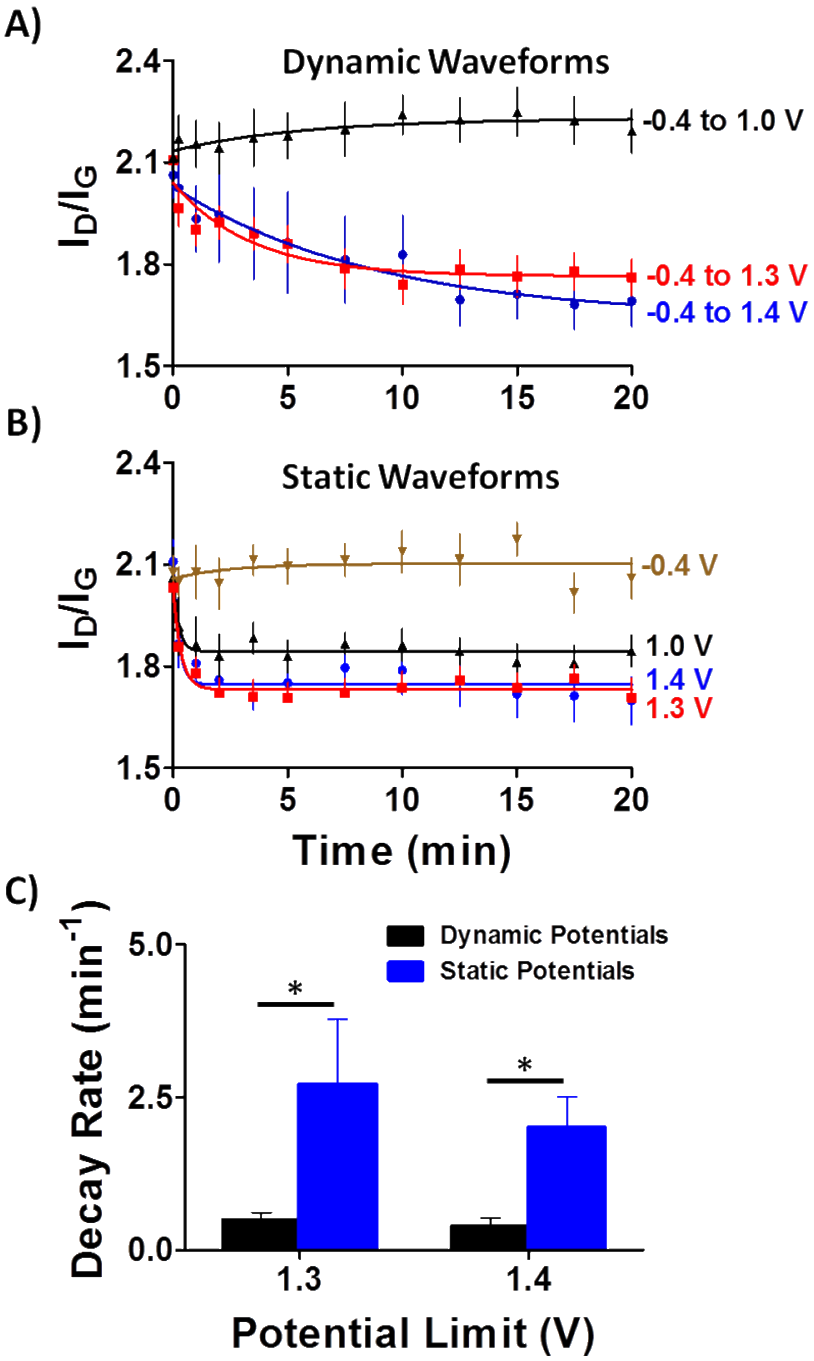

Figure 5.5. Static conditioning rapidly changes the carbon surface. Plots of I_D/I_G as a function of electrochemical conditioning time using A) dynamic and B) static waveforms. C) Rate constants determined by an exponential fit of the data in (A) and (B). (+1.3 V: *$p<0.05$, two-tailed t-test, n=5 static, n=9 dynamic; +1.4 V: *$p<0.05$, two-tailed t-test, n=7 static, n=7 dynamic)

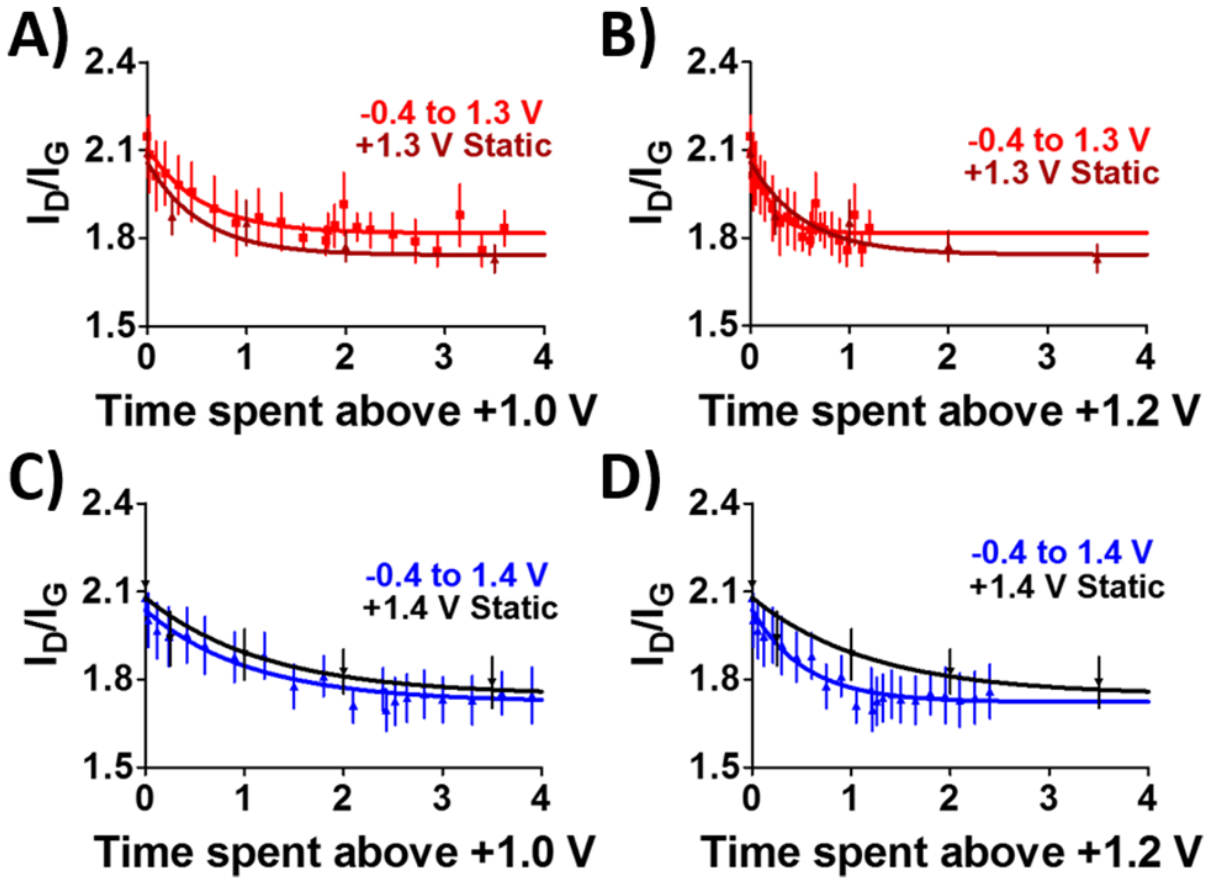

Figure 5.6. Structural changes to the carbon surface are dependent on the amount of time spent above +1.0 V. I_D/I_G is plotted *vs*. time spent above +1.0 V (A and C) and +1.2 V (B and D) for dynamic (triangular) waveforms with potential limits of +1.3 V (A and B) and +1.4 V (C and D), and static application of these potentials. (A-B: $p>0.05$, two-tailed *t*-test, n=11 dynamic, n=7 static; C-D: $p>0.05$, two-tailed *t*-test, n=11 dynamic, n=7 static)

5.3.3 Microstructural Changes to the Electrode Surface Correlate with Electrochemical Performance

Experiments were done to investigate how the structural changes described above correlate with electrochemical performance. Electrodes were conditioned with either a dynamic (60 Hz for 20 minutes) or static (1 minute) waveform, followed by voltammetric data

collection. In the case of static conditioning, data were collected using the first potential sweep (400 V/sec) after the conditioning period, with a holding potential of -0.4 V and a positive potential limit equal to the limit used for conditioning (+1.0 to +1.4 V). It has been shown previously that when using fast-scan cyclic voltammetry, the magnitude of the background current is predictive of electrode sensitivity.[48] As expected, the background current increased as the switching potential was raised for both dynamic and static conditioning (Figure 5.7A). This could only be due to an increase in electrode area or to chemical and structural changes occurring at the electrode surface. It is unlikely that electrode area would be substantially increased by the potentials applied herein, but more severe voltammetric sweeps have indeed been shown to fracture carbon surfaces.[22] To investigate if electrochemical conditioning was inducing substantial increases in electrode area, voltammograms for hexaaminеruthenium(III) chloride were collected on freshly polished electrodes, and then again on the same electrodes after dynamic conditioning for 20 minutes at 60 Hz. The equation for limiting current at a microdisc electrode is as follows:

$$i_{lim} = 4nFDCr \qquad (2)$$

where n is the number of electrons transferred, F is Faradays constant, D is diffusion coefficient, C is the concentration of the redox species in the bulk solution, and r is the radius of the electrode.[49] As shown in Equation 2, limiting current is directly related to the radius of the electrode. However, no significant difference was evident in the limiting currents collected at freshly polished vs dynamically conditioned electrodes (Figure H1 (Appendix H), $p>0.05$, paired t-test, n=3). While it is possible that very small changes in area would not be detected

due to error associated with the measurement,[50] it is more likely that the differences in electrochemical performance between these groups stem from chemical and structural changes at the surface of the carbon electrode, as hypothesized previously.[21, 51]

The background current is largely comprised of non-faradaic capacitive current, but also contains some current generated in redox processes that strongly depend on the nature of the carbon surface and its environment. For instance, oxygen-containing functional groups on the carbon surface (Figure 5.1) are critical in determining analyte adsorption, electrocatalysis, and capacitive behavior.[19, 52-54] The faradaic portion of the background current exceeds that expected for application of a triangular voltage sweep to an ideal RC circuit,[49] and is evident as peaks that develop at ~-0.3 V and +0.2 V (asterisks in Figure 5.7A). The area under the peak at ~+0.2 V, which we term the 'surface-dependent peak', was integrated to roughly estimate the population of oxygen on the surface of the electrode. The data suggest that the statically conditioned electrodes were significantly more oxidized than those that were dynamically preconditioned (bottom, $p<0.05$, one-tailed *t*-test, n=6 dynamic, n=8 static), except for the +1.4 V switching potential. The 'surface-dependent peak' attributed to oxygen-containing functionalities on dynamically preconditioned electrodes remained relatively low until potentials of +1.3 and +1.4 V were reached. As described above, this likely results because a dynamic triangular waveform only affords brief periods of time at potentials sufficient to break bonds and induce structural changes to the carbon surface.

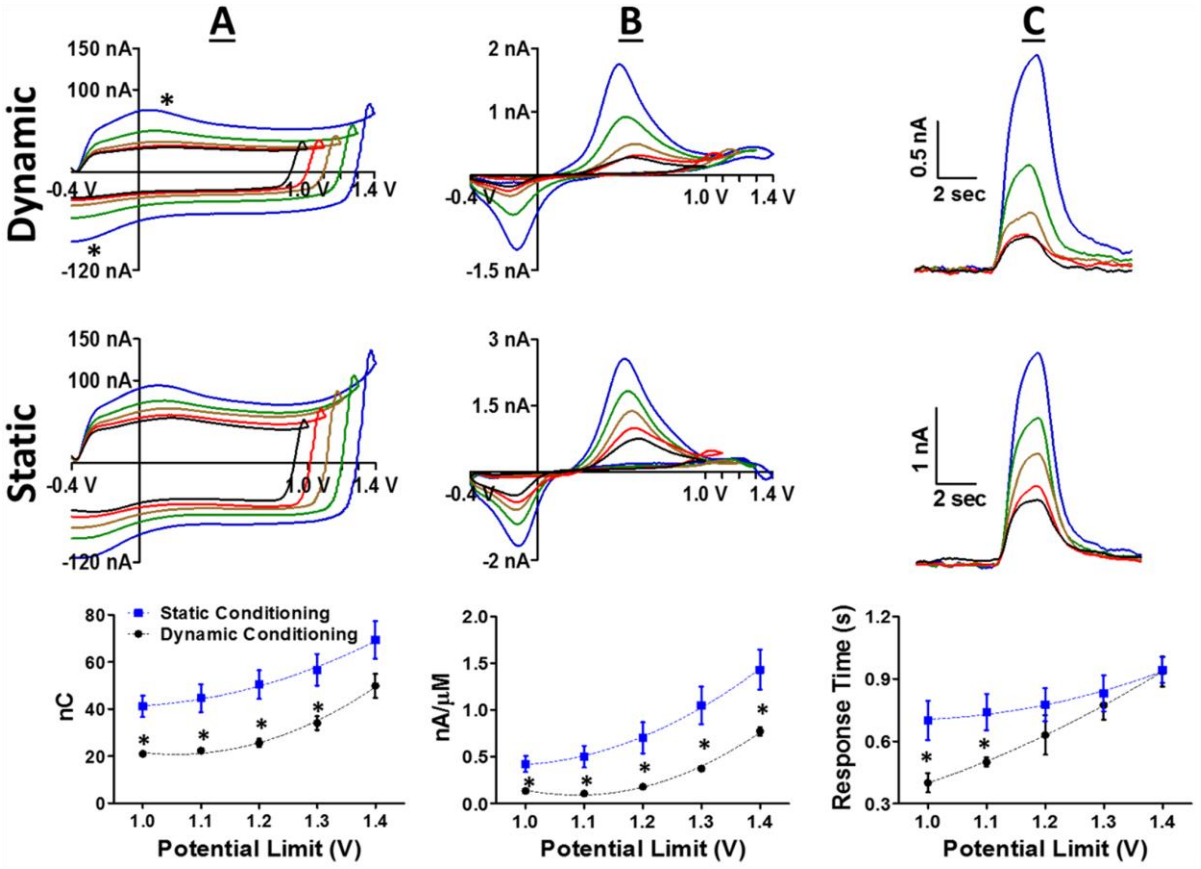

Figure 5.7. Conditioning affects electrochemical performance. Voltammetric data collected after dynamic (top) and static (middle) conditioning. Holding potential was -0.4 V, and switching potentials ranged from +1.0 V to +1.4 V. A) Averaged background voltammograms (400 V/sec, 10 Hz), with surface-related contributions denoted by asterisks (~+0.2 V). The charge for the portion of the background current that exceeds that expected for an ideal RC circuit is plotted verses the applied potential limit in the bottom panel. B) Averaged background-subtracted voltammograms for 2 µM dopamine. The bottom panel plots sensitivity to dopamine for these conditioning paradigms. C) Averaged current vs. time traces. The bottom panel plots response time (10%-90% rise time). Static and dynamic conditioning paradigms significantly affect background charge, sensitivity to dopamine, and responsivity. (*$p<0.05$, one-tailed *t*-test, n = 8 (static), n = 6 (dynamic)).

The adsorption-controlled electrochemical response to dopamine was also examined (Figure 5.7 B and C). As expected, sensitivity increased as the positive wavelimit increased,

consistent with the trend in the background current and with previous works.[21, 24] Sensitivity to dopamine was significantly greater for electrodes that were statically versus dynamically conditioned ($p<0.05$, one-tailed *t*-test, n=6 dynamic, n=8 static). However, electrode response time is a particularly important parameter when monitoring molecular dynamics in real time, and it has been shown that response time slows as oxidation of the carbon surface is increased.[24, 55] As expected, the electrode response is slowed as the positive limit is increased for both sets of conditioned electrodes (Figure 5.7C). Interestingly, the response time for static preconditioning is slow even when the lower potentials of +1.0 and +1.1 V are used. This again highlights how spending extended time at potentials sufficient to induce structural modifications at the carbon surface can affect electrode performance, even at these relatively mild potentials.

Electrochemically conditioning carbon electrodes has also been shown to increase the apparent electron transfer kinetics for a variety of molecules, including dopamine and ascorbic acid.[21, 56] The data presented here (Figure 5.7, Table 5.2) show that the peak-to-peak separation for dopamine oxidation and reduction (ΔE_p) decreases as the positive switching potential is increased. This indicates that the surface becomes better suited for electron transfer as the positive potential limit is extended. The detection of ascorbic acid was also characterized on the same set of electrodes (Figure 5.8). When using dynamically preconditioned electrodes, the oxidation wave for ascorbic acid was not well defined until a potential limit of +1.4 V was applied. However, statically conditioned electrodes exhibited a clear oxidation peak for ascorbic acid even with a positive wavelimit of only +1.0 V. This interesting result

demonstrates that lower potentials (+1.0 V) are sufficient to facilitate oxidation of ascorbic acid when statically applied.

Table 5.2. Peak-to-peak separation for the detection of 2 μM dopamine

Potential Limit	1.0 V	1.1 V	1.2 V	1.3 V	1.4 V
Dynamic Conditioning ΔE_p (V)	0.77 + 0.05	0.78 + 0.04	0.73 + 0.03	0.67 + 0.04*	0.60 + 0.02*
Static Conditioning ΔE_p (V)	0.74 + 0.09	0.7 + 0.1	0.68 + 0.06	0.64 + 0.05*	0.62 + 0.05*

- $p<0.05$, one-way ANOVA, n=6 (dynamic), n=9 (static), Tukey post-hoc tests compared to +1.0 V

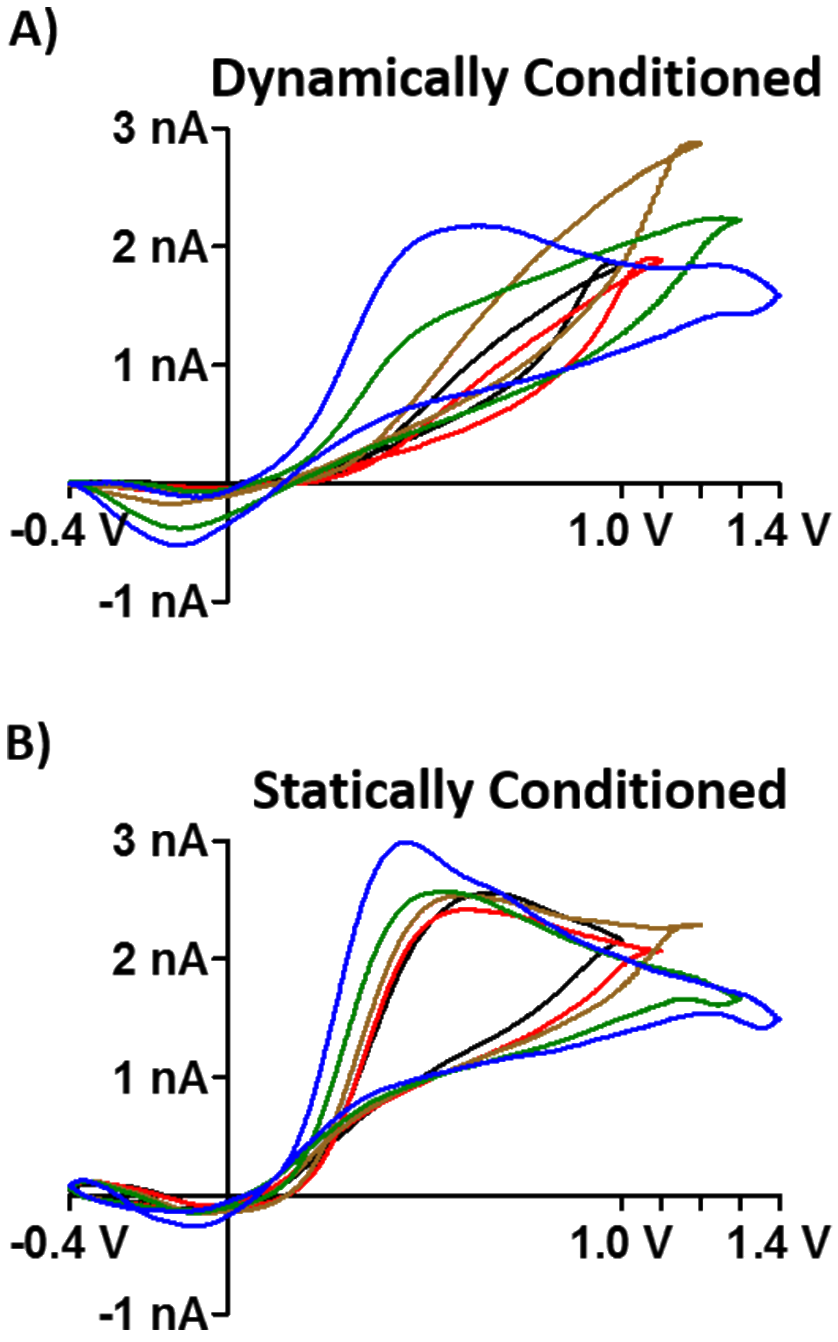

Figure 5.8. Conditioning alters the electrochemical response to ascorbic acid. Averaged background-subtracted voltammograms for 200 µM ascorbic acid collected using electrodes conditioned with A) dynamic and B) static potentials. Holding potential was -0.4 V and switching potentials varied: +1.0 V (black), +1.1 V (red), +1.2 V (gold), +1.3 V (green), and +1.4 V (blue).

5.3.4 The Dynamic Carbon Surface Quickly and Continually Undergoes Structural Reorganization in Response to Applied Potential

The data presented herein clearly demonstrate that the structure of the carbon surface is altered by potentials ranging from -0.4 V to +1.4 V; potentials that are commonly used in voltammetry. However, when performing voltammetric experiments, alternating negative and positive potentials are generally applied over the course of an experiment. In order to investigate if the carbon surface repetitively responds to changes in applied potential, -0.4 V and +1.4 V were applied in an alternating pattern and spectra were collected over time (Figure 5.9). Both I_D/I_G and I_D'/I_G were found to oscillate in response to the applied potential. These interesting data demonstrate that the carbon surface undergoes rapid structural reorganization as potential is applied, repeatedly alternating between a relatively ordered state, and one that exhibits greater disorder in the carbon lattice. This is likely a result of oxygen-containing surface species undergoing redox reactions in response to the applied potential. These data are consistent with a study by Stamford and coworkers that demonstrated that scanning to a positive wavelimit of +1.4 V increased adsorption and improved sensitivity to dopamine.[21] These benefits were attributed to a "semi-reversible" change to the electrode surface, and were lost when the positive wavelimit was subsequently decreased to +1.0 V. Importantly, the data presented herein directly demonstrate the dynamic nature of the graphitic layers in the carbon fiber. Rather than reaching a state of equilibrium, the carbon surface rapidly responds to potentials applied in repetitive voltammetric sweeps, allowing the voltammetric waveform to act as a continuous pretreatment.

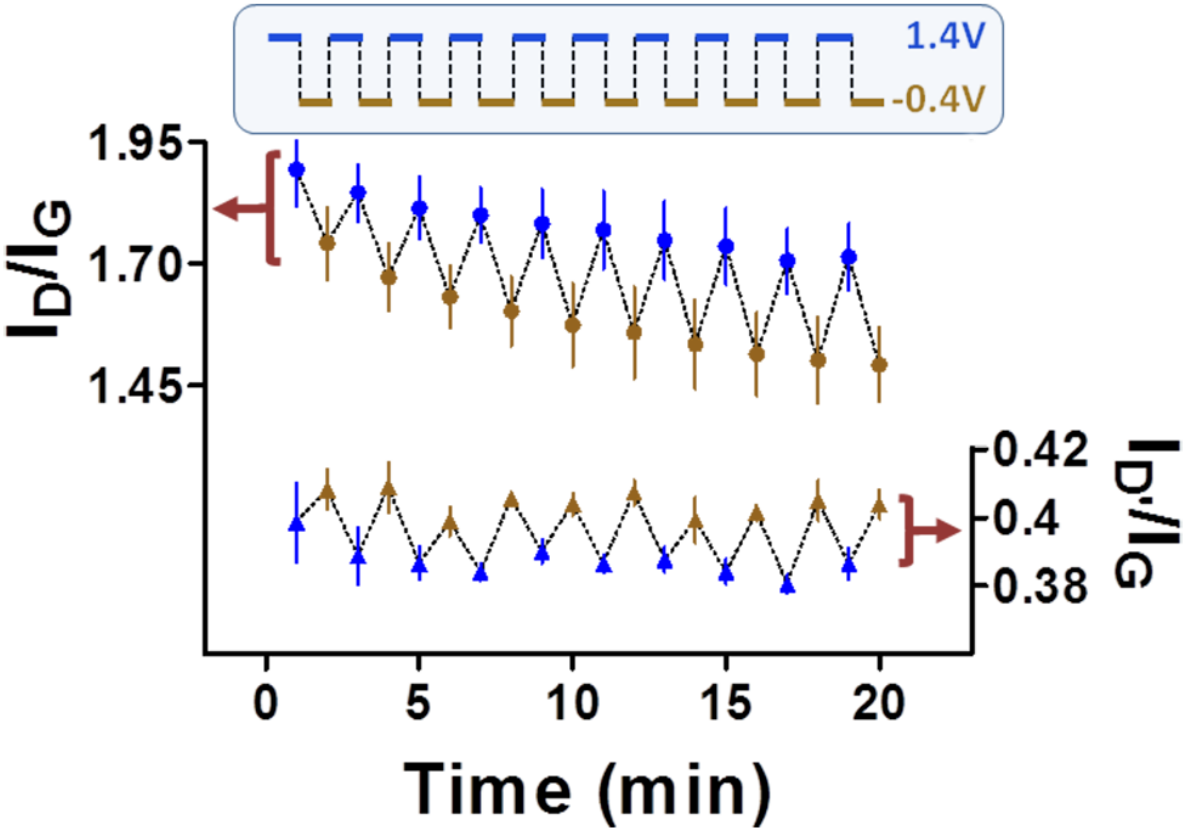

Figure 5.9. The carbon surface is dynamic and continually responds to applied potential. Plots of I_D/I_G (left y-axis) and $I_{D'}/I_G$ (right y-axis) as a function of time as static potentials of +1.4 and -0.4 V were alternately applied to the electrode (top).

5.4 Summary and Conclusions

The electrochemical performance of carbon-fiber microelectrodes is highly dependent on the surface characteristics of the fiber. Using Raman spectroscopy, we have shown that the carbon surface rapidly responds to applied potentials and that positive potentials are more effective than negative potentials at eliciting a microstructural response (Figure 5.5). In

addition, applying a static positive potential is more efficient than using a dynamic (triangular) waveform to elicit microstructural changes to the carbon surface that result in enhanced electrochemical performance (Figures 5.5, 5.7). For example, conditioning with a static potential of +1.0 V is sufficient to enable the voltammetric detection of ascorbic acid; however, conditioning with a dynamic waveform with a positive potential limit of +1.0 V is not (Figure 5.8). Likewise, conditioning with a static +1.0 V leads to a surface structure resembling that attained after conditioning with dynamic waveforms with larger positive potential limits (Figure 5.3). Thus, the amount of time spent at a potential sufficient to break bonds and rearrange the surface is critical in generating an ordered and oxidized carbon surface (Figure 5.6). Importantly, the carbon surface is a dynamic entity that continuously responds to applied potential (Figure 5.9). Overall these data provide valuable insight into deconstruction/reconstruction phenomena occurring at the carbon-fiber microelectrode surface in response to applied potential, addressing critical gaps in the fundamental understanding of electrochemical processes at carbon surfaces. The information presented herein will serve as a foundation to inform researchers designing waveforms to target specific molecules using carbon-fiber electrodes.

5.5 Acknowledgements

We thank Chuck Mooney (Analytical Instrumentation Facility, North Carolina State University) for assistance with SEM imaging, and both James Roberts and Rick McCreery for helpful discussion.

5.6 Associated Content

Supplemental Figure H1 is found in Appendix H. This material is available free of charge via the Internet at http://pubs.acs.org.

5.7 References

1. Meunier, C. J.; Roberts, J. G.; McCarty, G. S.; Sombers, L. A. Background Signal as an in Situ Predictor of Dopamine Oxidation Potential: Improving Interpretation of Fast-Scan Cyclic Voltammetry Data. *ACS Chem. Neurosci.* **2017,** *8* (2), 411-419.

2. Roberts, J. G.; Lugo-Morales, L. Z.; Loziuk, P. L.; Sombers, L. A. Real-time chemical measurements of dopamine release in the brain. *Methods Mol. Biol.* **2013,** *964*, 275-94.

3. Wightman, R. Probing Cellular Chemistry in Biological Systems with Microelectrodes. *Science* **2006,** *311* (5767), 1570-1574.

4. Kawagoe, K. T.; Zimmerman, J. B.; Wightman, R. M. Principles of Voltammetry and Microelectrode Surface-States. *J. Neurosci. Meth.* **1993,** *48* (3), 225-240.

5. Takmakov, P.; Zachek, M.; Keithley, R.; Walsh, P.; Donley, C.; McCarty, G.; Wightman, R. Carbon Microelectrodes with a Renewable Surface. *Anal. Chem.* **2010,** *82* (5), 2020-2028.

6. Keithley, R. B.; Takmakov, P.; Bucher, E. S.; Belle, A. M.; Owesson-White, C. A.; Park, J.; Wightman, R. M. Higher Sensitivity Dopamine Measurements with Faster-Scan Cyclic Voltammetry. *Anal. Chem.* **2011,** *83* (9), 3563-3571.

7. Kile, B. M.; Walsh, P. L.; McElligott, Z. A.; Bucher, E. S.; Guillot, T. S.; Salahpour, A.; Caron, M. G.; Wightman, R. M. Optimizing the Temporal Resolution of Fast-Scan Cyclic Voltammetry. *ACS Chem. Neurosci.* **2012,** *3* (4), 285-292.

8. Hashemi, P.; Dankoski, E. C.; Petrovic, J.; Keithley, R. B.; Wightman, R. M. Voltammetric detection of 5-hydroxytryptamine release in the rat brain. *Anal. Chem.* **2009,** *81* (22), 9462-71.

9. Pihel, K.; Hsieh, S.; Jorgenson, J. W.; Wightman, R. M. Electrochemical detection of histamine and 5-hydroxytryptamine at isolated mast cells. *Anal. Chem.* **1995,** *67* (24), 4514-21.

10. Park, J.; Aragona, B. J.; Kile, B. M.; Carelli, R. M.; Wightman, R. M. In vivo voltammetric monitoring of catecholamine release in subterritories of the nucleus accumbens shell. *Neuroscience* **2010,** *169* (1), 132-42.

11. Sanford, A. L.; Morton, S. W.; Whitehouse, K. L.; Oara, H. M.; Lugo-Morales, L. Z.; Roberts, J. G.; Sombers, L. A. Voltammetric Detection of Hydrogen Peroxide at Carbon Fiber Microelectrodes. *Anal. Chem.* **2010,** *82* (12), 5205-5210.

12. Schmidt, A. C.; Dunaway, L. E.; Roberts, J. G.; McCarty, G. S.; Sombers, L. A. Multiple Scan Rate Voltammetry for Selective Quantification of Real-Time Enkephalin Dynamics. *Anal. Chem.* **2014,** *86* (15), 7806-7812.

13. Gerhardt, G. A.; Oke, A. F.; Nagy, G.; Moghaddam, B.; Adams, R. N. Nafion-Coated Electrodes with High Selectivity for Cns Electrochemistry. *Brain Res.* **1984,** *290* (2), 390-395.

14. Qi, L.; Thomas, E.; White, S. H.; Smith, S. K.; Lee, C. A.; Wilson, L. R.; Sombers, L. A. Unmasking the Effects of L-DOPA on Rapid Dopamine Signaling with an Improved Approach for Nafion Coating Carbon-Fiber Microelectrodes. *Anal. Chem.* **2016,** *88* (16), 8129-36.

15. Lugo-Morales, L. Z.; Loziuk, P. L.; Corder, A. K.; Toups, J. V.; Roberts, J. G.; McCaffrey, K. A.; Sombers, L. A. Enzyme-modified carbon-fiber microelectrode for the quantification of dynamic fluctuations of nonelectroactive analytes using fast-scan cyclic voltammetry. *Anal. Chem.* **2013,** *85* (18), 8780-6.

16. Smith, S. K.; Lee, C. A.; Dausch, M. E.; Horman, B. M.; Patisaul, H. B.; McCarty, G. S.; Sombers, L. A. Simultaneous Voltammetric Measurements of Glucose and Dopamine Demonstrate the Coupling of Glucose Availability with Increased Metabolic Demand in the Rat Striatum. *ACS Chem Neurosci* **2017,** *8* (2), 272-280.

17. Liu, Y. D.; Kumar, S. Recent Progress in Fabrication, Structure, and Properties of Carbon Fibers. *Polym. Rev.* **2012,** *52* (3-4), 234-258.

18. Huang, X. Fabrication and Properties of Carbon Fibers. *Materials* **2009,** *2* (4), 2369-2403.

19. McCreery, R. Advanced carbon electrode materials for molecular electrochemistry. *Chem. Rev.* **2008,** *108* (7), 2646-2687.

20. Engstrom, R. C.; Strasser, V. A. Characterization of Electrochemically Pretreated Glassy-Carbon Electrodes. *Anal. Chem.* **1984,** *56* (2), 136-141.

21. Hafizi, S.; Kruk, Z. L.; Stamford, J. A. Fast Cyclic Voltammetry - Improved Sensitivity to Dopamine with Extended Oxidation Scan Limits. *J. Neurosci. Meth.* **1990,** *33* (1), 41-49.

22. Gonon, F. G.; Fombarlet, C. M.; Buda, M. J.; Pujol, J. F. Electrochemical Treatment of Pyrolytic Carbon-Fiber Electrodes. *Anal. Chem.* **1981,** *53* (9), 1386-1389.

23. Roberts, J. G.; Moody, B. P.; McCarty, G. S.; Sombers, L. A. Specific oxygen-containing functional groups on the carbon surface underlie an enhanced sensitivity to dopamine at electrochemically pretreated carbon fiber microelectrodes. *Langmuir* **2010,** *26* (11), 9116-22.

24. Heien, M.; Phillips, P.; Stuber, G.; Seipel, A.; Wightman, R. Overoxidation of carbon-fiber microelectrodes enhances dopamine adsorption and increases sensitivity. *Analyst* **2003,** *128* (12), 1413-1419.

25. Swain, G. M.; Kuwana, T. Electrochemical Formation of High Surface-Area Carbon-Fibers. *Anal. Chem.* **1991,** *63* (5), 517-519.

26. Pihel, K.; Walker, Q. D.; Wightman, R. M. Overoxidized polypyrrole-coated carbon fiber microelectrodes for dopamine measurements with fast-scan cyclic voltammetry. *Anal. Chem.* **1996,** *68* (13), 2084-9.

27. Bard, A. J.; Inzelt, G. r.; Scholz, F., *Electrochemical dictionary*. 2nd, rev. & extended ed.; Springer: Heidelberg, 2012; p vii, 991 p.

28. Ferrari, A. C.; Robertson, J. Interpretation of Raman spectra of disordered and amorphous carbon. *Phys. Rev. B* **2000,** *61* (20), 14095-14107.

29. Mcculloch, D. G.; Prawer, S. The Effect of Annealing and Implantation Temperature on the Structure of C Ion-Beam-Irradiated Glassy-Carbon. *J. Appl. Phys.* **1995,** *78* (5), 3040-3047.

30. Tougas, T. P.; Collier, W. G. Determination of Surface Carbonyl Groups on Glassy-Carbon with X-Ray Photoelectron-Spectroscopy Preceded by Derivatization with Pentafluorophenylhydrazine. *Anal. Chem.* **1987,** *59* (18), 2269-2272.

31. Collier, W. G.; Tougas, T. P. Determination of Surface Hydroxyl-Groups on Glassy-Carbon with X-Ray Photoelectron-Spectroscopy Preceded by Chemical Derivatization. *Anal. Chem.* **1987,** *59* (3), 396-399.

32. Boehm, H. P. Some Aspects of the Surface-Chemistry of Carbon-Blacks and Other Carbons. *Carbon* **1994,** *32* (5), 759-769.

33. Bowling, R. J.; Packard, R. T.; Mccreery, R. L. Activation of Highly Ordered Pyrolytic-Graphite for Heterogeneous Electron-Transfer - Relationship between Electrochemical Performance and Carbon Microstructure. *J. Am. Chem. Soc.* **1989,** *111* (4), 1217-1223.

34. McCreery, R. L., Carbon Electrodes: Structural Effects on Electron Transfer Kinetics. In *Electroanalytical chemistry*, Bard, A. J., Ed. Marcel Dekker, Inc.: New York, 1990; Vol. 17, pp 221-374.

35. Patel, A. N.; Collignon, M. G.; O'Connell, M. A.; Hung, W. O. Y.; McKelvey, K.; Macpherson, J. V.; Unwin, P. R. A New View of Electrochemistry at Highly Oriented Pyrolytic Graphite. *J. Am. Chem. Soc.* **2012,** *134* (49), 20117-20130.

36. Patel, A. N.; Tan, S. Y.; Miller, T. S.; Macpherson, J. V.; Unwin, P. R. Comparison and Reappraisal of Carbon Electrodes for the Voltammetric Detection of Dopamine. *Anal. Chem.* **2013,** *85* (24), 11755-11764.

37. Saito, R., *Physical Properties of Carbon Nanotubes*. Imperial College Press: United Kingdom, 1998.

38. Dresselhaus, M. S., *Graphite fibers and filaments*. Springer-Verlag: Berlin, 1988.

39. Chieu, T.; Dresselhaus, M.; Endo, M. Raman Studies Of Benzene-Derived Graphite Fibers. *Phys. Rev. B* **1982,** *26* (10), 5867-5877.

40. Pimenta, M. A.; Dresselhaus, G.; Dresselhaus, M. S.; Cancado, L. G.; Jorio, A.; Saito, R. Studying disorder in graphite-based systems by Raman spectroscopy. *Phys. Chem. Chem. Phys.* **2007,** *9*, 1276-1291.

41. Morita, K.; Murata, Y.; Ishitani, A.; Murayama, K.; Ono, T.; Nakajima, A. Characterization of Commercially Available Pan (Polyacrylonitrile)-Based Carbon-Fibers. *Pure Appl. Chem.* **1986,** *58* (3), 455-468.

42. Ferrari, A. C. Raman spectroscopy of graphene and graphite: Disorder, electron-phonon coupling, doping and nonadiabatic effects. *Solid State Commun.* **2007,** *143*, 47-57.

43. Mildred S. Dresselhaus, A. J., Mario Hofmann, Gene Dresselhaus, Riichiro Saito Perspectives on Carbon Nanotubes and Graphene Raman Spectroscopy. *Nano Lett.* **2010,** *10*, 751-758.

44. Y. Huang, R. J. Y. Effect of Fibre Microstructure Upon the Modulus of Pan- and Pitch-Based Carbon Fibres. *Carbon* **1995,** *33* (2), 97-107.

45. Alsmeyer, Y. W.; Mccreery, R. L. Surface Enhanced Raman Examination of Carbon Electrodes - Effects of Laser Activation and Electrochemical Pretreatment. *Langmuir* **1991,** *7* (10), 2370-2375.

46. Rice, R. J.; Allred, C. D.; McCreery, R. L. Fast Heterogenous Electron Transfer Rates For Glassy Carbon Electrodes Without Polishing or Activation Procedures. *J. Electroanal. Chem.* **1989,** *263*, 163-169.

47. Charles A. Goss, J. C. B., Eugene A. Irene, Royce W. Murray Imaging the Incipient Electrochemical Oxidation of Highly Oriented Py. *Anal. Chem.* **1993,** *65*, 1378-1389.

48. Roberts, J. G.; Toups, J. V.; Eyualem, E.; McCarty, G. S.; Sombers, L. A. In Situ Electrode Calibration Strategy for Voltammetric Measurements In Vivo. *Anal. Chem.* **2013,** *85* (23), 11568-11575.

49. Bard, A. J. F., L. R., *Electrochemical methods : fundamentals and applications*. 2nd ed.; John Wiley: New York, 2001.

50. Watkins, J. J.; Chen, J.; White, H. S.; Abruna, H. D.; Maisonhaute, E.; Amatore, C. Zeptomole voltammetric detection and electron-transfer rate measurements using platinum electrodes of nanometer dimensions. *Anal. Chem.* **2003,** *75* (16), 3962-71.

51. Keithley, R. B.; Takmakov, P.; Bucher, E. S.; Belle, A. M.; Owesson-White, C. A.; Park, J.; Wightman, R. M. Higher sensitivity dopamine measurements with faster-scan cyclic voltammetry. *Anal. Chem.* **2011,** *83* (9), 3563-71.

52. Adam K. Dengler, R. M. W., Gregory S. McCarty Microfabricated Collector-Generator Electrode Sensor For Measuring Absolute pH and Oxygen Concentrations. *Anal. Chem.* **2015,** *87*, 10556-10564.

53. Kawagoe, K. T.; Garris, P. A.; Wightman, R. M. Ph-Dependent Processes at Nafion(R)-Coated Carbon-Fiber Microelectrodes. *J. Electroanal. Chem.* **1993,** *359* (1-2), 193-207.

54. Johnson, J. A.; Hobbs, C. N.; Wightman, R. M. Removal of Differential Capacitive Interferences in Fast-Scan Cyclic Voltammetry. *Anal. Chem.* **2017,** *89* (11), 6167-6175.

55. Jian-Xing Feng, M. B., Kenneth Renner, Richard Kasser, Ralph N. Adams Electrochemical Pretreatment of Carbon Fibers for in Vivo Electrochemistry: Effects on Sensitivity and Response Time. *Anal. Chem.* **1987,** *59* (14), 1863-1867.

56. Engstrom, R. C. Electrochemical Pretreatment of Glassy Carbon Electrodes. *Anal. Chem.* **1982,** *54*, 2310-2314.

CHAPTER 6

Extending Fast-Scan Cyclic Voltammetry to Intracellular Measurements Using Nanocone Electrodes

This work was completed in collaboration with: Roberts, J.G., Mitchell, E.C., Dunaway, L.E., and Sombers, L.A., and is in preparation for submission to the Journal of Analytical Chemistry.

6.1 Introduction

Single cells from mammalian adrenal glands have been used extensively as models for studying exocytosis, the primary method by which cellular chemical communication occurs.[1-3] During exocytosis, vesicles containing chemical messengers fuse with the cell membrane where they subsequently release all or a portion of their contents into the synaptic cleft and/or extracellular space to propagate and regulate chemical communication.[4-5] Electrochemical approaches are well suited to monitor this vesicular release of redox active molecules with excellent temporal resolution and chemical selectivity.

Carbon-fiber microelectrodes are the most common electrode design when studying the dynamics of exocytosis, as the carbon substrate is sensitive to catecholamine release and the size is congruent with cell diameter. In general, 10 μm diameter, glass-insulated disk electrodes are placed directly on a cell to limit molecular diffusion and increase the likelihood of measuring individual release events.[6] Although it is less common, attempts have been made at acquiring electrochemical measurements within the cytosol, since having the ability to measure the uptake and packaging of neurochemicals would allow researchers to answer yet unaddressed questions regarding dynamics of and conditions required for these functions on a

sub-second time scale. In one related study, 2 μm platinum disk electrodes were inserted into giant snail neurons and linear-sweep pulsed voltammetry was used to monitor transport of dopamine bathed onto the cell as it crossed the cell membrane.[7] However, the slow scan rate and cleaning pulse phase significantly limited the temporal resolution and the electrochemical information obtained precluded qualitative analyte identification.

The ability to make intracellular measurements greatly expands the dimensionality of chemical information about the release, uptake, and packaging of neurotransmitters, as well as allowing for quantitation of other electroactive molecules that are generated within the cell or that cross the membrane. This type of information has been largely inaccessible due to the challenges of developing a stable electrode with the proper geometry to facilitate placement inside a single cell without causing extensive damage, while selectively sampling the cytosol and excluding the extracellular environment. Since the carbon fibers typically used for electrochemical experiments at single cells have a diameter of approximately 10 μm, which is roughly the same scale of the cells being studied, it is necessary to reduce the size of the probe in order to insert it into the interior of the cell. Ewing et. al. have recently implanted a flame etched carbon-fiber electrode within the cytosol of PC12 cells.[8] Interestingly, when this electrode was implanted, amperometric current spikes that resembled individual vesicular exocytosis events were observed which originated from within the cell. This perplexing finding was determined to be the result of individual vesicles lysing at the electrode and releasing their contents onto the surface.[9-10] Furthermore, intracellular vesicular content was compared to that measured at an extracellular disk electrode during exocytotic events, lending the finding that only a portion of the vesicular content was released to the environment.

Electrochemical measurements made at single cells generally employ amperometric detection, where the potential is held constant to drive chemical reactions at the electrode surface. Amperometry provides excellent sensitivity for measuring low quantities of analyte, and is unmatched in its temporal response, which is needed for studying dynamics of fast exocytotic events. However, this electrochemical technique provides little qualitative information as to which analyte is being detected, which can be limiting in complex biological preparations where multiple interfering species are present. Voltammetry dynamically scans through a range of potentials to drive redox reactions, which can lead to multiple oxidation and/or reduction peaks at discrete voltages to be used for analyte identification and quantification. This inherent chemical selectivity is crucial to researchers looking to distinguish the actions and origins of various neurotransmitters from one another due to the vastly diverse chemical content within cells. For example, voltammetry has proven capable of distinguishing and quantifying both serotonin and histamine released from mast cells.[11-12] Similarly, chromaffin cells are known to contain both norepinephrine and epinephrine, which are electrochemically active neurotransmitters. These catecholamines are structurally similar, and the enzymatic conversion of norepinephrine to epinephrine takes place within the cell through phenylethanolamine *N*-methyltransferase. Chromaffin cells secrete norepinephrine and epinephrine, however the relative amounts of these catecholamines, and by which cells they are secreted, remains in question.[13-14] Amperometric detection of exocytosis events at chromaffin cells allows for the quantification of the total catecholamine content being released; however, without chemical selectivity, the identity of the analytes being released cannot be determined. Fast scan cyclic voltammetry (FSCV) is able to provide sufficient selectivity

between norepinephrine and epinephrine and has been used to differentiate these molecules during exocytotic release events.[14-16] The combination of FSCV with a carbon based probe that can access the cytosol would permit chemically selective measurements to yield further insight into the transport and functions of these chemicals.

In this work, we developed carbon-fiber microelectrodes with a conical geometry, by way of a wet etching method and a phenolic-paraffin insulation. These innovative electrodes were used to penetrate the cell membrane to access the cytoplasm of chromaffin cells and subsequently identify and quantify intracellular vesicle content. Intracellular measurements using voltammetry with slow scan rates have been attempted before, but to our knowledge, FSCV has never been shown intracellularly.[7, 17-18] Additionally, most probes intended for cytosolic recording are not able to differentiate intra- and extracellular environments, as they the sensing surface bridges both regions. We sought to advance this field by adding a voltammetry technique with chemical selectivity, and highlight the utility of FSCV for making measurements intracellularly. Additionally, we used an extended voltammetric waveform to successfully distinguish norepinephrine and epinephrine in individual vesicles, as they adsorbed and lysed onto the electrode surface. The capability to qualitatively and quantitatively identify cytosolic neurotransmitters in real time has never been shown before and this research will permit exciting new studies about the dynamics of the vesicular packaging of these molecules and the effects of pharmacology on single cells from a new perspective.

6.2 Experimental Section

6.2.1 Chemicals

All chemicals were purchased from Sigma Aldrich Co. (St. Louis, MO) and used without additional processing. Aqueous solutions were made using doubly deionized water (Barnstead Easy Pure II, Dubuque, IA). Experiments done in a flow injection apparatus were carried out in phosphate-buffered saline (0.1 M PBS) at pH 7.4.

6.2.2 Electrode Fabrication

Cylindrical carbon-fiber microelectrodes were constructed using t-650 carbon fibers as previously described.[19] Briefly, a single carbon fiber was aspirated into a glass capillary (1.0 mm x 0.5 mm, A-M Systems, Carlsburg, WA). A tapered seal was subsequently formed by using a micropipette puller (Narishige, Tokyo, Japan) and the exposed carbon fiber was trimmed to 500 µm. An electrical connection was made with the fiber by coating a lead in silver paint (Silver Print II, GC Electronics) and inserting it into the back of the capillary. The exposed carbon fiber was next etched into a conical geometry by rapidly dipping and extracting the electrode into 4 M KOH while applying a +7 V potential to the carbon electrode, versus a platinum wire. The carbon fiber was insulated with a phenolic mixture by electropolymerization.[20] The tip (5 µm) of the conical electrode was masked, to prevent insulating this portion of the electrode intended to be inside the cell, by inserting it into a conductive silicon rubber (SSP1529 0.080, Specialty Silicone Products, Ballston Spa, NY, generous gift provided courtesy of Marian Inc., Salem, VA). All movements of the electrode were done with micromanipulators, including etching and insulation steps. The position of the electrode was monitored by measuring the impedance of the electrode/rubber interface with a

lock-in amplifier (7280, Ametek, Berwyn, PA). After the electrode was masked to the desired depth, the phenolic polymer insulation solution was electrodeposited onto the exposed carbon surface with +4 V applied to the carbon electrode, versus a platinum electrode, for 14 minutes. The electrode was removed from the mask and oven dried at 150 °C for 30 minutes. Electrode images were collected using scanning electron microscope (Hitachi S-3200N) with a 5 kV accelerating voltage, and electrodes were coated with a 60/40 gold/palladium alloy prior to imaging.

6.2.3 Flow Injection

Electrochemical data were collected using a flow injection apparatus that was housed within a custom built Faraday cage to reduce noise interference. The working electrode was positioned in the electrochemical cell using a micromanipulator (World Precision Instruments, Sarasota, FL). Buffered electrolyte was passed continuously over the working and reference electrode at 1 mL/min using a syringe pump (New Era Pump Systems, Wantagh, NY). A digital valve interface (Valco Instruments Company, Houston, TX) was used to control an air actuator connected to a six-port HPLC valve in order to introduce two-second bolus injections of analyte across the working electrode.

6.2.4 Electrochemical Data Acquisition

All potentials in voltammograms were reported versus a Ag/AgCl reference electrode (World Precision Instruments, Sarasota, FL). Analyte detection with FSCV was accomplished using triangular waveforms applied with an application frequency of 10 Hz. Waveform

application and current transduction was accomplished using open source software and custom instrumentation (HDCV, University of North Carolina at Chapel Hill, Department of Chemistry, Electronics Facility), along with a DAC/ADC card (NI 6363, National Instruments, Austin, TX). Current output was filtered with a four-pole low-pass Bessel filter. Background subtraction and signal averaging was software controlled. For amperometry experiments, electrodes were held at +850 mV with a patch-clamp amplifier (Axopatch 200B, Molecular Devices, Sunnyvale, CA) set to voltage-clamp mode in Whole Cell (ß = 1) configuration. The Axon Digidata 1440A (Molecular Devices, Sunnyvale, CA) was used to digitize data at 2 kHz. Axoscope software (Version 10.4.1.9, Molecular Devices) was used for amperometric data collection.

6.2.5 Primary Bovine Chromaffin Cell Culture

Bovine adrenal glands were obtained from a local slaughterhouse to establish primary culture. Adrenal glands were swiftly removed from the carcass and immediately trimmed of excess fat, perfused with cold W3 buffer (145 mM NaCl, 5.4 mM KCl, 1 mM NaH_2PO_4, 11.2 mM glucose, and 15 mM HEPES) through the adrenal vein, and submerged in ice-cold W3. Upon arrival in the lab, the glands were perfused with warm W3 and incubated at 37 ˚C for 10 minutes. The warm perfusion and incubation step was repeated in triplicate. Glands were then perfused with a digestion mixture containing 0.035 mg/mL DNAase and 1.4 mg/mL collagenase in W3 and then incubated for 15 minutes. Again, this digestion perfusion was repeated in triplicate. Nystatin (5 mL/L) was added to W3 and used for all remaining steps involving W3. After incubation, the glands were sliced longitudinally and the medullae were

removed from all glands, finely minced, placed in 36 ˚C digestion mixture, and stirred for 30 minutes. The digested solution was filtered (250 µm) and centrifuged to pellet the cells. After decanting, pellets were resuspended in a mixture of 90% Percoll and 10% 10x W3. The gradient was centrifuged to separate red blood cells, chromaffin cells, and cellular debris. The chromaffin cell layer, formed in the middle, was collected and filtered through a 40 µm sterile nylon filter. DMEM (Dulbecco's Modified Eagle Medium) was added to the filtrate and pelleted. The supernatant was removed and the pellets were resuspended in DMEM containing 10% FBS and 1% 100X Pen-strep. Cells were then plated on 35 mm culture dishes, and placed in the incubator. Cell media was changed every two days and initial testing occurred after three days of incubation.

6.2.6 Single Cell Experiments

Cell culture dishes were prepared for electrochemical measurements by replacing the DMEM with an isotonic buffer (150 mM NaCl, 5 mM KCl, 1.2 mM $MgCl_2$, 5 mM glucose, 10 mM HEPES, and 2 mM $CaCl_2$ at pH 7.4) and maintained at 37 ˚C using a culture dish incubator (DH-35iL, Warner Instruments, Camden, CT). To elicit exocytosis, a high potassium isotonic stimulating buffer (55 mM NaCl, 100 mM KCl, 1.2 mM $MgCl_2$, 5 mM glucose, 10 mM HEPES, and 2 mM $CaCl_2$) was loaded into a micropipette and puffed onto the cell with a 3 second, 20 psi pulse (Picospritzer II; General Valve Corporation, Fairfield, NJ). Cells were imaged on an inverted microscope (Olympus IMT-2) equipped with Hoffman Modulation Contrast optics and a 40x objective.

6.2.7 Data Analysis

Amperometric current peak areas were quantified using Mini Analysis software (Version 6.0.3, Synaptosoft). Custom Matlab scripts were used in voltammetric analysis (Matlab, MathWorks, Natick, MA). The limit of detection was defined as three times the standard deviation of the noise. Data are reported as the mean ± standard deviation. Graphical and statistical analysis was performed with Graph Pad Prism 5 (GraphPad Software, Inc., La Jolla, CA).

6.3 Results and Discussion

6.3.1 Electrode Development

In order to successfully position a carbon-fiber electrode inside the chromaffin cell cytosol, it was necessary to both reduce the diameter of the carbon fiber and alter its geometry so that it could penetrate the cell membrane with minimal force, as to not destroy the cell. Single chromaffin cells have diameters of ~10-20 μm, whereas carbon fibers have a diameter of approximately 10 μm.[21] Various techniques for reducing the dimensions of a carbon based electrode, such as flame etching, polishing, and wet etching, have been utilized for various aims.[22-24] For this work the wet etching procedure was chosen, because in our hands, it was proven to be effective, reproducible, and easily implemented (Figure 6.1). Briefly, a carbon-fiber electrode was lowered into a solution of 4 M potassium hydroxide, while a potential of +7 V was applied to the electrode versus a platinum reference wire, then removed from the solution. The process of dipping the electrode is essential to form a conical geometry, as the

tip of the electrode, being in contact with the solution for the longest, experiences more etching time than the remainder of the carbon surface. The applied potential was sufficient to rapidly etch the carbon, as the carbon fiber was exposed to the solution for about 1 to 1.5 seconds. The angle of the cone is dependent on the applied potential and the rate of movement, as a higher voltage and/or slower dipping rate will result in a more blunted point.

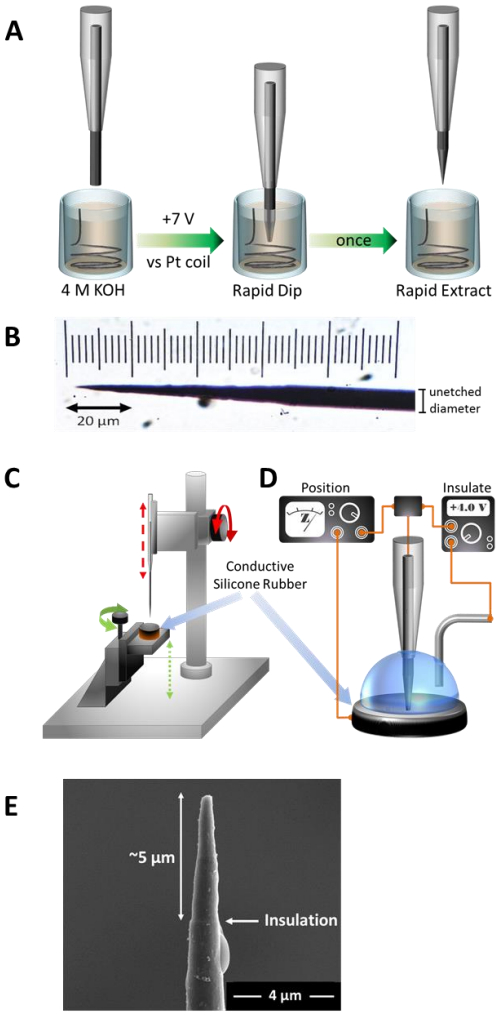

Figure 6.1. Fabrication of insulated conical nanoelectrodes. A) Schematic depicting the wet etching process. A carbon fiber cylinder electrode is positioned inside a solution of 4 M KOH. A potential of +7 V is applied to the carbon electrode, versus a coiled platinum wire. The electrode is rapidly lowered further into solution, then raised completely out of solution. B) Representative optical image of an etched electrode with a conical geometry. C) Diagram of the unit used to insulate the exposed carbon. An impedance meter is used to indicate when the carbon is directly above the conductive silicon rubber. Macro- and micro-positioners were used to vertically position the carbon fiber and the silicon rubber, respectively. D) Magnified view of the carbon fiber inserted into the silicon rubber. Once the fiber is masked to the desired length, a drop of polymer solution is placed and a platinum reference electrode is inserted, the insulation is electropolymerized around the fiber. E) Scanning electron micrograph of an insulated conical carbon fiber. An 8 µm diameter carbon fiber is tapered to a sharp point for insertion into cells. A ridge seen at ~5 µm from the tip indicates the formation of a thin layer of phenolic insulation.

An optical image of a representative electrode after the etching procedure is shown in Figure 6.1B, where the fiber tapers toward the tip of the electrode to form a sharp conical geometry. Even though the geometry of this design permitted cell penetration, a large portion of electroactive surface area remained outside of the cell. Having sections of the sensing surface both inside and outside of the cell would confound the origin of any electrochemical measurements. One means to address this potential shortfall without further modification of the sensor is to use a calcium free buffer. Without extracellular calcium present, the cell would be unlikely to undergo exocytosis and any measured events would be assumed to result from vesicular lysing. However, exocytotic events generated in response to intracellular calcium stores could not be ruled out. Additionally, this would limit experiments seeking to evaluate intracellular dynamics during exocytotic events. Another approach to selectively monitor the cytosol, is to insulate any electroactive portion of the electrode that would be outside the cell, so that the entirety of the electroactive electrode area is positioned inside the cell, and recorded events could safely be assumed to have resulted from intracellular measurements. This would also allow for intracellular measurements during exocytotic events.

Various attempts have been published for insulating carbon-fiber microelectrodes whereby the entire fiber is insulated and subsequently cut to expose carbon, or an extended length of exposed carbon protrudes from the insulation and is cut to length after the insulation process.[19, 25] These traditional approaches are not appropriate for this work, as the conical tip is created prior to any insulation step. To address this problem, the etched electrode tip was positioned inside conductive silicone rubber, using a micropositioner, to mask the desired surface area and shield it from insulation. A lock-in amplifier was used to measure the

impedance across the carbon/silicone interface to assist in positioning and indicators on the manipulators were used to quantify depth (Figure 6.1C). After masking, the phenolic solution used for insulating was dropped onto the silicon surface to cover the exposed carbon, and a platinum reference wire was positioned in the solution adjacent to the carbon electrode. The polymeric insulation was electropolymerized onto the carbon fiber to form a uniform insulating layer along the length of the exposed carbon fiber (Figure 6.1D). Since most chromaffin cells are in the ballpark of 20 μm in diameter we surmised that a sensing length of 5 μm would serve well for intracellular studies. A representative etched and insulated electrode is shown in Figure 6.1E, where this electrode has a tapered diameter of ~300 nm and a slight ridge 5 μm from the tip indicating the insulation boundary, where the silicone mask ended.

6.3.2 Electrochemical Characterization

Once the methodology was established for fabrication of the desired geometry, the electrochemical performance of these new electrodes was characterized *in vitro*. Carbon fiber electrodes are often electrochemically conditioned by continuously applying the potential waveform which is used for analyte quantification, for 10 to 20 minutes. This procedure serves to both populate and stabilize chemical functionalities on the electrode surface that enhance analyte detection.[26-27] As we conditioned these electrodes it was observed that the performance never stabilized, but instead the background voltammograms collected during the preconditioning phase gradually increased in magnitude. Steady state background current (i_c) generated during a potential sweep (v) is directly proportional to capacitance (C_d), which is fundamentally dependent on electrode surface area (Equation 1).[28]

$$Equation\ 1 \qquad |i_c| = C_d v$$

Thus we determined that the insulation was not stable, and slowly dissociated from the electrode surface as a result of extended electrochemical conditioning, exposing more carbon surface.

Several strategies were evaluated to improve the stability of the insulation, including thicker insulations and altering the ratio of the components of the polymerization solution, all with limited success. The method that was ultimately successful in improving the insulation stability was a strategy whereby we reinforced the polymer insulation by adding a second insulator. Wax coatings have been shown to function as a sealant material for glass insulated carbon electrodes.[29] As a means to reinforce the polymer coating and prevent degradation, we encased the electrode tip in paraffin wax. Doing so resulted in coating the bare carbon surface, which effectively insulated and prevented any electron transfer at the electrode surface. Figure 6.2A is the background-subtracted voltammogram of 1 μM dopamine that was collected using an electrode with the additional wax coating. There were no identifiable redox features present in this voltammogram, indicating that the entire carbon surface was insulated. Subsequent electrochemical conditioning removed the wax at the sensor surface,[29] to expose the small portion of carbon fiber without the phenolic insulation. Indeed, the same representative electrode used in Figure 6.2A was able to measure dopamine after conditioning for approximately 10 minutes (Figure 6.2B). In order to test the efficacy of the wax layer in protecting the polymeric later, insulation stability was assessed by monitoring dopamine oxidation current for a duration of three hours, at 15 min intervals. Failure of the insulation

would expose more surface area and oxidation current from a single concentration of dopamine would continue to increase, as peak current is proportional to surface area. After three hours of repeated electrochemical cycling, dopamine oxidation current remained stable ($p<0.05$, two-tailed t-test, Figure 6.2C). This result indicated that the use of a bilayer insulation provides a stable electrode for continual usage, where the paraffin wax layer was able to preserve the integrity of the phenolic insulation and not impede the carbon surface.

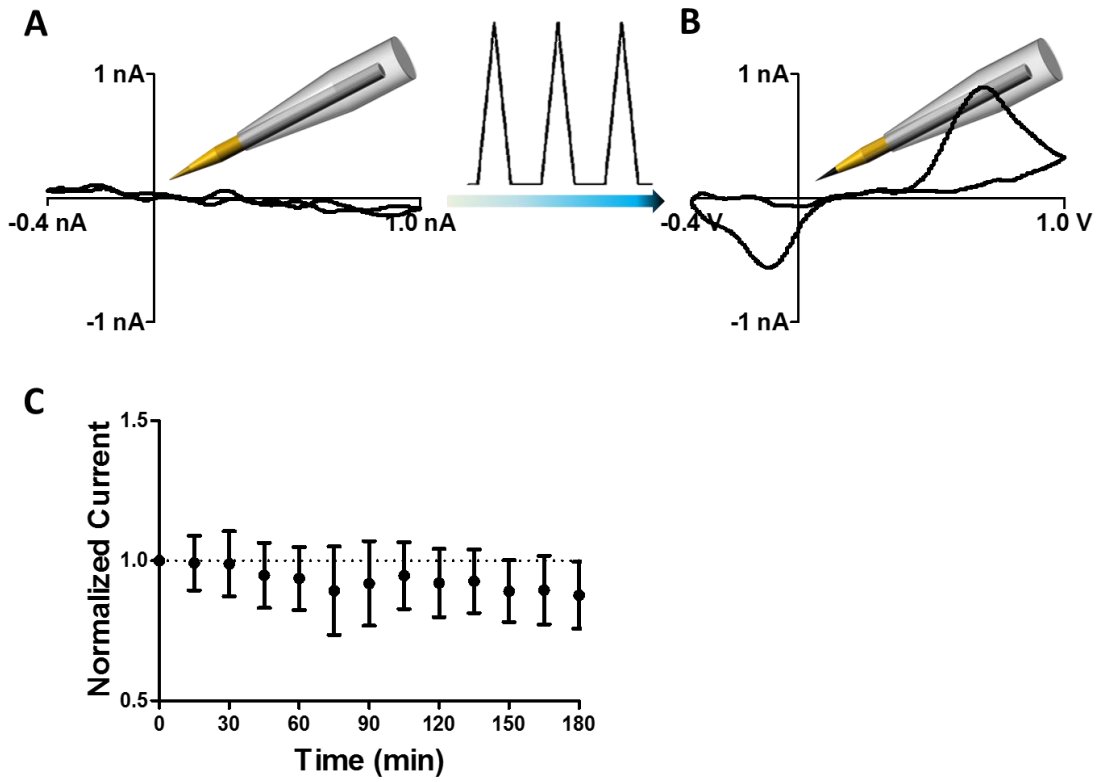

Figure 6.2. Wax coating to stabilize insulation. A) Dopamine redox was not observed when the electrode was fully coated in wax. B) Electrochemical conditioning effectively removed the wax coating from the portion of the fiber without phenolic insulation and dopamine was quantitated. C) The normalized oxidation current in response to 1 µM dopamine is plotted against collection time (n=3 electrodes, standard deviation). Data are normalized to the first response (time zero).

Additional analysis of this sensor focused on means of increasing peak redox currents without further modification, with the intent to increase the signal for analyte detection. Fundamental electrochemistry principles dictate that peak redox current (i_p) is proportional to the scan rate (ν) of the applied waveform for a surface adsorbed species (Equation 2),[28]

$$Equation\ 2 \qquad i_p = \frac{n^2F^2}{4RT}\nu A\Gamma$$

where the number of electrons (*n*), Faraday's constant (*F*), surface area (*A*), and surface concentration (Γ) are also proportional. Figure 6.3A highlights representative dopamine voltammograms collected using the same electrode at varying scan rates, and it was observed that peak current increased as the scan rate was raised from 400 to 2000 V/s. Additionally, a phenomenon observed with molecules that have quasi-reversible electron transfer kinetics, such as dopamine, is that the separation of the oxidation and reduction peaks increases as the scan rate is increased. Figure 6.3B shows normalized dopamine voltammograms collected at multiple scan rates, to highlight this peak shifting and separation. These data confirmed that the electrodes behaved according to principle and that the bilayer insulation did not interfere with the detection of dopamine.

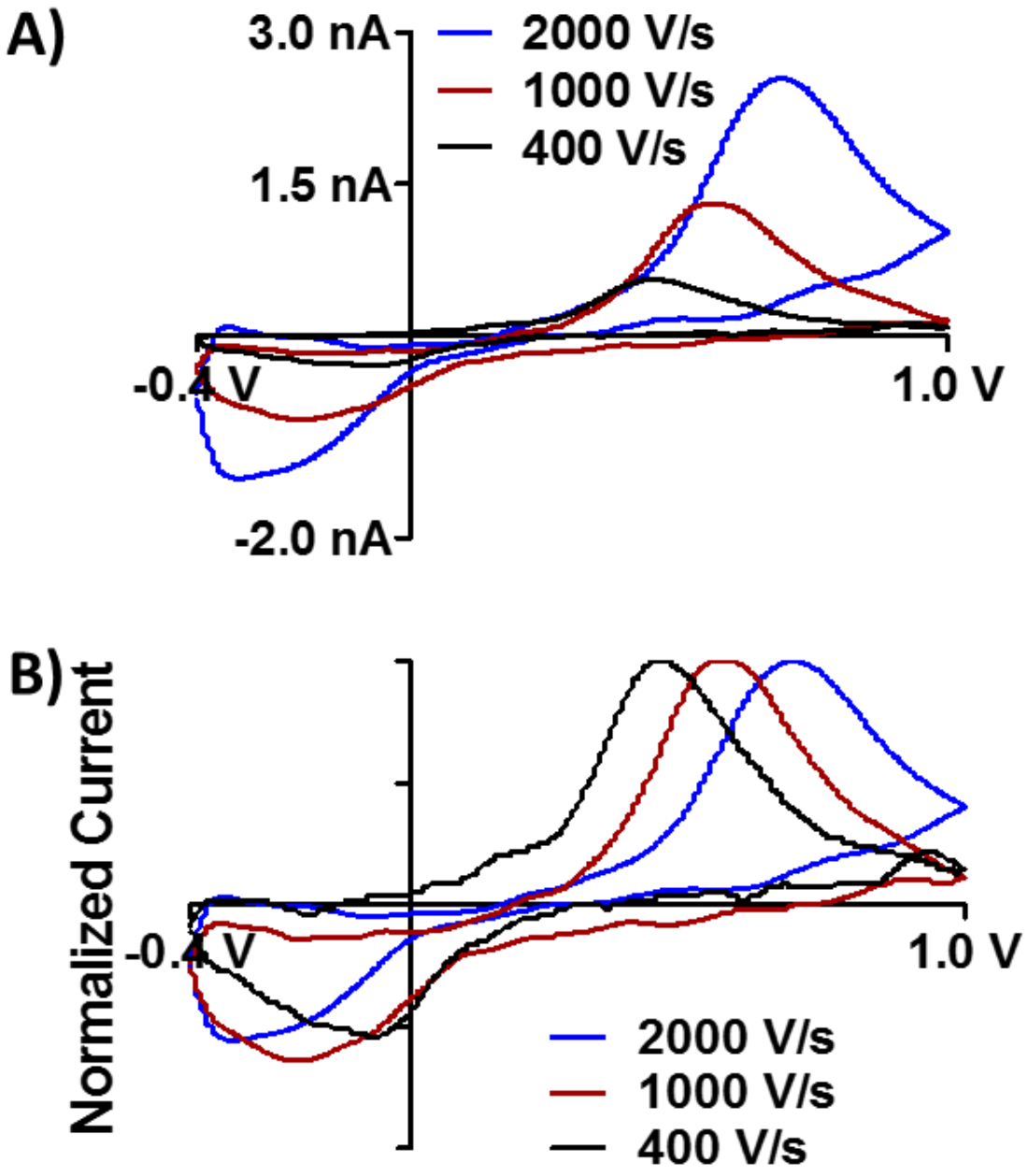

Figure 6.3. Electrochemical characterization of dopamine at conical electrodes. A) Representative voltammograms of 2 µM dopamine at multiple scan rates (blue line = 2 kV/s, red = 1 kV/s, black = 400V/s). B) Voltammograms from panel A that have been normalized to the magnitude of the oxidation peak.

6.3.3 Intracellular Characterization

As stated in the introduction, amperometry with carbon fiber disk electrodes is the most commonly used electrochemical technique for measuring vesicular release at single cells. Therefore, we initially assessed the performance of the new electrode design compared to a disk electrode by performing amperometric measurements at single cells. With the conical electrode positioned on the surface of a cultured chromaffin cell and held at +650 mV, no electrochemical activity was recorded unless chemically stimulated. Pressure-ejecting 100 mM KCl buffer (isotonically balanced with NaCl) resulted in the detection of amperometric spikes (Figure 6.4) rising from exocytotic events. The successful detection of exocytotic events indicated that the electrode design had sufficient sensitivity to quantify extracellular vesicular catecholamine release with amperometry.

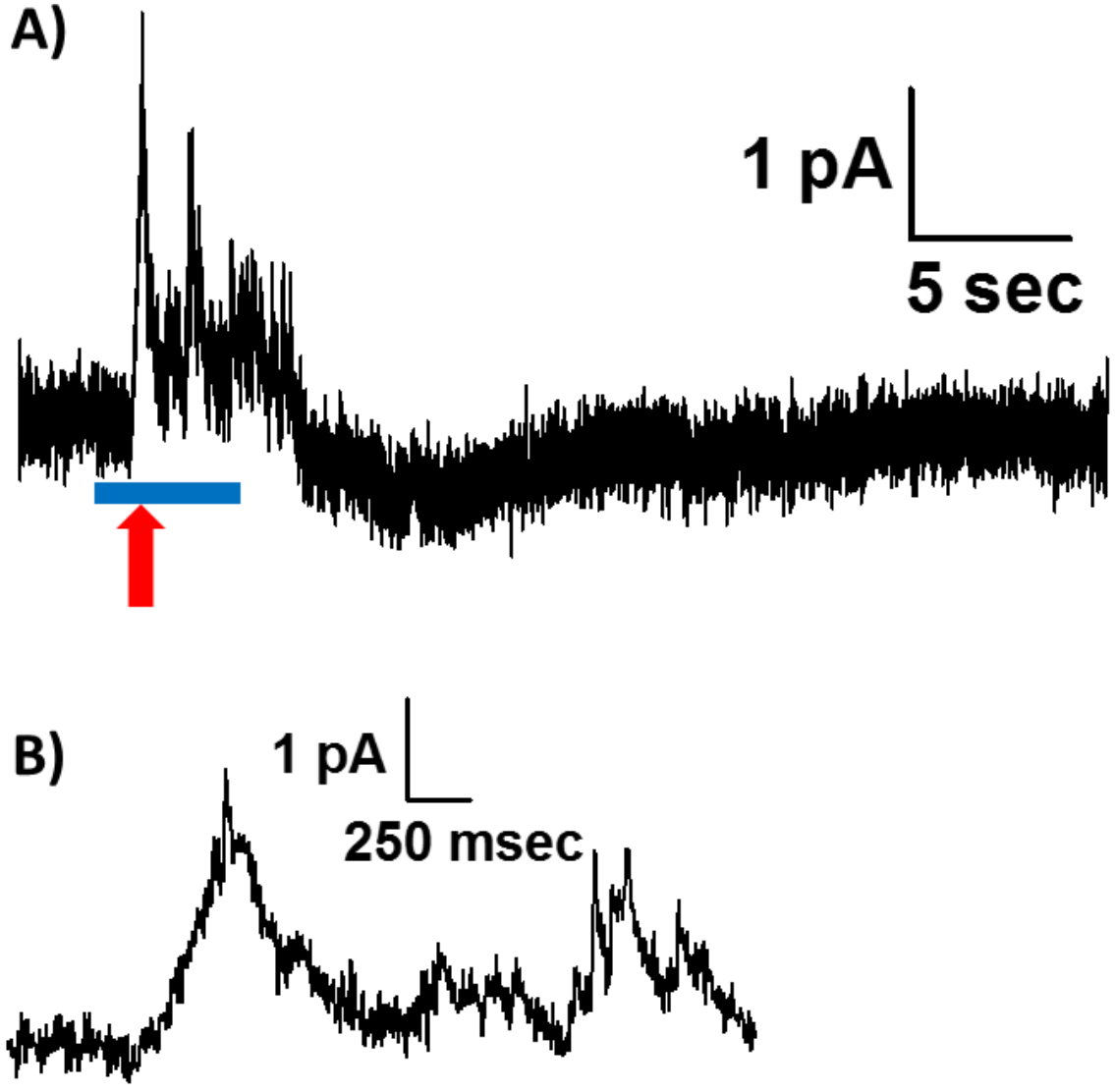

Figure 6.4. Individual exocytotic events recorded at conical electrodes. A) Amperometric trace recorded during potassium stimulation. The red arrow indicates the time of stimulation. B) Expanded view of the region highlighted by the blue bar in Panel A.

After establishing that the electrode could monitor vesicular release, it was inserted into the cell cytoplasm to obtain intracellular chemical measurements, illustrated in Figure 6.5. In

Figure 6.5A, an electrode was positioned next to a cell using piezoelectric micromanipulators, showing the relative scale of the task. The tip of the electrode was then pressed against the membrane, causing an indentation in the cell membrane (Figure 6.5B). Cells were selected that were firmly attached to the culture dish and would accept the force of the electrode without becoming dislodged. Application of sufficient force allowed for the electrode to penetrate the cell membrane and access the cytoplasm, forming a seal around the electrode (Figure 6.5C). From this position it was possible make chemical measurements intracellularly.

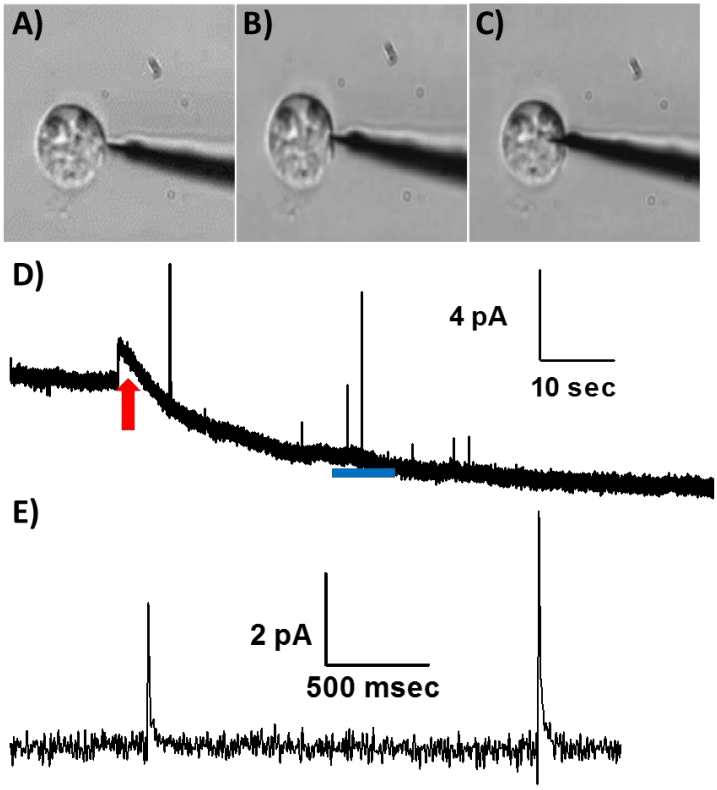

Figure 6.5. Intracellular recordings. A) The electrode is placed near the cell, B) pressed against the cell membrane, and C) inserted into the cell cytoplasm. D) Amperometric trace recorded during cellular penetration. The red arrow indicates the time point when the electrode gained access to the cytosol. E) Expanded view of the region highlighted by the blue bar shown in Panel D.

Upon insertion of the nanoelectrode into the cell, amperometric spikes were recorded that correlate to the collision and lysing of individual vesicles onto the electrode surface, replicating a previous report.[8] The amperometric trace shown in Figure 6.5D was collected as the electrode translated from outside the cell membrane to inside. The shifted baseline is the result of transporting the sensing surface from the buffered solution into the cytoplasm, where it encountered a different chemical environment and was further removed from the reference electrode (positioned in the extracellular buffer). Upon insertion of the nanoelectrode into the cytoplasm, amperometric spikes were recorded that correlate to the collision and lysing of individual vesicles onto the electrode surface, replicating a previous report.[8] As shown in Figure 6.5E, these events have sharp rise and decay times, similar to exocytotic events observed with an electrode positioned extracellularly. While the report by Ewing validated their intracellular measurements by comparing to a control where an electrode placed outside the cell recorded no spontaneous spikes, our results further validate the origin of these spikes by insulating the portion of the electrode that was outside of the cell, and recording the same spontaneous events.

6.3.4 Intracellular Voltammetry

Although amperometry offers outstanding benefits for measuring vesicular contents, it does not provide information on chemical identity. By contrast voltammetry offers qualitative information that can be used for analyte identification.[15] Thus, we sought to extend the utility of our electrodes by coupling them with FSCV to make both qualitative and quantitative chemical measurements. The Axopatch amplifier is commonly used to make electrochemical

measurements at single cells because of the low-noise electronics that it utilizes; therefore, for our initial investigation we used this system with the superior signal to noise ratio. Unfortunately, the desired waveform for catecholamine detection that results in greater sensitivity to catecholamines has a switching potential of +1.3 V,[30] but the maximal potential output of the Axopatch is only +1.0 V. With this limitation, the applied waveform ranged from -0.4 to +1.0 V. Figure 6.6 shows representative data collected using FSCV as the cell membrane was penetrated using the conical electrode. Upon insertion into the cell, a shifted baseline is observed in the color plot, as well as discrete vesicular release events (Figure 6.6A). A trace of the current collected at +0.75 V, the potential where peak current for catecholamines is observed, is shown in Figure 6.6C. These peaks clearly resemble those seen with amperometric detection (Figures 6.4 and 6.5). Figure 6.6B shows a voltammogram that was taken during one of the vesicular events (vertical dashed line in Figure 6.6A). The oxidation and reduction peaks identify the analyte as a catecholamine; however, we cannot distinguish between the two primary catecholamines, norepinephrine and epinephrine, present in the chromaffin cell using this voltammetric waveform. These data highlight the capacity of FSCV to gain more chemical information about the intracellular environment and still observe the spontaneous events.

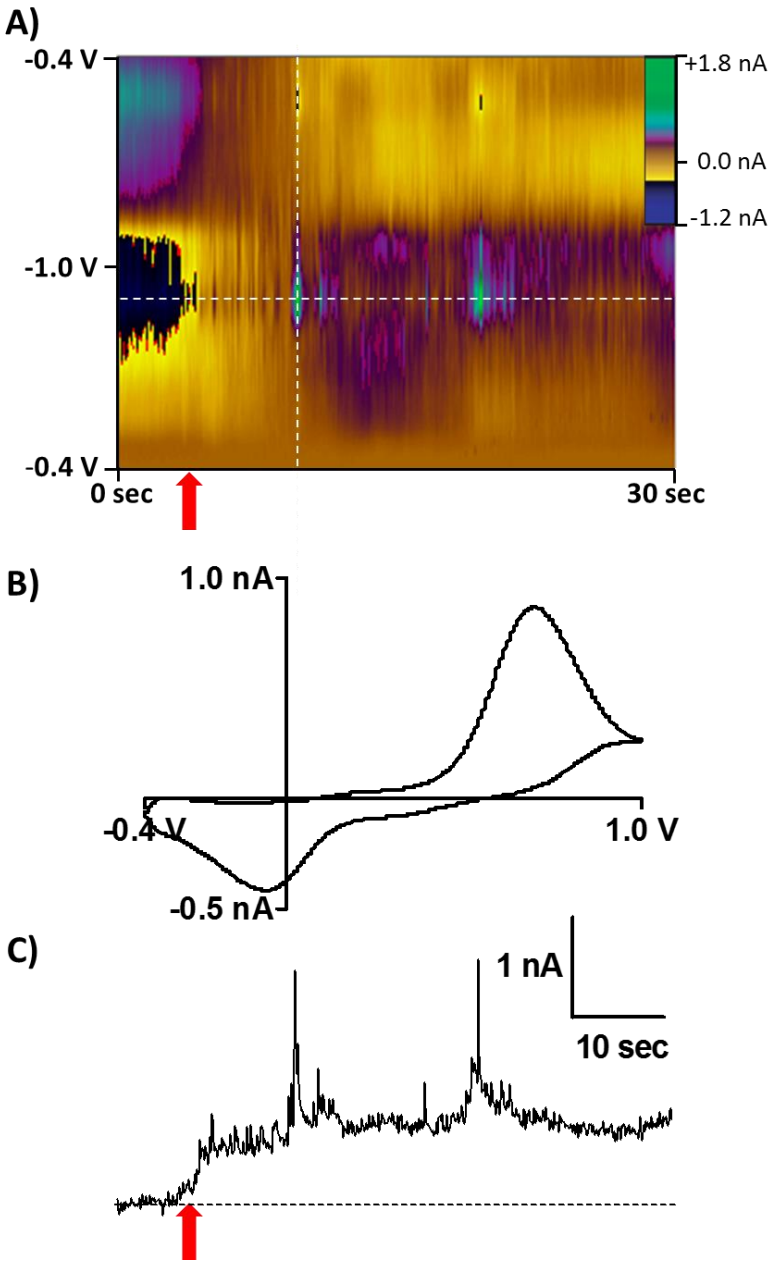

Figure 6.6: Intracellular voltammetry. A) Colorplot recorded during insertion of the electrode into the cell cytoplasm. The red arrow indicates the time of membrane penetration. B) Voltammogram taken from (A) indicated by the vertical white dashed line. The voltammograms show a clear catecholamine signal. C) Current verse time trace taken at the potentials shown by the horizontal white dashed line in (A). The red arrow indicates insertion into the cell.

The structural similarities between norepinephrine and epinephrine give way to similar voltammograms for these analytes at the potential limits employed in the previous experiment. However, by changing the applied waveform, Wightman and coworkers demonstrated that a second oxidation peak for epinephrine can be observed if the potential limit is extended to approximately +1.425 V.[15] In order to apply this capability in our own experiments, custom instrumentation was used to apply an extended cyclic waveform of +0.1 V to +1.45 V, as the Axopatch is limited to +1.0 V. This extended waveform was applied to the conical nanoelectrode *in vitro* and calibrated to both analytes. Figure 6.7 shows representative voltammograms demonstrating that the oxidation of norepinephrine results in a single peak, but the oxidation of epinephrine generates two distinct peaks. The first peak at approximately +0.65 V originates from oxidation of the hydroxyl groups to an ortho-quinone (Scheme 1.1), and the second peak at +1.45 V arises from the oxidation of the secondary amine (Scheme 1.2). Thus, the presence of the secondary peak provides a marker to distinguish norepinephrine from epinephrine.

Scheme 1: Electrochemical reactions for norepinephrine and epinephrine.

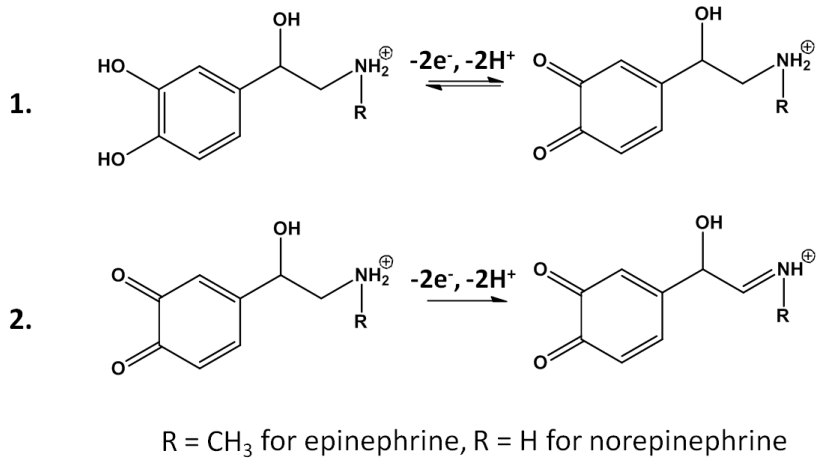

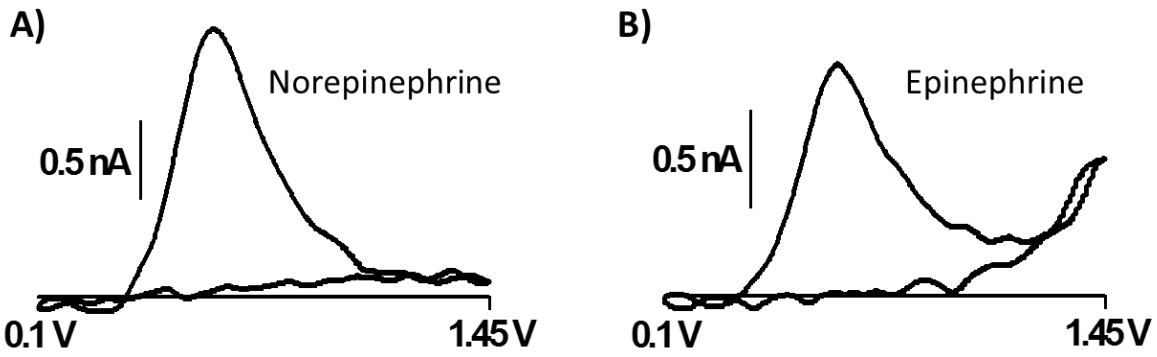

Figure 6.7. Norepinephrine and epinephrine voltammetry. A) 10 µM norepinephrine. B) 10 µM epinephrine.

Using this extended waveform, intracellular voltammetric data were collected using FSCV at conical electrodes. Spontaneous electrochemical events were observed, in Figure 6.8, while recording in the cytosol. To investigate the relationship between norepinephrine and epinephrine, current versus time traces were extracted from these data at two different

potentials (+0.65 and +1.425 V), and current was then converted to concentration using electrode sensitivity. For the data shown, the calibration factors were 0.29 nA/μM for norepinephrine, and 0.20 nA/μM for epinephrine's first peak and 0.08 nA/μM for the second. By comparing the peaks generated at these potentials it was possible to discern the two catecholamine species. Events that generated current at both potentials indicated the presence of epinephrine, whereas events that generated current only at +0.65 V corresponded to norepinephrine containing vesicles. The concentration versus time traces show that many of the vesicular lysing events indicated the presence of mostly epinephrine-containing vesicles. For example, the event marked by the red square had a corresponding peak in both traces. The extracted voltammogram in Figure 6.8C shows two oxidation peaks indicative of epinephrine. By contrast, the event marked by the blue square has no associated peak at +1.425 V. The voltammogram taken from this time point (Figure 6.8B) revealed that the event was generated from norepinephrine and had no discernable epinephrine. Interestingly, adrenal cells are thought to convert most of the norepinephrine to epinephrine, but these data show that there remains a store of intracellular norepinephrine.

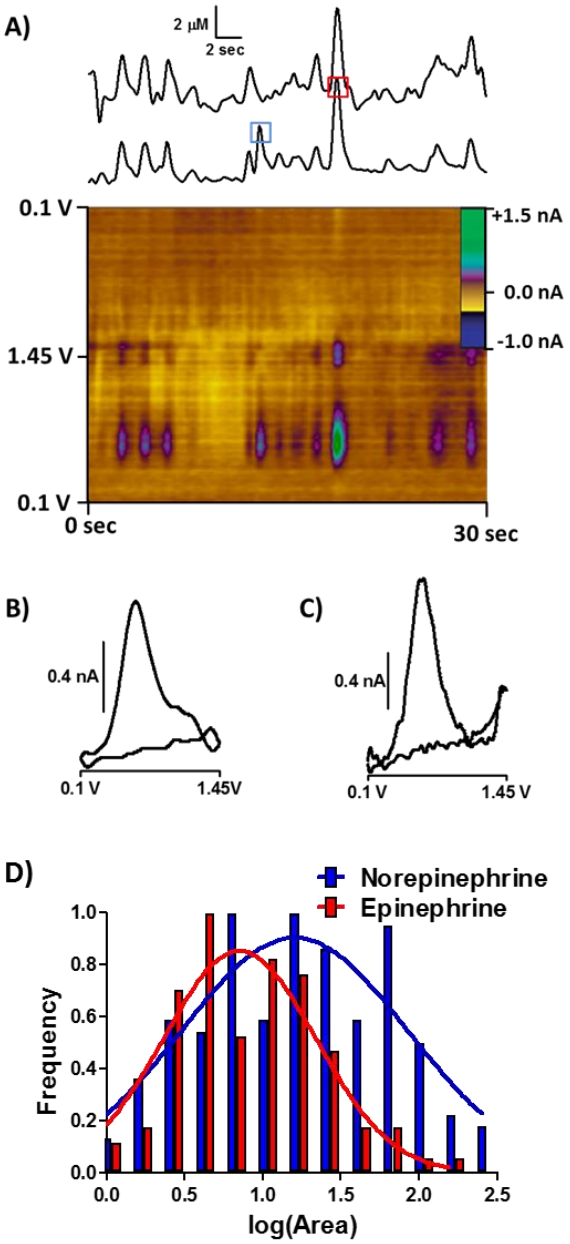

Figure 6.8. Chemical identification and quantification of intracellular vesicle content. A) Representative colorplot collected intracellularly with the extended waveform limits. Concentration vs. time traces are shown above the color plot, top: extracted at +1.45 V, bottom: extracted at +0.65 V. Voltammograms extracted from the color plot are shown for B) norepinephrine and C) epinephrine, collected at the time points marked by the blue and red squares, respectively. D) Histogram of log(Q) distribution for epinephrine (N=71 events) and norepinephrine (N=122 events) containing vesicles.

To further evaluate the chemical heterogeneity of each vesicle, the peak area of each spontaneous lysing event was calculated to determine the charge associated with the detection of norepinephrine and epinephrine, where the charge is proportional to the total number of molecules revealed. In Figure 6.8D, plotting a histogram of each event showed the distribution of epinephrine and norepinephrine containing vesicles. A single Gaussian fit for norepinephrine determined a mean of 2.24 $\pm$ 0.04 pC and epinephrine was 2.05 $\pm$ 0.06 pC. Based on these averages, norepinephrine accounted for approximately 61% of the released content and these data are in agreement with a previous finding that reported both norepinephrine and epinephrine are released from a random sample of chromaffin cells.[14] It is unclear at this point if individual vesicles lacking the enzyme phenylethanolamine N-methyltransferase were the source of norepinephrine, however, this will be the subject of future work.

6.4 Conclusions

Conical carbon-fiber microelectrodes with a bilayer insulation were developed and utilized for intracellular measurements to both identify and quantify vesicular content. By employing a wet etching technique, traditional cylinder carbon fibers were sharpened into a conical geometry with nanometer dimensions. This reduced dimensionality allowed the electrode to penetrate the cell membrane and enter the cytoplasm. The length of exposed surface area was regulated with an elegant masking procedure, and a bilayer insulation provided stable performance. By coupling these electrodes with FSCV, intracellular vesicle

content was measured with chemical selectivity and it was determined that approximately 61% of the vesicle neurotransmitter content corresponded to norepinephrine, over epinephrine. This technique has the potential to provide spatially resolved information on vesicular content within the cell, and to measure chemical transport across the cell membrane. Additionally, the intracellular chemical dynamics associated with manipulation using a variety of pharmacological agents can be revealed. This research provides a new tool that will resolve problematic questions that haven't been challenged due to technological hurdles.

6.5 References

1. Travis, E. R.; Wightman, R. M., Spatio-Temporal Resolution of Exocytosis from Individual Cells. *Annual review of biophysics and biomolecular structure* **1998,** *27*, 77-103.

2. Chen, G.; Ewing, A. G., Chemical Analysis of Single Cells and Exocytosis. *Critical reviews in neurobiology* **1997,** *11* (1), 59-90.

3. Kim, D.; Koseoglu, S.; Manning, B. M.; Meyer, A. F.; Haynes, C. L., Electroanalytical Eavesdropping on Single Cell Communication. *Analytical chemistry* **2011,** *83* (19), 7242-7249.

4. Mellander, L. J.; Trouillon, R.; Svensson, M. I.; Ewing, A. G., Amperometric Post Spike Feet Reveal Most Exocytosis is via Extended Kiss-and-Run Fusion. *Scientific reports* **2012,** *2*, 907.

5. Sudhof, T. C.; Rizo, J., Synaptic Vesicle Exocytosis. *Cold Spring Harbor perspectives in biology* **2011,** *3* (12).

6. Schulte, A.; Schuhmann, W., Single-Cell Microelectrochemistry. *Angewandte Chemie* **2007,** *46* (46), 8760-8777.

7. Lau, Y. Y.; Wong, D. K. Y.; Ewing, A. G., Intracellular Voltammetry at Ultrasmall Platinum-Electrodes. *Microchem J* **1993,** *47* (3), 308-316.

8. Li, X.; Majdi, S.; Dunevall, J.; Fathali, H.; Ewing, A. G., Quantitative Measurement of Transmitters in Individual Vesicles in the Cytoplasm of Single Cells with Nanotip Electrodes. *Angewandte Chemie* **2015,** *54* (41), 11978-11982.

9. Dimitrievski, K.; Kasemo, B., Simulations of Lipid Vesicle Adsorption for Different Lipid Mixtures. *Langmuir* **2008,** *24* (8), 4077-4091.

10. Dunevall, J.; Fathali, H.; Najafinobar, N.; Lovric, J.; Wigstrom, J.; Cans, A. S.; Ewing, A. G., Characterizing the Catecholamine Content of Single Mammalian Vesicles by Collision-Adsorption Events at an Electrode. *J Am Chem Soc* **2015,** *137* (13), 4344-4346.

11. Travis, E. R.; Wang, Y. M.; Michael, D. J.; Caron, M. G.; Wightman, R. M., Differential Quantal Release of Histamine and 5-Hydroxytryptamine from Mast Cells of Vesicular Monoamine Transporter 2 Knockout Mice. *Proceedings of the National Academy of Sciences of the United States of America* **2000,** *97* (1), 162-167.

12. Pihel, K.; Hsieh, S.; Jorgenson, J. W.; Wightman, R. M., Quantal corelease of histamine and 5-hydroxytryptamine from mast cells and the effects of prior incubation. *Biochemistry* **1998,** *37* (4), 1046-52.

13. Cooper, B. R.; Jankowski, J. A.; Leszczyszyn, D. J.; Wightman, R. M.; Jorgenson, J. W., Quantitative-Determination of Catecholamines in Individual Bovine Adrenomedullary Cells by Reversed-Phase Microcolumn Liquid-Chromatography with Electrochemical Detection. *Analytical chemistry* **1992,** *64* (6), 691-694.

14. Ciolkowski, E. L.; Cooper, B. R.; Jankowski, J. A.; Jorgenson, J. W.; Wightman, R. M., Direct Observation of Epinephrine and Norepinephrine Cosecretion from Individual Adrenal-Medullary Chromaffin Cells. *J Am Chem Soc* **1992,** *114* (8), 2815-2821.

15. Pihel, K.; Schroeder, T. J.; Wightman, R. M., Rapid and Selective Cyclic Voltammetric Measurements of Epinephrine and Norepinephrine as a Method to Measure Secretion from Single Bovine Adrenal-Medullary Cells. *Analytical chemistry* **1994,** *66* (24), 4532-4537.

16. Troyer, K. P.; Wightman, R. M., Temporal Separation of Vesicle Release from Vesicle Fusion During Exocytosis. *J Biol Chem* **2002,** *277* (32), 29101-29107.

17. Lau, Y. Y.; Chien, J. B.; Wong, D. K. Y.; Ewing, A. G., Characterization of the Voltammetric Response at Intracellular Carbon Ring Electrodes. *Electroanal* **1991,** *3* (2), 87-95.

18. Meulemans, A.; Poulain, B.; Baux, G.; Tauc, L.; Henzel, D., Micro Carbon Electrode for Intracellular Voltammetry. *Analytical chemistry* **1986,** *58* (9), 2088-2091.

19. Kawagoe, K. T.; Zimmerman, J. B.; Wightman, R. M., Principles of Voltammetry and Microelectrode Surface-States. *J Neurosci Meth* **1993,** *48* (3), 225-240.

20. Strein, T. G.; Ewing, A. G., Characterization of Submicron-Sized Carbon Electrodes Insulated with a Phenol Allylphenol Copolymer. *Analytical Chemistry* **1992,** *64* (13), 1368-1373.

21. Plattner, H.; Artalejo, A. R.; Neher, E., Ultrastructural Organization of Bovine Chromaffin Cell Cortex - Analysis by Cryofixation and Morphometry of Aspects pertinent to Exocytosis. *J Cell Biol* **1997,** *139* (7), 1709-1717.

22. Strand, A. M.; Venton, B. J., Flame etching enhances the sensitivity of carbon-fiber microelectrodes. *Analytical Chemistry* **2008,** *80* (10), 3708-3715.

23. Huang, W. H.; Pang, D. W.; Tong, H.; Wang, Z. L.; Cheng, J. K., A Method for the Fabrication of Low-Noise Carbon Fiber Nanoelectrodes. *Analytical chemistry* **2001,** *73* (5), 1048-1052.

24. Kawagoe, K. T.; Jankowski, J. A.; Wightman, R. M., Etched carbon-fiber electrodes as amperometric detectors of catecholamine secretion from isolated biological cells. *Analytical Chemistry* **1991,** *63* (15), 1589-94.

25. Robinson, D.; Hermans, A.; Seipel, A.; Wightman, R., Monitoring rapid chemical communication in the brain. *Chem. Rev.* **2008,** *108* (7), 2554-2584.

26. Roberts, J. G.; Moody, B. P.; McCarty, G. S.; Sombers, L. A., Specific Oxygen-Containing Functional Groups on the Carbon Surface Underlie an Enhanced Sensitivity to Dopamine at Electrochemically Pretreated Carbon Fiber Microelectrodes. *Langmuir* **2010,** *26* (11), 9116-22.

27. Mitchell, E. C.; Dunaway, L. E.; McCarty, G. S.; Sombers, L. A., Spectroelectrochemical Characterization of the Dynamic Carbon-Fiber Surface in Response to Electrochemical Conditioning. *Langmuir* **2017**.

28. Bard, A. J. F., L. R., *Electrochemical Methods: Fundamentals and Applications*. 2nd ed.; John Wiley: New York, 2001.

29. Ramsson, E. S.; Cholger, D.; Dionise, A.; Poirier, N.; Andrus, A.; Curtiss, R., Characterization of Fast-Scan Cyclic Voltammetric Electrodes Using Paraffin as an Effective Sealant with In Vitro and In Vivo Applications. *Plos One* **2015,** *10* (10).

30. Heien, M.; Phillips, P.; Stuber, G.; Seipel, A.; Wightman, R., Overoxidation of carbon-fiber microelectrodes enhances dopamine adsorption and increases sensitivity. *Analyst* **2003,** *128* (12), 1413-1419.

CHAPTER 7

Summary and Outlook

7.1 Research Summary

Background-subtracted fast scan cyclic voltammetry (FSCV) has made a tremendous impact in the field of neuroscience, allowing researchers to monitor neurotransmitter and neuromodulator dynamics in live tissue, in real time. Prior to the introduction of FSCV in 1984,[1] chemical measurement techniques in neuroscience were largely limited to those which require tissue sampling followed by offline analysis[2] or immunoassay,[3] which provide chemical data only at one time point, most often post-mortem. By contrast, FSCV has been used extensively to study catecholamine release in the brain[4-5] and periphery,[6] and the dysregulation of dopamine neurotransmission resulting from certain disease states.[5, 7] The ability to monitor neurotransmitter release from cells in real time has allowed neuroscientists to better understand the links between certain behaviors and the chemical mechanisms that dictate them. For instance, many researchers have investigated the effects of cocaine on spontaneous dopamine transient release events in the nucleus accumbens of rats, and found that intravenous infusions of cocaine result in an increase in both amplitude and frequency of these dopamine transients.[8-9]

One health issue of particular importance to the United States today is the current nationwide drug epidemic – this is a health crisis that stands to gain a lot from the type of information provided by FSCV. As of 2014, over 7 million adults in America struggle with a drug abuse disorder.[10] An estimated 4.3 million Americans use prescription opiate pain killers

for nonmedical purposes.[10] Opiates are commonly prescribed for pain, but they are also commonly abused drugs which bind to opioid receptors. These opioid receptors are found throughout the nervous system alongside endogenous opioids, and are particularly prevalent in adrenal chromaffin cells. It has been established that both the catecholamines and endogenous opioids contribute to motivated behavior and reward processing;[11-13] however, the precise mechanisms by which these two neurochemicals modulate the reward circuitry are poorly understood. With improved analytical techniques such as FSCV, the intertwined roles of opioid and catecholamine signaling could be better investigated and understood, lending valuable insight into improved therapeutic strategies for pain with an end goal of dissociating the pain-relieving properties of these drugs from the effects on motivated behavior. The research outlined in this document describes steps taken to advance chemical measurements made with FSCV. The work has enabled the first direct detection of opioid peptide dynamics in adrenal tissue, and has discovered that endogenous opioids can evoke catecholamine secretion in chromaffin cells. Additionally, the type of sensor used for studying sub-second dynamics of exocytotic release events from single chromaffin cells in culture by amperometry has been improved upon, allowing for the more complete detection of neurotransmitters released into the extracellular space.

Chapter 2 describes the design and fabrication of a novel cavity ultramicroelectrode for improved sensitivity in monitoring exocytotic release from individual cells in culture. This electrode was fabricated using a plasma-etching strategy to recess the carbon back from the tip of the glass insulation. Compared to the disc microelectrode geometry typically employed in single cell work, cavity electrodes displayed an increased sensitivity to dopamine, as well as

evidence of confined mass transport. When used to monitor subsecond dynamics of exocytotic release from chromaffin cells, the cavity electrodes detected larger overall quantal sizes compared to disk electrodes. This interesting and unexpected result upends a major assumption in the field - that disk electrodes detect all of the neurotransmitters released from cells. With improved electrodes such as the cavity electrode described in this chapter, the field can better monitor vesicular release events, and draw more accurate conclusions from the data collected in these studies. A more complete picture of the biophysical aspects of vesicular fusion is crucial when a large number of pharmacological therapies rely on modulating neurotransmitter dynamics in the extracellular space.

Chapter 3 describes the investigation of a mechanism by which an endogenous opioid peptide, met-enkephalin (M-ENK), elicits catecholamine release in the adrenal glands. In order to investigate this phenomenon using FSCV, a sawhorse waveform was developed which allows for catecholamines to be detected in the presence of M-ENK, a fouling agent, by incorporating a holding step into the waveform at +1.3 V to clean the electrode surface. By performing pharmacological manipulations, it was discovered that M-ENK can elicit catecholamine secretion from chromaffin cells by way of the mu-opioid receptor (MOR), and that this response is sensitive to blockade by the opioid receptor antagonist naltrexone. This phenomenon was further studied using patch-clamp electrophysiology in a collaborative effort with Dr. John Meitzen's lab in Biological Sciences. By monitoring chromaffin cell membrane potential in response to bath infusion of various drugs, it was found that activation of MOR by the selective MOR agonist, DAMGO, depolarizes the cell. Further experiments determined that this response is dependent on activation of the muscarinic acetylcholine receptor, as

application of its antagonist, scopolamine, abolishes the depolarization by DAMGO. Together, these results provide a previously unknown mechanism by which M-ENK can act to elicit catecholamine release in the adrenal glands. This represents a major step forward in understanding the dependence of catecholamine release on opioid signaling, as opioids can excite post-synaptic cells.

Chapter 4 is a paper published in *Analytical Chemistry* in collaboration with a former Sombers Lab graduate student, Dr. Andreas Schmidt, who is the first author.[14] In this work, we developed a multiple scan-rate waveform which allows for the reliable detection of M-ENK with FSCV (described above). This new waveform was developed in order to decrease the electrochemical signal from interferents such as catecholamines, while mitigating the fouling of the electrode surface by M-ENK. I contributed to this work by using the waveform in a rat adrenal slice preparation to perform the first direct, real-time detection of M-ENK in live tissue using FSCV. This work introduces an exciting new method which allows researchers to detect M-ENK in real-time, providing a first look at opioid neuropeptide dynamics in live tissue. This is tremendously significant to the field of neuroscience, as many scientists are interested in opioid signaling. The development of this waveform also sets the stage for the detection of other peptides using FSCV, which could provide an entirely new avenue into which FSCV can be used in neuroscience.

Chapter 5 is a paper recently published in *Langmuir* in collaboration with another former Sombers Lab graduate student, Dr. Edwin Mitchell, who is the first author.[15] This work outlines the role that preconditioning with a positive potential plays in modifying the surface of carbon electrodes to improve electrochemical performance. Electrodes were conditioned

either statically or dynamically, with voltammetric waveforms that had upper limits ranging from +1.0 V to +1.4 V, or by holding at static potentials ranging from +1.0 V to +1.4 V. Electrode performance was then assessed with FSCV, and surface characterization was simultaneously performed with Raman spectroscopy and slow scan cyclic voltammetry. It was found that conditioning with higher potentials yielded improved electrochemical performance, and that static conditioning was more efficient than dynamic conditioning in eliciting the structural changes that underlie improved performance. I contributed by performing the slow scan voltammetric measurements, as well as lending major contributions to the development of the project and the overall manuscript preparation. This work provides valuable insight into how carbon surfaces change in response to application of positive potentials, which will aid researchers in improving sensors and in developing customized waveforms for better electrochemical performance when studying chemical signaling in the nervous system.

Chapter 6 describes another novel carbon-fiber sensor developed in the Sombers Lab, a nanoelectrode with a conical tip on the order of 200 nm in diameter. The nanoelectrode was implanted inside single chromaffin cells to monitor intracellular catecholamines as the vesicles containing them lysed onto the electrode. This work was also a collaborative effort with data collection performed by Edwin Mitchell, Sombers Lab post-doctoral fellow Dr. James Roberts, and myself. My contribution included aiding with establishing chromaffin cell culture according to the protocol that I wrote, as well as helping to collect the FSCV data on the single cell experimental setup that I built. We report the first implementation of FSCV inside individual cells, and successfully distinguished epinephrine from norepinephrine intracellularly. This work has exciting future outlooks, as performing intracellular FSCV will

allow neuroscientists to quantitatively investigate intracellular vesicular content and compare it to measurements of neurotransmitters released and detected outside of the cell. This will allow for insights into different populations of vesicles inside the cell, conditions required for differential release of these pools of vesicles, the partial vs full fusion debate, and many more questions.

Overall, the work presented herein represents a major step forward in advancing electroanalytical approaches to monitoring chemical communication between cells, while also providing fundamental insights into opioid and catecholamine signaling. Thus, it serves to advance two separate fields, analytical electrochemistry and neuroscience. For instance, Chapter 2 outlines the fabrication and characterization of a new cavity microelectrode which, when used to detect exocytotic neurotransmitter release from individual cells, revealed that traditionally used sensors in this preparation likely yield incomplete information into quantal size of the vesicles. Chapter 3 describes a previously unknown mechanism by which activation of mu-opioid receptors can elicit exocytotic release of catecholamines, and provides evidence for the presence of excitatory opioid receptors on chromaffin cells. Chapter 4 describes a new voltammetric approach that allows for the first detection of the dynamics of met-enkephalin in tissue, while Chapter 5 investigates the effect that the applied waveform has on the electrode performance. Chapter 6 describes another novel sensor, a nanoelectrode, which can be implanted into individual cells to monitor intracellular content. Together, this work provides researchers with exciting new tools to address crucial questions in neuroscience which were inaccessible with the methods previously available, and will undoubtedly lead to many more

advances in understanding opioid signaling in the nervous system to facilitate the development of improved opioid therapeutics.

7.2 References

1. Stamford, J. A.; Kruk, Z. L.; Millar, J., Regional Differences in Extracellular Ascorbic-Acid Levels in the Rat-Brain Determined by High-Speed Cyclic Voltammetry. *Brain Res.* **1984,** *299* (2), 289-295.

2. Zestos, A. G.; Kennedy, R. T., Microdialysis Coupled with LC-MS/MS for In Vivo Neurochemical Monitoring. *AAPS J* **2017**.

3. Tiong, G. K. L.; Olley, J. E., Use of Methionine-Enkephalin Sulfoxide and Leucine-Enkephalin Radioimmunoassays for the Measurement of Enkephalins in the Rat-Brain. *Clinical and Experimental Pharmacology and Physiology* **1989,** *16* (2), 89-95.

4. Robinson, D. L.; Hermans, A.; Seipel, A. T.; Wightman, R. M., Monitoring rapid chemical communication in the brain. *Chem. Rev.* **2008,** *108* (7), 2554-84.

5. Qi, L.; Thomas, E.; White, S. H.; Smith, S. K.; Lee, C. A.; Wilson, L. R.; Sombers, L. A., Unmasking the Effects of L-DOPA on Rapid Dopamine Signaling with an Improved Approach for Nafion Coating Carbon-Fiber Microelectrodes. *Anal. Chem.* **2016,** *88* (16), 8129-36.

6. Petrovic, J.; Walsh, P. L.; Thornley, K. T.; Miller, C. E.; Wightman, R. M., Real-time monitoring of chemical transmission in slices of the murine adrenal gland. *Endocrinology* **2010,** *151* (4), 1773-83.

7. Ferris, M. J.; Calipari, E. S.; Yorgason, J. T.; Jones, S. R., Examining the Complex Regulation and Drug-Induced Plasticity of Dopamine Release and Uptake Using Voltammetry in Brain Slices. *ACS Chem. Neurosci.* **2013,** *4* (5), 693-703.

8. Stuber, G. D.; Roitman, M. F.; Phillips, P. E. M.; Carelli, R. M.; Wightman, R. M., Rapid dopamine signaling in the nucleus accumbens during contingent and noncontingent cocaine administration. *Neuropsychopharmacology* **2005,** *30* (5), 853-863.

9. Heien, M. L. A. V.; Khan, A. S.; Ariansen, J. L.; Cheer, J. F.; Phillips, P. E. M.; Wassum, K. M.; Wightman, R. M., Real-time measurement of dopamine fluctuations after cocaine in the brain of behaving rats. *Proceedings of the National Academy of Sciences of the United States of America* **2005,** *102* (29), 10023-10028.

10. Azofeifa, A.; Mattson, M. E.; Schauer, G.; McAfee, T.; Grant, A.; Lyerla, R., National Estimates of Marijuana Use and Related Indicators - National Survey on Drug Use and Health, United States, 2002-2014. *Mmwr Surveillance Summaries* **2016,** *65* (11), 1-Cover3.

11. Le Merrer, J.; Becker, J. A. J.; Befort, K.; Kieffer, B. L., Reward Processing by the Opioid System in the Brain. *Physiological Reviews* **2009,** *89* (4), 1379-1412.

12. Smith, K. S.; Berridge, K. C., Opioid limbic circuit for reward: Interaction between hedonic hotspots of nucleus accumbens and ventral pallidum. *J. Neurosci.* **2007,** *27* (7), 1594-1605.

13. Mahler, S. V.; Vazey, E. M.; Beckley, J. T.; Keistler, C. R.; McGlinchey, E. M.; Kaufling, J.; Wilson, S. P.; Deisseroth, K.; Woodward, J. J.; Aston-Jones, G., Designer receptors show role for ventral pallidum input to ventral tegmental area in cocaine seeking. *Nature Neuroscience* **2014,** *17* (4), 577-U136.

14. Schmidt, A. C.; Dunaway, L. E.; Roberts, J. G.; McCarty, G. S.; Sombers, L. A., Multiple Scan Rate Voltammetry for Selective Quantification of Real-Time Enkephalin Dynamics. *Anal. Chem.* **2014,** *86* (15), 7806-7812.

15. Mitchell, E. C.; Dunaway, L. E.; McCarty, G. S.; Sombers, L. A., Spectroelectrochemical Characterization of the Dynamic Carbon-Fiber Surface in Response to Electrochemical Conditioning. *Langmuir [Just Accepted]* **2017**.

APPENDIX A

Primary Bovine Adrenal Chromaffin Cell Culture

A.1 Sombers Lab BACC Protocol

A.1.1 Materials

Chemicals

- Benzalkonium Chloride
- W3 Buffer (NaCl, KCl, NaH_2PO_4, glucose, HEPES)
- Penicillin-Streptomycin
- Gentamicin
- Nystatin
- Collagenase
- DNAase
- Percoll
- Dulbecco's Modified Eagle's medium (DMEM)

Hardware/Instruments

- Autoclave
- Incubator
- 15, 50 mL centrifuge tubes
- Centrifuge (room temp, 260 to 13,000 rpm)
- Centrifuge tube rack
- Stirring hotplate
- Scalpel
- Scissors
- Insulated container
- Hemocytometer
- Microscope
- Automatic pipetter
- 1000 µL Eppendorf pipet
- 5, 10 and 20 mL serological pipettes
- Parafilm

Glassware/Disposables

- 500+ mL beaker to transport glands
- 250 mL beaker (x2)

- 150 mL beaker (x7)
- 100 mL beaker
- 250 mL graduated cylinder
- 15 cm petri dish
- 50 mL centrifuge tubes
- Glass rod
- Aluminum foil
- 250 µm nylon mesh
- 40 µm cell strainer (Corning Falcon, blue)
- Cell culture dishes
- 5 mL syringes

A.1.2 Procedures

A) **Day before cell culture**
   1. Set CO_2 level on incubator to 7.0 % (12 psi) and temperature to 37˚ C
   2. Fill water bath up with 50 mL/L of 1% benzalkonium chloride
   3. Reserve vehicle to transport glands
   4. Confirm appointment with slaughterhouse (Chaudhry Halal Meat, 919-742-9292)
   5. Autoclave all glassware and surgical tools
   6. Place the following in the hood (all sterile)
      - Eppendorf pipette tips
      - 50 mL centrifuge tubes
      - 1, 5, and 20 mL serological pipettes
      - Centrifuge tube rack
      - Automatic pipette
      - Cell culture dishes
   7. Make 10X W3 stock solution with autoclaved water (store at 4˚ C)
      - 1450 mM NaCl 84.75 g/L
      - 54 mM KCl 4.03
      - 10 mM NaH_2PO_4 1.38
      - 112 mM glucose 20.00
      - 150 mM HEPES 35.75
   8. Make 1 L of W3 solution with autoclaved water from 10X stock solution and divide into to 500 mL aliquots and adjust W3 to pH 7.4 with NaOH
   9. Add antibiotics to all aliquots
      - Pen-strep 30 mL/L (of 100x to dilute to 3x final)
      - Gentamicin 2 mL/L (of 50 mg/mL)
      - Nystatin 5 mL/L (only add to one aliquot)

B) **At the Slaughterhouse**

1. Bring large transport beaker, W3 without nystatin, 1 mL syringe, Parafilm, and insulated container
2. Obtain ~6 undamaged adrenal glands (no cuts or perforations) and trim off large pieces of excess fat
3. Repeatedly wash glands by perfusion through adrenal vein with cold W3 (sans nystatin) in syringe, until buffer comes out from gland clear and free of blood (~10 mL/gland)
4. Submerge glands in beaker under W3, cover with parafilm and store in ice

C) **In the lab, Under Laminar Flow Hood**

1. Warm leftover W3 to RT in water bath on hotplate
2. Carefully, trim glands of all remaining fat
3. Use syringe to flush W3 through adrenal veins to make glands swell (~4 mL)
4. Place each gland in sterile 150 mL beaker, cover, and incubate for 10 min at 37˚ C
5. While incubating, prepare 37˚ C water bath on stir plate (observe step 7 and 8)
6. Repeat steps 3 and 4 two additional times, emptying beaker after each flush
7. During incubation, prepare digestion mixture
    - Dissolve 200 mg collagenase in 140 mL W3
    - Add 5 mg DNAase
8. During incubation, prepare Percoll gradient
    - For 6 adrenal glands, mix 4 mL 10X W3 and 36 mL Percoll
9. After last W3 flush, rinse each beaker with W3. Then, syringe 4 mL collagenase/DNAase solution into each gland, cover, and incubate for 15 minutes
10. Repeat digestion mixture flush and incubation step, two additional times
11. One at a time, cut open glands using a scalpel or scissors along longitudinal axis, and place external side down. Remove medulla by scraping with scalpel and place into 15 cm petri dish.
12. Pool medullae in one dish, add a few mL's of collagen/DNAase solution, and mince with scalpel (finer mincing will yield higher cell count, ~1mm pieces)
13. Add W3 to remaining collagen/DNAase solution to double its volume.
14. Pour mince into sterile 150 mL beaker with stir bar and add remaining digestion mixture. Place beaker in warm water bath and stir at a moderate rate (a few revs/second) for 30 minutes
15. Filter digestion mixture through 250 µm nylon mesh, into sterile glass beaker. Facilitate with glass rod and rinse filtrate with W3
16. Evenly divide mixture into four 50 mL centrifuge tubes and dilute to 50 mL with W3
17. Centrifuge at 1500 rpm (300-400 G) for ~15 minutes to pellet cells
18. Carefully, discard supernatant. Resuspend pellets in 2 batches of 20 mL W3 and carefully mix each batch with 20 mL Percoll gradient by gently upending capped tube.
19. Centrifuge both tubes are about 10,000 RPM (3,400-20,000 Gs) at RT for 20 minutes

20. Red blood cells collect at bottom of gradient, chromaffin cells band in the middle, and cellular debris at the top. Remove the cellular debris from the top with a pipette (roughly 1/10 of gradient)
21. Collect the middle chromaffin cell containing layer, 50-60% of gradient volume, with a 10 mL pipette.
22. Filter this layer through a 40 µm sterile nylon filter.
23. Put filtrate into a 500 mL sterile bottle and add 200 mL sterile DMEM medium.
24. Aliquot 400 mL into four or five 50 mL centrifuge tubes and centrifuge at ~800 rpm (~400 G) for 10 min at RT to pellet cells
25. Remove supernatant and resuspend cell pellets into 40 mL DMEM with 10% FBS and 1% 100x pen-strep.
26. Use hemocytometer to dilute to density of 3 x 10^5 cells/mL and pipette 2 mL in each culture dish.
27. On 3rd, 5th and 7th days of culture, remove old medium and replace with fresh growth medium, without FBS. Cells are typically viable for about a week.

A.2 Protocol Considerations

Sterile technique is crucial to the establishment of a healthy primary cell culture. While obtaining the glands from the slaughterhouse is not sterile, all other aspects of this preparation should be carefully performed. A laminar flow hood with UV sterilization should be used for all chemical preparations, as well as all steps involving glands following return from the slaughterhouse. Everything placed into the flow hood, aside from live tissue, should be sterilized with 70% ethanol. Chemicals and supplies that are stable upon exposure to UV light should be placed in hood prior to UV sterilization. Chemicals with proteins that denature upon exposure to UV light should be added to the sterile environment afterwards. Glassware and instruments should be autoclaved before placement into the hood. Benzalkonium chloride solution for the incubator can be autoclaved after mixing, and poured directly into the incubator. Allow it to cool down prior to pouring into the tray; otherwise it will substantially

raise the temperature of the incubator. In order to avoid contamination, it is beneficial to have an incubator dedicated solely to the chromaffin cells.

At the slaughterhouse, the adrenal glands are often damaged when cutting the carcass sagittal. In our experience, damaged glands do not produce healthy cell cultures. Additionally, there are smaller kidney bean-shaped glands in the same general area; avoid these and obtain the larger glands that appear heart-shaped or L-shaped. They are easily distinguished by the presence of adrenal arteries and veins.

APPENDIX B

Instrumentation for Single Cell Analysis

B.1 Instrumentation

The Axon Instruments Axopatch 200B was used for amperometry experiments, because it is capable of detecting sub-picoampere current with extremely low noise (~0.5 pA RMS in voltage-clamp, whole cell configuration). The Axon Instruments CV 203B headstage has a built in peltier cooler, which helps lower the electrical noise. The Axopatch is coupled to an Axon Instruments Digidata 1440A digitizer, for an uncomplicated USB interface with the computer. While homemade breakout boxes are substantially cheaper, they typically introduce more electrical noise relative to the Digidata connection. For instrumentation setup, grounding, and troubleshooting, consult The Axon Guide that is available from Molecular Devices, LLC.

B.2 Components

After considering instrumentation, many other components are required to image the cells, maintain viability, manipulate electrode placement, and stimulate the cells. The experimental rig is built around a research-grade inverted microscope. Inverted microscopes allow for placement of the electrode and injector without interference from the optics, as well as visualizing the cells without the electrode obstructing the view. The Olympus IMT-2 platform was used for all experiments. Contrast optics are necessary in order to visualize and distinguish cells from one another, as well as to assess the health and overall shape of a cell. Hoffman Modulation Contrast was selected, as it is superior to phase contrast and comparable to differential interference contrast (DIC).

The entire experimental rig must be isolated from building vibrations in order to minimize electrical noise from the electrode responding to the environment. While anti-vibration tables are an effective way to do this, benchtop vibration isolators (Newport Instruments) are equally effective, and can be placed inside a Faraday cage.

Micromanipulators are required in order to position electrodes and injectors adjacent to the cell of interest. Companies including Siskiyou, Narishige, and Sutter offer motorized manipulators that allow for very precise electrode positioning. The Burleigh PCS-5000 Series has piezoelectric control, which offer exceptionally low electrical noise, and minimal electrode drift over time.

Finally, the cell plate holder used for mounting the cell dish onto the rig must allow for constant temperature control, as this preparation leaves the cells in a bath, without need for perfusion of a buffered saline solution. The Warner Instruments chamber with heated base was

selected to allow for constant temperature control. The heated base was controlled by a Warner Instruments TC-324B temperature controller. The cell chamber was mounted on a Siskiyou three-axis micromanipulator to allow for movement of the cell dish with respect to the optics of the microscope. This allows for the microscope to be fixed on the table, rather than fixing the cell dish and moving the microscope with respect to the cells. A custom stage was designed in order to mount the cell chamber onto the manipulator.

B.3 Experimental Considerations

Grounding all of the components to one another is essential for minimizing electrical noise. At the same time, avoid creating ground loops that tend to amplify the noise. Consult the Axon Guide for information on this topic. Electrode length is also a factor in dealing with electrical noise. Longer electrodes tend to vibrate more and act as larger antenna to pick up more electrical noise. The electrode should also have a proper seal with the glass insulation. Additionally, the electrode may need to be held at a static potential of +1.0 V vs. Ag/AgCl for up to an hour before being sensitivity to catecholamines is optimal.

APPENDIX C

Patch-Clamp Electrophysiology Experiments on Chromaffin Cells in Rat Adrenal Slice

C.1 Materials and Solutions

Adrenal Slicing Solution- bicarbonate buffered saline (BBS) (low calcium version)

NaCl (125 mM), $NaHCO_3$ (26 mM), KCl (2.5 mM), $NaH_2PO_4 \bullet H_2O$ (1.25 mM), Glucose (10 mM), HEPES (10 mM), $CaCl_2 \bullet H_2O$ (0.1 mM), $MgCl_2 \bullet 6H_20$ (3 mM), pH set to 7.2 with NaOH, osmolarity set to 320 mOsm with sucrose

Adrenal Incubation Solution- BBS

NaCl (125 mM), $NaHCO_3$ (26 mM), KCl (2.5 mM), $NaH_2PO_4 \bullet H_2O$ (1.25 mM), Glucose (10 mM), HEPES (10 mM), $CaCl_2 \bullet H_2O$ (2 mM), $MgCl_2 \bullet 6H_20$ (1 mM), pH set to 7.2 with NaOH, osmolarity set to 320 mOsm with sucrose

HEPES-Buffered Ringer Solution

NaCl (150 mM), HEPES (10 mM), Glucose (10 mM), $CaCl_2 \bullet H_2O$ (2.8 mM), KCl (2.8 mM), $MgCl_2 \bullet 6H_20$ (2 mM), pH set to 7.2 with NaOH, osmolarity set to 320 mOsm with sucrose

Internal Pipette Solution

Gluconate (145 mM), HEPES (10 mM), NaCl (8 mM), MgATP (2 mM), $MgCl_2$ (1 mM), EGTA (0.1 mM), NaGTP (0.3 mM), phosphocreatine (10 mM) pH set to 7.2 with NaOH, osmolarity set to 310 mOsm with sucrose

C.2 Instrumentation

For patch clamp experiments, Axon instruments' (Molecular Devices, LLC., Sunnyvale, CA) MultiClamp 700B amplifier, DigiData 1440A digitizer, and pCLAMP 10 software were used to collect electrophysiological data. Tissue was visualized using a Zeiss Axioscope, equipped with IR-DIC optics for contrast, a DAGE IR-1000 camera for images, 10x and 40x objective lenses, and optical zoom.

C.3 Experimental Procedures and Considerations

C.3.1 Acute Adrenal Slice Preparation

Animal care and use was in complete accordance with NIH and NC State University institutional guidelines (IACUC). Male Sprague-Dawley rats (250−550 g, Charles River Laboratories, Raleigh, NC) were deeply anesthetized with isofluorane, and euthanized by decapitation. The adrenal glands were rapidly removed, trimmed of fat tissue, and embedded in agarose gel (3% agarose in low calcium BBS). The gel blocks containing the adrenal glands were placed in cold low calcium BBS while 300 μm thick slices were obtained with a vibroslicer (World Precision Instruments, Sarasota, FL). The slices were allowed to rest in the buffer for at least 1 hour before the start of an experiment.

C.3.2 Electrophysiological Recording

After resting for at least one hour, slices were placed in the recording chamber of the microscope and perfused with oxygenated ringer solution heated to 27° C. Whole-cell patch-clamp recordings were made from healthy cells in the medulla. Ideal cells have a defined three-dimensional contour without a well-defined nuclear envelope, which is indicative of cell death. Recordings were made using glass electrodes (2-4 MΩ) pulled on a Sutter Instrument (Novato, CA) P-97 Micropipette Puller. Electrodes were backfilled with internal pipette solution, and air bubbles removed from the pipette tips either with gentle perturbation, or positive pressure. Signals were filtered at 2 kHz and digitized at 10 kHz. Membrane potential was recorded in current-clamp mode.

C.4 Data Analysis

Electrophysiological properties were characterized using pCLAMP 10 software. After gaining access, the membrane potential was allowed to stabilize three to four minutes. Quiescent cells were kept at resting potential with no holding current, while cells firing spontaneous action potentials were suppressed using negative current (15-30 pA). Three hyperpolarizing current injections were applied in order to calculate input resistance, both before and after each experimental manipulation.

When assessing cell response to particular drugs, membrane potential was allowed to rest for 5 minutes before the drug was applied. Drugs were applied via bath application for 10-15 minutes before washing out. Membrane potential was averaged in thirty second increments to assess its response to the applied drug.

Statistics

Data were analyzed using two-tailed *t* tests, linear regressions, and ANCOVAs (Prism version 5.0, GraphPad Software). Significance was determined by p values <0.05. Data are presented as the mean ± SEM.

APPENDIX D

Considerations for Adrenal Slice Experiments

D.1 Procedural Notes

Removing the adrenal glands from an animal and slicing them is a delicate procedure, and the utmost care must to taken in order to yield healthy cells in this preparation. This section will add to the methods, and note considerations as to what works well and what does not.

The first consideration is the weight of the animal. With the Sprague-Dawley rat, we have used animals ranging from 250 grams to 550 grams. While repurposing animals that have already been used for other experiments results in better stewardship of our resources, older rats tend to gain weight and present some problems in these experiments. After extracting the glands, there is far more fat surrounding the tissue, which increases the time to locate and remove the glands. Additionally, the cortex could become damaged while trimming the excessive fat. Thus, it is desirable to use younger animals for ease of access to the glands without causing damage in the extraction process. Also, younger glands have less connective tissue in the medulla and permit easier access to the chromaffin cells themselves. In this work, rats ranging from 250 to 350 grams have produced the best results.

It is important to extract the glands and place them in oxygenated, ice cold BBS as quickly as possible following decapitation, without damaging the cortex. When in doubt, cut out a bigger piece of tissue with more fat around the gland. Once glands are in cold BBS, more care can be taken to trim the gland of remaining fat. Any fat remaining on the gland tends to get caught in the blade during slicing and pulls the gland out of agarose, resulting in unusable

slices. However, the researcher must be careful not to cut into the cortex, as this damages the gland and results in less healthy cells within the medulla. Once trimmed of all fat, the agarose solution is prepared. 3% agarose in BBS is roughly the same density as the adrenal gland, so that the glands don't immediately sink to the bottom of the container. If they do sink, the agarose was probably not all dissolved in solution, resulting in a less dense gel. Heating and stirring the agarose mixture at a high rate helps to disperse all of the powdered gel into solution. Even if some chunks remain at first, the solution can stay on the hot plate until all powder is dissolved. Once the agarose solution is created, it must be cooled to 33-34 C˚ before embedding the glands. For low-gelling agarose, this temperature is slightly above the gelling point, so temperature control is key. However, adding the glands to the gel at a temperature higher than 34 C˚ can damage the cells.

Once the gel solidifies, it is important to immediately return the embedded glands into ice cold BBS. Once the cooled block of agarose is trimmed and glued to the stage, it is ready to be sliced. The ideal slice thickness seems to be around 300 μm. Thicker slices result in difficulty visualizing the cells with DIC optics. Slicing less than 300 μm results in marginally better visualization, but less healthy tissue. A sharp blade must be used with slicing; double sided platinum-edged blades tend to work . Slicing the gland must be done at a constant, slow rate; ideally each pass of the blade through the gland will take 60-75 seconds. The obtained slices are added to an incubation chamber and bubbled with 95% O_2/5% CO_2. Direct contact with rigorous bubbling can damage the cells, so the pressure must be low enough that the bubbles don't perturb the glands. At the same time, it must be sufficiently high to keep the

solution saturated and the pH stable. A careful preparation yields slices that are viable for 6-8 hours.

APPENDIX E

Implementing Optogenetics for FSCV Experiments

E.1 Expression of Channelrhodopsin

Optogenetics was implemented to gain neuron-specific excitation in the rat brain, to address selectivity issues for measuring neurotransmitter release. For proof of concept, the dopamine projection from the ventral tegmental area (VTA) to the nucleus accumbens was targeted for expression of channelrhodopsin. Viral vectors were purchased from the UNC Vector Core (Chapel Hill, NC) and kept frozen until infused into the rats. The neural activator vector AAV-CAG-ChR2-GFP was chosen, with GFP for verification of infection and ChR2 for activation of expressed neurons. 2 μL of the viral vector was microinfused via a cannula guide into the VTA. Infection was verified after 8 weeks for maximum expression, utilizing fluorescence microscopy on coronal tissue slices.

E.2 Hardware

In order to stimulate release, a 470 nm LED (Thor Labs, Newton, NJ) was coupled to the epi-illuminator port on the microscope, to direct light through the optics to the sample. The

LED was powered by a Thor Labs LED driver with a maximum output of 1.2A. Stimulation trains were generated using the “stim” feature built into HDCV.

E.3 Optically Stimulated Dopamine Release in the Striatium

After allowing eight weeks for maximum expression of ChR2, an acute brain slice experiment was performed, targeting the nucleus accumbens. The recording electrode was placed in the caudal portion of the nucleus accumbens, where GFP expression was most prevalent. A variety of experiments were performed, with various stimulation parameters. Dopamine release was detected multiple times, with 10 Hz stimulation frequency proving most effective for pulsatile stimulation (Figure E1A), while a constant five seconds stimulation elicited substantially more release (Figure E1B).

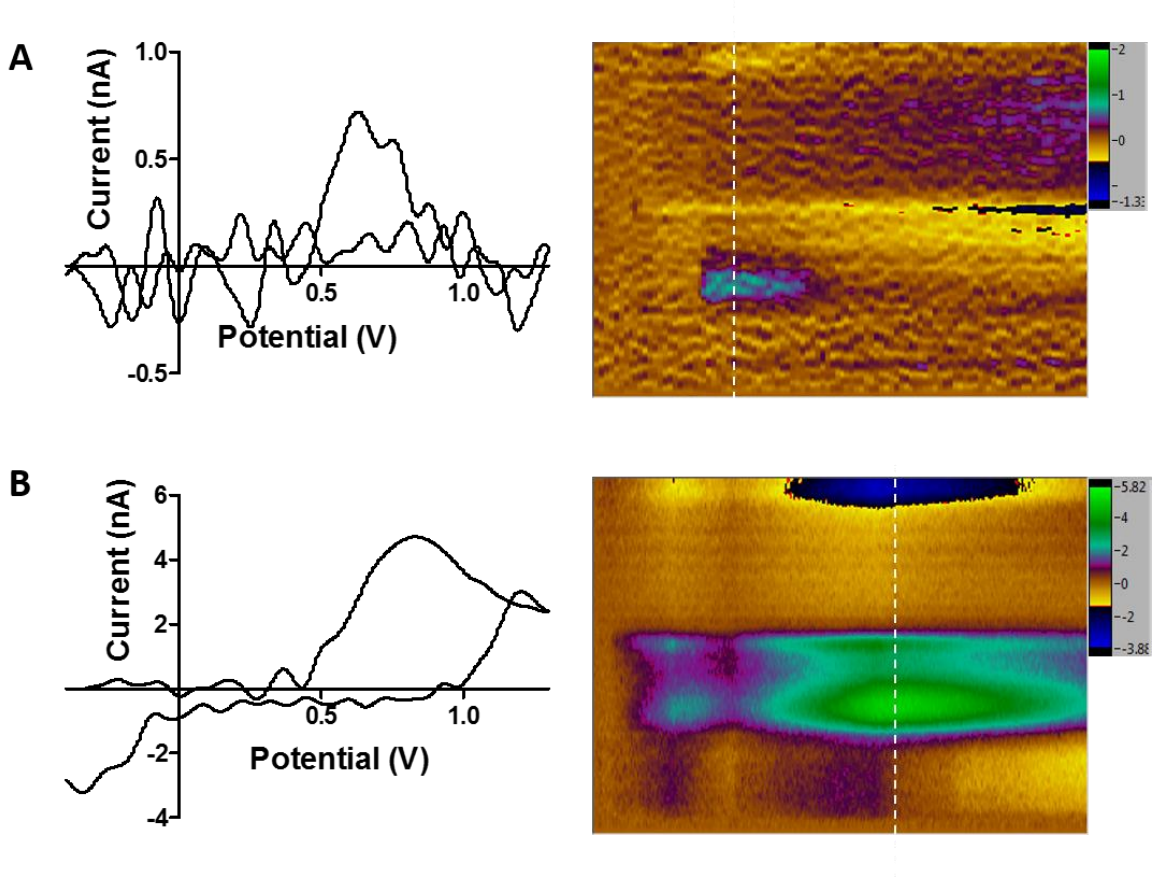

Figure E1. Optically stimulated dopamine release in the nucleus accumbens. A) 20 pulses at 10 Hz. B) 1 pulse for 5 seconds.

E.4 Optically Stimulated Met-Enkephalin Release in the VTA

Data were collected in collaboration with Howard Fields' lab at UCSF, where a rat was microinfused with a viral vector containing the AAV2/1-CAG-ChR2-tdtomato sequence in the ventral pallidum (VP) 6 weeks prior to the experiment. Infection with the virus leads to membrane-localized expression of ChR2 in ENK neurons projecting from the VP to the ventral tegmental area (VTA), so terminals in the VTA that originate from the VP should then express

this sequence. Infection was verified by fluorescence microscopy with a tdtomato filter cube (data not shown).

Data collected utilizing this method are shown in Figure E2. Optical stimulation in the VTA occurs at the red arrow in Figure E2A, and voltammetric data is extracted (dashed white line) and shown in Figure E2B. The peaks collected in the tissue align well with the tyrosine and methionine peaks of a voltammogram collected *in vitro*.

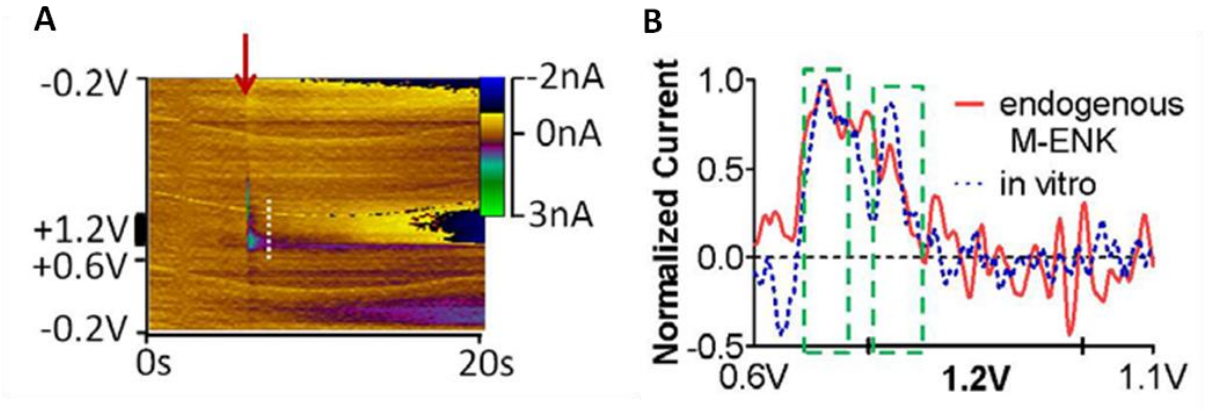

Figure E2. Optically evoked M-ENK release in the VTA of a rat brain slice. A) Color plot with optical stimulation at the red arrow. Optical stimulation consists of a single 5 msec pulse of 470 nm light. B) Normalized voltammetric data extracted from the color plot in Figure E2A (red line), overlaid with a voltammogram collected *in vitro* (blue dashed line). Green squares highlight oxidation peaks for tyrosine and methionine, respectively.

APPENDIX F

Supplemental Information to Chapter 3

F.1 Supporting Information

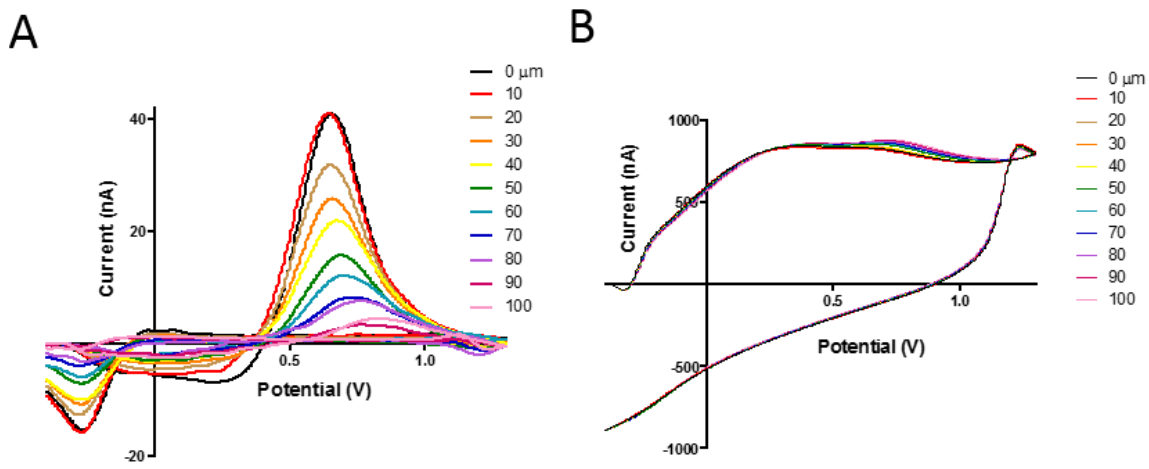

Figure F1. Shifting peak oxidation potential. A) Voltammograms collected by pressure ejecting 10 µM norepinephrine onto electrode as it is lowered into adrenal tissue. Electrode begins outside of tissue, and is lowered into tissue 10 µm at a time. As electrode is lowered, magnitude of the signal is decreased, and the impedance shift pushes peaks to a higher potential. B) Non background-subtracted voltammograms collected as electrode is lowered into adrenal tissue. Basal catecholamine signal in the background increases in magnitude as electrode is lowered, accompanied by similar response to impedance pushing peaks to higher potentials.

APPENDIX G

Supplemental Information to Chapter 4

G.1 Supporting Information

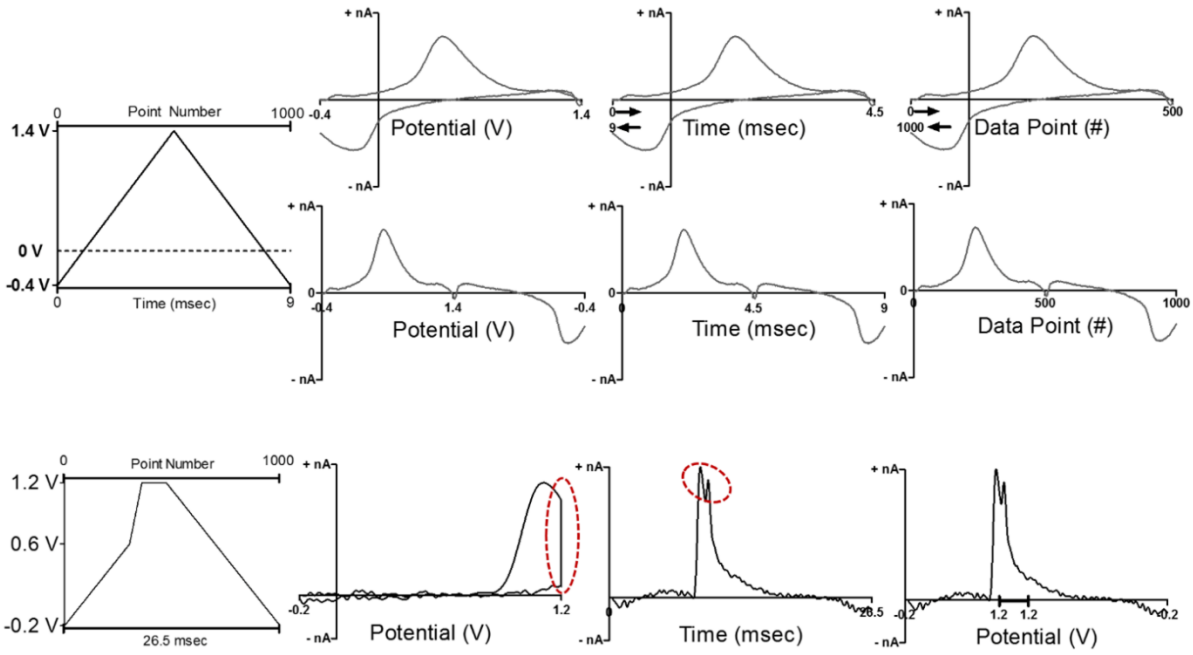

Figure G1. Cyclic voltammograms are typically plotted as current (y-axis) vs. potential (x-axis). Typically, two separate y values are plotted for each x value, one corresponding to the current measured during the forward scan (anodic current) and one from the reverse scan (cathodic current). However, when the potential is held constant, as is the case with the MSW, there will be multiple y-values collected at a single potential (x-value), making it difficult to visualize the electrochemical response at that potential. Each cycle of the MSW consists of 1000 individual data points. Data collected using the MSW are easily visualized when displayed in a linear fashion with current (y-value) plotted versus data point number (in time) of the applied waveform. The benefits of this approach are highlighted by the red ellipses; the second peak is only visible when the data is plotted linearly (vs. time or data point number converted to potential).

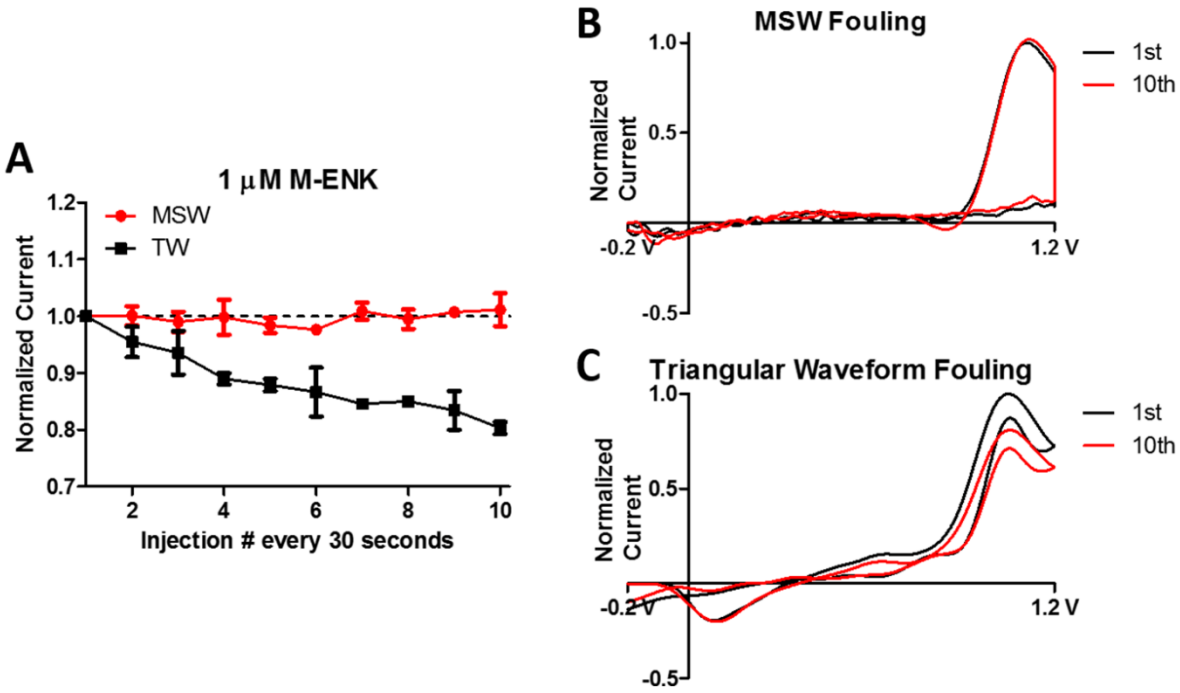

Figure G2. (A) 10 consecutive injections of 1 µM M-ENK. The MSW retained sensitivity, but the performance of the triangular waveform (TW) rapidly declined. (B, C) Representative voltammograms from 1st and 10th injections using the MSW (top) and TW (bottom). The effects of electrode surface fouling are evident when using a conventional TW.

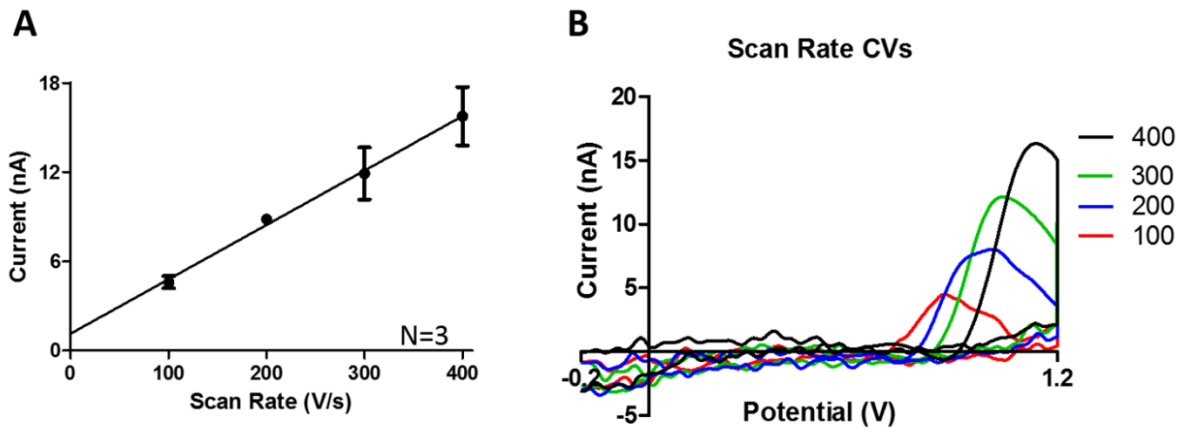

Figure G3. Incrementally increasing the scan rate from 100 V/s to 400 V/s in the second portion of the anodic scan (0.6-1.2V) increases the (A) current and (B) oxidation potential inherent to the first (tyrosine-derived) peak in the voltammetric detection of 1 μM M-ENK. A scan rate of 400 V/s was chosen for the second portion of the anodic scan, as it provides the best option for sensitivity and peak resolution.

APPENDIX H

Supplemental Information to Chapter 5

H.1 Supporting Information

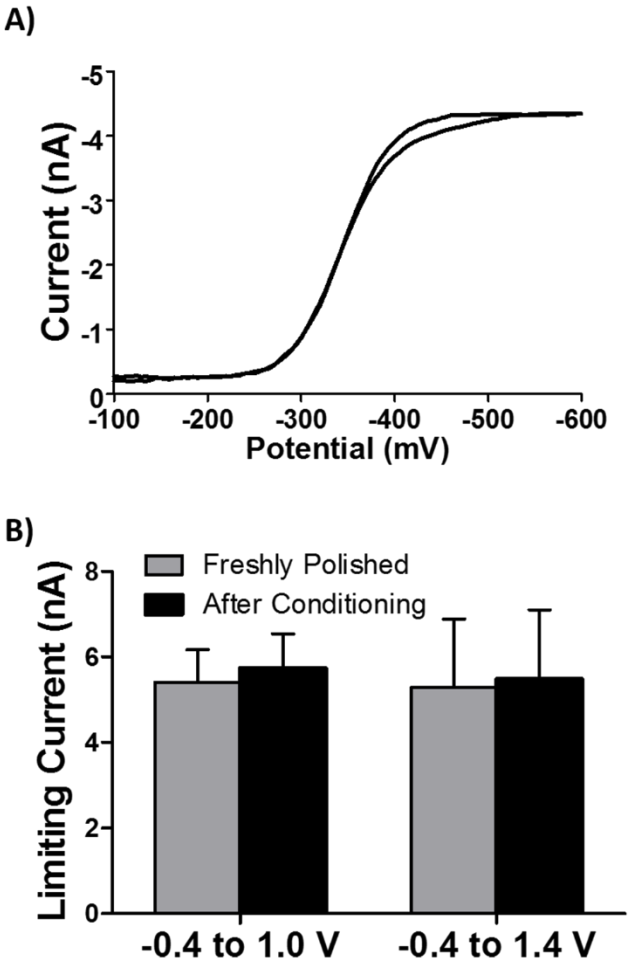

Figure H1. Electrochemical conditioning does not significantly alter electrode surface area. A) Representative voltammogram from a freshly polished electrode. B) Limiting current generated in the reduction of hexaminerutheniumIII) chloride collected after polishing (grey) and after conditioning the polished electrodes with dynamic waveforms (black). No significant difference was detected ($p>0.05$, paired *t*-test, n=3 for both conditioning methods).